

Global buckling of sheet piles

The influence of soil to the global buckling behaviour of sheet piles

Vincent van Delft



Global buckling of sheet piles

The influence of soil to the global buckling
behaviour of sheet piles

MSc Thesis by:
Vincent van Delft, 4345088

to obtain the degree of Master of Science
at the Delft University of Technology
to be defended on May 28, 2020, 11:00

| | | | |
|----------------------|----------------------|----------------------------|--------------------------------|
| Graduation company | Iv-Infra, Sliedrecht | | |
| Graduation committee | Chair | Prof. dr. ir. S.N. Jonkman | Delft University of Technology |
| | Member | Ir. W.F. Molenaar | Delft University of Technology |
| | Member | Dr. ir. R. Abspoel | Delft University of Technology |
| | Member | Ir. H.J. van der Giessen | Iv-Infra B.V. |

An electronic version of this thesis is available at: <http://repository.tudelft.nl/>.

Cover: Construction pit Cherry Park, Stratford, London, UK. Source: [1]

Preface

This report presents the reader the thesis which is written to conclude my Master in Civil Engineering at the Delft University of Technology. After obtaining my Bachelor of Science degree, I started this Master in September 2017 to follow the track of Hydraulic Engineering with the specialisation of Hydraulic Structures and Flood Risk. During my studies, an interest was developed in the combination of hydraulic structures, geotechnical engineering and structural mechanics. I therefore did not need much time to decide when I was offered the opportunity to write a thesis about *the influence of soil to the global buckling behaviour of sheet piles* at Iv-Infra B.V., a subsidiary of Iv-Groep B.V. responsible for the design of many infrastructural structures. This is a thesis topic in where all three interests of my are represented.

I want to express my gratitude to the thesis committee, chaired by Bas Jonkman, for their support during the past 9 months. Wilfred Molenaar and Roland Abspoel I would like to thank for their criticism during the committee meetings and elsewhere, which strengthened, with their help, the theoretical arguments in this thesis. Harm-Jan van der Giessen from Iv-Infra B.V. has provided a significant support and was always quick with his answers, for which I am thankful. Furthermore, I would like to thank academic staff at the Delft University of technology, supporting staff from Iv-Infra B.V. and friends who provided ideas for this thesis and answers to questions.

Finally, I want to say thanks to my family and friends for their support during almost 6 years of academic education, which ends up at this point, with a Master thesis at the Delft University of Technology.

*Vincent van Delft
Rijnsburg, May 2020*

"All models are wrong, but some are useful"
G. Box, 1976

Summary

In the construction of excavation pits, quay walls and soil reinforcing structures steel sheet piles may be used to retain the soil at its place. Due to the difference in soil or water levels or external forces, the sheet piles are loaded and may fail due to insufficient strength or instability. Several mechanism may lead to failure of the pile, which all should be checked in order to declare a sheet piling design safe according to the Eurocode NEN-EN 1993-5. A sheet pile will deform due to the loading, visualised in figure 1 by w_0 . If a vertical load, a normal force, is applied to the sheet pile, this displacement will grow, visualised by w . This effect is known as the global buckling mechanism, main topic of this thesis. In the current practice, the verification or unity check on this mechanism depends on the critical global buckling load F_{cr} . If the normal force approaches this load, the growth of the deformation will go to infinity, which will obviously give failure of the sheet pile. Currently, the value of F_{cr} is determined based on the resistance the steel material of the sheet pile gives against deformation. However, the soil must be deformed as well for the global buckling mechanism to occur, but this is currently left out of account. This thesis aims to investigate the influence of the soil to the global buckling mechanism.

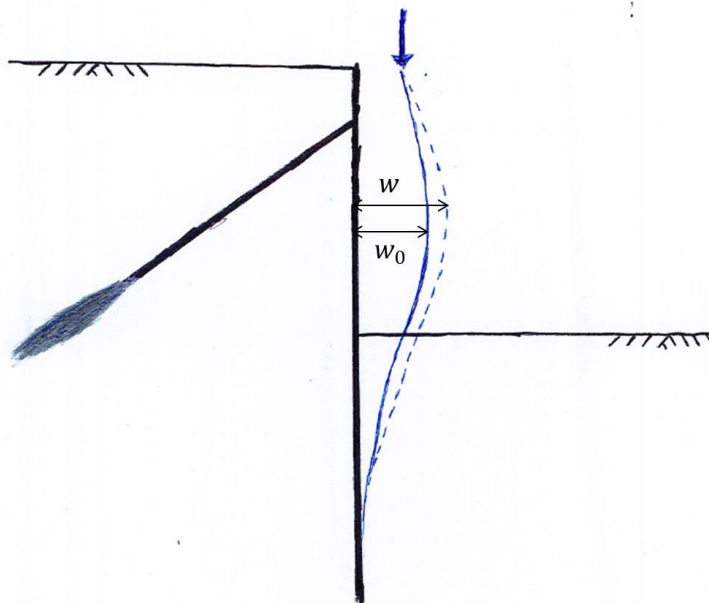


Figure 1: Principle of global buckling in a sheet pile. Sheet pile anchored by a grout body anchor

From a literature study, it turned out that the verification of the global buckling mechanism in the Eurocode for steel sheet piles is a check on the normal stress in the steel. Due to the displacement of the pile, the normal force will introduce a bending moment in the pile, causing an additional normal stress above the already present stress. For most calculations, this bending moment is not embedded in the results of the calculation and should be taken into account separately. To do so, a distinction was made between the type of the deformation. Firstly, the pile deforms due to loading to the pile. Secondly, a deformation will be present because a pile is never perfectly straight or has other (production) errors, known as the imperfections. Though both types of deformation are initiating the global buckling mechanism, they are differently taken into account. The global buckling mechanism initiated by imperfections is taken into account by reducing the capacity of the normal force with a reduction factor χ_b . This factor is based on a mathematical derivation and dependent to F_{cr} , but an important term is determined by experiments. From those experiments it was concluded that the global buckling mechanism can be ignored for normal force less than 4% of F_{cr} . Unfortunately, this factor χ_b does make an error resulting in an overestimation of the effects by the global buckling mechanism, which is taken into account by a factor $k_{yy}(=1.15)$. Besides representing this error, k_{yy} does also represent the

effects of the global buckling mechanism initiated by the deformations of the pile caused by loading. Though complex formula's are present to determine k_{yy} for each case separately, the value of it was set to a constant but conservative value of 1.15, valid for all sheet piling structures. Both the factors χ_b as 1.15 should be added to the unity check on steel stress. This check is given in the left hand side of equation 1 and changes to the check at the right hand side with the added factors, including an extra safety factor γ_{M1} . Both checks are from NEN-EN 1993-5.

$$\gamma_{M0} \frac{N_{Ed}}{N_{Rd}} + \gamma_{M0} \frac{M_{Ed}}{M_{Rd}} < 1.0 \xrightarrow{\text{if } N_{Ed} > 4\% \text{ of } F_{Cr}} \frac{N_{Ed}}{\chi_b N_{Rd} (\gamma_{M0} / \gamma_{M1})} + 1.15 \frac{M_{Ed}}{M_{Rd} (\gamma_{M0} / \gamma_{M1})} < 1.0 \quad (1)$$

Software packages are available which are able to calculate the deformation of the sheet pile due to loading, including the influence of the normal force and so the global buckling effect. If this is done, this effect should not be represented by the factor k_{yy} (=1.15), which therefore only remains to represents the error made by χ_b . Because this error is relatively small and overestimating, it can be ignored without the design becoming unsafe. With both effects represented by k_{yy} (=1.15) differently taken into account or even ignored, this thesis proposes to remove the factor from the unity check. Taking the global buckling effect to the bending moment M_{Ed} into account by software, the unity check could be reduced without much effort.

For the factor χ_b , the influence of the soil should be taken into account through F_{Cr} , which can be determined by the use of linear elastic stiffnesses of the materials of the structure. Unfortunately, the stiffness of soil is not elastic, let alone linear elastic, which gives that the exact influence of the soil to F_{Cr} can not be determined. Nonetheless, an approach of F_{Cr} is given in this thesis. The interaction between the soil and the structure must be described by one of the available models, where the stiffness of the soil is dependent to the deformation of the pile and the soil. Only one model is existing which describes the soil stiffness partly elastic, which is the spring model using the modulus of subgrade reaction to describe the soil stiffness. To determine the value of F_{Cr} , the soil must be modelled as an elastic support to the sheet pile, with a support stiffness based on the available modulus of subgrade reaction of the soil. The exact value of F_{Cr} can only be approached because the soil stiffness might decrease during the mechanism of global buckling.

Because the influence of the soil to the value of F_{Cr} can only be approached if the spring model is used to model the interaction between the soil and the structure, the influence of the soil to χ_b can not be determined for other soil-structure interaction models, like those used in finite element software. Purpose of this factor χ_b is to take the bending moment by the normal force due to imperfections relatively simple into account. As alternative, this thesis proposes to model the imperfections manually into a calculation program or model which should be able to model an imperfect sheet pile. If this is done, the effects of the global buckling mechanism due to imperfections are embedded in the results of the calculation, where the influence of the soil is taken into account automatically. The factor χ_b will no longer be required when the sheet pile is modelled including imperfections.

Recently, a method was proposed by the POVM¹ to take the bending moment caused by the normal force due to imperfections into account by taking the product of the maximal initial imperfection and maximal normal force as an additional bending moment. However, the growth of the imperfection, see figure 1, is neglected by this method, which should therefor result in an underestimation of the actual bending moment. Fortunately, due to changing soil stresses due to the global buckling mechanism, the maximal bending moment caused by soil pressure reduces. For this reason, it was found that the method proposed by the POVM gives a small overestimation instead of an underestimation for relatively low normal forces and is therefor valid.

In three example calculations it is shown that the proposed improvements for the unity check on global buckling can lead to a significant reduction of this check. The order of the reduction is case dependent, but can be up to 10% or even more based on the three example calculation. Taking the soil influence to F_{Cr} into account or the removal of χ_b gives roughly half the reduction to the check. The other improvement, removing the factor 1.15 if the influence of the normal force to the bending moment is determined by software, is responsible of the rest of the reduction to the global buckling check. For larger values of the normal force, the effect of the normal force to the bending moment will be larger and so the effect of the removal of the factor 1.15 will be less than for low values of the normal force.

¹The POVM, or POV Macrostablieit, is a Dutch regulation for the design of dikes.

Contents

List of Symbols

| | | |
|----------|---|-----------|
| 1 | Introduction | 1 |
| 1.1 | Problem statement | 1 |
| 1.2 | Research objectives and approach | 2 |
| 1.3 | Report structure | 3 |
| 2 | Sheet pile design | 5 |
| 2.1 | Sheet pile design lay-out | 5 |
| 2.1.1 | Conventional sheet piling | 5 |
| 2.1.2 | Sheet pile profiles | 7 |
| 2.2 | Subsoil model | 8 |
| 2.2.1 | Soil stress. | 8 |
| 2.2.2 | Drainage subsoil | 12 |
| 2.3 | Soil-structure interaction models | 13 |
| 2.3.1 | Blum's method | 13 |
| 2.3.2 | Spring model. | 14 |
| 2.3.3 | FE-models | 15 |
| 2.4 | Friction and vertical bearing capacity | 16 |
| 2.4.1 | Wall friction | 16 |
| 2.4.2 | Vertical stability | 18 |
| 2.5 | Structural analysis of sheet piles | 19 |
| 2.5.1 | Elastic structural analysis | 19 |
| 2.5.2 | Reduced bending stiffness | 21 |
| 3 | The mechanisms of global buckling for steel structures | 23 |
| 3.1 | Global buckling | 23 |
| 3.1.1 | Interaction between normal force and displacements | 23 |
| 3.1.2 | Critical global buckling load | 26 |
| 3.1.3 | Global buckling in sheet piles | 28 |
| 3.2 | Global buckling due to geometrical imperfections. | 30 |
| 3.2.1 | Geometrical imperfections, global buckling check and the Eurocode | 31 |
| 3.2.2 | Introducing geometrical imperfections into the model. | 35 |
| 3.3 | Conclusions to the general global buckling theory. | 36 |
| 4 | Global buckling in sub-soil structural elements | 39 |
| 4.1 | Elastic supported beams. | 39 |
| 4.1.1 | Derivation of critical global buckling load F_{cr} | 40 |
| 4.1.2 | Mobilisation of the horizontal soil pressure | 41 |
| 4.2 | Global buckling in foundation piles | 41 |
| 4.2.1 | Vogt et al.. | 42 |
| 4.2.2 | Shields | 44 |
| 5 | Critical global buckling load F_{cr} of sheet piles | 45 |
| 5.1 | Method 1: F_{cr} based on Euler's buckling theory and the spring model | 45 |
| 5.1.1 | Derivation of the theoretical critical global buckling load for sheet piles | 46 |
| 5.1.2 | Mobilisation of horizontal soil pressure | 49 |
| 5.1.3 | Parametric determinant coefficient matrix. | 55 |
| 5.1.4 | Parameter sensitivity analysis | 58 |
| 5.2 | Method 2: F_{cr} based on first and second order displacements | 60 |
| 5.2.1 | Example of the method. | 61 |

| | | |
|----------|---|------------|
| 5.3 | Comparison of method 1 and method 2 | 64 |
| 5.4 | Proposed method compared with the Eurocode method. | 66 |
| 5.5 | Conclusions to the determination of F_{cr} for sheet piles | 70 |
| 6 | Effect of geometrical imperfections to the soil-structure interaction calculation model | 71 |
| 6.1 | Discussion of the global buckling mechanism in sheet piles | 72 |
| 6.2 | Second order effects due to geometrical imperfections | 76 |
| 6.2.1 | Method 3: Second order effects to imperfections determined by geometrical imperfections in the model. | 76 |
| 6.2.2 | Method 4: simplified approach of the POVM. | 79 |
| 6.3 | Comparison of proposed method's with current Eurocode method | 82 |
| 7 | Discussion | 85 |
| 8 | Conclusions | 87 |
| 8.1 | Conclusions | 87 |
| 8.2 | Recommendations. | 89 |
| | Bibliography | 91 |
| | List of Figures | 93 |
| | List of Tables | 97 |
| A | Derivation of the critical global buckling load according to Rayleigh | 101 |
| B | Derivation of global buckling reduction factor χ_b | 103 |
| C | M-N Interaction for structural cross sections by the k_{yy} factor | 107 |
| C.1 | Error made by the buckling equation | 108 |
| C.2 | Amplification of bending moment. | 111 |
| C.3 | Conclusions to the k_{yy} interaction factor | 112 |
| D | Determinant of schematised sheet pile chapter 5.1 | 113 |
| E | Examples of displacement based critical buckling loads | 117 |
| E.1 | Calculation of deformation | 117 |
| E.2 | Calculations of displacements for the examples in section 5.2.1 | 117 |
| E.2.1 | Example A | 118 |
| E.2.2 | Example B | 120 |
| E.2.3 | Example C | 122 |
| E.2.4 | Example D | 125 |
| E.2.5 | Example E | 127 |
| E.3 | Critical buckling loads based on displacement of sheet piles in section 5.3 | 129 |
| F | Input data of Diana FEA | 131 |
| F.1 | Diana FEA model | 133 |
| G | Second order effects determined by D-sheet piling | 143 |
| H | Plaxis model data | 145 |

List of Symbols

Latin symbols

| | | |
|-------------------------------|---|-------------------|
| A | Cross-sectional area | $[m^2]$ |
| b | Width single sheet pile | $[m]$ |
| Cohesion | $[kPa]$ | c |
| E | Elasticity | $[kN/m^2]$ |
| EI | Bending stiffness | $[kNm^2]$ |
| EA | Axial stiffness | $[kN]$ |
| 50% secant value of stiffness | | E_{50} |
| E_{ur} | Unloading/reloading stiffness | $[kN/m^2]$ |
| E_v | Strain energy | $[Nm]$ |
| e_0 | First order maximal imperfection | $[m]$ |
| F | Point load | $[kN]$ |
| F_{cr} | Critical Euler buckling load | $[kN]$ |
| f_ϕ | Ratio between internal friction angle and skin friction angle | $[-]$ |
| f_α | Reduction factor for cohesion component in skin friction | $[-]$ |
| f_y | Yield stress of material | $[N/mm^2]$ |
| f_{undr} | Undrained shear strength | $[kPa]$ |
| h | Sheet pile height (profile height) | $[mm]$ |
| h | Thickness of soil layer | $[m]$ |
| h_w | Water head | $[m]$ |
| I | Moment of inertia | $[mm^4]$ |
| k | Spring stiffness | $[kN/m]/[kN/m^2]$ |
| K_a | Active soil pressure coefficient | $[-]$ |
| K_n | Neutral soil pressure coefficient | $[-]$ |
| K_p | Passive soil pressure coefficient | $[-]$ |
| k_{yy} | Design factor for bending moment in Eurocode buckling check | $[-]$ |
| L | Beam / Pile length | $[m]$ |
| L_k | Critical buckling length | $[m]$ |
| M_{Ed} | Acting bending moment | $[kNm]$ |
| M_{Rd} | Bending moment capacity | $[kNm]$ |
| M_{Ed}^I | First order bending moment | $[kNm]$ |
| M_{Ed}^{II} | Second order bending moment | $[kNm]$ |
| n | Ratio between normal force and Euler buckling load | $[-]$ |
| N_{Ed} | Acting normal force | $[kN]$ |
| N_{Rd} | Normal force capacity | $[kN]$ |
| $N_{b,Rd}$ | Normal force buckling capacity | $[kN]$ |
| $N_{pl,Rd}$ | Normal force plastic capacity | $[kN]$ |
| p | Pore water pressure | $[kPa]$ |
| p_{hydr} | Hydrostatic pore water pressure | $[kPa]$ |
| S_u | Undrained shear strength | $[kPa]$ |
| s | Sheet pile thickness (web) | $[mm]$ |
| t | Sheet pile thickness (flange) | $[mm]$ |
| V | Structural shear force | $[kN]$ |
| w | Displacement (field) | $[mm]$ |
| w_0 | First order displacement | $[mm]$ |
| w^I | First order displacement | $[mm]$ |
| w^{II} | Second order displacement | $[mm]$ |
| W | Section modulus | $[m^3]$ |
| W_{el} | Elastic section modulus | $[m^3]$ |

| | | |
|----------|-------------------------|----------|
| W_{pl} | Plastic section modulus | $[m^3]$ |
| q | Distributed line load | $[kN/m]$ |
| q_c | Cone resistance | $[kPa]$ |

Greek symbols

| | | |
|------------------------------|---|----------------|
| γ | Material density | $[kN/m^3]$ |
| γ_{sat} | Saturated soil density | $[kN/m^3]$ |
| γ_{unsat} | Unsaturated soil density | $[kN/m^3]$ |
| γ_w | Water density | $[kN/m^3]$ |
| γ_{M0} | Structural safety factor for cross sectional resistance | [-] |
| γ_{M1} | Structural safety factor for stability | [-] |
| δ | Buckling correction factor by Dischinger | [-] |
| δ | Soil-structure friction angle | [°] |
| κ | Curvature of structural cross section | [-] σ_v |
| Vertical soil stress $[kPa]$ | | |
| σ'_v | Effective vertical soil stress | $[kPa]$ |
| σ'_h | Effective horizontal soil stress | $[kPa]$ |
| $\sigma'_{h,neutral}$ | Effective neutral horizontal soil stress | $[kPa]$ |
| $\sigma'_{h,active}$ | Effective active horizontal soil stress | $[kPa]$ |
| $\sigma'_{h,passive}$ | Effective passive horizontal soil stress | $[kPa]$ |
| $\sigma'_{h,max}$ | Maximal horizontal soil stress | $[kPa]$ |
| τ_{max} | Maximal skin friction on a sheet pile | $[kPa]$ |
| ϕ | Angle of internal friction | [°] |
| ϕ | Structural rotation | [°] |
| χ_b | Buckling reduction factor | [-] |

Abbreviations

| | |
|--------|---|
| c.t.c. | centre to centre |
| CPT | Cone Penetration Test |
| EC | Eurocode |
| FE | Finite Element |
| FEA | Finite Element Analysis |
| FEM | Finite Element Method |
| POVM | Project Overstijgende Verkenning Macrostabiteit |
| u.c. | Unity Check |

Introduction

In geotechnical engineering, soil retaining structures are used to retain soil at a position where it will be unstable otherwise. Not seldom these structures are made of steel sheet piles like the structure in the cover image. These sheet piles are made of thin steel plates with a relatively large cross section as in figure 1.1 in order to create a stiff structure. A sheet pile wall consists of multiple single sheet piles connected to each other by interlocks, see figure 1.1. The design of structures and thus of sheet piles has to be done conform the Eurocode, the European standard for structural design. For steel sheet piling structures, the design has to be done according to NEN-EN 1993-5 (Eurocode 3: Design of steel structures - part 5: piling). Several failure mechanisms are described in this standard, such as the exceedance of the yield stress, structural instability, local buckling, global buckling, system failure, attack by corrosion, unacceptable deformations etc.. Not seldom the governing mechanism of the design of steel sheet piles is the global buckling mechanism¹. If a deformed sheet pile is loaded by a normal load, a load in the axial direction of the sheet pile, the normal load will introduce a bending moment due to the deformation of the pile, enlarging the deformation. This is the global buckling mechanism, where this thesis will review the verification check to this mechanism applied to steel sheet piling.

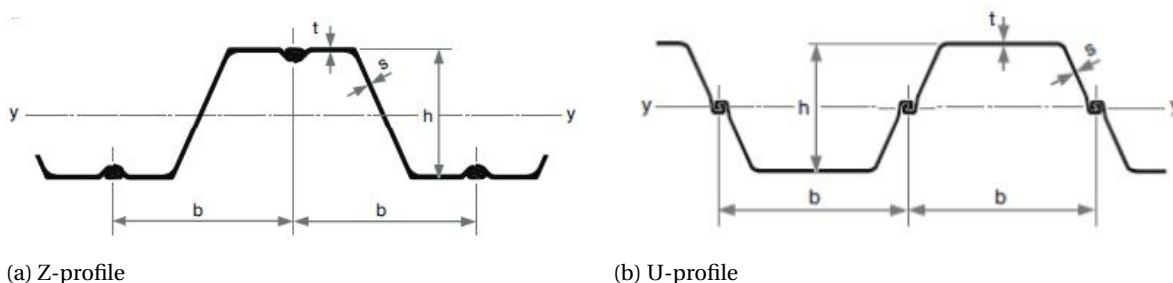


Figure 1.1: Cross sections of sheet pile profiles (figure 39-1 and 39-2 from [2])

1.1. Problem statement

Conform the Eurocode, the verification of the global buckling mechanism should be executed if the normal force exceeds the value of 4% of the critical global buckling load F_{cr} [3]. Below this percentage, the global buckling mechanism may be fully ignored and only the verification of the cross sectional capacity should be checked. This results in the reality of expression 1.1 giving both the check of the cross sectional steel stress of the sheet pile (left hand side) as the check of the global buckling mechanism (right hand side) as given in NEN-EN 1993-5. Taking a close look learns that both checks are quite similar. The bending moment M_{Ed} is increased with 15% and the normal force capacity N_{Rd} is reduced by reduction factor χ_b , which is smaller than 1 at all times. The partial safety factor γ_{M0} (=1.0) must be applied to design checks of the steel stress, but this factor is replaced by γ_{M1} (=1.1), which must be applied to design checks on stability. All this differences are giving that the check on the buckling mechanism is (much) more unfavourable compared to the check on

¹In literature, global buckling is also referred to as column buckling, flexural buckling or just buckling.

cross sectional capacity. Because the check of global buckling should only be done with a value of the normal force above 4% of F_{cr} , it could hypothetically be that an increase of the normal force of just 1% or even smaller results in a growth of a unity check² in the order of 30%. Because the influence of the subsoil to the global buckling mechanism is neglected in this design check, it is thought among engineers that this buckling check is too conservative. The objective of this thesis is to obtain the background of the factors χ_b and 1.15 and describe possibilities to estimate the effects of global buckling in sheet piles more precisely. The partial safety factor γ_{M1} is prescribed by the Eurocode and won't be an objective of this thesis.

$$\gamma_{M0} \frac{N_{Ed}}{N_{Rd}} + \gamma_{M0} \frac{M_{Ed}}{M_{Rd}} < 1.0 \xrightarrow{\text{if } N_{Ed} > 4\% \text{ of } F_{cr}} \frac{N_{Ed}}{\chi_b N_{Rd} (\gamma_{M0} / \gamma_{M1})} + 1.15 \frac{M_{Ed}}{M_{Rd} (\gamma_{M0} / \gamma_{M1})} < 1.0 \quad (1.1)$$

Next to obtaining the background of the above global buckling check, the influence of the subsoil to the critical global buckling load F_{cr} will be an important objective as well. Not only because the buckling mechanism should not be checked if the acting normal force is less than 4% of F_{cr} , but also because χ_b depends directly to F_{cr} . In the current practice, the soil is left out of account for the determination of F_{cr} , which is based only on the structural resistance against global buckling. However, global buckling will deform the sheet pile and consequently, it will deform the soil. This means that some force is required to deform the soil. If the soil resistance is taken into account, it is thought that the value for F_{cr} will rise significantly. Consequently, the check on the buckling mechanism would only be required at higher normal loads, which gives that the unfavourable check of the global buckling mechanism should be executed in less designs.

Besides having a positive effect to the critical global buckling load F_{cr} , the soil pressure will have a negative effect as well. In the first place, the soil pressure causes deformations of the sheet pile, and with that the global buckling mechanism is initiated. On top of that, the soil pressure might introduce the normal force in the sheet pile, enlarging the effects of the global buckling mechanism. Those negative effects will be discussed in the thesis as well.

1.2. Research objectives and approach

The main objective of this thesis is to determine the influence of soil to the global buckling mechanism and to improve the current global buckling check for steel sheet piles, which is thought to be too conservative among engineers. Based on the previous, this objective can be answered qualitatively by stating the first two research questions below, divided to several sub-questions. Based on the answers of both questions, a model, or possibly several models, will be described to approach the global buckling mechanism more precisely compared to the current approach with the global buckling check. To describe the significance of possible improvements a third research question is stated.

What is the background of the current global buckling check for steel sheet piles?

- Which effects leads to the reduction factor χ_b and 1.15 in the current global buckling check?
- How is the critical global buckling load F_{cr} derived for steel structures in general?
- Why should global buckling only be checked if the acting normal force exceeds 4% of the critical global buckling load?

What are possible improvements to the current global buckling check to take the influence of the soil into account?

- How can the influence of soil to the critical global buckling load F_{cr} be modelled?
- Can the current global buckling check be changed for steel sheet piles such that the resistance of the soil is included in the check?

What is the quantitative effect of the found improvements of the current global buckling check?

The scope of the thesis will stick to the global buckling mechanism in steel sheet piles. Any other failure mechanism will only be discussed when it is to support the theory of the global buckling mechanism. It

²A unity check is a check like given in expression 1.1 at the left hand side of the < sign. If a unity check of a mechanism is larger than 1.0, the resistance of the structure against the mechanism is insufficient.

might be that some aspects of the buckling mechanism are a minor detail in the design of steel sheet piles, but when discussed it is of importance in order to understand the global buckling mechanism and the check on this mechanism.

The global buckling mechanism is mainly a structural mechanism, but the structural behaviour of a sheet pile is strongly correlated with the behaviour of the soil around the pile. For this reason, an important subject of this report is the description of the available models the soil-structure interaction. This interaction tends to have a time dependent behaviour due to the time dependent behaviour of soil, but this will be fully neglected in the scope of this thesis. The global buckling effect develops at a short time scale, which indicates that the most unfavourable design conditions in time could be used.

1.3. Report structure

As already written earlier, the interaction between the soil and the structure is of great importance to the behaviour of the sheet pile. This is certainly also the case for the buckling mechanism. For this reason, the first chapter will describe the soil-structure interaction models available. Besides, this chapter will discuss the other relevant aspects of a sheet piling structure as well. Chapter two contains the description and the relevant backgrounds of the global buckling mechanism. For foundation piles, some models are already available to determine the influence of the soil to the global buckling mechanism more correctly. Though sheet piles are a different type of geotechnical structures than foundation piles, the models for foundation piles might deliver some important insights for possible models for sheet piles. Therefore, those models will be described in chapter three.

Based on the results of the literature study, chapter four will propose two models to approach the effect of the soil resistance in the determination of the critical global buckling load F_{cr} . This will be done by the description of two methods which will firstly be discussed qualitatively with some supporting examples. This examples may not be realistic for sheet piles, but they will support the proposed method to approach the effects of the soil to the global buckling mechanism. Once the methods for sheet piles are described, an example will be treated to quantify the effects of the improved models compared to the current check on the global buckling mechanism. Chapter five will discuss a method to determine the effects of the global buckling mechanism with finite element techniques. The quantitative effects of the proposed method's will be discussed by two example cases.

Chapter six discusses the validity, relevance and limitations of the model's and method's described in the thesis. Finally, chapter seven gives the conclusions and recommendations of this thesis.

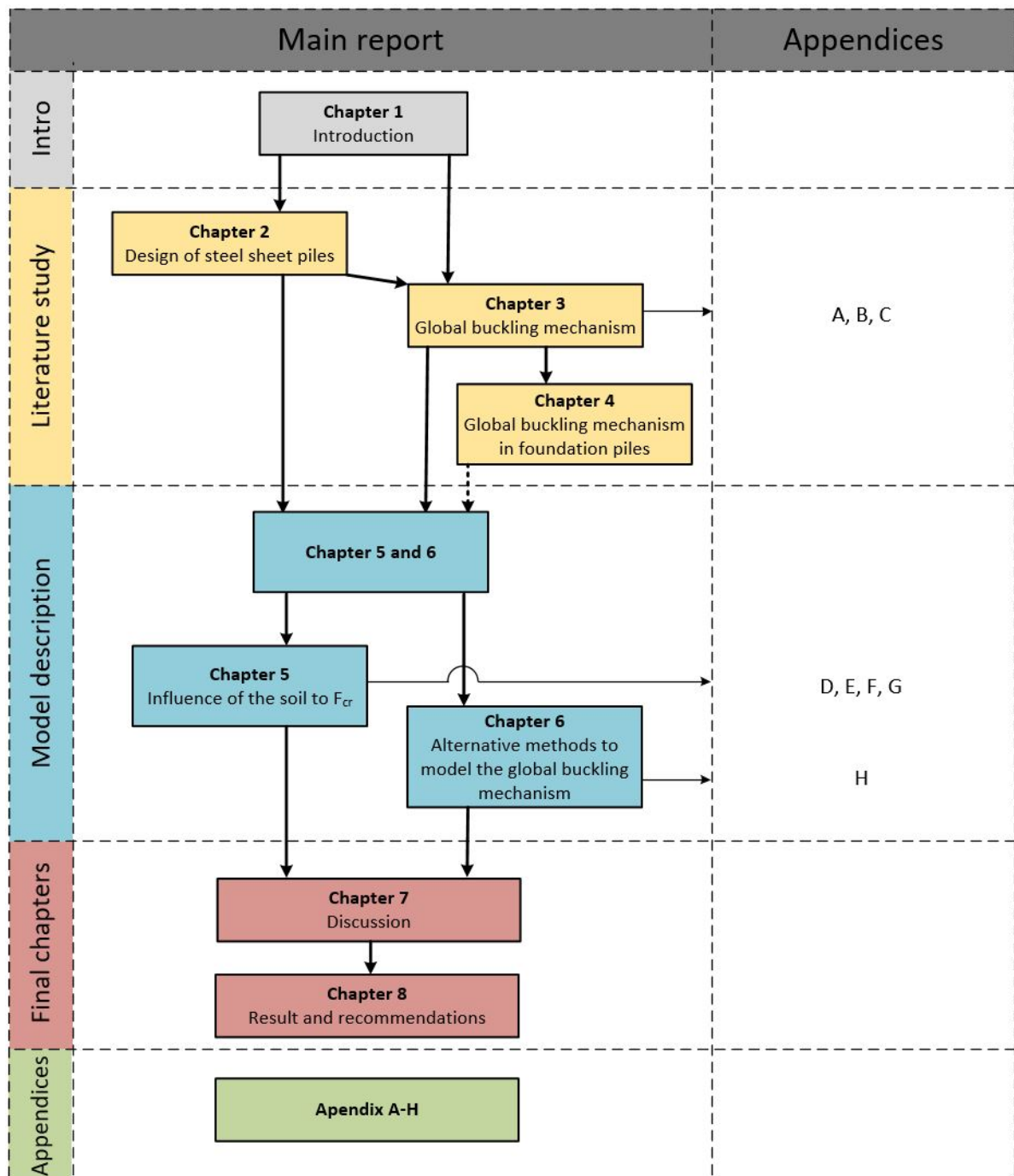


Figure 1.2: Visual representation of the report structure

2

Sheet pile design

This chapter discusses the relevant requirements, models and lay-outs for sheet pile design in the current design practice. An important aspect of the design is the soil-structure interaction and will be an important subject of this chapter.

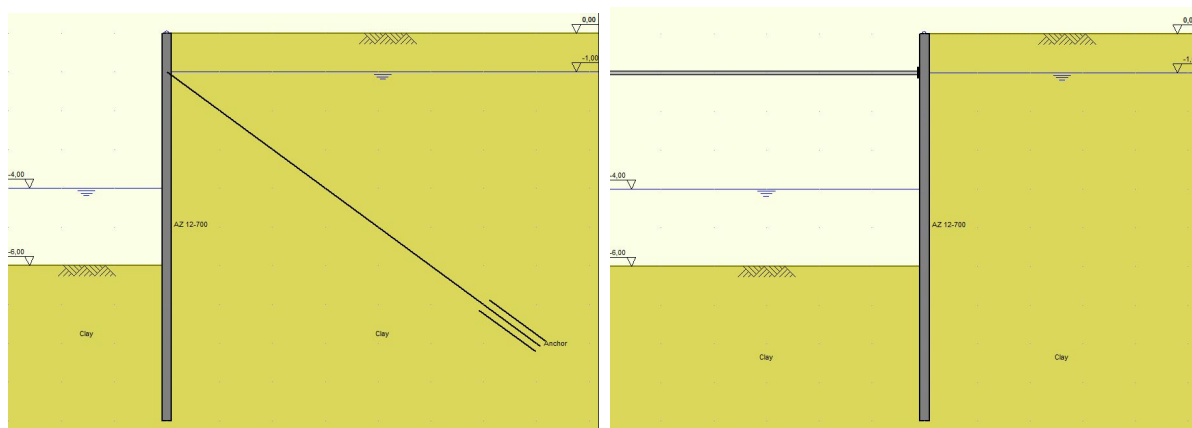
2.1. Sheet pile design lay-out

For those familiar with the lay-out of a steel sheet pile and combi-walls may skip through paragraph 2.2

To understand the mechanisms acting in a soil retaining sheet pile wall, it is important to understand lay-out of the structure. With the lay-out clear, the reader of this thesis will be able to understand some choices made better.

2.1.1. Conventional sheet piling

A steel sheet pile is designed to retain soil from displacement. Most times, a sheet pile is used to overcome a soil surface and/or water level difference. Examples are quay walls, building pits, seepage screens, but also reinforcement structures for dikes or embankments. To give an idea, figure 2.1 gives two examples of sheet piling structures.



(a) Sheet pile supported by an anchor

(b) Sheet pile supported by a strut

Figure 2.1: Sheet pile profiles (figures from D-sheet piling)

The horizontal soil pressure acting to the sheet pile can be divided between the active, neutral and passive soil pressure. If the sheet pile moves away from the soil, the soil pressure will be active. Movement towards the soil results in passive soil pressure, no movement of both the pile as the soil gives the neutral soil pressure. Both the active as the passive soil pressure are dependent on the displacement of soil and sheet pile. The displacement of the pile is directly dependent to the loading, which is (for a significant part) the soil pressure. Consequently, the deformation of the sheet pile depends partly to itself and therefore the calculation of the

forces and deformation of the pile is a complex process. This complex process is an important aspect of the soil-structure interaction model, described in section 2.3.

Horizontal support

To ensure horizontal stability, the horizontal soil pressures and possibly external horizontal loads should be in equilibrium. If an equilibrium is not reached or the displacements or cross sectional forces in the sheet pile become too large, a horizontal support could be applied, which can be an anchor (figure 2.1a) or strut (figure 2.1b). Alternative is to choose a larger sheet pile profile with more bending stiffness or a longer sheet pile, but this won't always be an economical solution.

The horizontal supports, the anchors or struts, are placed to the sheet pile wall with a certain distance between each support. This centre to centre (c.t.c.) distance is regularly in the order of a meter to a couple of meters. In order to distribute the support from the anchors or struts along the sheet pile wall, a steel beam can be placed in between the wall and the supports. A structural scheme of the cross section is given in figure 2.2, a more detailed scheme of the connection with the anchor/strut, wale and sheet pile is given by figure 2.3.

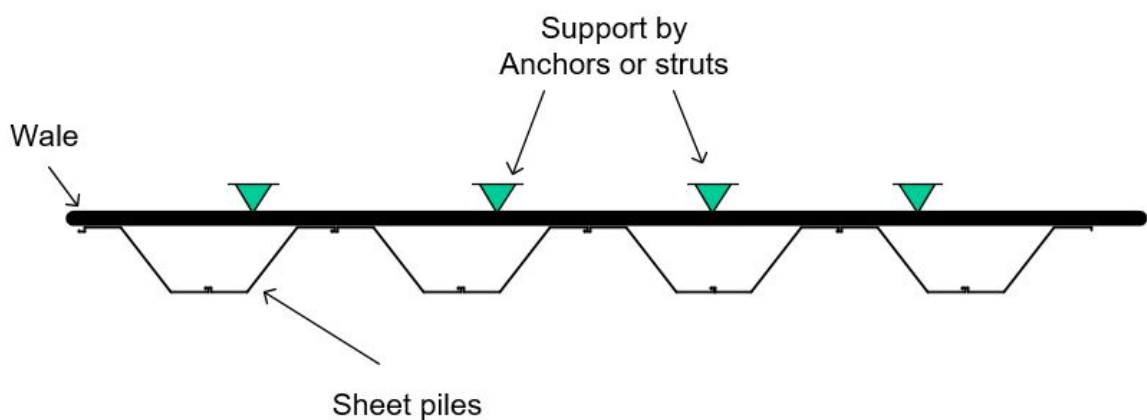


Figure 2.2: Structural scheme of waling and horizontal support (top view)

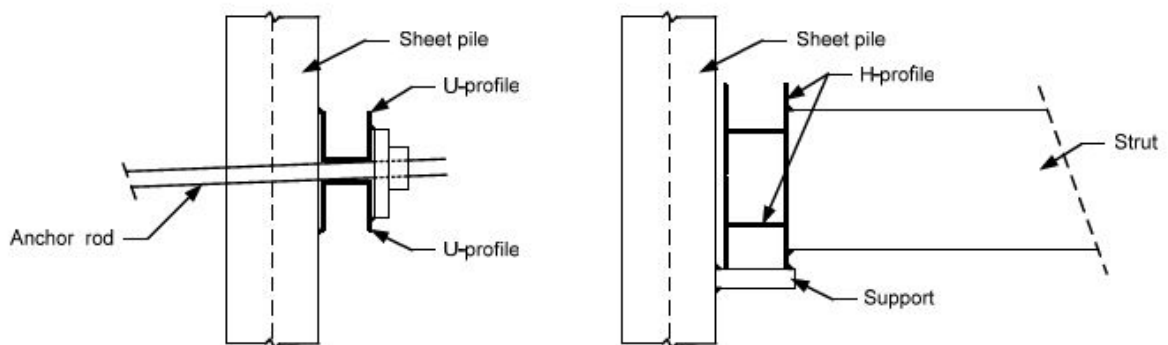
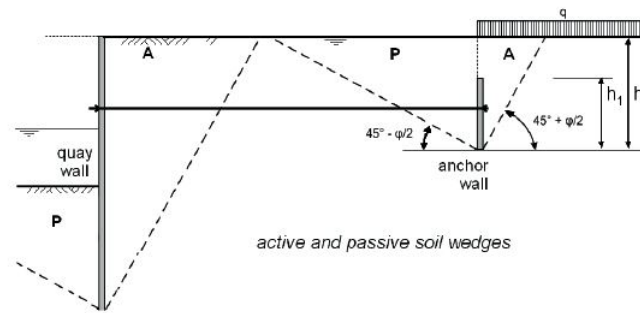


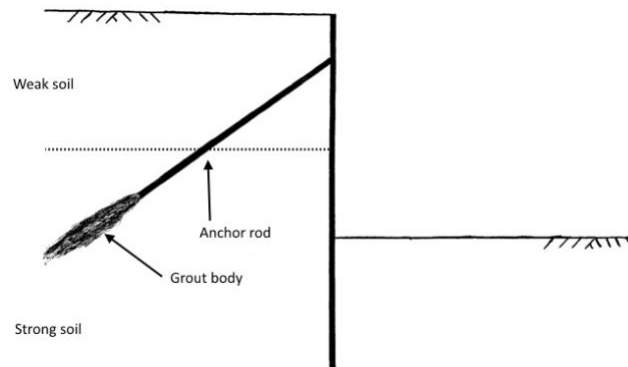
Figure 2.3: Cross sectional lay-out of a wale supported sheet pile (figure 40-1 from [2])(side view)

Struts can only be applied in a excavation pit, where the other end of the strut can be supported horizontally. Usually, this support is given by another soil retaining structure, in unique cases special structures could be applied to redirect the strut force. If struts cannot be applied, anchors can be applied which will be installed in the soil behind the wall. The anchors can be fixed by a wall or plate placed far enough behind the wall, see figure 2.4a. If it is impossible or inconvenient to use this anchor structures, an anchor could be installed with a grout body as in figure 2.4b. To create enough strength of structure, the grout body is often installed in a deeper situated stiff soil layer, while the support to the sheet pile wall is needed at a relatively high level. This means that the anchors must be installed with an angle, which introduces a vertical force in the wall. This

normal force from the anchor is affecting the global buckling mechanism.



(a) Example quay wall supported with an anchor and anchor wall (figure 41-4 from [2])

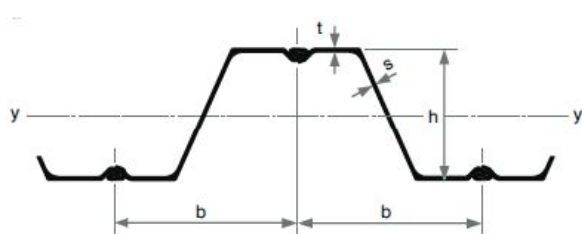


(b) Example soil retaining wall supported by grout anchor

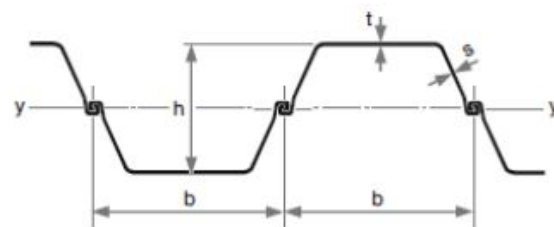
Figure 2.4: Types of anchor systems

2.1.2. Sheet pile profiles

The profile of the sheet pile is of great importance to the behaviour of the wall. The thicker the steel plates or the larger the profile height of the cross section is, the stiffer the pile will react resulting in less deformations. Besides, the resistance to cross sectional forces (bending moment, normal forces or shear forces (respectively the M-,N- and V-forces)) is larger if the cross section is larger. To create stiff and strong cross sections with relatively little material, sheet piles are usually made of Z- or U- shaped profiles like in figure 2.5. Those profiles consists of the flange (with thickness t in figure 2.5) and the web (with thickness s). One single pile has width b and is connected to the next pile by an interlock. Sheet piles can be installed singular or in pairs (2, 3 or 4 piles in once). Sheet piles installed in pairs are clamped or welded to each other at the interlocks before installation such that they act as on structural element. For U-type profiles, extra care should be taken into account due to asymmetry, which is further explained in section 2.5.2.



(a) Z profile (figure on page 4 from [4])



(b) U profile (figure on page 1 from [4])

Figure 2.5: Sheet pile profiles [2]

Combi-walls

Most of this section is based on paragraph 3.3.5 of CUR 166 part 2 [5]

When sheet piles made from Z or U shaped cross sections are not stiff or strong enough, the structure can be reinforced by stiffer piles in between the sheet piles (i.e. tubular piles (most common) or I profiles), creating a combi-wall like the profiles in figure 2.6. Typically, relatively large tubular piles (diameter of about a meter) are applied with 2 or 4 Z-profile sheet piles or 2 or 3 U profile sheet piles placed in between [5]. The stiffness of the combined cross section is for a large part given by the stiff elements, but the sheet piles generate some stiffness as well. The average stiffness of both the stiff elements as the sheet piles can be used as the stiffness of the combined section.

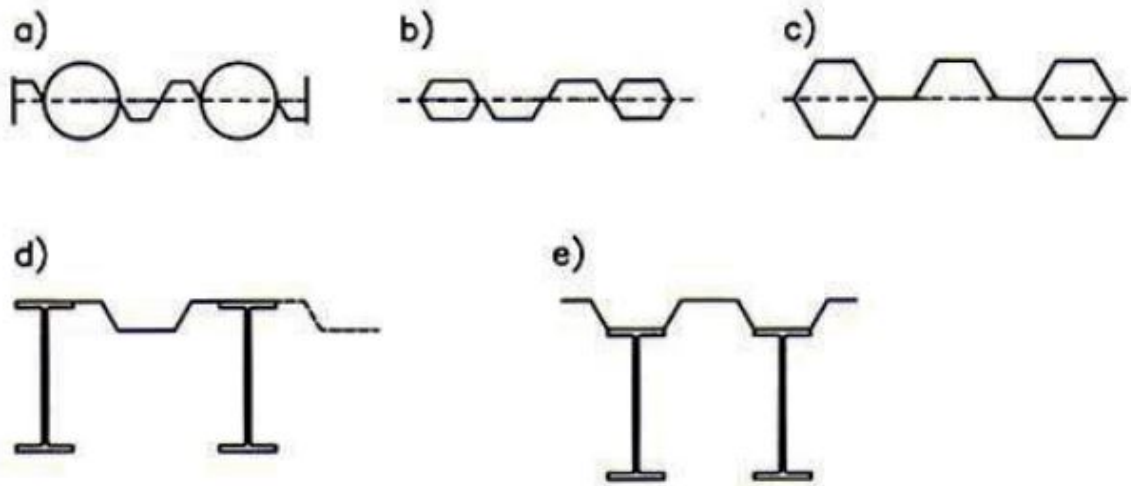


Figure 2.6: Several cross sections for combi-walls: a) Tube piles with two Z-profiles in between; b) double U-profiles with two U-profiles in between; c) quadruple Z-profiles with two Z-profiles in between; d) and e) IPE profiles as stiffeners behind U- or Z-profiles (figure 39-21 from [2])

Due to significant stiffness differences between the stiff piles and sheet piles, the sheet piles will transfer much of the load to the stiff parts. Because of this redirection of forces, the sheet piles will tend to deflect more compared to the stiff parts of the wall. As a consequence, the soil behind the sheet piles will deform more compared to the soil behind the stiffer piles. This gives that an arch effect will occur in the horizontal soil pressure, see figure 2.7. Due to this effect, the active horizontal soil pressure on the sheet piles will be less than the soil pressure on the stiff piles which will take most pressure from the soil.

If a combi wall is anchored, the anchors are usually connected to the wall in the stiff elements. For this reason, most, if not all, of the vertical anchor force is redirected to the soil via the stiff element. Other vertical loads to the sheet pile are likely to be redirected to the stiff parts as well. This makes that most, if not all, of the normal force in the combi-wall is inside the stiff elements. This normal force distribution in the combi-wall will result in the fact that the global buckling mechanism will mostly occur in the stiff element, but the mechanism will be resisted by both the soil and the weaker elements (the sheet piles) between the stiffer elements. This makes a possible theory to describe the global buckling mechanism in combi-walls even more complex compared to the regular sheet pile wall.

2.2. Subsoil model

In order to design a sheet pile, a soil-structure interaction model must be used. In order to describe such a model, the basic principles of soil pressure must be known. This will be treated in this section.

2.2.1. Soil stress

The soil stress is the main loading to sheet piles, especially the horizontal soil stress. For the vertical soil stress, simple equations can be used to determine the vertical (effective) soil stress (see equation 2.1). The pore water pressure is based on the drainage of the soil. For purely hydrostatic water pressure (drained soil)

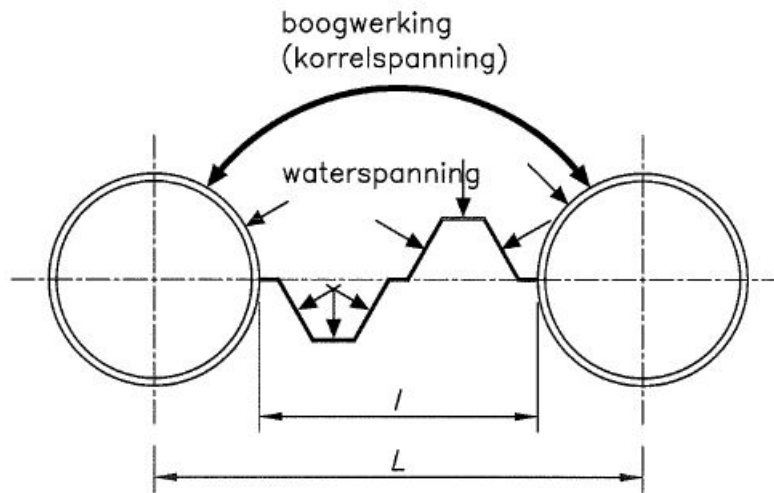


Figure 2.7: Arch effect in horizontal soil pressure on combi-walls (figure 3.15 from [5])

the pore water pressure p_{hydr} can be defined as in equation 2.1. For undrained soils where the water pressure is not purely hydrostatic, the over- or under waterpressure should be added to the hydrostatic water pressure. For the remainder of this thesis, the soil conditions will assumed to be drained.

$$\begin{aligned}
 \sigma_v &= \gamma * h \\
 \sigma'_v &= \sigma_v - p \\
 p_{hydr} &= \gamma_w * h_w
 \end{aligned}
 \tag{2.1}$$

where:

γ = Soil density

p = Pore water pressure

h = Thickness of soil layer

The horizontal soil pressure is dependent to the vertical soil pressure, but also to the deformation of the soil. Without any movement of the soil, the horizontal soil pressure is neutral. However, due to this horizontal soil pressure, the sheet pile will start to deform. The deformation of the sheet pile will cause deformation, and ultimately failure, of the soil. If the soil is compressed (movement of the pile towards the soil), the soil pressure will grow to the passive soil pressure. If the soil relaxes (movement of the pile from the soil), the soil pressure will go to the active soil pressure. This development develops gradually until the passive or active soil pressure is reached, see figure 2.8[6]. When the soil deforms more due to the movement of the sheet pile, the soil will fail and the soil body will move along the slip plane, like sketched in figure 2.9. In this case, the limit state of the horizontal soil pressure has been reached. The sheet pile will stop the active soil body from sliding away by a reaction force to the soil pressure. At the other side, the deformation of the pile will push the passive soil body away.

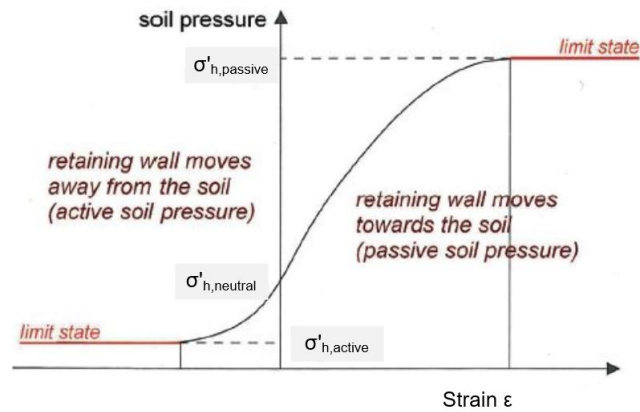


Figure 2.8: Soil deformation behaviour (figure 24-3 from [2] (adapted))

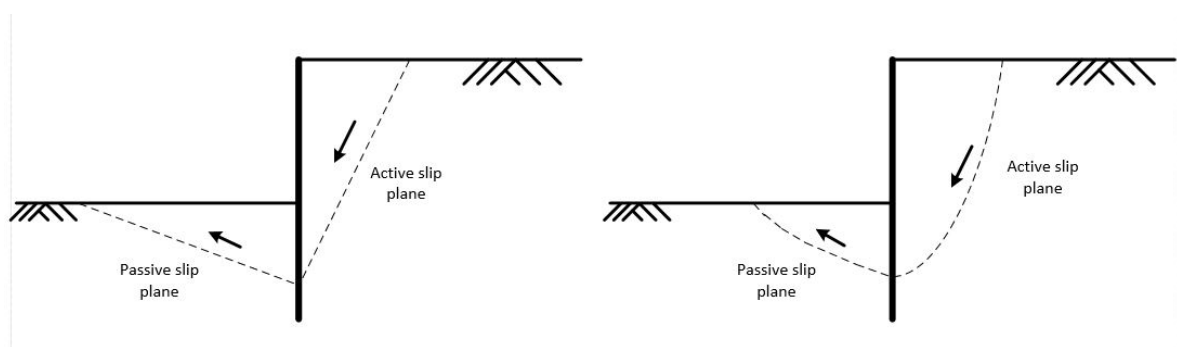


Figure 2.9: Sketch of both straight (left) as curved (right) slip planes

The force delivered by the sheet pile to both soil bodies can be determined based on the principle of horizontal force equilibrium. This can be best shown by figure 2.10, where all the forces to the soil body are sketched. With this figure, the force from the sheet pile to the soil can be derived parametric (based on soil parameters) based on the force balance. Using Newton's third law (action is reaction), the force from the sheet pile to the soil equals the acting soil pressure. [6]

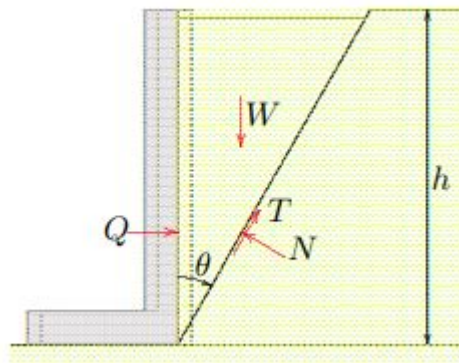


Figure 2.10: Forces acting to the soil body sliding away (figure 34.1 from [6])

In literature [6] the derivation of equations 2.2 to 2.6 can be found, where the vertical soil pressure (known) can be multiplied with the horizontal pressure coefficient K in order to find the horizontal soil pressure. The pressure coefficient can be determined for the active, neutral and passive soil pressure (relatively equations 2.3, 2.4 and 2.6 [7]). The value for K can be determined by either straight (Müller-Breslau) or curved (Kötter) slip planes. Straight planes are known to underestimate the active horizontal soil pressure and overestimate the passive horizontal soil pressure [5]. This does lead to an unsafe design and therefore curved slip planes

are preferred. However, for friction angle ϕ lower than 30° the made error is relatively small and straight slip planes are allowed to use [5]. The horizontal pressure coefficients are defined by Kötter as in equations 2.3, 2.4 and 2.6, which are from [8]. In this equations, the cohesion c of the soil is introduced.

The active or passive soil pressure is reached when a certain displacement of the sheet pile and the soil occurs. As long the active or passive soil pressure is not reached, the soil pressure can be expressed in percentages of the passive soil pressure. This is called the mobilisation of the horizontal soil pressure ¹

$$\sigma'_{h,active} = \sigma'_v * K_a - 2c\sqrt{K_a} \quad (2.2)$$

$$K_a = \frac{1 - \sin(\phi)\sin(2\alpha_a + \phi)}{1 + \sin(\phi)} \exp\left(-\frac{\pi}{2} + \phi + 2\alpha_a\right) \tan(\phi) \quad (2.3)$$

$$K_0 = 1 - \sin(\phi) \quad (2.4)$$

$$\sigma'_{h,passive} = \sigma'_v * K_p + 2c\sqrt{K_p} \quad (2.5)$$

$$K_p = \frac{1 + \sin(\phi)\sin(2\alpha_p - \phi)}{1 - \sin(\phi)} \exp\left(\frac{\pi}{2} + \phi - 2\alpha_p\right) \tan(\phi) \quad (2.6)$$

with:

$$\alpha_a = \frac{1}{2}(\cos^{-1}\left(\frac{\sin(\delta)}{\sin(\phi)}\right) - \phi + \delta)$$

$$\alpha_p = \frac{1}{2}(\cos^{-1}\left(\frac{\sin(\delta)}{\sin(\phi)}\right) + \phi - \delta)$$

ϕ = Soil friction angle (Radians)

δ = Soil-structure friction angle (Radians)

For horizontal stresses below non-horizontal soil surfaces, the horizontal soil pressure coefficients becomes more complex. Tables are available to withdraw the horizontal soil pressure coefficient, based on the angle of the slope, the friction angle and the skin friction angle [9].

The sheet pile is not fixed to the soil and thus it is possible that the sheet pile will displace vertically with respect to the soil. This relative settlement creates friction between the pile and the soil, which is influencing the force balance of the soil body (as given in figure 2.10). For this reason, the skin friction is affecting the horizontal soil pressure coefficients. To determine the angle δ of skin friction, various relationships are given by the design codes. Figure 2.11 represents the values given by the NEN 9997-1 [10], while the same code states that the design value of the angle δ should not be more than $0.67*\phi$ at sheet piles. Based on experience at the Rijkswaterstaat Bouwdienst, CUR166 [5] presents the values given in table 2.1. For peat, it is stated that the skin friction angle must be 0° .

Tests to determine the skin friction angle are hard to execute and the correctness is limited [5]. Tests have been done by Pontyondy [11] on various soils with various materials to determine the coefficient between the wall friction angle and the soil friction angle. The results of the experiments are discussed at the end of paragraph 2.4.1. This experiments however are not done specifically with sheet piles, so one should use the values of Potyondy with care.

| Soil | δ |
|---------------------------|------------|
| Gravel ($d_{50} > 8$ mm) | 0 |
| Sand ($d_{50} > 2$ mm) | $1/3 \phi$ |
| Sand ($d_{50} < 2$ mm) | $2/3 \phi$ |
| Loam | $1/2 \phi$ |
| Clay | $1/3 \phi$ |

Table 2.1: Skin friction angle based on experience of the Rijkswaterstaat Bouwdienst [5]

¹Short example: $K_a = \frac{1}{2}$, $K_0 = \frac{2}{3}$ and $K_p = 2$. In this case, the active horizontal soil pressure has a mobilisation ratio of 25%, the neutral horizontal soil pressure has a mobilisation ratio of 33.3%. The passive horizontal soil pressure has always a mobilisation ratio of 100%

| Relatieve ruwheidsbenaming van het wandoppervlak | Nadere definitie van de ruwheid van de wand | Wandwrijvingshoek (δ) | |
|--|---|--------------------------------|--|
| | | Recht glijvlak | Gekromd glijvlak |
| Getand | $> 10 d_{50}$ | $0,67 \varphi'_k$ | $\leq \varphi'_k$ |
| Ruw | $0,5 d_{50} - 10 d_{50}$ | $0,67 \varphi'_k$ | $\leq \varphi'_k - 2,5^\circ$ met een maximum van $27,5^\circ$ |
| Half ruw | $0,1 d_{50} - 0,5 d_{50}$ | $0,33 \varphi'_k$ | $0,5 \varphi'_k$ |
| Glad | $< 0,1 d_{50}$ | 0° | 0° |

Figure 2.11: Skinfriction angle δ based on the friction angle [10]

2.2.2. Drainage subsoil

When the soil profile or water heads in the subsoil are changing, it has a significant effect to the effective soil pressure. When a sheet pile is installed and the conditions in the soil are changed, the soil will react. How quickly the soil pressure changes depends on how easy the pore water can flow through the soil (drainage). Some soils, like sands, have a quick drainage time and will respond relatively fast to the new circumstances. Other soils, the cohesive soils, have a relatively long drainage time, which means that the soil and water pressure are changing over a longer time scale. Besides, deformation of cohesive soils occurs after time, affecting the soil pressure as well. This means that the load to the sheet pile, and with that the behaviour of the pile and load to the soil, changes over time. This might result in large forces or deformations of the sheet pile after time. It is therefore important to think about what the most critical moment in time is when it comes to the global buckling mechanism. Because the global buckling mechanism occurs on a relatively short timescale, the most critical state should be used to determine the required resistance against global buckling.

In the years 1999-2000 an experiment was conducted on a small construction pit in the port of Rotterdam. The soil retaining walls in the construction pit were sheet piles supported by struts and were made of two different types of profiles. Because a thick clay layer is present in the surrounding of the clay layer, it takes time for the water pressure and with that the effective soil pressure to adapt to the new situation. Kort [12] has evaluated the behaviour of the walls and concluded that time effects are occurring in the sheet pile, as visible in figure 2.12. The soil supporting the sheet pile at the excavation side consist for an important part of clay. If the excavation pit is pumped dry, it will take some time before the water pressure in the soil has reduced to the lowered water head. Because the water pressure will resist the sheet pile to deform, the deformation of the pile will grow after time. This can be seen in figure 2.12, where both the slope (rotation) as the bending moment of the pile are increasing. [12]

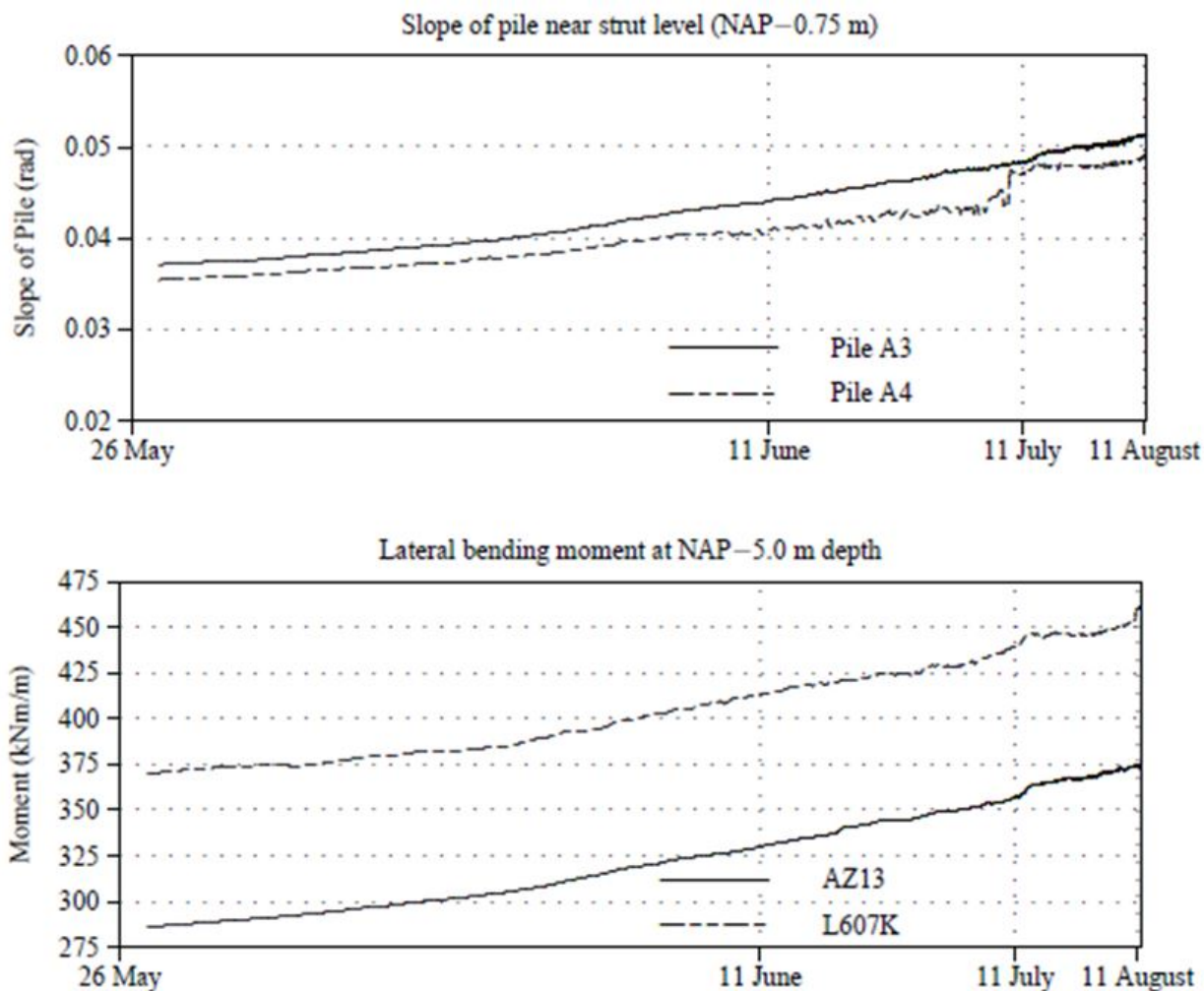


Figure 2.12: Reaction of sheet pile against log-scale time (figure 4.45 from [12])

2.3. Soil-structure interaction models

Based on the theories for soil pressure described in section 2.2, several calculation methods can be described. In this section, a manual method (Blum), a method based on the spring model and a FE method will be elaborated.

2.3.1. Blum's method

A much used method in manual calculations is Blum's method. This method assumes that the soil has failed and thus that the horizontal soil pressure is fully active or passive, see figure 2.13. Blum's method is based on determining the point of zero bending moments in a sheet pile (point D in figure 2.13). This point is at an unknown depth t . By describing the bending moment at the pile tip using t as a variable, the value for t can be determined such that M equals zero. Blum's assumption is that the length based on this calculation is not sufficient. If in reality the sheet pile is just a bit too short or the soil delivers a lower passive pressure, the pile will become unstable. Therefore, the pile length must be a bit longer in order to guarantee stability [6]. The extra length can be determined by applying a factor (see figure 2.14) over the embedded depth of the sheet pile. Once the length of the sheet pile is known, the soil pressure to the pile can be determined and the internal forces of the sheet pile can be calculated.

For an anchored or strut supported wall, the bending moment should be calculated around the support instead of the pile tip. To reach a bending moment equilibrium, a certain embedded depth t is required. For multiple supports, Blum's method is unable to be used.

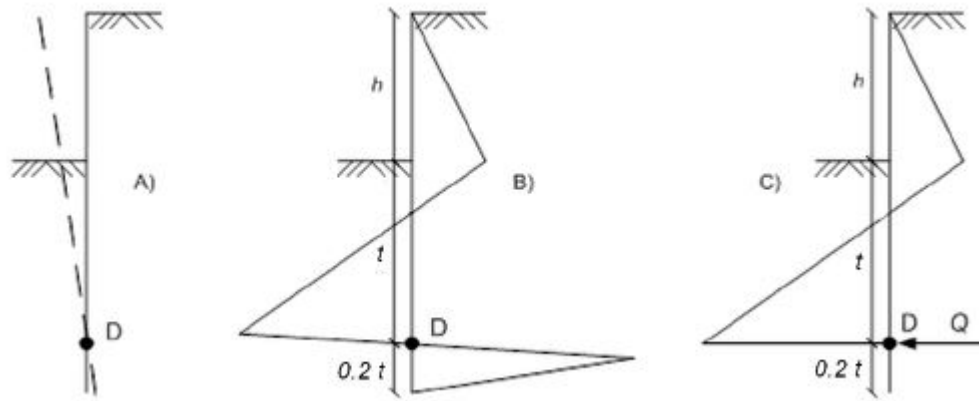


Figure 2.13: Schematisation of displacement, loading and effective loading by Blum (figure 39.7 from [2])




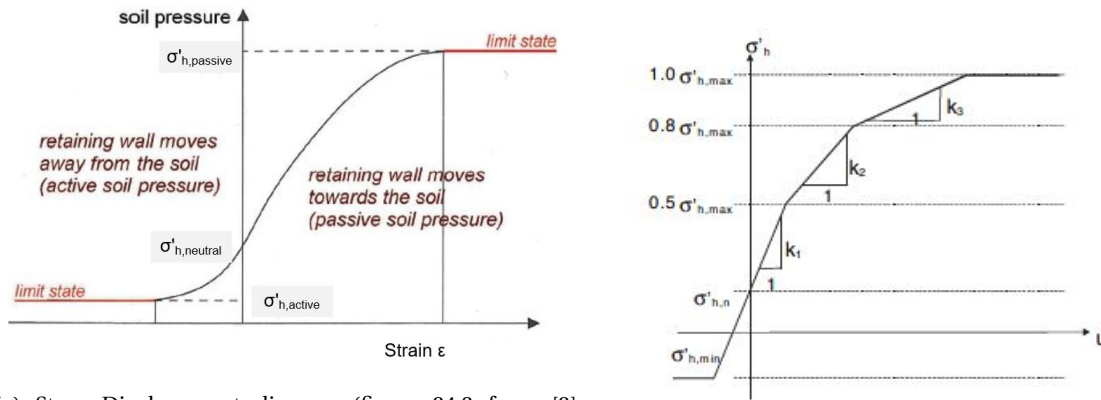
| wall type |  small water head |  big water head |  very big water head or only water pressure |
|---------------------------------|--|---|--|
| cantilever | 1,20 | 1,30 | 1,40 - 1,60 |
| anchored and fixed toe | 1,10 | 1,15 | 1,20 - 1,30 |
| anchored and toe free supported | 1,05 | 1,10 | 1,15 - 1,20 |

Figure 2.14: Factor for embedded depth by Blum's method (table 39.4 from [2])

2.3.2. Spring model

As already presented in figure 2.8 and again in figure 2.15a, the soil pressure is dependent to the strain of the subsoil. The displacement of the soil and thus the sheet pile is directly dependent to the strain of the soil. Therefore, the relationship between the horizontal soil stress and displacement of the sheet pile will be of similar shape as the graph in figure 2.15a. Based on this relationship, the soil can be modelled as a spring, where a certain displacement results in a certain reaction force. This is visualised in figure 2.15b, where the curved graph of figure 2.15a graph is simplified and split up in 3 linear parts. In this pressure-displacement curve, the soil pressure to the sheet pile is based to the displacement of the sheet pile at that specific point. At the neutral pressure, there is zero displacement. The active soil pressure (lower left part of figure 2.15b) is already reached with just a little displacement. To reach the passive soil pressure, much more displacement is required, which gives that the passive horizontal soil pressure is not always reached. [2]

The spring stiffness values of the 3 branches in figure 2.15b are generalised for the Dutch practice and are given in figure 2.16. The stiffness is based on the cone resistance q_c for sands and the undrained shear strength f_{undr} for clays and peat (see second column). Two values are given, k_{low} and k_{high} . For displacement calculations, k_{low} should be used. In most cases, this value is also governing for the force distribution in the sheet pile, but it should be checked whether or not k_{high} leads to higher internal forces [2].



(a) Stress-Displacement diagram (figure 24.3 from [2] (adapted))

(b) Stress-Displacement diagram (figure 33.5 from [2])

Figure 2.15: Stress-deformation relationships

| | | k_1 [kN/m ³] | | k_2 [kN/m ³] | | k_3 [kN/m ³] | |
|-------------|------------------|----------------------------|------------|----------------------------|------------|----------------------------|------------|
| | | k_{low} | k_{high} | k_{low} | k_{high} | k_{low} | k_{high} |
| sand | q_c [MPa] | | | | | | |
| loose | 5 | 12000 | 27000 | 3270 | 7360 | 1000 | 2250 |
| moderate | 15 | 20000 | 45000 | 5460 | 12270 | 1670 | 3750 |
| firm | 25 | 40000 | 90000 | 10900 | 24550 | 3330 | 7500 |
| clay | f_{undr} [kPa] | | | | | | |
| weak | 25 | 2000 | 4500 | 400 | 900 | 200 | 450 |
| moderate | 50 | 4000 | 9000 | 1090 | 2460 | 240 | 530 |
| firm | 200 | 6000 | 13500 | 2570 | 5790 | 670 | 1500 |
| peat | f_{undr} [kPa] | | | | | | |
| weak | 10 | 1000 | 2250 | 275 | 615 | 85 | 185 |
| moderate | 30 | 2000 | 4500 | 400 | 900 | 200 | 450 |

Figure 2.16: Spring stiffness values for different soils (table 33.1 from [2])

The previous section stated Blum's method, which neglects the above described theory that some displacement of the soil should take place in order to reach the active/passive soil pressure. The calculation will be closer to reality if this is taken into account. However, because the displacement of the soil is dependent to the displacement of the sheet pile and thus the soil pressure to the sheet pile, a manual calculation with this spring model will become way to complex and labour intensive (iterations should be done). So for manual calculation's Blum's method should give a good estimation of reality. However, with available software it is easy and more precise to use the above described spring model.

2.3.3. FE-models

In the spring model, the whole soil body is simplified to a set of horizontal springs. This schematisation neglects the fact that the soil is also redistributing the forces vertically to the subsoil. This redistribution is done in a non-linear and complex way, depending to the soil model used to describe the relationship between the soil parameters, soil stresses and deformations. It is possible to split up the soil body in a number of small soil parts, creating a mesh of soil elements. For each part, the stress and deformation can be determined based to the stress and deformations of all neighbouring elements. Such a method is called a Finite Element Method (FEM) and is able to model the soil more precisely compared to the spring model. A finite element method takes into account that soil close to the sheet pile will be more affected by the displacement of the sheet pile compared to soil further away. This is clearly visible in figure 2.17, which gives the horizontal soil stress of a sheet pile in an excavation pit determined with a FEM. At the left, far from the sheet pile, the soil stress is not affected. Just before the sheet pile, the horizontal soil stress starts to decrease towards the active

soil pressure. At the excavation side of the sheet pile, the local increase of the soil stress can be very large, but as can be seen, it is quickly redirected to other parts of the subsoil. The stress distribution in the soil is of great influence to the soil deformation and therefore to the sheet pile. This soil behaviour, and therefore the soil-structure interaction, is complex and non-linear, which gives that FE-models can only be evaluated with FE-program's. In this thesis, Plaxis 2D will be used as a FE-program. The sheet pile itself is modelled and evaluated with linear mechanics, thus without finite elements in this program [13]. How this structural modelling is done is discussed in section 2.5.

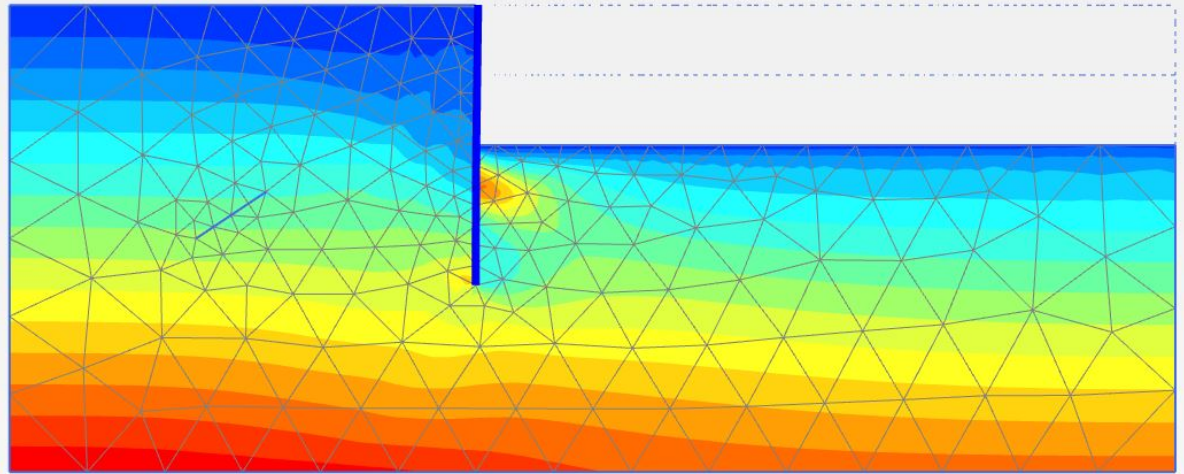


Figure 2.17: Horizontal soil stress around an excavation with a sheet pile wall

For the modelling of the soil in a FEM multiple soil models are available to describe the relationship between the soil parameters, deformation and stress in the soil elements. The FE program Plaxis for instance has the ability to imply no less than 13 soil models, of which a description can be found in literature [13]. Based on the situation and the type of soil, it might differ which soil model should be used. By Dutch regulations for the design of dikes ² it is stated that the Hardening Soil (HS) model is preferred for non-cohesive soils, where for cohesive soils (clay, peat) the Soft Soil Creep (SSC) model should be used [14]. For undrained soils, the NGI-ADP model should be used, which can take the undrained shear strength into account [14]. For the remaining of this thesis, the HS and SSC models will be used as to model the behaviour of the soil in FE programs.

2.4. Friction and vertical bearing capacity

Besides horizontally, the sheet pile is also loaded in the vertical direction. This load can originate in the vertical anchor component, an external vertical force or, not in the last place, the earlier discussed skin friction between the soil and the sheet pile. This section will discuss how the normal loading can be redirected to the soil.

2.4.1. Wall friction

The skin friction between the soil and the sheet pile will only occur if the sheet pile moves with respect to the soil directly besides the pile. When the soil settles harder than the sheet pile, the pile experience a downward directed friction force (the soil 'hangs' on the pile). When the pile settles harder, an upward directed friction force is experienced (the pile 'hangs' on the soil). In figure 2.18, it is assumed that the soil at the right side (active soil pressure) settles more than the sheet pile, the soil at the left side (passive soil pressure) settles less than the sheet pile. The friction between the soil and sheet pile at the right side will lead to an additional normal force in the sheet pile. At the left side, the friction will lead to a reduction in the normal force. The maximal friction can be determined by using equation 2.7, but this value is not necessarily reached by the soil-structure interaction. Just as with the horizontal soil stress, some displacement is required in order to create all the friction possible between the soil and structure. Again, this is dependent on the non-linear behaviour of the soil and the soil-structure interaction. The linear relation between the friction and the displacement is

²In the Netherlands, dikes should be designed according to the POVM: Project Overstijgende Verkenning Macrostabieleit

given in figure 2.19. The displacement where the maximal friction τ_{max} is being reached equals to 10 mm for sand and 20 mm for cohesive soils according to the Dutch "CUR166: Handboek damwandconstructies" [5].

$$\tau_{max} = \sigma'_h \tan(\delta) \quad (2.7)$$

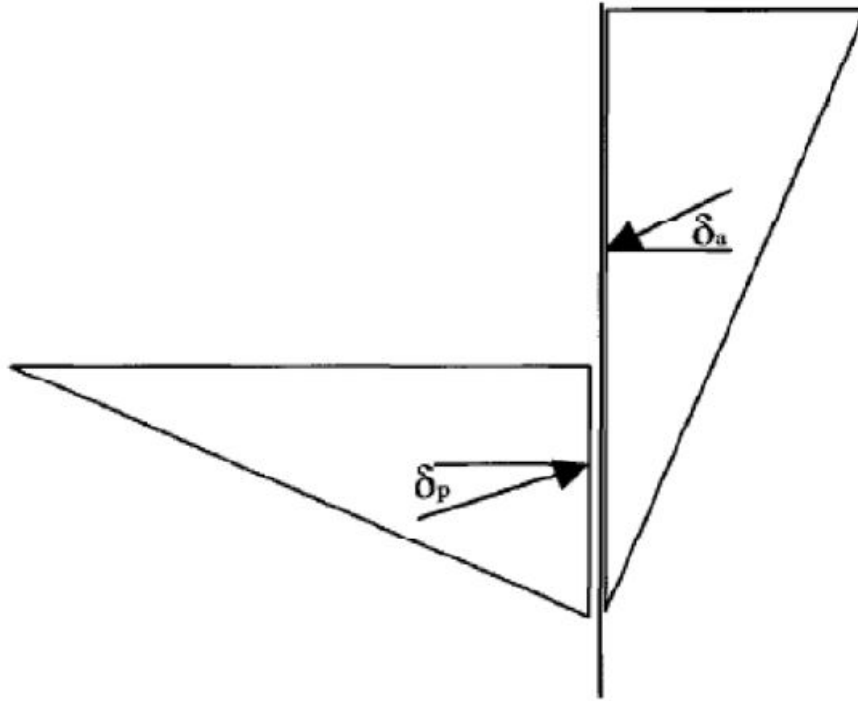


Figure 2.18: interaction between horizontal soil pressure and sheet pile (figure 5.1 from [5])

In the friction formula given in equation 2.7 the cohesion of the soil is neglected. However, when cohesion is present, this does affect the shear stress in the soil (and thus the skin friction). Pontyondy et al. [11] took this into account for his research to the relation between the skin friction angle δ and the internal friction angle ϕ . He used formula 2.8 instead of formula 2.7 to account for the cohesion term in the skin friction. With experiments he carried he was able to derive the factors f_δ and f_c , given in table 2.2. For shallow soils, the account of cohesion can be significant, where for deep soils, this significance reduces where soil stress becomes larger and more important.

$$\tau_{max} = f_c c + \sigma'_h \tan(\delta) \quad (2.8)$$

With:

$$\delta = f_\phi * \phi$$

| | Sand | | Cohesionless silt | | Cohesive granular soil | | Clay | | | |
|-------------------------|----------|----------|-------------------|----------|------------------------|----------|-------|----------|-------|-------------|
| | Dry | Sat. | Dry | Sat. | - | - | - | - | - | |
| | Dense | | Dense | Loose | Dense | - | - | - | - | - |
| Steel surface roughness | f_ϕ | f_ϕ | f_ϕ | f_ϕ | f_ϕ | f_ϕ | f_c | f_ϕ | f_c | $f_{c,max}$ |
| Smooth polished steel | 0.54 | 0.64 | 0.79 | 0.40 | 0.68 | 0.40 | - | 0.50 | 0.25 | 0.50 |
| Rusted rough steel | 0.76 | 0.80 | 0.95 | 0.48 | 0.75 | 0.65 | 0.35 | 0.50 | 0.50 | 0.80 |

Table 2.2: f_ϕ and f_c values based on experiments (values from [11])

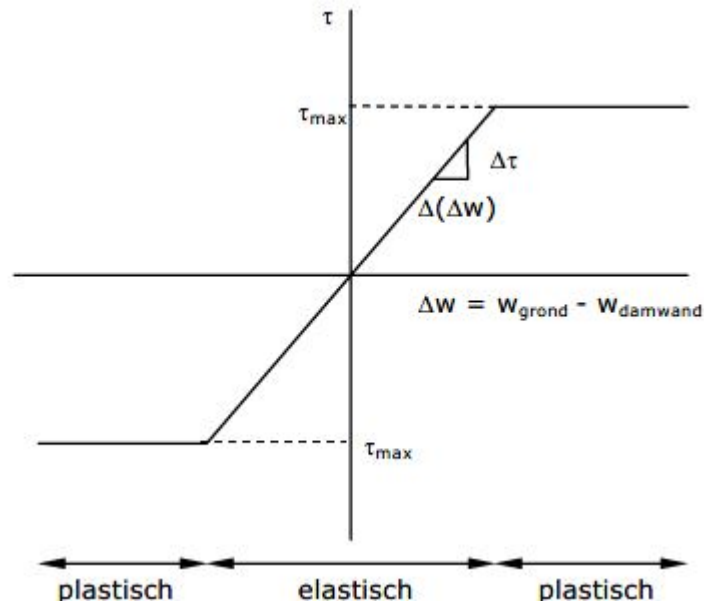


Figure 2.19: Mobilisation curve skin friction (figure 21 from [7])

2.4.2. Vertical stability

Due to the vertical loading to the sheet pile it might be that the pile becomes unstable vertically and fails. Vertical stability should be reached by mobilising enough skin friction and toe bearing capacity. The resistance against vertical settlement consists of the bearing capacity of the pile tip and the upward directed skin friction at the passive soil pressure. If not enough resistance is given by the soil, the pile will become unstable and start to settle.

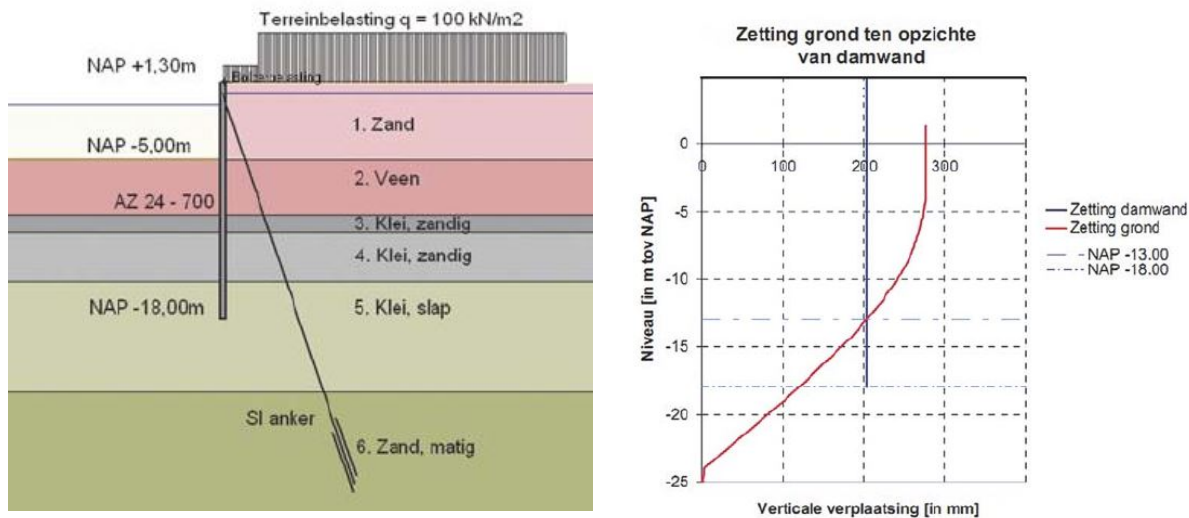
Slip method

The vertical stability of the sheet pile can be determined with the slip method. The above derived theory for the skin friction is the basis for the slip method as described in [15]. This method assumes that if the vertical bearing capacity is not enough, the pile starts to settle. In this way it can occur relatively quickly that the lower parts of the sheet pile settle more than the soil at both sides. In that case, the skin friction angle δ at the side with the active soil pressure should be reduced or completely reversed where the pile settles more than the soil. A reduction of the friction angle would mean that the friction between the soil and the pile is reducing as well. A reversing of the angle would mean that the friction force is directed upward instead of downward. With less downward directed friction forces, vertical stability might be reached. One can split up the soil in small layers (let say a meter) and may then reverse the angle starting with the lowest layer. If the reversed friction of this layer alone does not result in enough vertical stability, the skin friction angle δ of the next layer should be reversed. This process repeats itself until vertical stability is reached. It should be noticed that with a lower or even negative angle for the skin friction, the horizontal soil pressure factor K_a rises. With that, the loading from the soil to the sheet pile and thus the deformations will increase.

In the magazine of Geotechniek a case study has been conducted with the slip method [15], see figure 2.20. The sheet pile was constructed in extreme conditions (thick peat layer (4.5 m), founded in thick clay layers (at a sum of 14.5 m) and a relatively steep anchor (45°)). Because of the weak soil, the soil settlement was significant at the top (275 mm) and vertical stability was not reached without settlement of the sheet pile. The settlement of the pile was enlarged to no less than 200 mm to reach stability, such that the soil above NAP -13m settled and the soil below this level raised with respect to the pile. This made the friction below this level at the right side directed upwards, and above this level directed downwards. In figure 2.20b it can be seen that only a small part of the friction along the wall was not fully mobilised (over less than a meter in vertical direction the settlement difference between the soil and the pile are less than 20 mm).

q_c method

Another method to determine the vertical stability is the q_c method. This method states that if the sheet pile



(a) Soil profile case study vertical stability (figure 6 from [15])

(b) Settlement of the soil and sheet pile (figure 7 from [15])

Figure 2.20: Case study Geotechniek

is fixed and undeformed (negligible deformations) in the soil below the lower zero shear force point (at this point a horizontal force balance is reached), that the part of the pile below the zero shear point may be seen as foundation pile. In that case, the bearing capacity may be calculated in the same way it is done with foundation piles. The bearing capacity of foundation piles can be determined based on the cone resistance q_c , which is determined by a Cone Penetration Test (CPT). Limitation to this method is that it can only be used until a vertical displacement of the sheet pile of 25 mm or 10% of the piletip diameter. [15]

The q_c method is used to verify the above described case study. This method gave an significant lower bearing capacity compared to the slip method. However, considering the displacements of this case, the q_c method is not allowed to be used. The same structure was calculated by a FE program, showing that the displacement found with the slip method was indeed (more or less) correct. [15]

2.5. Structural analysis of sheet piles

The previous sections focused to the behaviour of soil around a sheet pile, where this section will focus to the structural behaviour of the sheet pile. Steel has a certain maximum stress it could take without permanent deformation: the yield stress. Steel has some extra capacity for stresses larger than the yield stress, but the steel fibres will deform permanent if such stresses are reached and the sheet pile won't return to it's original shape after unloading (plastic deformation). Besides, once the steel starts to yield, the deformations becomes large as well. For those reasons, sheet piles are generally designed with the yield stress as upper limit [14]. The design with the yield stress as upper limit is an elastic design. If the yield stress may be exceeded, the design is plastic. Because the design of sheet piles should be elastic most times, this section will focus to the elastic structural behaviour of steel elements.

2.5.1. Elastic structural analysis

In order to check if the capacity of the sheet pile is exceeded or not, the relationship between the loading, deformation and internal forces must be known. This relationship for elastic design is presented in equations 2.9 to 2.12 assuming a normal force is not present. The derivations have been done based on the structural element given in figure 2.21. First of all, a displacement w of the sheet pile is assumed, which can be derived in order to find the rotation of the sheet pile (equation 2.9). It is known that the bending moment is the product of the bending stiffness EI and the curvature of the cross section (equation 2.10).

$$\frac{dw}{dx} = -\phi \quad (2.9)$$

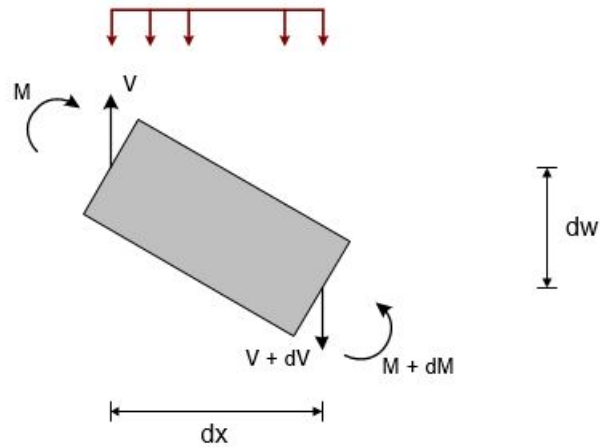


Figure 2.21: Structural element loaded by bending moment M and shear force V

$$EI \frac{d\phi}{dx} = EI * \kappa = M \quad (2.10)$$

$$\frac{dM}{dx} = V \quad (2.11)$$

$$\frac{dV}{dx} = -q \quad (2.12)$$

The above equations are valid for a structural element loaded with a bending moment M and a shear force V . But for the global buckling mechanism the influence of the normal force N should be known. If a normal force N is added, equation 2.11 will change, where equations 2.9, 2.10 and 2.12 remain to be valid. For an element loaded with the M -, V - and N -forces (figure 2.22), the expression of the shear force is derived in equation 2.13 based on the moment balance of the element in figure 2.22 (bending moment taken around right centre of forces).

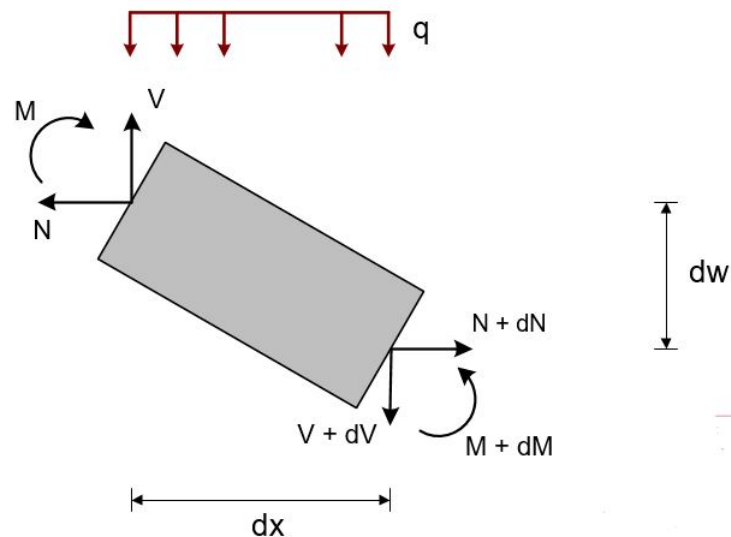


Figure 2.22: M -, V - and N - forces on small structural element

$$\begin{aligned}
 M + dM &= M + V * dx - N * dw \\
 \frac{dM}{dx} + N \frac{dw}{dx} &= V \\
 -EI \frac{d^3 w}{dx^3} + N \frac{dw}{dx} &= V
 \end{aligned}
 \tag{2.13}$$

$$EI \frac{d^4 w}{dx^4} - N \frac{d^2 w}{dx^2} = q
 \tag{2.14}$$

In the last derivation given in this section, an elastic support is connected to the structural element with a spring stiffness k , see figure 2.23. The force from the support equals $k * w$ (the extra displacement dw is negligible with respect to w) and will act as a distributed load directed upwards. This results in equation 2.15, where the reaction of the elastic support is subtracted from the distributed load. This equation is of importance in the spring model, as will be seen in the derivation of the critical global buckling load F_{cr} for sheet piles which are designed according to the spring model.

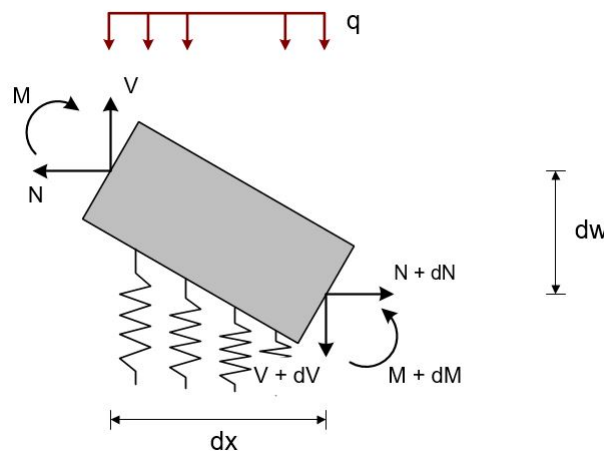


Figure 2.23: M-,V- and N- forces on small structural element with an elastic support

$$EI \frac{d^4 w}{dx^4} - N \frac{d^2 w}{dx^2} = q - k * w
 \tag{2.15}$$

2.5.2. Reduced bending stiffness

In the derived relation between the displacement, loading and internal forces, the bending stiffness EI is of great importance. This can be taken as a constant from the cross sectional properties of the sheet pile. However, there are some influences which affects the bending stiffness negatively. Two of them are discussed in this section: Asymmetrical cross sections and corrosion.

Asymmetrical cross sections

The reduction to the bending stiffness due to asymmetrical cross sections is a problem occurring in U-shaped cross sections. This is best described with the help of figure 2.24. The first situation is the most ideal situation: all the interlocks between the single sheet piles are fixed to each other and the neutral axis³ goes straight through centre of the combined profile. In this case, the cross section is symmetric and the bending stiffness should not be reduced. However, because of practical reasons not all of the interlocks can be fixed to each other before installation. If an interlock is not fixed, the cross sectional forces can not be fully transmitted to the next sheet pile by the interlock. The friction in the interlock will only transfer a part of the cross sectional forces. This results in less resistance against bending and thus in a lower bending stiffness EI . Three more situations are given in figure 2.24. In situation two, non of the interlocks are fixed, and the bending stiffness is

³The neutral axis is the axis in the cross section where zero normal stress occurs

reducing significantly. The neutral axis is no longer in the centre of the combined profile but in the centre of the single pile. If only half of the interlocks (situation three) are connected, two single piles acts as one single profile. With the profile being present over the full height of the combined profile, the bending stiffness is not reduced, but an other problem occurs. The cross section is asymmetrical, resulting in bending in two directions and larger normal stresses in the steel, known as oblique bending. To account for this effect, the bending stiffness should be reduced. The reduction factor to the bending stiffness is given in equation 2.16 [5]. The reduction to the section modulus W , an important parameter to determine the bending moment capacity⁴, can be determined by equation 2.17.

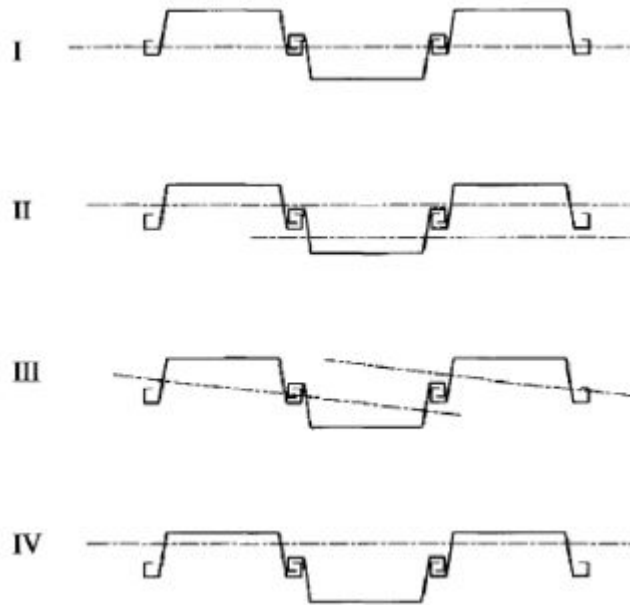


Figure 2.24: Oblique bending of U-shaped sheet piles (figure 3.7 from [5])

$$\beta_B = \frac{I_z I_y - I_{yz} I_{zy}}{-I_{yz} y + I_z z} \frac{h}{2I_y} + \sum_{n=1}^6 \Delta\beta_{B,n} \leq 1.0 \quad (2.16)$$

$$\beta_D = 1 - \frac{I_{yz} I_{zy}}{I_z I_y} + \sum_{n=1}^6 \Delta\beta_{D,n} \leq 1.0 \quad (2.17)$$

If two out of three interlocks are fixed before installation (situation four in figure 2.24), the effect of oblique bending does not occur. However, the neutral axis is still not in the centre of the combined profile. Therefore, the bending stiffness should be reduced in theory. However, for sheet piles where two out of three (or more) interlocks are fixed, the reduction in the bending stiffness can be neglected [5].

Corrosion of steel sheet piles

Due to the environment of steel sheet piling structures, the steel piles are prone to corrosion over its life time. This corrosion reduces the thickness of the sheet pile and with that the bending stiffness reduces. The magnitude of the corrosion depends to the local circumstances. For instance, a sheet pile applied in a quay wall has multiple parts with different rates of corrosion. Above the splash zone and the high water level, water will be less present than at lower parts, resulting in less corrosion than in the parts where water and oxygen are often present. At lower parts, water or/and soil will always be present reducing the corrosion rate. This gives that several bending stiffness are present along the sheet piles once corrosion occurs after time. This might result in complex calculations, especially for the global buckling mechanism which is strongly dependent to the bending stiffness along the sheet pile.

⁴The bending moment capacity M_{Rd} can be determined by the product of the section modulus W and the yield strength f_y

3

The mechanisms of global buckling for steel structures

To determine the influence of soil on the global buckling mechanism in sheet piles, it is important to know what the cause of the mechanism is, what the theoretical background of the mechanism is and how the current global buckling check for sheet piles in the Eurocode is derived in the first place. This will be described in this chapter, neglecting all influences of the soil against the mechanism.

3.1. Global buckling

When an initial displacement is present in a structural element, eccentricities will occur between the deformed element and the line of action of the normal force, visualised in the left part of figure 3.1. The normal force in combination with the eccentricity introduces a bending moment in the element, increasing the displacement and so the bending moment itself. An equilibrium will be reached where the driving bending moment from the normal force is in balance with the resisting bending moment from the beam. It may be possible that the enlarged bending moment exceeds the moment capacity leading to failure, which would be failure due to the global buckling mechanism.

3.1.1. Interaction between normal force and displacements

The initial displacement and bending moment due to the normal force are the first order effects to the structure. The increase of both the displacement as the bending moment is the second order effect. The growth of the deformation from the first to the second order is called the amplification. This section will discuss the derivation and formula's in order to describe the second order effects. [16]

As example, two cases are given below. The first case results in a well known formula from the structural mechanical theory, which is often used to calculate the second order displacement for structures in general. As will be seen by the second case, this is not completely correct.

Amplification with an initial sinusoidal displacement field

In figure 3.1 a displacement field of a beam is given. In this example, the first order displacement field w_0 is described by equation 3.1. If the structural element is loaded with a normal force, the displacement will increase to an unknown displacement w .

$$w_0(x) = \hat{w}_0 * \sin\left(\frac{\pi x}{l}\right) \quad (3.1)$$

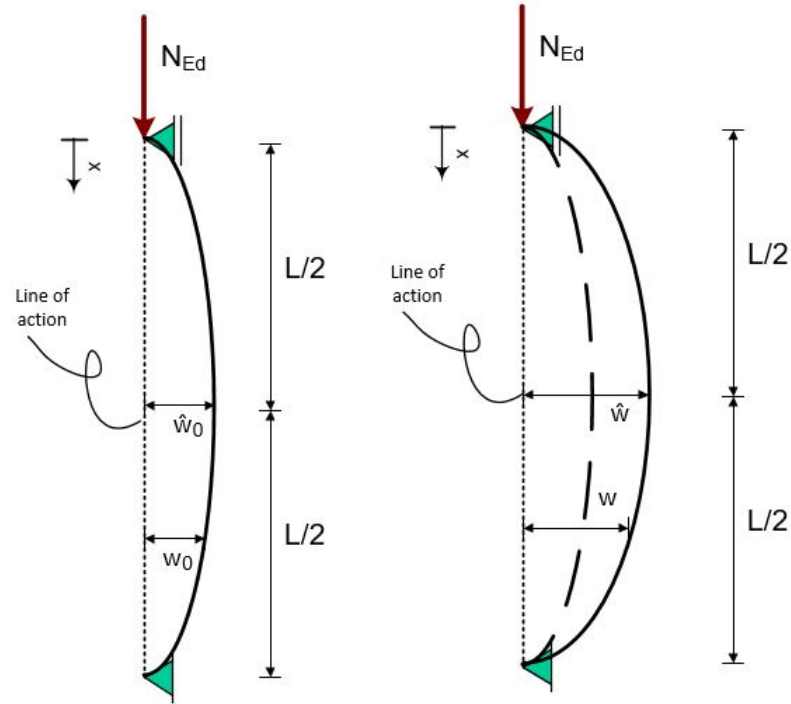


Figure 3.1: First order (left) and second order (right) displacement field (figure 11.4 from [16])

In section 2.5 the relation between the displacement, normal force and bending stiffness was derived, represented by equation 3.2. Because there is no distributed load q present, the equation could be set equal to zero. Expression 3.3 gives a solution of $w(x)$ for which the equilibrium of equation 3.2 is valid¹. Four unknowns are included in this equation: C_1, C_2, C_3 and C_4 . These could be found by solving equation 3.3 for the situation sketched in figure 3.1. It is known that at both $x = 0$ as $x = L$ both the displacement w as the bending moment M_{Ed} must be zero, leading to conditions 3.4 and 3.5. Solving those four boundary equations gives that all four unknown constants are equal to zero. The equation for the displacement can be rewritten to equation 3.6.

$$EI\left(\frac{d^4 w}{dx^4} - \frac{d^4 w_0}{dx^4}\right) + N_{Ed} \frac{d^2 w}{dx^2} = q = 0 \quad (3.2)$$

$$w(x) = EI \frac{\hat{w}_0 \pi^2 \sin\left(\frac{x\pi}{L}\right) + \left(L^2 - \frac{\pi^2}{N_{Ed}}\right) C_1 \cos\left(\frac{\sqrt{N_{Ed}} x}{\sqrt{EI}}\right) + \left(L^2 - \frac{\pi^2}{N_{Ed}}\right) C_2 \sin\left(\frac{\sqrt{N_{Ed}} x}{\sqrt{EI}}\right)}{EI\pi^2 - N_{Ed}L^2} + C_3 x + C_4 \quad (3.3)$$

for both $x = 0$ as $x = L$:

$$w(x) = 0 \quad (3.4)$$

$$M(x) = -EI\left(\frac{d^2 w}{dx^2} - \frac{d^2 w_0}{dx^2}\right) = 0 \quad (3.5)$$

$$w(x) = \frac{EI * \pi^2}{EI * \pi^2 - N_{Ed}L^2} \hat{w}_0 \sin\left(\frac{x\pi}{L}\right) = \frac{1}{1 - N_{Ed}/F_{cr}} \hat{w}_0 \sin\left(\frac{x\pi}{L}\right) = \frac{1}{1 - n^{-1}} \hat{w}_0 \sin\left(\frac{x\pi}{L}\right) \quad (3.6)$$

with:

$$F_{cr} = \frac{EI\pi^2}{L^2}$$

$$n = \frac{F_{cr}}{N_{Ed}}$$

The second order displacement $w(x)$ can grow very large when the normal force N_{Ed} goes to the critical buckling load F_{cr} . When this happens, the ratio n becomes close to 1 and the amplification factor $(1/(1 - n^{-1}))$

¹Computations are done with Maple TA. Maple TA is a powerful software program able to solve non-linear algebraic complex functions.

becomes large. This effect is visualised in figure 3.2. With the displacement, the bending moment due to the normal force becomes very large as well. Dependent to the quantity of the initial displacement and normal force, the maximal resisting bending moment will be reached (long) before the critical global buckling load is reached.

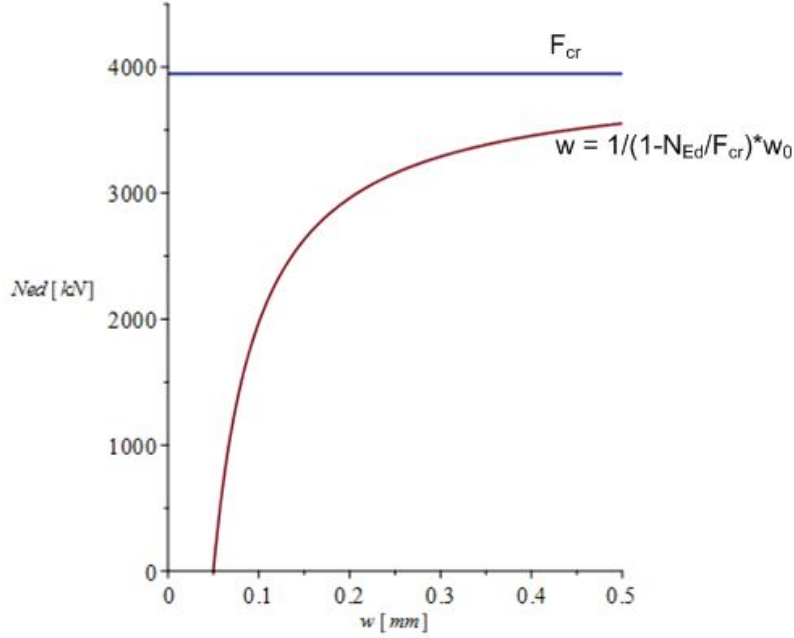


Figure 3.2: Deformation w against the axial force F

Amplification with an initial parabolic displacement field

The above derivation for the example gave an equation to take the second order effects into account which is rather convenient. As said, this expression yields for a sinusoidal displacement field, but the next example will treat the expression for the displacement field described by equation 3.7 (this example is taken from literature [16]). Again, a general solution must be found which full-fills the equilibrium of expression 3.2. This general solution is found by Maple TA¹ and presented in equation 3.8. With the conditions 3.4 and 3.5, the four unknowns C_1 to C_4 can be determined, which gives equation 3.9 for the displacement field including the second order effects.

$$w_0 = \frac{4\hat{w}_0}{L^2}(Lx - x^2) \quad (3.7)$$

$$w(x) = C_1 + C_2x + C_3\sin(\alpha x) + C_4\cos(\alpha x) \quad (3.8)$$

$$\alpha = \sqrt{\frac{N_{Ed}}{EI}}$$

$$w(x) = \frac{8}{(\alpha L)^2} \hat{w}_0 \left(\frac{\sin(\alpha L - \alpha x) + \sin(\alpha x)}{\sin(\alpha L) - 1} \right) \quad (3.9)$$

The above derived amplification factor differs obviously from the amplification factor for a sinusoidal displacement field, which is less complex. For the middle of the beam, at $x = L/2$, both equations 3.6 and 3.9 are compared with each other for several values of the ratio n . In order to express equation 3.9 in terms of n , the term αL has been rewritten in expression 3.10. The comparison is made for several values for n in table 3.1, which shows that the amplification factor ($n/(n-1)$) is a well approximation of the exact amplification. The error is limited to only 2.8% for a normal force of 90% of the critical buckling load. Because of its simplicity and its relative small error, equation 3.6 is often used to determine the second order displacement independent from the shape of the first order displacement (parabolic, triangular, sinusoidal etc).

$$\alpha L = \sqrt{\frac{N_{Ed} l^2}{EI}} = \sqrt{\frac{\pi^2 N_{Ed}}{F_{cr}}} = \frac{\pi}{\sqrt{n}} \quad (3.10)$$

| n | Parabolic amplification | Sinusoidal amplification |
|------|-------------------------|--------------------------|
| 100 | 1.01 | 1.01 |
| 50 | 1.021 | 1.020 |
| 20 | 1.054 | 1.053 |
| 10 | 1.114 | 1.111 |
| 5 | 1.257 | 1.250 |
| 2.50 | 1.686 | 1.667 |
| 2 | 2.030 | 2.000 |
| 1.50 | 3.061 | 3.000 |
| 1.25 | 5.125 | 5.000 |
| 1.11 | 10.284 | 10.000 |

Table 3.1: Amplification factor's for both sinusoidal and parabolic displacement fields

Dischinger correction factor

As described, the simplification made when one use's the simple amplification factor from equation 3.6, an error is made. Dischinger [17] proposed to introduce a correction factor δ for other type of displacement fields to account for this error. The sinusoidal amplification factor can be rewritten as in equation 3.11. For the example above with the parabolic initial displacement field, the correction factor can be set to 0.031. This value will reduce the maximal error from 28% to only 0.6%, a significant reduction of the error with a factor 47.

$$\frac{1}{\frac{1 - n^{-1}}{1 + \delta n^{-1}}} \quad (3.11)$$

3.1.2. Critical global buckling load

In the above derivations of the second order effects, a critical value for the normal force F_{cr} was introduced. Apparently, it is impossible for the normal force to grow beyond this value since the displacement will go to infinity if the the normal force goes to F_{cr} . Even with the smallest thinkable initial deformation, the value of displacement including the second order effect will rocket if F_{cr} is approached. Since a beam is never perfectly straight, F_{cr} will be the absolute upper limit for the normal force N_{Ed} . Let's consider the, what seems to be straight, beam of figure 3.3 with an imperfection of 1 μm (own weight not considered). If N_{Ed} equals 99.9999% of F_{cr} , the displacement including the second order effect equals a meter according to equation 3.6. This shows that even the smallest displacements may leads to significant second order effects.

This section discusses the derivation of F_{cr} . Based on the described theories, a method will be described in chapter 5 to determine F_{cr} taking into account the resistance of the soil.

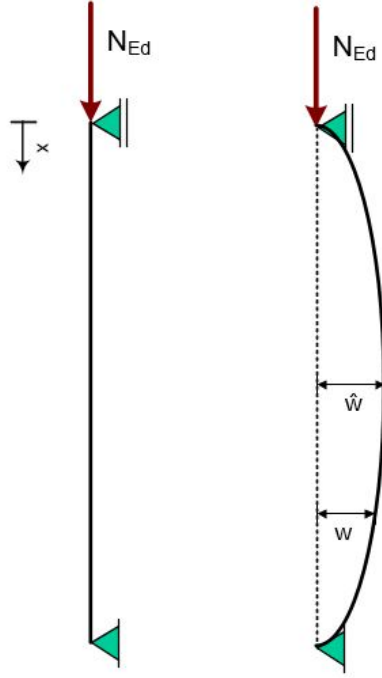


Figure 3.3: Global buckling of a straight structure without initial displacement ($F_k = F_{cr}$)

Derivation critical buckling load according to Euler

A well known method to determine the critical global buckling is derived by Euler [16], which is based on the earlier derived equilibrium equation 3.12. In theory, a perfectly straight beam does not exist and a displacement w_0 will always be present. The value for F_{cr} can be derived for w_0 going to 0, which can therefore be neglected. This resulted in the right hand side of equation 3.12. The general solution to this simplified equation 3.12 is given in equation 3.13.

$$EI\left(\frac{d^4 w}{dx^4} - \frac{d^4 w_0}{dx^4}\right) + N_{Ed} \frac{d^2 w}{dx^2} = q \longrightarrow EI \frac{d^4 w}{dx^4} + N_{Ed} \frac{d^2 w}{dx^2} = 0 \quad (3.12)$$

$$w(x) = C_1 \cos(\alpha x) + C_2 \sin(\alpha x) + C_3 x + C_4 \quad (3.13)$$

$$\alpha = \sqrt{\frac{N_{Ed}}{EI}}$$

The four unknowns C_1 , C_2 , C_3 and C_4 can be determined by solving the boundary conditions given in expressions 3.14 and 3.15. Those four conditions can be rewritten into the matrix shape given in equation 3.16. The buckled shape of the structural element in figure 3.3 occurs when the normal force N_{Ed} equals F_{cr} . The buckling shape has clearly a non-zero displacement field, which means that it is not possible that all the constants C_1 to C_4 are zero. Yet, all the boundary conditions must be zero, which means that the determinant of the coefficient matrix should be zero [16]. The determinant of this coefficient matrix is given by equation 3.17, which equals zero if N_{Ed} is set equal to F_{cr} as given in equation 3.18. This value for F_{cr} is the well known (Euler's) critical global buckling load.

Boundary conditions:

$$w(0) = C_1 + C_4 = 0 \quad (3.14)$$

$$w(L) = C_1 \cos(\alpha L) + C_2 \sin(\alpha L) + C_3 L + C_4 = 0$$

$$M(x) = -EI \frac{d^2 w}{dx^2} = EI\alpha^2 (C_1 \cos(\alpha x) + C_2 \sin(\alpha x)) = 0$$

$$M(0) = EI\alpha^2 C_1 = N_{Ed} C_1 = 0 \quad (3.15)$$

$$M(L) = EI\alpha^2 (C_1 \cos(\alpha L) + C_2 \sin(\alpha L)) = N_{Ed} (C_1 \cos(\alpha L) + C_2 \sin(\alpha L)) = 0$$

$$\begin{pmatrix} N_{Ed} & 0 & 0 & 0 \\ 1 & 0 & 0 & 1 \\ N_{Ed} \cos(\alpha L) & N_{Ed} \sin(\alpha L) & 0 & 0 \\ \cos(\alpha L) & \sin(\alpha L) & L & 1 \end{pmatrix} \begin{pmatrix} C_1 \\ C_2 \\ C_3 \\ C_4 \end{pmatrix} = \begin{pmatrix} 0 \\ 0 \\ 0 \\ 0 \end{pmatrix} \quad (3.16)$$

$$L * N_{Ed}^2 \sin\left(\sqrt{\frac{N_{Ed}}{EI}} L\right) = 0 \quad (3.17)$$

$$N_{cr} = F_{cr} = \frac{\pi^2 EI}{L^2} \quad (3.18)$$

Apart from Euler, Rayleigh [16] has derived a method based on an energy approach to determine the critical buckling load. In appendix A, the derivation of Rayleigh is given.

Buckling length

The above derived equation 3.18 only yields for the structural element given in figure 3.3. For other structural elements with other boundary conditions, the formula will change. It was found [16] that the critical global buckling load for structural elements could be determined by equation 3.19, where L_k is not the length of the structural element, but the critical buckling length. In literature (for example [16]), various examples could be found of the critical buckling length for different boundary conditions. Three examples are given in figure 3.4 with the critical buckling length given as fraction of the structure length. Once the beam has buckled, a displacement occurs, which is different for each structure in figure 3.4. This shape of the displacement is the buckling shape, which will be mentioned more in this thesis.

$$N_{cr} = F_{cr} = \frac{\pi^2 EI}{L_k^2} \quad (3.19)$$

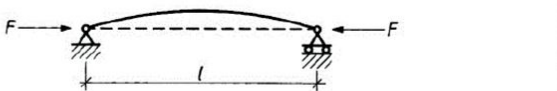
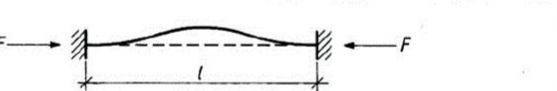
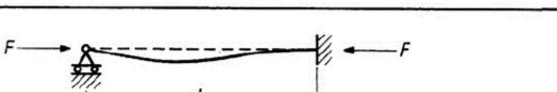
| | | |
|---|--|-----------------|
| a |  | $L_k = L$ |
| b |  | $L_k = L/2$ |
| c |  | $L_k = 0.7 * L$ |

Figure 3.4: Several values for the critical buckling length L_k (figure 36-2 from [2](adapted))

The lower the critical buckling length is compared to the structure length, the more the structure has to bend, see also the examples of figure 3.4. Bending of a structure requires energy and thus a force. The larger the bending must be, the larger the force must be. So a smaller critical buckling length requires a higher critical global buckling load F_{cr} . The critical buckling length therefore says something about the resistance against global buckling delivered by the bending stiffness of the structure.

3.1.3. Global buckling in sheet piles

Above the background of global buckling mechanism has been derived for regular structural elements. In this derivation, the global buckling mechanism and the second order effects strongly depends to the critical global buckling load F_{cr} . CUR 166 states equation 3.20 to determine the bending moment due to the normal

force. In this equation, w_0 is the first order displacement of the sheet pile [5]. Though it is known to be incorrect, this equation should be used independent from the shape of the deformation. Previously, it has been found that the amplification ratio in equation 3.20 (the fraction) is only correct if and only if the shape of the deflection is of the same shape as the global buckling shape (see figure 3.4). For any other deflection shape, a small error is made for this equation. The error made by this simplification can for a large part be removed by Dischinger's correction factor δ . In chapter 5.3 it will be concluded that values of δ are negative for sheet piles. This gives that equation 3.20 is an overestimation of the actual second order effect to the displacement.

$$M = N_{Ed} \frac{1}{1 - n^{-1}} w_0 \quad (3.20)$$

Back in the days, when software was not or hardly available, the above described method was a well approximation to determine the second order effects in sheet piles. However, nowadays, this could be done more precisely using the available software. This would mean that the above described method could be replaced. However, as will be seen later, the amplification ratio used in equation 3.20 will be of importance for the design check to the global buckling mechanism.

Critical buckling length

The value of F_{cr} for steel sheet piles must be known before the structure could be checked on the global buckling mechanism. Eurocode 1993-5 for sheet piles recommends equation 3.19 in order to determine F_{cr} . The code defines the critical buckling length as presented in figure 3.5. If the toe of the sheet pile is fixed² in the soil (figure 3.5b), the critical buckling length becomes to be 70% of the distance between the lowest anchor and the toe. If the toe is not fixed³, the critical buckling length is not reduced (figure 3.5a).

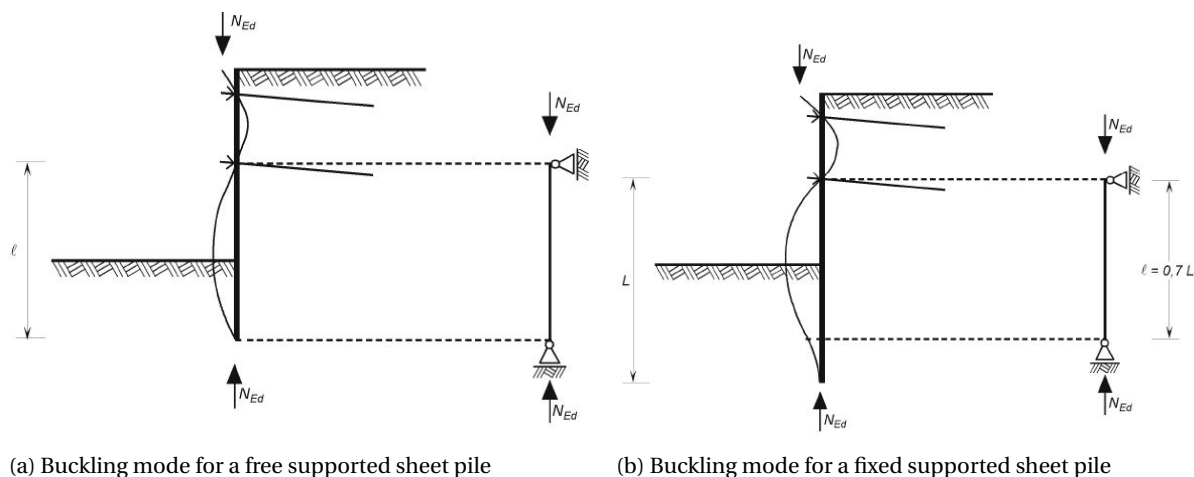


Figure 3.5: Buckling length according to Eurocode

The effect of corrosion to the buckling capacity

Over the life time of a sheet pile, the pile gets affected by corrosion reducing the thickness, and with that the bending stiffness EI , of the sheet pile. It is possible that the rate of the corrosion is not constant over the length of the pile. If the steel is constantly above the water level, the corrosion will be less compared to the steel which is around the water line. Due to this various corrosion rates, the bending stiffness will be variable over the height of the sheet pile as well [5].

Because of variation in the bending stiffness, the sheet pile must be split up in the calculation model in different sections with different bending stiffnesses, like the example in figure 3.6a. When the buckling verification check of the Eurocode is done, it is not seldom done to use the bending stiffness of the cross section of consideration to determine the critical global buckling load F_{cr} . However, because other sections of other stiffness's

²A fixed toe gives that the sheet pile can hardly rotate at the pile tip

³A non fixed toe gives that the sheet pile can rotate quite easily at the pile tip

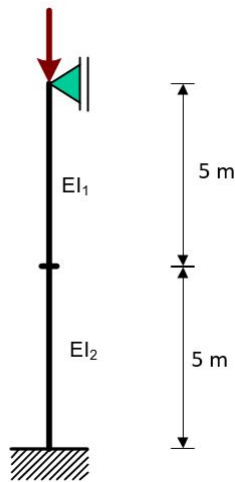
influence critical load F_{cr} as well, this is false. This section will give a model to determine the size of this effect and if it can be ignored or not.

As an example, a sheet pile is modelled as in figure 3.6a, which is belonging to the buckling shape figure 3.5b with a fixed tip of the sheet pile. The stiffness EI_1 of the top has been reduced by 20%, while the other part has still the initial stiffness ($100\,000\text{ kNm}^2$). In order to find the critical buckling load, Euler's method described in section 3.1.2 should be used. For this method, equation 3.21 should be solved to find the critical buckling shape. This equation is solved by equations 3.22 and 3.23 for respectively the upper and lower half of the sheet pile in figure 3.6a. Both equations are very similar, but the difference is between the bending stiffness EI_1 and EI_2 . These two equations have combined 8 unknown parameters, which could be found by stating the boundary conditions, like done in section 3.1.2. These conditions could be rewritten into the shape of equation 3.16. If the normal force N_{Ed} equals the critical global buckling load, the determinant of the coefficient matrix equals zero. The determinant of this matrix is plotted in figure 3.6b, where it is visible that the determinant equals zero if the normal force equals $17\,431\text{ kN}$. With the current design practice, where only one single bending stiffness EI is used, the top and bottom half of the sheet pile would have a critical global buckling load of respectively $16\,153\text{ kN}$ (-7.3%) and $20\,191\text{ kN}$ (+15.8%). So the current design practice will be conservative for the top part of the pile, but will be progressive for the bottom part of the wall. This is a significant error which might be solved quite easily, based on the above theory.

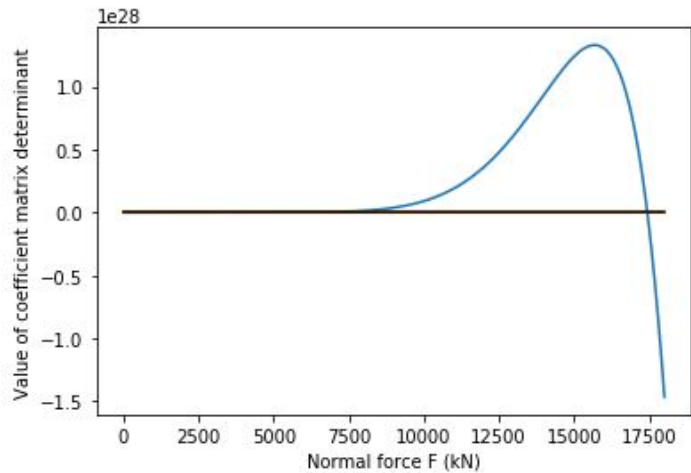
$$EI * \frac{d^4 w}{dx^4} + F * \frac{d^2 w}{dx^2} = 0 \quad (3.21)$$

$$w_1 = C_1 + C_2 x + C_3 \sin\left(\frac{\sqrt{F}x}{\sqrt{EI_1}}\right) + C_4 \cos\left(\frac{\sqrt{F}x}{\sqrt{EI_1}}\right) \quad (3.22)$$

$$w_2 = C_5 + C_6 x + C_7 \sin\left(\frac{\sqrt{F}x}{\sqrt{EI_2}}\right) + C_8 \cos\left(\frac{\sqrt{F}x}{\sqrt{EI_2}}\right) \quad (3.23)$$



(a) Model



(b) Determinant of coefficient matrix

Figure 3.6: Example of fixed sheet pile with variable stiffness

3.2. Global buckling due to geometrical imperfections

The initial displacement introducing second order effects and with that the global buckling mechanism can have two causes: Loading to the sheet pile or geometrical imperfections of the sheet pile. The displacement due to loading to the sheet pile can be calculated with the available soil-structure interaction models and software. As already discussed above, some software is able to determine the second order effect of those displacements, also for sheet piling structures. With the second order effect known, the consequences of global

buckling mechanism are known, including the impact of the soil resistance. At this point, it seems to be that the influence of the soil to the global buckling mechanism can simply be determined with the use of software. However, the global buckling mechanism caused by geometrical imperfections is not discussed yet. As will be seen, this effect is not so easy determined with a software package.

Geometrical imperfections are errors in the structure which weren't taken into account in the design. This might for example be that the profile of the sheet pile is a bit thinner or that the pile is not perfectly straight. Those imperfections are dependent on the fabrication (possible errors/deviations), history (new or used pile) and installation of the pile. Several geometrical imperfections might occur in sheet piles, for which NEN-EN 10248 [18] defines tolerances for the thickness, height, width and other geometrical parameters. This tolerances leads to imperfections which may bring small reductions into the stiffness (both axial (EA) as bending (EI)). Other imperfections can be residual stresses, pre-deflections of the sheet pile, lower yield stress etc.. But mostly, this imperfections will lead to a sheet pile which is not perfectly straight, which leads to the global buckling mechanism.

Figure 3.7 is an example of an geometrical imperfection, where the thickness of the sheet pile has a tolerance and so a possible imperfection of 6%. The geometrical imperfections are unknown in the design. Therefore, tests were conducted to develop standard values for imperfections which were included in Eurocode 3 for steel structures [17]. Below, the derivation and the application of this value is described.

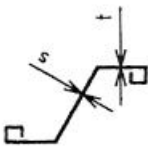
| Afmetingen in mm | | | |
|------------------|--|--------------------------|---------------------------|
| Omschrijving | Figuur | Nominale afmeting | Tolerantie |
| Dikten s en t |  | t, s ≤ 8,5 t, s > 8,5 | ± 0,5 ± 6 % van s en t |

Figure 3.7: Example of possible imperfections in steel sheet piling (table 9 from [18])

3.2.1. Geometrical imperfections, global buckling check and the Eurocode

Geometrical imperfections may result in an initial displacement and cause the global buckling mechanism. To take all imperfections into account, a representative eccentricity e_0 for all geometrical imperfections is introduced like in figure 3.8. The bending moment due to the interaction between the normal force and imperfections is given by equation 3.24, which is basically an extension of equation 3.20 but with geometrical imperfection e_0 instead of displacement w_0 . The normal force and the bending moment will induce normal stresses in the cross section. This normal stress should not exceed the yield stress, leading to the unity check presented in equation 3.25. The bending moment M_{Ed} represents the bending moment caused by all loads to the structural element including the second order effect. The initial imperfection e_0 is still an unknown. [17]

$$M = N_{Ed} \frac{n}{n-1} e_0 \quad (3.24)$$

$$\frac{N_{Ed}}{N_{pl,Rd}} + N_{Ed} \frac{1}{1 - \frac{N_{Ed}}{F_{cr}}} \frac{e_0}{M_{Rd}} + \frac{M_{Ed}}{M_{Rd}} \leq 1 \quad (3.25)$$

A complex derivation has been conducted in order to derive the current method used in the Eurocode. With rewriting the first two terms equation 3.25, the first term of equation 3.26 is derived. Reduction factor χ_b can be found with equation 3.27. The full derivation of this equation can be found in appendix B. Though the initial imperfection e_0 is lost in the derivation (it is represented by α together with other parameters), the critical global buckling load F_{cr} is still of importance.

$$\frac{N_{Ed}}{\chi_b N_{pl,Rd}} + \frac{M_{Ed}}{M_{Rd}} \leq 1 \quad (3.26)$$

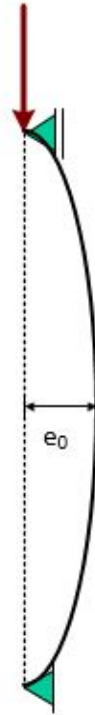


Figure 3.8: Imperfections represented by eccentricity e

With:

$$\chi_b = \frac{1}{\Phi + \sqrt{\Phi^2 - \bar{\lambda}_b^2}}$$

$$\Phi = 0.5(1 + \alpha * \epsilon * (\bar{\lambda}_b - 0.2) + \bar{\lambda}_b^2)$$

$$\bar{\lambda}_b = \sqrt{\frac{N_{pl,Rd}}{F_{cr}}}$$

$$\epsilon = \sqrt{\frac{235}{f_y}}$$
(3.27)

Parameter α has been introduced to represent several parameters (8 parameters in total, see appendix B). To determine the value for α , tests have been conducted with sheet piles, of which the results are presented in figure 3.9. Based on those results, the reduction factor χ_b could be determined using the European buckling curve d⁴, as presented in figure 3.9. All the test results are (well) above this curve, meaning that the curve is a bit conservative. The buckling curve could be described using equation 3.27 with a value for α of 0.76, corresponding to an initial eccentricity e_0 of 5.5‰ for Z-profiles or 5‰ for U-profiles of the sheet pile length [17].

When the relative slenderness $\bar{\lambda}_b$ is smaller than 0.2, the reduction factor χ_b is constant 1.0 (see figure 3.9). In principle, the buckling curves results in larger values for the reduction factor for those low slenderness values. However, a reduction factor larger than 1.0 results in fact in an increment instead of a reduction of the normal force capacity, which is impossible. For this reason, the second order effects of the imperfections must be neglected if the value of $\bar{\lambda}_b$ is lower than 0.2. Based on the definition of $\bar{\lambda}_b$ in equation 3.27, the Eurocode for the design of steel structures (NEN-EN 1993-1-1) states that the second order effects initiated by the geometrical imperfections should be neglected if the acting normal load N_{Ed} is less than 4% of the critical global buckling load F_{cr} .

⁴Buckling curves a₀, a, b and c are also existing, but those are valid for other steel profiles than sheet pile profiles

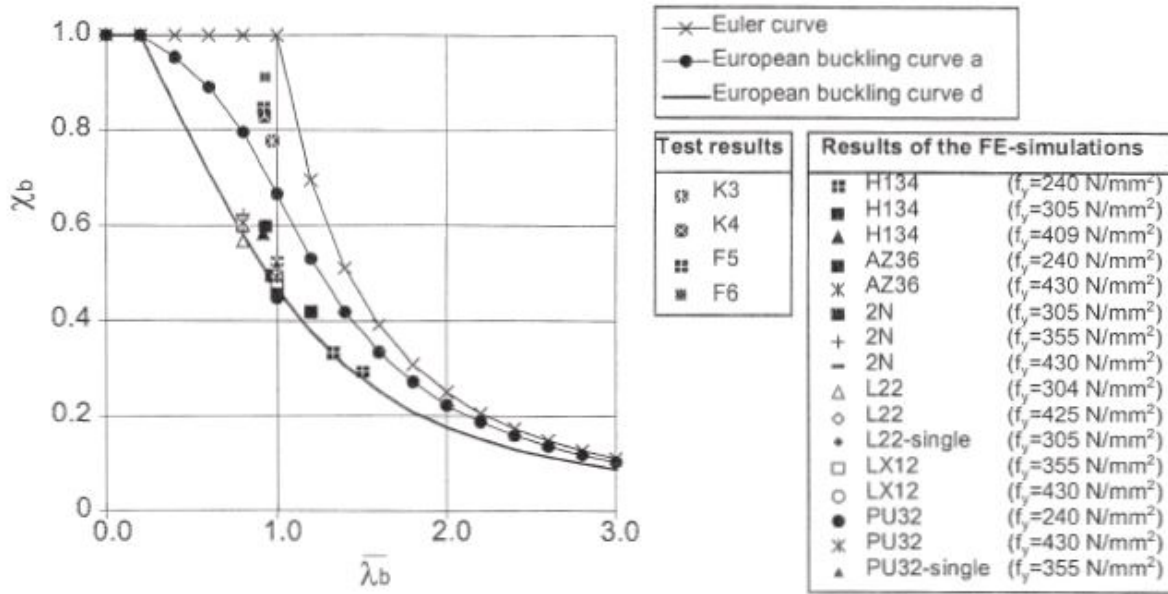


Figure 3.9: Experimental results of buckled sheet piles (figure 2.6-9 from [17])

In principle, the global buckling mechanism initiated by displacements caused by loading is still present for those low normal forces (<4% of F_{cr}). However, those effects will be limited and as stated by the Eurocode, can be neglected as well.

Because both the normal load as the bending moment are causing a normal stress in the structural element, the two are influencing each others capacity. If the normal load increases, the normal stress capacity left for the bending moment capacity reduces (M-N interaction). This interaction for the elastic design of steel structures is represented by the unity check in equation 3.28. Because the first two terms in equation 3.28 are rewritten to one term in equation 3.29, this M-N interaction isn't as straight forward anymore. Equation 3.28 depends non-linear to the normal load N_{Ed} , while equation 3.29 depends linearly to N_{Ed} . The two equations are only equal if the acting normal force N_{Ed} equals the normal force capacity $\chi_b N_{pl,Rd}$. For any lower normal force, the first term of equation 3.29 is larger than the first two terms of equation 3.28 and thus an overestimation. This means that extra capacity of the cross section is left for the bending moment M_{Ed} , which is visible in figure 3.10. If the normal force equals 50% of the capacity (so $\frac{N_{Ed}}{\chi_b N_{Rd}} = 0.5$), the bending moment can be 50% of the capacity (M_{Rd}) according to equation 3.29, but it could be 54.2% according to the exact equation 3.28. To account for this error, the acting bending moment M_{Ed} can be reduced by a factor 0.92 such that the error is removed. This factor is included in k_{yy} as in equation 3.29, appendix C discusses the derivation of this factor.

$$\frac{N_{Ed}}{N_{pl,Rd}} + N_{Ed} \frac{1}{1 - \frac{N_{Ed}}{F_{cr}}} \frac{e}{M_{Rd}} + \frac{M_{Ed}}{M_{Rd}} \leq 1 \quad (3.28)$$

$$\frac{N_{Ed}}{\chi_b N_{Rd}} + k_{yy} \frac{M_{Ed}}{M_{Rd}} \leq 1 \quad (3.29)$$

Annex A of the Eurocode for steel structures gives complex formula's to calculate k_{yy} [19]. In appendix C of this thesis, this factor is treated, from which it comes clear that k_{yy} is also representing the amplification of the bending moment M_{Ed} due to second order effects. Consequently, the used value for M_{Ed} must be the first order bending moment.

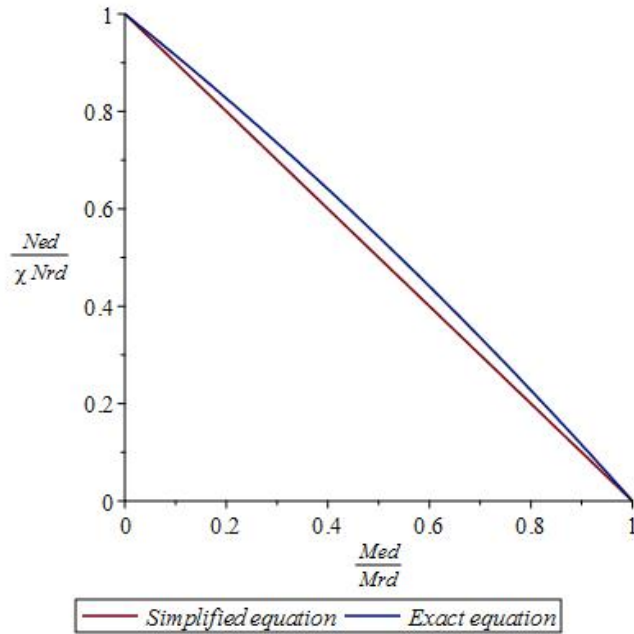


Figure 3.10: Comparison between equation 3.28 (exact equation) and equation 3.29 (simplified equation)

For steel sheet piles, it was decided to derive one constant, but conservative, value for k_{yy} [17]. In total, 30 experiments were carried out, of which the results are presented in figure 3.11. Based on this results, a line was sketched such that all the experimental results were above this line. This line could be described by equation 3.29 if k_{yy} is set to 1.15. It could be argued that for small normal forces the value of 1.15 is much too high for k_{yy} , but the Eurocode for sheet piles (NEN-EN 1993-5) prescribes the value of 1.15 independent to the value of the normal force [3]. This results in equation 3.30 for the unity check on the global buckling mechanism, including the partial safety factor γ_{M1} (=1.1) [3].

$$\frac{N_{Ed}}{\chi_b N_{Rd}(\gamma_{M0}/\gamma_{M1})} + 1.15 \frac{M_{Ed}}{M_{Rd}(\gamma_{M0}/\gamma_{M1})} \leq 1 \tag{3.30}$$

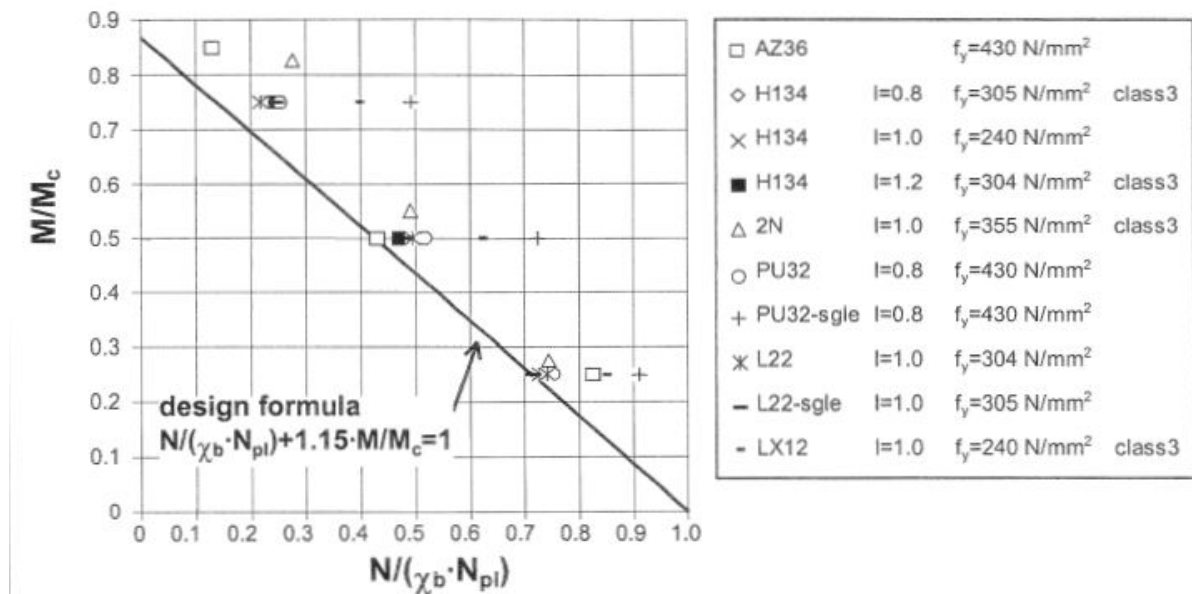


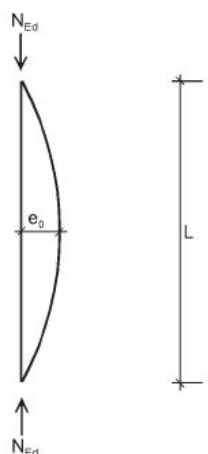
Figure 3.11: Test results of failure points by M-N interaction (figure 2.6-12 from [17])

Based on the results of appendix C, the factor k_{yy} and with that the factor 1.15 is introduced to account for the error made by the reduction factor χ_b and the second order effects to the bending moment M_{Ed} . With the current state of technology, the second order effects to the bending moment M_{Ed} can simply be determined using software ([20] and [8]). This requires only a little effort, it is usually only opting a option on or off in the program or calculation settings. If this is done, it is no longer necessary to take the second order effects into account by the use of factor k_{yy} . If k_{yy} is totally left out of account, it would be neglected that the reduction factor χ_b makes an error. In sheet piling structures, the normal force is usually in the order of 0 to 30% of the capacity ($\chi_b * N_{Rd}$). For this range of the normal force, the error made by χ_b is only small, see figure 3.10. Consequently, the design would be slightly conservative if k_{yy} is neglected, but it won't be unsafe. This means that the factor 1.15 could be removed from equation 3.30 if the second order effects to M_{Ed} are determined exactly. In other words, the bending moment M_{Ed} should not be increased with 15%. Due to the second order effect, the first order bending moment will increase usually in the order of 5 to 10% by a normal force (low normal forces). This means that the value of 1.15 can be replaced by a value of about 1.05, depending on the structure and the size of the load. If the normal force in the sheet pile increases, the enlargement of the bending moment increases as well. In theory, the enlargement of the bending moment could become more than the removed value 1.15. However, the ignored error made by the reduction factor χ_b starts to increase as well and so the overestimation made by this error will become large. If this error taken into account, the enlargement of the bending moment may be reduced. As can be seen from the experimental results presented in figure 3.11, the enlargement of the bending moment will not be larger than 15%, independent to the value of the normal force.

To conclude, the removal of the factor $k_{yy}(=1.15)$ by taking the second order effects to the bending moment into account is may be done for all values of the normal force. For large values of the normal force, where the second order effects become large, it might be more wise to use the value of 1.15 which is proven by experiments to be the upper limit of the factor k_{yy} .

3.2.2. Introducing geometrical imperfections into the model

The global buckling effect due to initial imperfections could be taken into account by applying the reduction factor $\bar{\chi}_b$ to the normal force capacity, but Eurocode 1993-1-1 section 5.3 gives an alternative. Instead of a perfectly straight sheet pile, a geometrical imperfect sheet pile could be modelled in the soil-structure model. If the model can determine the second order effects, the effect of the geometrical imperfections is embedded in the outcome of the model. The shape of this imperfection should be of the same shape of the buckling shape. The maximal geometrical imperfection is predefined by the Eurocode (see figure 3.12) based to the buckling curve (curve d for steel sheet piles) and the type of analysis [19]. As a result, the reduction factor $\bar{\chi}_b$ should not be applied and the value of the critical global buckling load F_{cr} is no longer a point of interest.



(a) Initial imperfection shape (figure 5.4 from [19])

| Buckling curve acc. to Table 6.1 | elastic analysis | plastic analysis |
|----------------------------------|------------------|------------------|
| | e_0 / L | e_0 / L |
| a ₀ | 1 / 350 | 1 / 300 |
| a | 1 / 300 | 1 / 250 |
| b | 1 / 250 | 1 / 200 |
| c | 1 / 200 | 1 / 150 |
| d | 1 / 150 | 1 / 100 |

(b) Values for initial imperfections (table 5.1 from [19])

Figure 3.12: Imperfection model according to Eurocode 1993-1-1

With a model taking geometrical imperfections into account, expression 3.31 becomes valid as a unity check for a structural element loaded by and only by a normal force. When the reduction factor $\bar{\chi}_b$ is used, expression 3.32 should be used as unity check. For several sheet pile cross sections both unity checks 3.31 and 3.32 have been conducted. For the initial imperfection e_0 a value is assumed of $e_0/L = 1/150$ (see figure 3.12b). The results are shown in table 3.2, where it comes clear that the unity check presented in equation 3.31 is more conservative as equation 3.32. Main explanation for this difference in the unity checks is that an initial imperfection e_0 of $0.0067 * L$ is used. However, from the experiments discussed in section 3.2.1 (figure 3.9) it became clear that the initial imperfection e_0 should be maximal $0.0055 * L$ for Z-profile sheet piles or $0.005 * L$ for U-profile sheet piles, but the initial imperfections may even be lower [17]. Therefore, an initial geometrical imperfection e_0 of $0.0067 * L$ is too conservative and thus equation 3.31 results in higher unity checks compared to the unity check 3.32.

$$u.c. = \frac{N_{Ed}}{N_{Rd}} + \frac{F_{cr}/N_{Ed}}{F_{cr}/N_{Ed} - 1} * \frac{N_{Ed} * e_0}{M_{Rd}} < 1.0 \quad (3.31)$$

$$u.c. = \frac{N_{Ed}}{\bar{\chi}_b N_{Rd}} < 1.0 \quad (3.32)$$

| Sheet pile profile | length (m) | N_{Ed} (kN) | Equation 3.31 | | | | Equation 3.32 | |
|--------------------|------------|---------------|---------------|----------------|----------------|------|----------------------------|------|
| | | | e_0 (mm) | e_{2nd} (mm) | M_{Ed} (kNm) | u.c. | $\bar{\chi}_b N_{Rd}$ (kN) | u.c. |
| AZ 12-700 | 10 | 1 500 | 0.0667 | 0.108 | 162 | 1.09 | 1 573 | 0.95 |
| AZ 18-700 | 10 | 2 200 | 0.0667 | 0.093 | 203 | 1.09 | 2 218 | 0.99 |
| AZ 36-700N | 10 | 3 800 | 0.0667 | 0.084 | 318 | 1.13 | 3 875 | 0.98 |
| AU 16 | 10 | 2 100 | 0.0667 | 0.096 | 202 | 1.14 | 2 194 | 0.96 |
| AU 25 | 10 | 3 000 | 0.0667 | 0.090 | 269 | 1.14 | 3 090 | 0.97 |
| Hoesch 1605 | 10 | 1 900 | 0.0667 | 0.099 | 188 | 1.09 | 1 977 | 0.96 |
| Hoesch 2605 | 10 | 3 000 | 0.0667 | 0.098 | 293 | 1.09 | 3 080 | 0.97 |
| L23 | 10 | 2 800 | 0.0667 | 0.098 | 275 | 1.19 | 2 899 | 0.97 |

Table 3.2: Unity check of normal load

Based to the above, it seems to be that the method using the reduction factor $\bar{\chi}_b$ is results in better (lower) unity checks compared to the method including the initial geometrical imperfection e_0 in the calculation. However, it is not always possible to use this method as it is meant to be. Firstly, the method with the reduction factor is derived and determined experimentally for a structural element loaded by a constant normal force. Secondly, it may not be possible to determine F_{cr} correctly for sheet piles (influence of the soil), while modelling an imperfect sheet pile in the soil-structure interaction software might be possible. As stated before, the value of F_{cr} is no point of interest if the imperfections are modelled into the soil-structure interaction model. For those two reasons, it might be useful to determine the effects of geometrical imperfections by modelling an imperfect sheet pile in the soil-structure model instead of the use of buckling reduction factor χ_b .

3.3. Conclusions to the general global buckling theory

The global buckling mechanism is a result of an interaction between the normal force in a sheet pile and displacements. This displacements are caused by either loading to the sheet pile or geometrical imperfections. To determine the second order effects of the buckling mechanism, a relation is derived between the first order displacement w^I , the normal load in the structure N_{Ed} and the critical global buckling load F_{cr} .

For displacements caused by loading, the second order effects can be determined by software (D-sheet piling, Plaxis 2D). However, in the current global buckling check for steel sheet piles, those second order effects are represented by a constant factor of 1.15 to the bending moment M_{Ed} determined without second order effects. If the second order effect to M_{Ed} is determined by software, this factor 1.15 can be neglected. In chapters 5 and 6, examples has been derived in which the factor 1.15 has been removed.

To determine the second order effects caused by geometrical imperfections, two approaches are available.

The first method is the most common in the current design practice, which uses F_{cr} to determine a reduction factor χ_b to the normal force capacity. Because this method is the most common in the current design practice, chapter 5 will solely focus on the influence of the soil to the value of F_{cr} .

A second approach to determine the second order effects of geometrical imperfections is to model a sheet pile with the geometrical imperfections, discussed in the previous section. This approach is likely to be the most convenient method to take the effect of the soil resistance against the second order effects caused by the imperfections into account. Chapter 6 describes how this method can be used for sheet piles and does describe some limitations of this method as well.

Development of the normal force in the sheet pile

Important in the global buckling mechanism or for the second order effects is the development of the normal force in the sheet pile. A typical diagram of the normal force in a sheet pile is given in figure 3.13. At the top of the pile, a normal force of 200 kN is introduced by an external vertical load. At the anchor level, just a meter below the top, the vertical anchor force is introduced and thus a jump is visible. The soil-structure friction gives that the normal force is not constant in the sheet pile. This friction is present at both sides of the pile, but the absolute value of the friction at the passive soil pressure (right side) is significantly larger than the friction at the active soil pressure (left side). Therefore, below the excavation level, the friction has a larger effect to the normal force as above and the normal force increases rapidly.

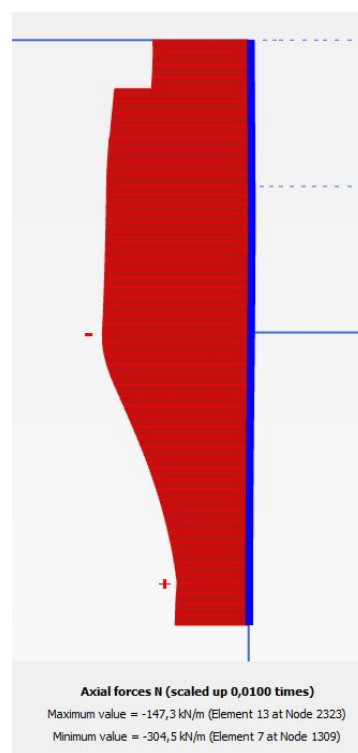


Figure 3.13: Example of normal force development in sheet piles (Figure from Plaxis 2D)

The effect of this development in the normal force to the second order effect is hard to determine by a manual method. The first method described above to approach the second order effects due to geometrical imperfections using the reduction factor χ_b , is manually derived (see appendix B), and is not able to be adapted for a non-constant normal force. So unfortunately, the acting normal force should be constant and the exact effect of the normal force as given in figure 3.13 cannot be determined by this method. As a solution, one could use the maximum occurring normal force in the diagram. In the case of figure 3.13, this would be 304.5 kN. This would lead to an overestimation of the global buckling effect, but the method will result in a safe design.

If the second approach of section 3.2.2 is used to determine the second order effects of the geometrical imper-

fections, the non-linear development of the normal force will be taken into account directly by the software used. The software will see the external force, the anchor force and the soil-structure friction as a load and will determine the effect of each load to the force distribution and deformation of the sheet pile. If imperfections are already introduced, the effect of each separate load to this imperfection is taken into account. In other words, the problem with the non-constant occurring normal force in the first approach is no problem in the second approach.

4

Global buckling in sub-soil structural elements

For free beams with known boundary conditions, known deformations and load schemes derivations are known and the mechanism of global buckling is quite well understood. When it comes to in soil founded structures, additional factors influence the global buckling behaviour and this behaviour is not known well. In the first place the resistance of the soil against bending and thus against global buckling is not taken into account by determining the buckling load. For the structure to buckle, it will have to displace the soil and so more force is required to overcome this resistance. In the second place the friction between the soil and structure influences the normal force, which is not taken into account. This chapter focuses on theories which are already known for subsoil elements.

4.1. Elastic supported beams

Figure 4.1 gives two structural beams loaded by a normal force F . The right beam is horizontally supported by two supports at both sides. The left beam is also continuous supported by horizontal springs with a spring stiffness k ($kN/m/m$), an elastic support. This horizontal support will resist against global buckling and will therefore influence F_{cr} .

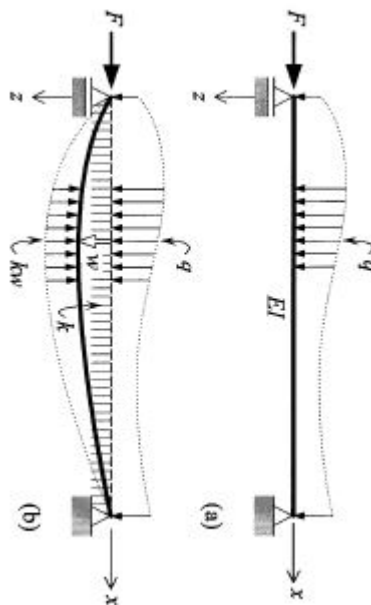


Figure 4.1: Displacement of an elastic supported beam (Left: elastically supported; Right: not elastically supported) (figure 7.20 from [16])

The elastic support as given in figure 4.1 is able to take both compression as tension forces. Soil however, is only able to take compression forces. In the case of foundation piles, soil is situated at all sides of the pile and can be modelled with an elastic support. For sheet piling structures however, only below the excavation level the soil is present at both sides and only below this level the soil can be modelled as an elastic support.

4.1.1. Derivation of critical global buckling load F_{cr}

For the derivation of the critical global buckling load, the fourth order differential equation derived in section 2.3.2 is used. This equation is given once more in equation 4.1, where the distributed load q is set to zero.

$$\begin{aligned} EI * \frac{d^4 w}{dx^4} + F * \frac{d^2 w}{dx^2} &= q - k * w \\ EI * \frac{d^4 w}{dx^4} + F * \frac{d^2 w}{dx^2} + k * w &= 0 \end{aligned} \quad (4.1)$$

The buckling shape of this elastic supported beam is assumed and sketched in figure 4.2 and described by equation 4.2. Parameter m represents the buckling mode governing in the beam. For example, the buckling shape in figure 4.2 has a value of 4 for m , the maximal displacement occurs four times in the buckling shape. Which buckling mode is governing for the structure depends on the bending stiffness of the beam and the spring stiffness of the elastic support. A higher mode results in less resistance from the elastic support (less deformation of the soil), but to more resistance from the beam itself (more bending of the structure) and vice versa. The critical buckling mode is the mode resulting in the lowest buckling load.

$$w(x) = \hat{w} * \sin\left(\frac{m * \pi * x}{L}\right) \quad (4.2)$$

Solving equation 4.1 with the displacement described by equation 4.2 results in the buckling load derived in equation 4.3. Setting the spring stiffness of the elastic support to zero, one should obtain the critical buckling load derived in section 3.1.1 for a simple, non elastic supported beam.

$$\begin{aligned} (EI * \frac{m^4 * \pi^4}{L^4} - F * \frac{m^2 * \pi^2}{L^2} + k) * \hat{w} * \sin\left(\frac{m * \pi * x}{L}\right) &= 0 \\ EI * \frac{m^4 * \pi^4}{L^4} - F * \frac{m^2 * \pi^2}{L^2} + k &= 0 \\ EI * \frac{m^4 * \pi^4}{L^4} + k &= F * \frac{m^2 * \pi^2}{L^2} \\ (EI * \frac{m^4 * \pi^4}{L^4} + k) * \frac{L^2}{m^2 * \pi^2} &= F \\ EI * \frac{m^2 * \pi^2}{L^2} + k * \frac{L^2}{m^2 * \pi^2} &= F = F_{cr} \end{aligned} \quad (4.3)$$

Approach of F_{cr} by Engesser

Based on equation 4.3, Engesser derived a formula to determine the critical buckling mode m and with that the critical buckling load. He rewrote equation 4.3 to equation 4.4 and argued that the combined terms between brackets would be minimal if the both terms are equal to each other. With this argumentation, the critical buckling mode m can be described by equation 4.5, where it should be mentioned that m should be a whole number. The critical buckling mode results in the critical buckling load described by equation 4.6, independent to the length L of the beam. In the end, the critical global buckling load by Engesser in equation 4.6 is a simplified approach of equation 4.3 by Euler. [16]

$$F_{cr} = \frac{\pi^2 * EI}{L^2} * \left(m^2 + \frac{k * L^4}{m^2 \pi^4 EI}\right) \quad (4.4)$$

$$m = \sqrt[4]{\frac{k * L^4}{\pi^4 EI}} \quad (4.5)$$

$$F_{cr} = 2 * \sqrt{k * EI} \quad (4.6)$$



Figure 4.2: Fourth buckling mode of an elastically supported beam (figure 7.21) from [16])

4.1.2. Mobilisation of the horizontal soil pressure

As already discussed in section 2.3.2, the interaction between the horizontal soil pressure and the displacement could be schematised by springs. Using this schematisation, it could be possible to use the above theory in order to determine the critical global buckling load for sub-soil elements. However, the above derived value for F_{Cr} yields for elastic supports with linear spring stiffness where the spring stiffness is independent from the displacement of the spring. For soil however, the soil pressure (modelled by a spring force) does have a limit in the minimal (active) or maximal (passive) soil pressure. The relationship between the deformation of the modelled soil and the soil stress is given in figure 4.3. This relationship makes it complex to derive a value for F_{Cr} for sub-soil structures, but, as will be seen in chapter 5, not completely impossible.

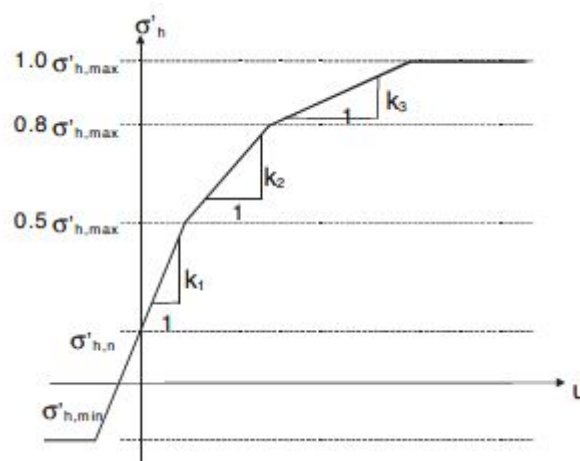


Figure 4.3: Stress-Displacement diagram (figure 33.5 from [2])

4.2. Global buckling in foundation piles

For reference the global buckling mechanism in foundation piles will be reviewed, for which other regulations applies. Dutch regulations (NEN-EN 1997-1) states that the global buckling mechanism does not has to be checked for foundation piles situated in subsoil where undrained shear strength of the soil is 10 kPa or more

[9], where the German design codes requires a minimal strength of 15 kPa [21]. Research has been done to the resistance of the soil to the global buckling mechanism, with the conclusion that the above stated boundaries of 10 kPa and 15 kPa can lead to an unsafe design [22].

Methods to determine the critical global buckling load in foundation piles are derived by Shields [21] and Vogt et al. [22]. Tests are done by Vogt et al. to compare the proposed model with the reality. The tested foundation piles are piles with a steel core, with a grout body around the core. Result is a foundation pile with a cross section combining steel and grout. Results of this tests are represented in figure 4.4 by the green dots. Also graphs are plotted for Vogt et al. (TUM, blue line), Shields and a new method. This new method is the result of a master thesis by Lankreijer [23], and is clearly the best one to fit with the tests.

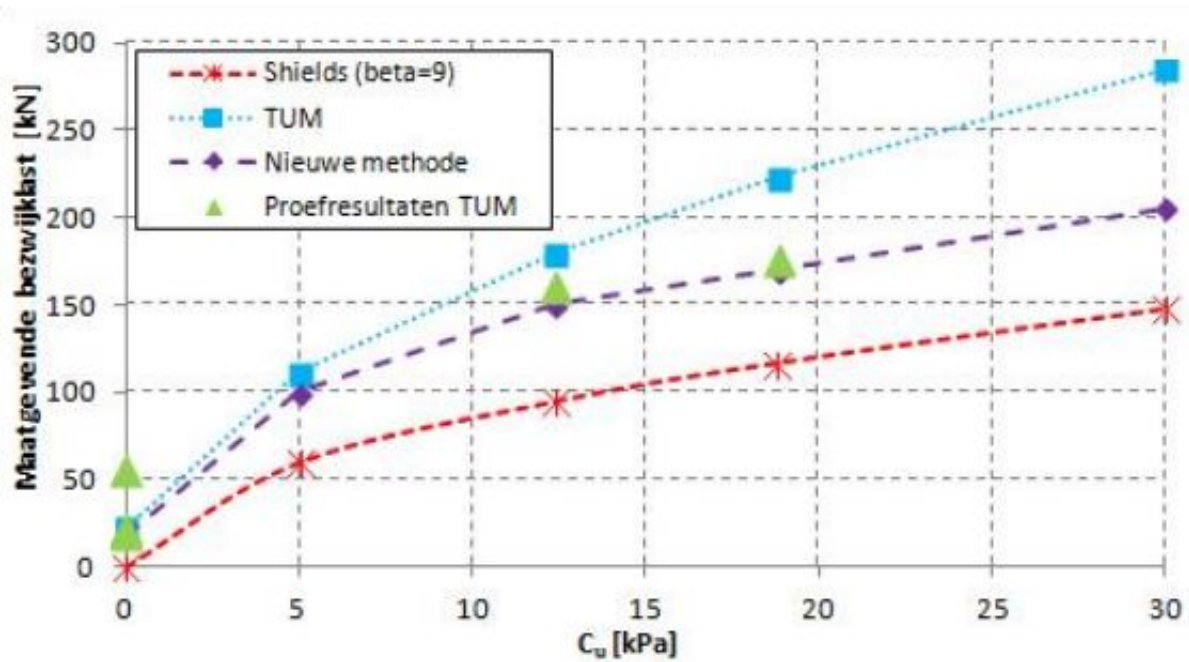


Figure 4.4: Comparison of several methods and tests for pile buckling (figure 7-1 from [23])

4.2.1. Vogt et al.

Vogt et al. made a derivation of the buckling load based on equilibrium of momentum, as drawn in figure 4.5. The derivation will be shortly discussed based on this figure.

A foundation pile is loaded by and only by a normal force. Therefore, displacements of the pile do not occur, except for possible geometrical imperfections. Those imperfections are represented by an eccentricity of the pile, $w_{0,M}$, see figure 4.5. Due to the normal force, this eccentricity will grow. With the growing eccentricity, the soil will be displaced. The resulting soil pressure can be defined as p_M , the resisting bending moment M_M can be determined based on the curvature of the foundation pile.

Where $w_{0,M}$ is the first order imperfection, $w_{N,M}$ is the second order imperfection. With little displacements of the soil, the soil reacts with a certain stiffness. When the deformation of the soil starts to grow, the stiffness of the soil will decrease. When the reduction of the stiffness starts, the resistance of the soil against buckling of the foundation pile will decrease. Therefore, the critical global buckling load will decrease if the soil stiffness decreases. For this reason, there is a maximum displacement of the sheet pile, w_{ki} , see also figure 4.6 (at the line named 'bilinear gebetteter Stab'). For this reason, the critical global buckling load can be derived using the value of this critical displacement w_{ki} for $w_{N,M}$.

$$N_{buc} = \frac{w_{N,M} \frac{\pi^2}{L_{Hw}^2} E_p I_p + \frac{1}{\pi^2} p_m L_{Hw}^2}{w_{N,M} + w_{0,M}} \quad (4.7)$$

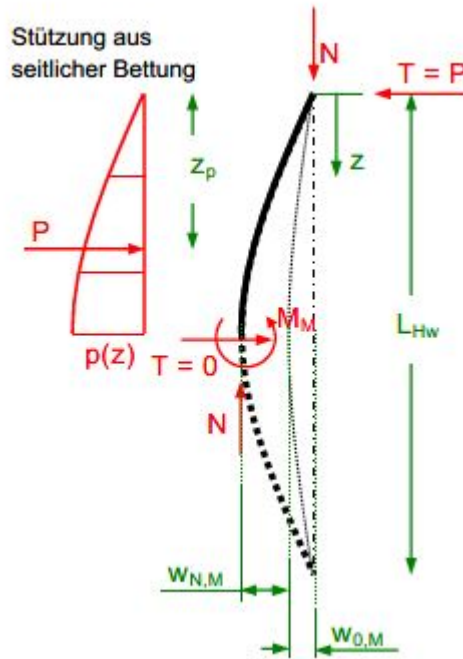


Figure 4.5: Equilibrium of momentum at buckling (figure 2 from [22])

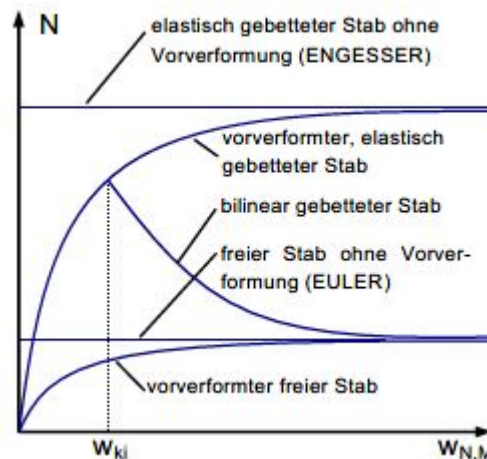


Figure 4.6: Normal force - displacement curves based on different models (figure 3 from [22])

Adaption of Vogt’s method by Lankreijer

Lankreijer showed the shortcomings of the model by Vogt. In the model of Vogt, a constant value for the bending stiffness of the foundation pile is used. However, due to crack development in the grout body of the pile, the bending stiffness reduces when the normal load grows. When this is not taken into account, an overestimation occurs of the bending stiffness and critical global buckling load. This appeared to be the most significant error by the method of Vogt. Lankreijer does put effort into the determination of the soil stiffness leading to significant better results as can be seen in figure 4.4. [23]

The error made by Vogt was mainly caused by the neglect of the cracked grout body. Because this error won’t occur in steel sheet piles, Vogt’s method should be a good approximation of the Euler buckling load of sheet piles. However, Vogt method only yields for foundation piles, not for soil retaining structures like regular sheet piling structures and is therefore only valid if the sheet pile is used as a foundation pile.

4.2.2. Shields

Shields came up with a single formula to determine the critical global buckling load based on the formula of Engesser, see section 4.1. To model the soil stiffness, Shields used a spring stiffness k of $90 \cdot S_u$, where S_u is the undrained shear strength of the soil [23]. Doing this Shields defined the buckling force capacity as given in equation 4.8 with a value of β of 19, which corresponds to equation 4.6. This factor is based on a perfect formed beam. However, just as in section 3.2, this perfect beam does not exist. In reality, the factor β lies between 8 and 14, which takes these imperfections into account [23]. In the Netherlands, it is advised to use a β value of 11 (CUR 236 [24]).

$$F_{cr} = \beta \sqrt{S_u EI} \quad (4.8)$$

5

Critical global buckling load F_{cr} of sheet piles

Based on the theories discussed in the previous chapters, two methods will be described in order to derive the critical global buckling load F_{cr} for steel sheet piles. Nevertheless, the first discussed examples will be non-realistic for the conditions of the soil or sheet piles. Though not realistic, those examples will help to explain the proposed method.

The first described method is discussed in section 5.1. This method is an analytical derivation of the critical global buckling load F_{cr} of which the derivation is based on Euler's buckling theory discussed in chapter 3. For this method, the soil-structure interaction must be described by the use of the spring model. Using this method it is possible to approach the critical global buckling load F_{cr} .

A numerical method to determine F_{cr} is introduced in section 5.2. This second method is based on the amplification factor previously discussed in section 3.1.1. This relation consists of the first order displacement, the second order displacement, Disschinger's correction factor δ , the normal force and the unknown critical normal force. With the use of available software able to determine second order effects to displacements caused by loading, the only unknowns in this relation are the critical buckling load and Disschinger's correction factor. Based on multiple examples evaluated by the software, from which the normal force and both first and second order displacements are known, those two unknowns can be determined.

Because the second, numerical, method can be used independent to the soil-structure interaction model, this method might be more interesting than the analytical method discussed firstly in section 5.1. A comparison between those methods is made in section 5.3 from which it will become clear that only the analytical method is valid to determine the critical load F_{cr} for sheet piles. Finally, in section 5.4 the proposed analytical method to derive F_{cr} for sheet piles will be compared with the method stated by the Eurocode, used in the current practice.

5.1. Method 1: F_{cr} based on Euler's buckling theory and the spring model

The soil-structure interaction of a sheet pile can be schematised by the spring model, where the soil can be modelled as an elastic-plastic support¹. Based on section 4.1, it became clear that it is possible to determine the critical global buckling load for a structure supported by an elastic support.

This section will treat the theoretical derivation of the critical buckling load of an elastic-plastic supported structural element. This will be done firstly for elastic supports without taking into account the mobilisation of the horizontal soil pressure. Afterwards, the effect of the soil pressure mobilisation will be discussed. The sensitivity of the global critical buckling load to the parameters used in the model are included as well.

Chapter 3 discusses the relevance of the critical buckling length for structures. Because the value of F_{cr} for steel structures in general can be determined quite easily using the critical buckling length, this length is historically of importance to determine the global buckling effect. Though this historical importance, this section will propose a method to determine F_{cr} without using the critical buckling length. This is done for two

¹Elastic-plastic behaviour of material, and in this case support, is the behaviour of material which is elastic for small displacements, but will be plastic for large displacements

reasons. Firstly, this length is based on the buckling shape of the sheet pile, which is significantly influenced by the subsoil. For each sheet piling structure, the buckling shape and with that the critical buckling length should be determined separately. In contrast with steel structures above the soil surface, there are no simplified equations available to determine the critical length. Secondly, with the critical buckling length, only the resistance against global buckling from the bending stiffness of the sheet pile can be taken into account. The critical buckling length does not say anything about the resistance against global buckling delivered from the soil. For those two reasons, the critical buckling length is no point of interest in the following method.

5.1.1. Derivation of the theoretical critical global buckling load for sheet piles

For the derivation of the critical global buckling load Euler's theory will be applied, see section 3.1.2. This theory has also been used for the elastically supported beam in section 4.1, so it should be possible to determine F_{cr} by Euler's theory for sheet piles using the spring model. Firstly, for the derivation of F_{cr} , the sheet pile is modelled as in figure 5.1. The excavation of the pile will be at the right side so that the soil level at the left side is at a higher level than at the right side of the pile. This gives that the pile will buckle rightwards since there is less resistance of the soil. The soil at the left side will therefore not resist against global buckling and only an elastic support at the right side is schematised. In the example of figure 5.1 soil is only present at the lower part of the pile at the right side and so only an elastic support is schematised at this lower part.

Some inconsistencies with this schematisation are made compared to the actual structural model of steel sheet piles. First of all, supports are added at both tips of the sheet pile. Secondly, the modelled elastic support at the lower half has an elastic spring stiffness k which is independent to the displacement of the pile. The non-linear behaviour of the soil pressure will be reviewed later.

Without deformation of the sheet pile and therefore the soil, the soil pressure at both sides equals the neutral horizontal soil pressure $\sigma'_{v,n}$. Once the sheet pile starts to deform, the pressure at the left (side with the higher soil surface) will deform the sheet pile to the right (at the right side, the soil surface is at a lower level). This means that the horizontal soil pressure at the left side will decrease towards the active horizontal soil pressure. Because the active soil pressure is reached with a relatively small displacement, the horizontal soil pressure at the left side is assumed to be fully active in this example. This soil pressure will be modelled as a load to the pile.

At the right side, the horizontal soil pressure will increase towards the passive horizontal soil pressure. This increase in the soil pressure is represented by the force from the elastic support to the pile and will therefore not have to be modelled as a separate load. Though the elastic support can take both compressive as tensile forces, soil can only take compressive forces. So it would seem that this schematisation is false, since it is possible that the elastic support is loaded with a tensile force. However, the soil is at both sides of the pile which gives that a tensile force of the elastic foundation represents compression of the soil at the left side of the pile². The initial, neutral horizontal soil pressure can be modelled as a load to the sheet pile. Together with the active horizontal soil pressure, the load to the sheet pile can be modelled as in figure 5.1.

²If the pile moves to the right in figure 5.1, the elastic foundation is compressed and a compressive force will occur. If the pile moves to the left, the elastic foundation is elongated and a tensile (rightward) force occurs. Because the soil at the left side is compressed with this movement, this soil generates a rightward force, in the direction of the elastic foundation force. With that, this schematisation is valid.

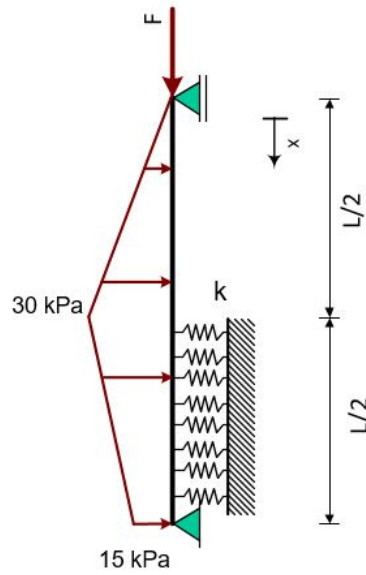


Figure 5.1: Schematisation of the sheet pile neglecting the mobilisation of the soil

Euler's theory is based to the equation of equilibrium given by expression 5.1, derived in section 2.5. In the schematisation of figure 5.1, the pile should be split up in two parts (upper and lower half), where each part has different conditions. For both parts, equation 5.1 yields and the bending stiffness EI and normal force F are equal. However, the spring stiffness k differs over both parts. Clearly, the upper half does not have any support from the soil, and so k should be set to zero. The lower half is supported horizontally by the soil and a spring stiffness k is present.

Because of the difference between the upper and lower part, the solution for the displacement w of equation 5.1 differs for both parts of the sheet pile. The solution of the upper part can be described by equation 5.2, for the lower part the solution is given by equation 5.3. This two equations contains of 8 unknowns in total (C_1 to C_8), which could be solved by the 8 conditions given expression 5.4. The first and last two conditions are to ensure that the pile does not displace or create a resisting bending moment at both pile tips. At the intersection of the two parts at $x = L/2$, both the equations 5.2 and 5.3 are valid. This gives that the four conditions at $x = L/2$ as given are valid.

$$EI * \frac{d^4 w}{dx^4} + F * \frac{d^2 w}{dx^2} + k * w = 0 \quad (5.1)$$

$$w_1 = C_1 + C_2 x + C_3 \sin\left(\frac{\sqrt{F}x}{\sqrt{EI}}\right) + C_4 \cos\left(\frac{\sqrt{F}x}{\sqrt{EI}}\right) \quad (5.2)$$

$$w_2 = C_5 e^{-\frac{\sqrt{-2EI(F+\sqrt{-4EI k+F^2})}x}{2*EI}} + C_6 e^{\frac{\sqrt{-2EI(F+\sqrt{-4EI k+F^2})}x}{2*EI}} + C_7 e^{-\frac{x\sqrt{-2EI(F-\sqrt{-4EI k+F^2})}}{2*EI}} + C_8 e^{\frac{x\sqrt{-2EI(F-\sqrt{-4EI k+F^2})}}{2*EI}} \quad (5.3)$$

$$\begin{aligned}
\text{For } x = 0: \quad & w_1(x = 0) = 0 \\
& M_1(x = 0) = 0 \rightarrow -EI \frac{d^2 w_1}{dx^2} = 0 \\
\text{For } x = L/2: \quad & w_1(x = L/2) = w_2(x = L/2) \\
& \phi_1(x = L/2) = \phi_2(x = L/2) \rightarrow -\frac{dw_1}{dx} = -\frac{dw_2}{dx} \\
& M_1(x = L/2) = M_2(x = L/2) \rightarrow -EI \frac{d^2 w_1}{dx^2} = -EI \frac{d^2 w_2}{dx^2} \\
& V_1(x = L/2) = V_2(x = L/2) \rightarrow -EI \frac{d^3 w_1}{dx^3} - F \frac{dw_1}{dx} = -EI \frac{d^3 w_2}{dx^3} - F \frac{dw_2}{dx} \\
\text{For } x = L: \quad & w_2(x = L) = 0 \\
& M_2(x = L) = 0 \rightarrow -EI \frac{d^2 w_2}{dx^2} = 0
\end{aligned} \tag{5.4}$$

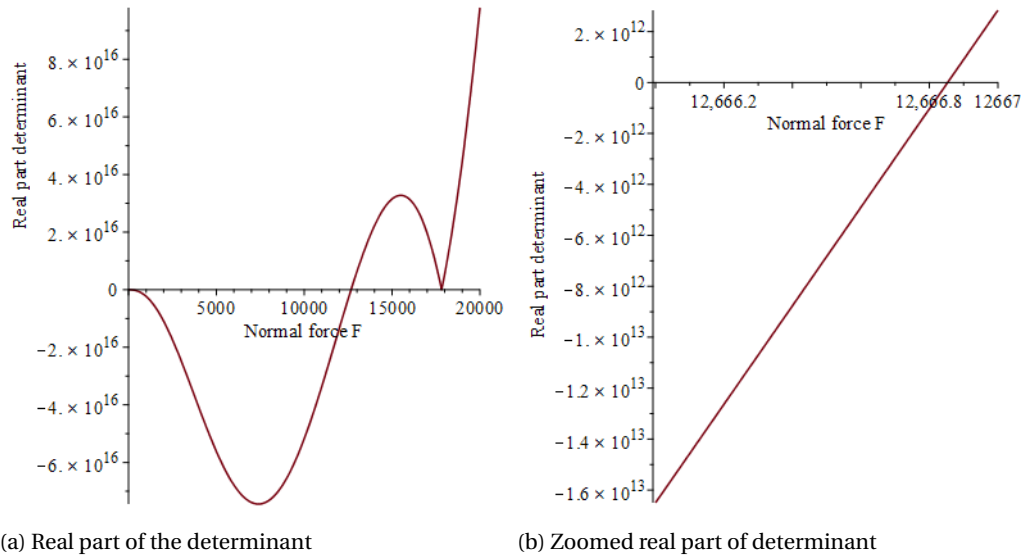
Equation 5.2 and 5.3 will be solved by the given conditions. As already discussed in section 3.1.2, all conditions as given in expression 5.4 are valid if all constants are set to zero. However, if all the 8 constants are set to zero, the displacements of w_1 or w_2 are zero, independent to x . It is known that if a structural element buckles, displacements will occur. Therefore, the solution of all constants being zero won't be a solution for the buckling problem.

As described in section 3.1.2, the 8 conditions could be rewritten into the shape of equation 5.5. By definition, a non-zero solution for the 8 constants and therefore displacement is only possible if the determinant of the coefficient matrix equals zero. Unknown parameters in this matrix are EI , k , L and F . Since EI , k and L are known, the determinant could only be set to zero by varying the normal force F . Based on this theory, the critical value F_{cr} for the normal force could be found. Below an example has been discussed, in which this method is used.

$$\text{Coefficient matrix} * \begin{pmatrix} C_1 \\ C_2 \\ C_3 \\ C_4 \\ C_5 \\ C_6 \\ C_7 \\ C_8 \end{pmatrix} = 0 \tag{5.5}$$

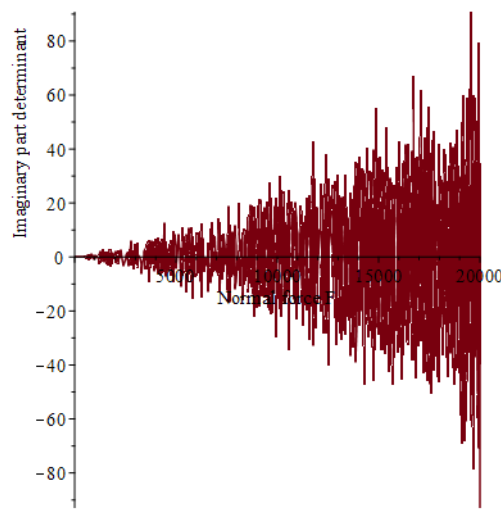
A sheet pile with a length of 10 m and profile AZ 18-700 ($EI = 79\,380 \text{ kNm}^2$) has been modelled as an example according to the model in figure 5.1. The soil stiffness of the spring foundation equals $1\,000 \text{ kN/m/m}^2$. Based on these parameters and the above given boundary conditions, the determinant of the coefficient matrix has been determined. Because of the size, the matrix has been given in (see appendix D), where also the determinant of this matrix is given. In this appendix it becomes clear how complex the derivation of the critical global buckling load F_{cr} can be. In this case, it is not possible to write a short equation to determine F_{cr} . It is more convenient to plot the determinant against the normal force. This is done in figure 5.2, from which it appears that the determinant consists of a real part and an imaginary part. The imaginary part could be ignored if this part is negligible compared to the real part of the determinant, which can be confirmed using the plots of both parts in figure 5.2.

From figure 5.2b, it is visible that the critical global buckling load equals 12 666.85 kN. In addition, the second time the determinant becomes to be zero is at 17 819 kN. For the critical global buckling load of the structure this value is not of use, but it is interesting to see that this value equals Engesser's approximation of an elastic supported structural element ($F_{cr} = 2 * \sqrt{k * EI}$, see section 4.1). This means that, mathematically, the structure buckles at this normal load because the embedded part of the sheet pile (lower half) becomes unstable.



(a) Real part of the determinant

(b) Zoomed real part of determinant



(c) Imaginary part of determinant

Figure 5.2: Determinant of coefficient matrix plotted against the normal force F

5.1.2. Mobilisation of horizontal soil pressure

In the above executed example, the soil stiffness k is independent to the displacement of the soil. However, the soil stiffness does depend on the deformation and is thus not linear (see figure 5.4). Euler's derivation of F_{cr} uses equation 5.1, which requires constant parameters and thus a constant soil stiffness. It is important to realise that the critical global buckling load F_{cr} itself is much higher (about a factor ten) than regular occurring normal load in sheet piles. The critical global buckling load is used to calculate second order effects, caused by the interaction between the normal force and displacements of the pile (see chapter 3.1). This second order effect is represented by figure 5.3, the initial displacement w_0 will grow to displacement w_1 when the pile is loaded by a normal force. Because the normal load is typically relatively small compared to F_{cr} , the growth of the initial displacement (by the second order effects) will be small as well. This small displacement will result in only a small reduction of the soil stiffness. This fact will be the crux of the solution in order to determine the influence of soil to the critical global buckling load (when the spring model is used).

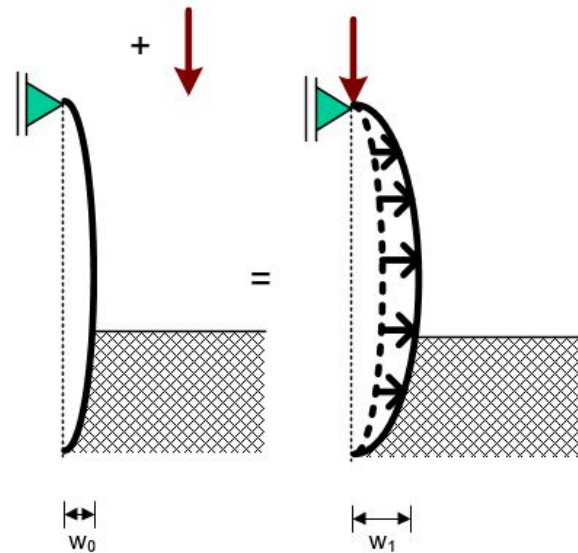


Figure 5.3: Effect of imperfections and normal force combined

When the spring model is used to model the soil-structure interaction, the modelled soil stiffness is semi-linear, see figure 5.4. The soil stiffness does only change if the soil stress grows across a certain value. In the case of figure 5.4, which is much used in the Dutch design practice [5], the soil stiffness decreases when the horizontal soil stress σ'_h reaches 50%, 80% or 100% of $\sigma'_{h,max}$ ($\sigma'_{h,max} = \sigma'_{h,passive}$). Between these three percentages, the soil stiffness k is constant, and consequently, the critical global buckling load could be derived. The extra displacement due to the second order effects will be relatively small, which means that the soil stiffness can be seen as constant according to the spring model.

For example, if the initial horizontal soil stress³ equals 35% of $\sigma'_{h,max}$, soil stiffness k_1 must be used. Due to the second order effect, the displacement of the sheet pile and with that the soil displacement will grow. A growth in the soil displacement could lead to an decrease of the soil stiffness. The soil stress should grow to more than 50% of $\sigma'_{h,max}$ for the soil stiffness to reduce, to stiffness k_2 . Such a growth of the horizontal soil stress due to second order effects is unlikely. Therefore, to determine the critical global buckling load F_{cr} , soil stiffness k_1 can be used to model a linear spring stiffness. However, if the initial horizontal soil stress equals 45% of $\sigma'_{h,max}$, it is likely that the soil stiffness changes due to the global buckling mechanism. If this happens, the soil stiffness reduces during the global buckling mechanism, but this can not be described by the critical global buckling load F_{cr} , which requires a constant elastic stiffness. To tackle this problem, the soil stiffness could be modelled with the value of stiffness k_2 instead of k_1 . If the soil stress increases from 45% to over 50% of $\sigma'_{h,max}$, the modelled soil stiffness may be too low for the part between 45 and 50%, but it is not too high for the part above 50%. For this reason, it would be wise to use spring stiffness k_2 instead of k_1 to determine F_{cr} when the initial horizontal soil stress exceeds 40% of $\sigma'_{h,max}$. Result of this approach gives that F_{cr} is not determined exactly, but approached from a safe side. For the same reason, above an initial horizontal stress of 70% instead of 80% of $\sigma'_{h,max}$, k_3 should be modelled and above an initial stress of 90% instead of 100% of $\sigma'_{h,max}$, no soil stiffness should be modelled.

The mobilisation of the horizontal soil stress, and with that the soil stiffness, is variable over the depth of the soil. This gives that the soil stiffness varies as well over the depth of the soil and several soil layers should be modelled with each a constant soil stiffness. This model is shown in figure 5.5, which does also take the horizontal support of the anchor (or strut) into account. This support is not fully rigid, but will displace when loaded. Therefore, this support should be modelled as a spring.

³The initial horizontal soil stress refers to the horizontal soil stress where the second order effects are not taken into account

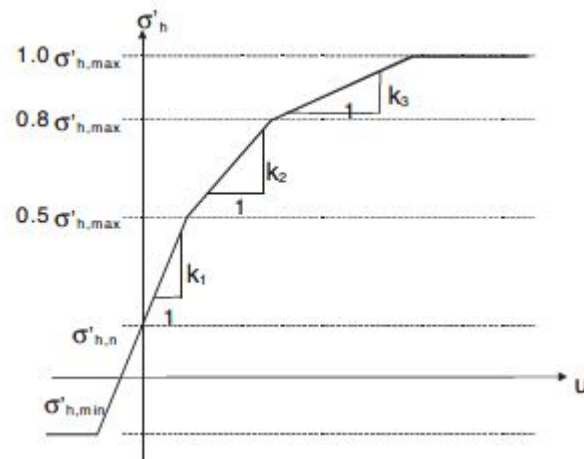


Figure 5.4: Stress-Displacement diagram (figure 33.5 from [2])

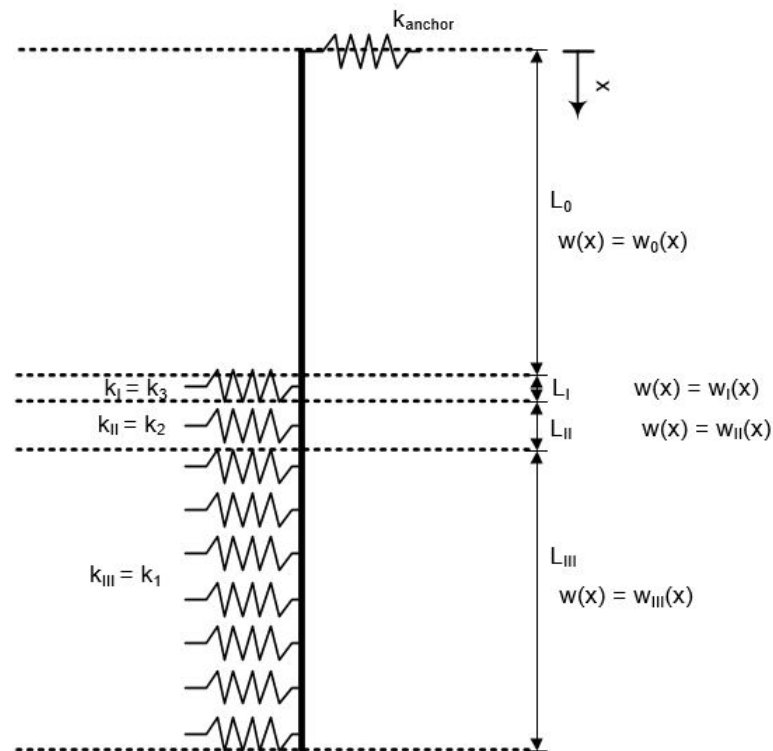


Figure 5.5: Structural model of sheet pile example

Example calculation

As an example, the sheet pile given in figure 5.6 has been evaluated with the help of the D-sheet piling software. The relevant technical details of the sheet pile, the anchor and the sand as used in the D-sheet piling model are given in table 5.1. The initial horizontal soil stress of the horizontal soil pressure is determined and given in figure 5.7a.

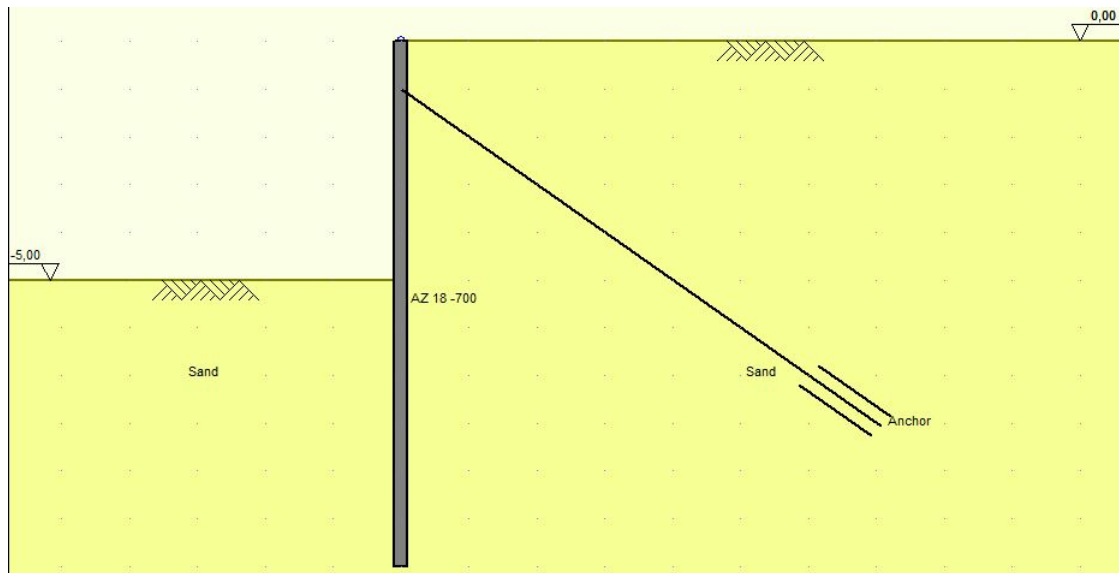


Figure 5.6: Example calculation of the global critical buckling load based on partly elastic support

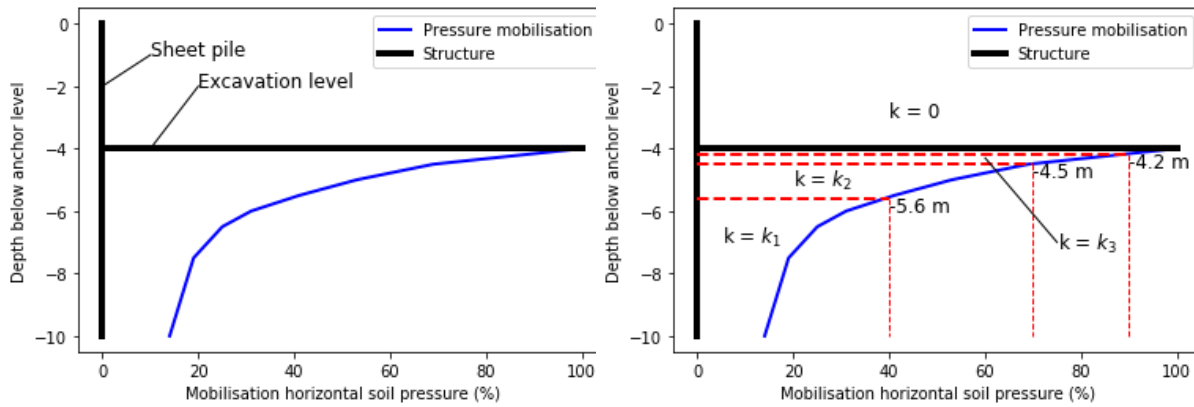
| | Property | Value | Unit |
|------------|--|----------|-----------|
| Sand | Unsaturated unit weight sand | 18 | kN/m^3 |
| | Saturated unit weight sand | 20 | kN/m^3 |
| | Cohesion | 0 | kN/m^2 |
| | Friction angle ϕ | 30 | $^\circ$ |
| | Delta friction angle δ | 20 | $^\circ$ |
| | Spring stiffness k_1 | 12 000 | kN/m^3 |
| | Spring stiffness k_2 | 3 270 | kN/m^3 |
| Sheet pile | Spring stiffness k_3 | 1 000 | kN/m^3 |
| | Profile | AZ18-700 | |
| | Bending stiffness EI | 79 380 | kNm^2/m |
| | Bottom tip level | -11 | m |
| Anchor | Level excavation | -5 | m |
| | Original surface level | 0 | m |
| | Level at sheet pile | -1 | m |
| | Axial stiffness EA | 840 000 | kN/m |
| Anchor | Length | 10 | m |
| | Angle | 45 | $^\circ$ |
| | Horizontal anchor stiffness k_{anchor} | 42 000 | $kN/m/m$ |

Table 5.1: Soil and material properties of the structure given in figure 5.6

Based on the calculations with D-sheet piling, the sheet pile was schematised as a structural element like given in figure 5.8. It is easy to see that the meter sheet pile above the anchor level is not modelled in figure 5.8. The normal force is introduced at the anchor level, and thus the top part of the pile will not be loaded by the normal force. However, due to the buckling shape of the buckling mechanism, this part might rotate towards the soil. In theory, this rotation would be resisted by the subsoil and should therefore increase F_{cr} . For simplicity of the calculation, this resistance to the global buckling mechanism.

The anchor is modelled as a spring, a spring stiffness of $42\,000\text{ kN/m/m}$ is found based on the cross sectional properties and length of the anchor⁴. The mobilisation ratio horizontal soil stress is already known from the D-sheet piling calculation and is given in figure 5.7a. Based on this ratio, the soil stiffness can be determined, figure 5.7b gives how the soil stiffness for the calculation of F_{cr} is divided over the depth of the soil.

⁴It is assumed that the other end of the anchor, deep in the soil, will not displace



(a) Ratio initial horizontal soil pressure / passive horizontal soil pressure (b) Division of soil stiffness based on the ratio initial horizontal soil pressure / passive horizontal soil pressure

Figure 5.7: Initial soil pressure mobilisation of the model

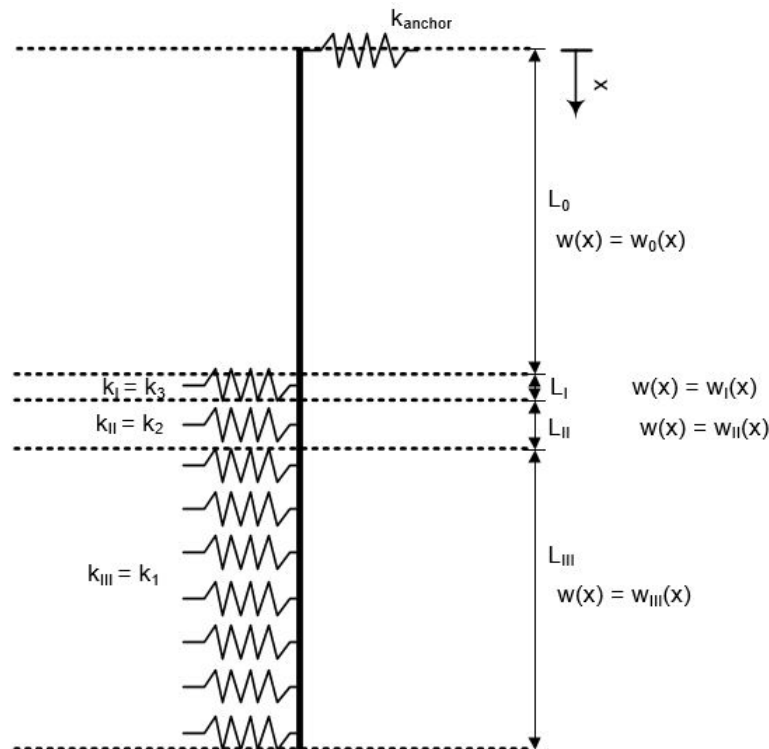


Figure 5.8: Structural model of sheet pile example

In order to find the critical global buckling load of the structural model in figure 5.8, the equilibrium equation given in equation 5.6 has to be full filled for each part of the sheet pile. Solution to this equation is given in equation 5.7 for w_0 and equation 5.8 for w_I, w_{II} and w_{III} . The lengths of L_0, L_I, L_{II} and L_{III} are, based on figure 5.7b, respectively 4.2 m, 0.3 m, 0.9 m and 4.6 m. With the 4 equations to describe the displacement of the sheet pile (1 equation for each part of the pile), there are 16 unknowns. This unknowns could be found by solving the 16 conditions stated below.

$$EI * \frac{d^4 w}{dx^4} + F * \frac{d^2 w}{dx^2} + k * w = 0 \tag{5.6}$$

$$w_0 = C_1 + C_2 x + C_3 \sin\left(\frac{\sqrt{F}x}{\sqrt{EI}}\right) + C_4 \cos\left(\frac{\sqrt{F}x}{\sqrt{EI}}\right) \quad (5.7)$$

$$w_{I;II;III} = C_5 e^{-\frac{\sqrt{-2EI(F+\sqrt{-4EI k+F^2})}x}{2*EI}} + C_6 e^{\frac{\sqrt{-2EI(F+\sqrt{-4EI k+F^2})}x}{2*EI}} + C_7 e^{-\frac{x\sqrt{-2EI(F-\sqrt{-4EI k+F^2})}}{2*EI}} + C_8 e^{\frac{x\sqrt{-2EI(F-\sqrt{-4EI k+F^2})}}{2*EI}} \quad (5.8)$$

Boundary and interface conditions:

| | | |
|--|--|--|
| $x = 0:$ $M_0(0) = 0$ $V_0(0) = 42\,000 * w_0$ | $x = 4.5 \text{ m}:$ $w_{II}(4.5) = w_I(4.5)$ $\phi_{II}(4.5) = \phi_I(4.5)$ $M_{II}(4.5) = M_I(4.5)$ $V_{II}(4.5) = V_I(4.5)$ | $x = 5.4 \text{ m}:$ $w_{III}(5.4) = w_{II}(5.4)$ $\phi_{III}(5.4) = \phi_{II}(5.4)$ $M_{III}(5.4) = M_{II}(5.4)$ $V_{III}(5.4) = V_{II}(5.4)$ |
| $x = 4.2 \text{ m}:$ $w_0(4.2) = w_I(4.2)$ $\phi_0(4.2) = \phi_I(4.2)$ $M_0(4.2) = M_I(4.2)$ $V_0(4.2) = V_I(4.2)$ | $x = L = 10 \text{ m}:$ $M_{III}(L) = 0$ $V_{III}(L) = 0$ | |

With the above 16 conditions rewritten into a coefficient matrix, the critical global buckling load F_{cr} could be found. The determinant of this matrix equals zero when the normal load F equals F_{cr} . For this example, it appeared to be impossible to calculate F_{cr} for this model with three different types of soil stiffness because of the complexity⁵. Therefore, only spring stiffness $k_{III}(=k_1)$ and $k_{II}(=k_2)$ are modelled and the resistance to buckling of the rest of the soil, with spring stiffness $k_I(=k_3)$, is neglected (see figure 5.8). The determinant is plotted against the normal force in figure 5.9, where it can be seen that the critical global buckling load equals 22 390 kN. In comparison, conform the current Eurocode for sheet piles the buckling length is set to 7 m (fixed bottom tip), resulting in a value for F_{cr} of 16 027 kN.

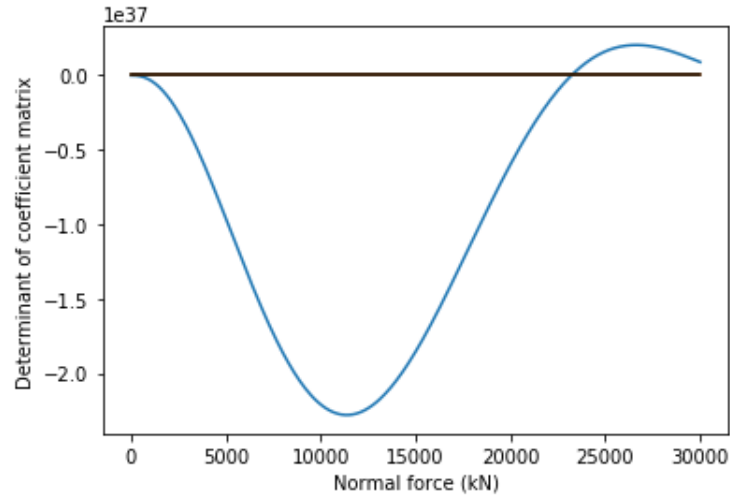


Figure 5.9: Plot of determinant against the normal force. Critical global buckling load F_{cr} equals 22 390 kN

Verification of extra stress mobilisation

At the start of the derivation, it was assumed that the second order effects of the imperfections would not increase the soil stress mobilisation in such an extent that the spring stiffness should change according to the spring model. Once the critical buckling load is known, this can simply be verified by equation 5.9 where w_I is the initial displacement of the soil.

⁵The number of terms in the determinant depends on the size of the matrix (in this case a 16x16 matrix). A n x n matrix has a determinant with n! terms. For two displacement fields (n=8), the determinant has 40 320 terms, with 3 fields it has 479 million terms and with 4 fields this equals 21 trillion (1E12) terms. As long the sheet pile is not elastically supported, most of the terms cancels because of the relatively simple equation (see equation 5.7, w_0). When an elastic support is introduced, the terms becomes more complex and less terms cancels (but still far most of the terms fall out). This makes it hard to impossible to determine the theoretical critical buckling load for models with more than two different kind of soil stiffness values.

The value of F_{cr} is determined to quantify the effect of the geometrical imperfections in the sheet pile. In corresponding with section 3.2.2, the maximal geometrical imperfection e_0 in equation 5.9 should be set to 66.67 mm ($e_0 = L/150$). If the normal force is set to 400 kN (additional external loading), the maximal imperfection grows to $e_{2nd,order} = 67.88$ mm. Because the exact buckling shape is unknown, it is unknown where the maximal imperfection occurs. Therefore, it is assumed that the growth of the imperfection may be 1.21 mm all along the pile. It is possible to use FE-software to find the precise critical buckling shape and load, but this will be discussed later. If this is done, the exact value of the imperfection at the point of interest can be determined.

The question is that if the soil may be modelled with the soil stiffness which is assumed. In the above example, it is assumed that for the soil at 5.4 m and more below the anchor, the stiffness may be set to 12 000 kN/m³ (k_1). With a growth of the imperfection of 1.21 mm, the horizontal soil pressure grows with 14.57 kPa. At 5.4 m below the anchor, the mobilisation ratio horizontal soil stress equals 39%. With an increase of 14.57 kPa, this ratio would have a value of 50%, and so soil stiffness k_1 may be modelled for the soil lower than this point. Above this level, the soil should be modelled using k_2 because the soil pressure will be more than 50% of $\sigma'_{h,max}$. This means that the found critical buckling load of 22 390 kN can be used as an approach to the actual critical buckling load F_{cr} .

$$e_{2nd,order} = \frac{1}{1 - n^{-1}} * e_0 \quad (5.9)$$

To conclude, it is possible to take the resistance of the soil into account in the determination of F_{cr} . When the soil displacement increases due to the buckling mechanism such that the soil stiffness decreases to another, lower, modelled soil stiffness, this lower soil stiffness should be used in the derivation. If this is done, the found value for the critical buckling load is a safe side approximation of the actual critical buckling load.

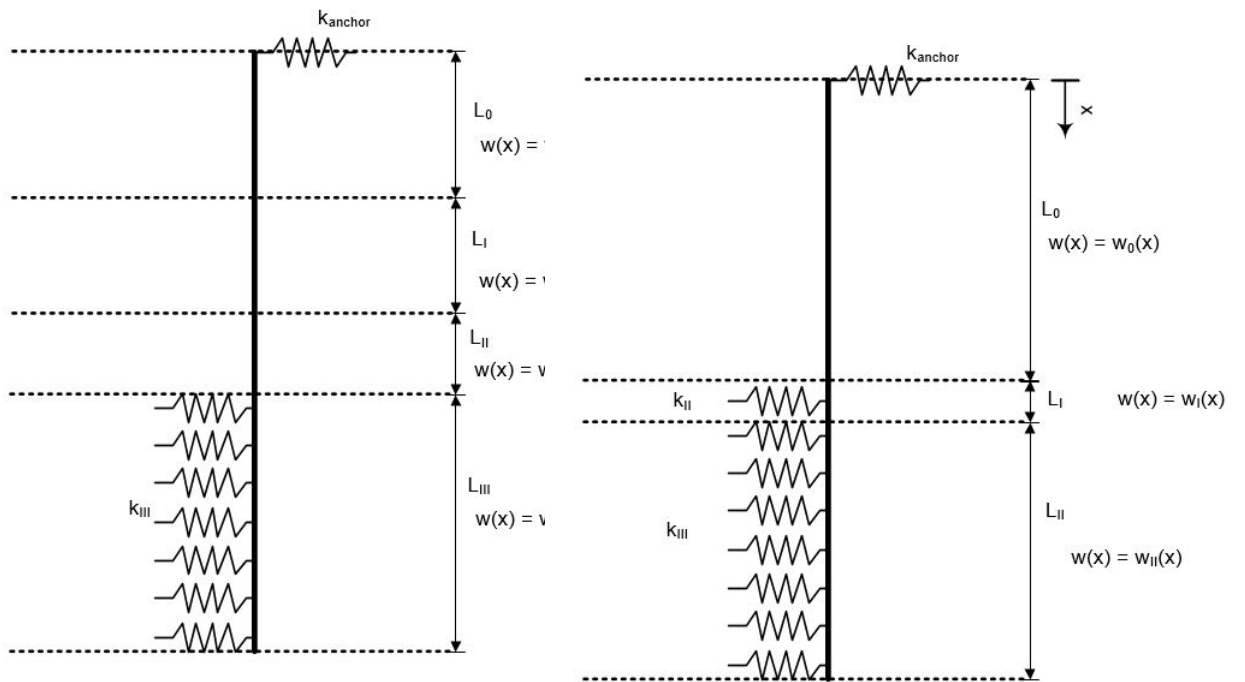
5.1.3. Parametric determinant coefficient matrix

The above example has been done with known parameters. Based on this calculation, it is known that it takes a long time to calculate the determinant of the coefficient matrix. Besides, the scripting of the formula's requires significant time as well and is prone to errors. Therefore, the determinant of the coefficient matrix has been determined parametric for the two models in figure 5.10. The model of figure 5.10a is capable to take into account 4 different stiffness values EI for the sheet pile into account and can model only 1 soil stiffness. The model in figure 5.10b can model 3 different stiffnesses for the sheet pile and 2 different values for the soil stiffness. This parametric model will be used in section 5.1.4 to determine the importance of the input parameters to the value of F_{cr} . More complex models were not derived by hand because it was impossible to run the derivation of the parametric formula.

Determining critical load with FE-software

To determine the critical global buckling load for more complex cases, it is possible to run a buckling analysis with structural finite element analysis (FEA) tools. In this report, the FEA-program Diana FEA is used to model the sheet pile and the spring supports like modelled in figure 5.8. In principle, such a program is able to analyse the most complex schemes with many different soil stiffnesses and bending stiffnesses of the sheet pile. The limitation is rather on the time to put the data into the program as in the calculation time of the model.

In appendix F the FEA model is given for the example in section 5.1.2. Based on the model of the previous example a stability analysis was done, which has shown a critical global buckling load of 22 369 kN, just 21 kN off from the value which was found with Euler's theory. The buckling shape of the structure is shown in figure 5.11. In addition, the soil stiffness which was ignored before (k_3) is added to the calculation using Diana FEA, which returns a critical global buckling load of 22 627 kN (+1.15%).



(a) 1 elastic stiffness value, 4 sheet pile stiffness values (b) 2 elastic stiffness values

Figure 5.10: Structural model for the critical buckling load calculation/approach of a sheet pile

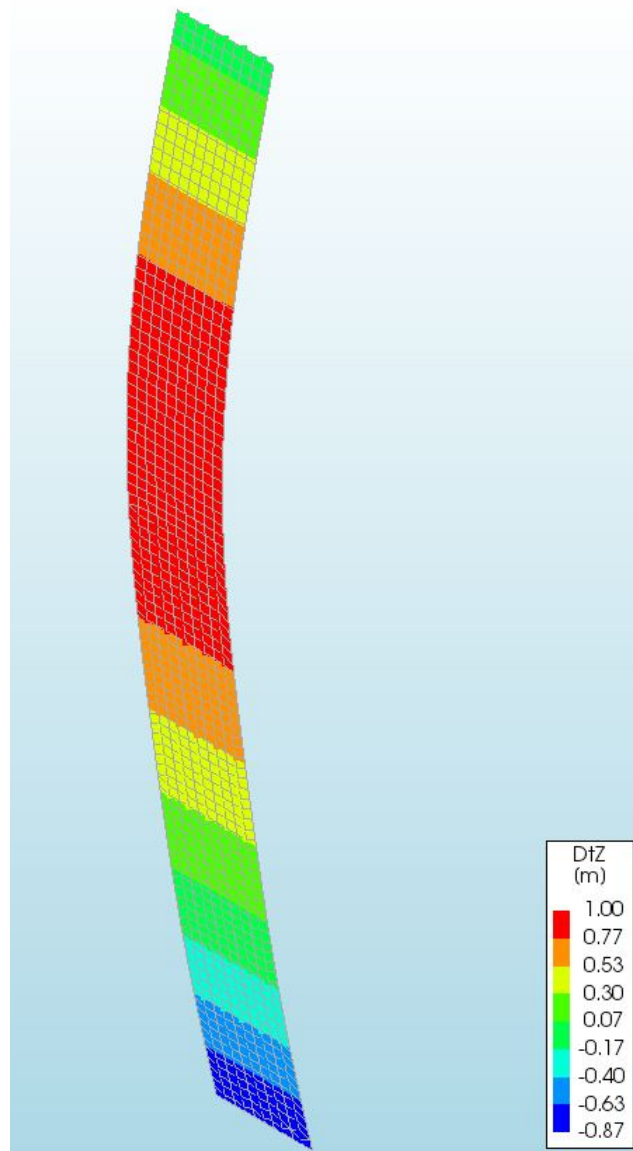


Figure 5.11: Buckling shape computed by Diana FEA

With the use of Diana FEA, more complex models can be analysed. In the example above, the part of the sheet pile above the anchor level was neglected. However, because this part will rotate into the soil due to the global buckling mechanism, the soil around this part of the pile will resist against global buckling as well. Because of the complexity, this was cancelled in earlier calculations. With the use of Diana FEA, this could be taken into account easily. This is done according the structural model given in figure 5.12. The soil stiffness k_{top} was set to $12\,000\text{ kN/m/m}^2$. This structural model has, based on calculations with Diana FEA, a value of F_{cr} of $23\,519\text{ kN}$, which is just 4% more compared to the value of F_{cr} found without the top part taken into account. Besides, it's questionable if the soil stiffness of $12\,000\text{ kN/m/m}^2$ is present at this level in the soil. Because the soil is shallow at this location, the maximal horizontal stress is quickly reached, resulting in not much resistance of the soil. If one takes the resistance of this part of the soil into account, it should be done with care.

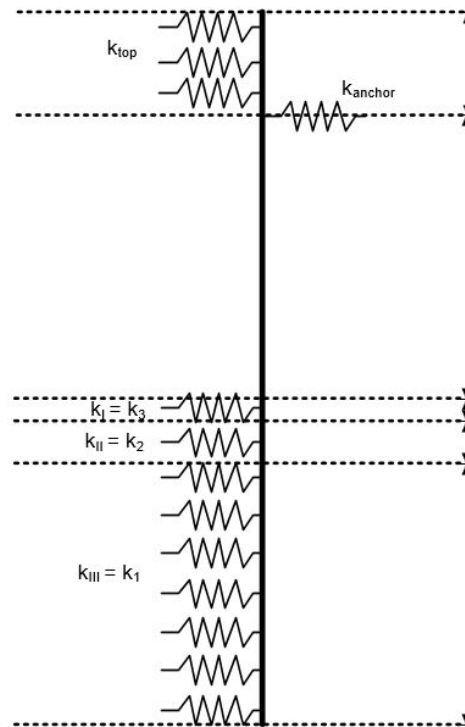


Figure 5.12: Structural model of sheet pile in figure 5.6

5.1.4. Parameter sensitivity analysis

The model presented in section 5.1.2 requires 4 input values: the anchor stiffness, the bending stiffness of the sheet pile, the soil stiffness and the length of the sheet pile. Because the parameters may be uncertain during the design, this section treats the sensitivity of F_{cr} to the stiffness parameters. The length is assumed to be known and certain, therefore the sensitivity of the critical buckling load to the length of the sheet pile is left out of account.

The value of the critical global buckling load is based on the stiffness of the system. Three different types of stiffness are influencing the value. If one of the three stiffnesses reduces and the other two stiffnesses remain constant, it should be expected that the critical global buckling load reduces as well, but less strongly since it is also dependent two the other two stiffnesses.

The influence of the parameters is determined by varying the parameters with a certain deviation around the mean value. For a large amount of values for the parameters the value for F_{cr} is calculated for the example of section 5.1.2. In total, 1 000 calculations have been done for each parameter. Based on this set calculations, the sensitivity of the critical global buckling load to the parameter can be determined.

Influence of soil stiffness

The example of section 5.1.2 has been used to determine the sensitivity of the critical global buckling load. The soil stiffness has been varied around its original values of $12\,000\text{ kN/m}^2$ and $3\,270\text{ kN/m}^2$ (for k_1 and k_2 respectively) by a reduction factor. The reduction factor has a mean of 1.0 and standard deviation of 0.05. Thousand random numbers based on this distribution are plotted in figure 5.13. For each of these 1 000 values, the soil stiffness has been determined and with that the critical buckling load is determined. This load has been divided by the mean value found in section 5.1.2 ($22\,390\text{ kN}$) in order to plot its normal distribution in figure 5.13. The mean of this distribution equals 1.0, the value of the standard deviation is 0.0276.

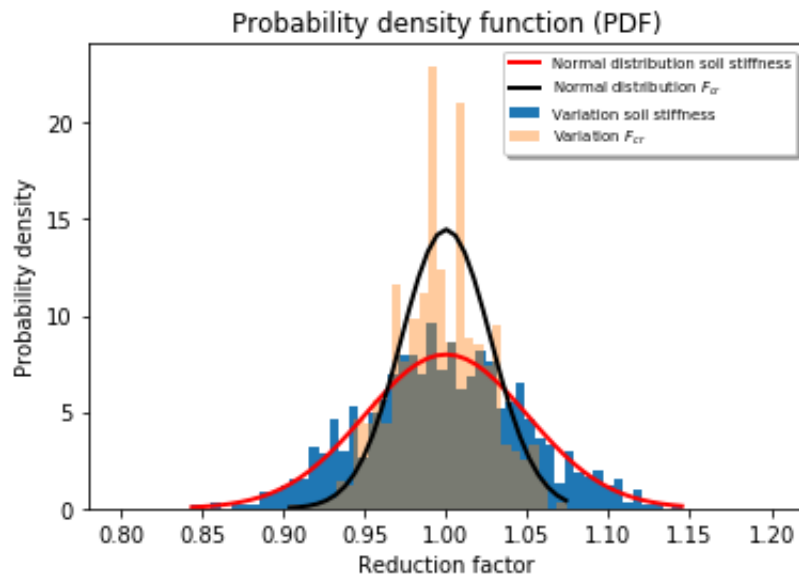


Figure 5.13: Normal distribution of soil stiffness and critical buckling load with varying soil stiffness as input

Influence of bending stiffness

The bending stiffness has been varied similar to the soil stiffness with a variable reduction factor normally distributed with a mean of 1.0 and standard deviation of 0.05. The values for the critical normal force, divided by the critical force found in section 5.13, were found to be normal distributed around 1.0 with a standard deviation of 0.0210.

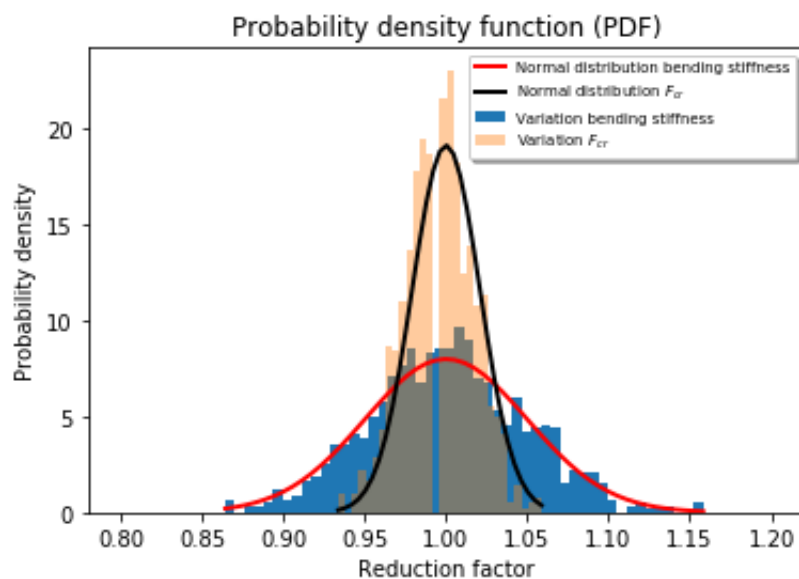


Figure 5.14: Normal distribution of bending stiffness and critical buckling load with varying bending stiffness as input

Influence of anchor stiffness

At last the influence of the anchor stiffness has been determined with the same normal distribution as the previous two parameters. As visible in figure 5.14, the critical buckling load is only very limited influenced by the anchor stiffness. When the anchor stiffness deviates with a standard deviation of 5%, the critical buckling has a standard deviation of 0.03%. Even with a reduction of 50% to the anchor stiffness, the critical buckling load reduces with only 0.67%.

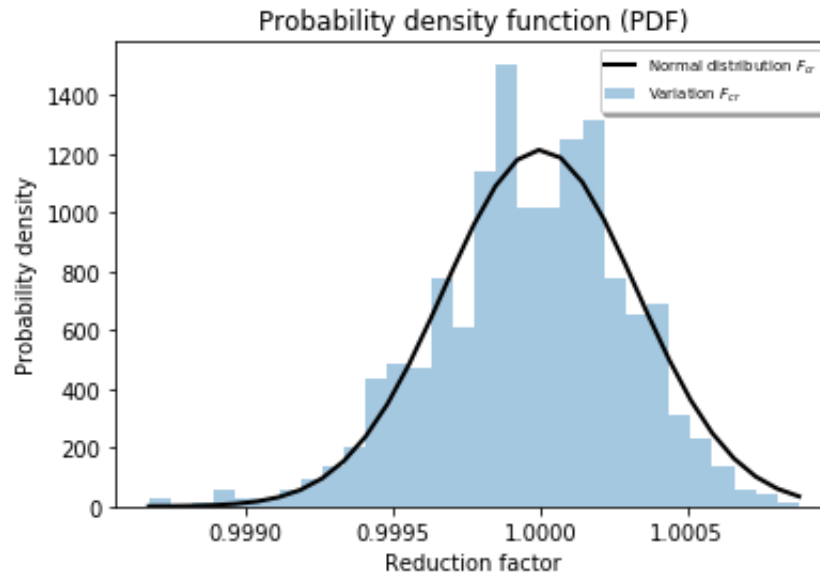


Figure 5.15: Normal distribution of bending stiffness and critical buckling load with varying bending stiffness as input

Conclusion of sensitivity analysis

As seen, the critical global buckling load depends strongly to the bending stiffness of the sheet pile and the soil stiffness. The anchor stiffness however has only very limited impact. Before the results were presented the expectation was stated that the reduction to the critical global buckling load would be less than the reduction to the stiffness. Based on the results, this is indeed the case.

It is important to realise that the found sensitivity is only valid for this particular case. For another set of parameters, the sensitivity is likely to be different.

5.2. Method 2: F_{cr} based on first and second order displacements

The method derived in the previous section is unfortunately only available if the spring model is used to model the soil-structure interaction. For other models, this section proposes a numerical method to find F_{cr} , based on the relationship between the critical buckling load F_{cr} , the acting normal load N_{Ed} , the first order displacement w^I and the second order displacement w^{II} . In this section, examples are used to explain the method. Those examples are not representative for sheet piling structures. In section 5.3, it will be reviewed if this numerical method is valid or not for sheet piles.

Section 3.1.1 introduced the relationship between the critical buckling load F_{cr} , the acting normal load N_{Ed} , the first order displacement w^I and the second order displacement w^{II} . As reminder, this relation is presented again in equation 5.10 including Dischinger's correction factor δ . In theory, the critical buckling load could be determined based on equation 5.10 if the other parameters are known (N_{Ed} , w^I , w^{II} and δ).

$$w^{II} = w^I \frac{1 + \delta n^{-1}}{1 - n^{-1}} \quad (5.10)$$

Relation 5.10 is rewritten in equation 5.11 resulting in a function for F_{cr} . This equation includes Dischinger's correction factor δ , which is unknown. Because the value of δ is unknown, the determination of F_{cr} is less straightforward than it might seem.

$$\begin{aligned}
\frac{w^{II}}{w^I}(1 - n^{-1}) &= 1 + \delta n^{-1} \\
\frac{w^{II}}{w^I} - 1 &= n^{-1}(\delta + \frac{w^{II}}{w^I}) \\
n^{-1} &= \frac{w^{II}/w^I - 1}{w^{II}/w^I + \delta} \\
n &= \frac{w^{II}/w^I + \delta}{w^{II}/w^I - 1} \\
F_{cr} &= \frac{w^{II}/w^I + \delta}{w^{II}/w^I - 1} N_{Ed}
\end{aligned} \tag{5.11}$$

The displacements w^I and w^{II} can be calculated using software or manually in the case of relatively simple structures. When a value is assumed for δ (for example 0.00), the critical buckling load can be calculated. Doing this for multiple values for N_{Ed} , multiple values for F_{cr} will be found. Based on those multiple values, the average could be used as a value for F_{cr} . For each acting normal force N_{Ed} , the found value for F_{cr} will deviate from the average value. Of all this deviations, an average error should be determined. To minimise this error, δ should be varied⁶ for a certain range of values. From every different value for δ , a value for F_{cr} and the error will be found. The F_{cr} belonging to the minimal error should be the value for the critical global buckling load. Examples are executed to show this method.

5.2.1. Example of the method

To support the above theory, an example with the beam given in figure 5.16 is worked out. The beam is supported at both ends with a rigid support and with a spring foundation in between (parameters given below). Though this is not a sheet pile, it does give a relatively simple insight of the theory proposed above. Besides, the critical global buckling load could be determined with existing buckling theories and therefore this proposed method could be verified.

The beam in the example is loaded with a distributed load of 100 kN/m causing a parabolic deformation given in figure 5.17 (first order displacement)⁷. When the beam is loaded by a normal force N_{Ed} , the displacements of the beam will grow with the second order effects. For a normal force of 2 000 kN, the second order displacement is given in figure 5.17. For 15 values of the normal force (ranging from 1 000 kN to 15 000 kN) the critical global buckling load is determined, of which the results are given in table 5.2. The values of the displacement given in this table were calculated manually, the calculation is given in appendix E.1. Due to the precision of the displacement (5 decimals are known), it is possible to calculate F_{cr} quite precisely. In total, the calculations are done for 2 000 values for δ . For each of the 15 values for the normal load, the value of F_{cr} has been determined based on the found data (6th column in table 5.2). The error between this value and the average value of F_{cr} is given by the 7th column of the same table. For all 2 000 values of δ , the average error is plotted in figure 5.18. From this figure, it can be seen a correction factor δ of 0.006 results in a minimal error. The average found critical buckling load equals 17 955.6 kN with an average error of just 0.08‰ (last column of the table).

⁶Variation should be done for a large set of δ values. This can be done by and only by a powerful calculation tool. For this examples, Python has been used to run the calculation

⁷Calculation of deformations are given in appendix E.1

$EI = 79\,380\text{ kNm}^2$ (Sheetpile profile AZ18-700)

$k = 1\,000\text{ kN/m}^2$

$L = 10\text{ m}$

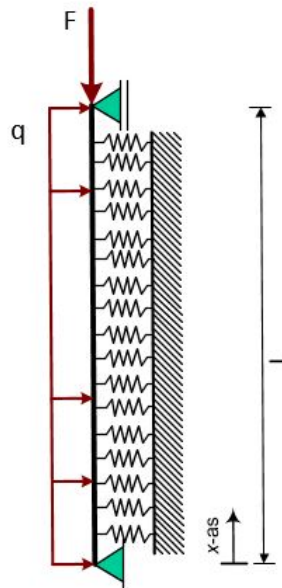


Figure 5.16: Example A: Elastic founded beam loaded by a distributed load of 100 kN/m

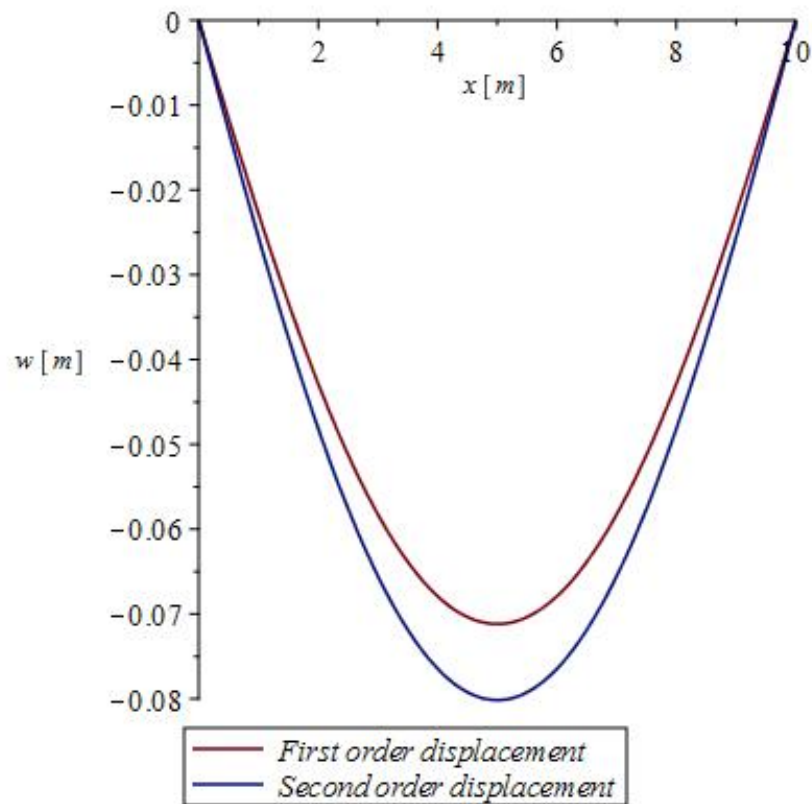
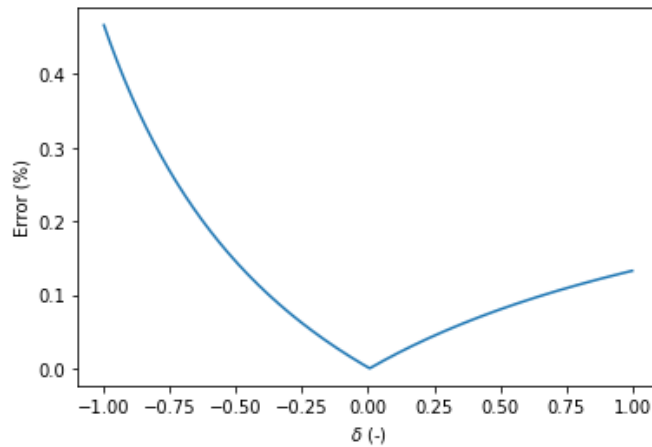


Figure 5.17: First and second order displacement of the example, loaded by a normal force of $2\,000\text{ kN}$

| N_{Ed} (kN) | w^I (mm) | w^{II} (mm) | w^{II}/w^I | n | F_{cr} | Error (‰) |
|---------------|------------|---------------|--------------|---------|----------|-----------|
| 1 000 | 71.18115 | 75.40399 | 1.059 | 17.957 | 17 957.4 | 0.10 |
| 2 000 | 71.18115 | 80.15667 | 1.126 | 8.978 | 17 956.3 | 0.04 |
| 3 000 | 71.18115 | 85.54544 | 1.202 | 5.985 | 17 955.5 | 0.01 |
| 4 000 | 71.18115 | 91.70697 | 1.288 | 4.489 | 17 954.8 | 0.04 |
| 5 000 | 71.18115 | 98.82012 | 1.388 | 3.591 | 17 954.2 | 0.07 |
| 6 000 | 71.18115 | 107.12351 | 1.505 | 2.992 | 17 953.8 | 0.10 |
| 7 000 | 71.18115 | 116.94281 | 1.643 | 2.565 | 17 953.7 | 0.11 |
| 8 000 | 71.18115 | 128.73441 | 1.809 | 2.244 | 17 953.7 | 0.09 |
| 9 000 | 71.18115 | 143.15828 | 2.011 | 1.995 | 17 953.9 | 0.07 |
| 10 000 | 71.18115 | 161.20580 | 2.265 | 1.795 | 17 954.3 | 0.03 |
| 11 000 | 71.18115 | 184.43752 | 2.591 | 1.632 | 17 954.9 | 0.01 |
| 12 000 | 71.18115 | 215.46026 | 3.027 | 1.496 | 17 955.8 | 0.08 |
| 13 000 | 71.18115 | 258.98028 | 3.638 | 1.381 | 17 956.9 | 0.08 |
| 14 000 | 71.18115 | 324.44976 | 4.558 | 1.283 | 17 958.3 | 0.15 |
| 15 000 | 71.18115 | 434.06564 | 6.098 | 1.197 | 17 960.0 | 0.25 |
| | | | | Average | 17 955.6 | 0.08 |

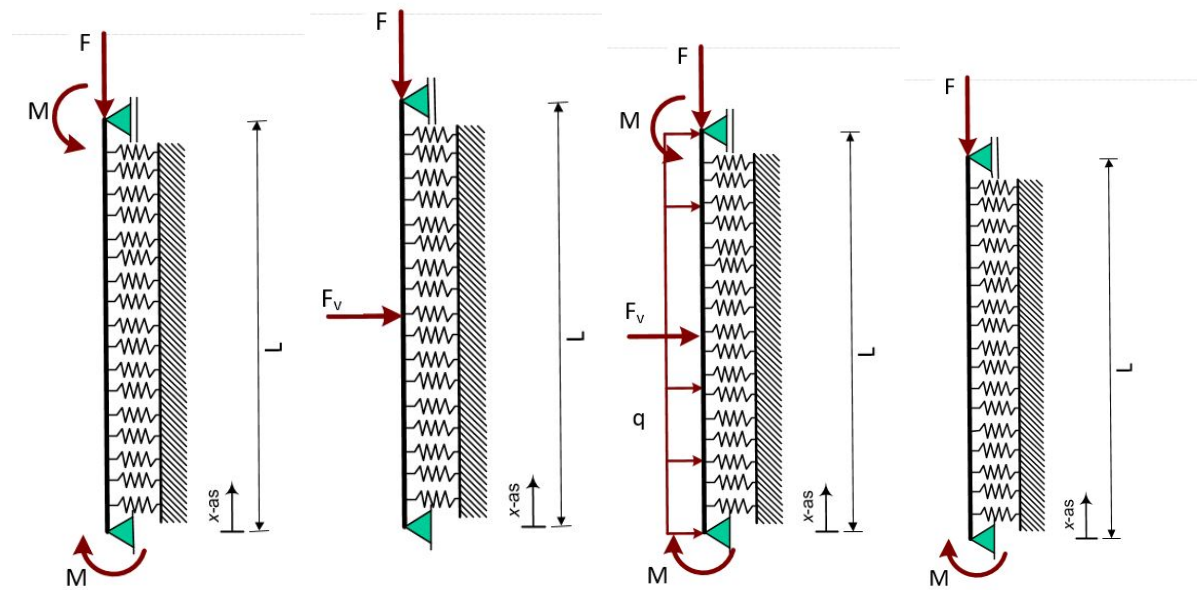
Table 5.2: Determination of critical buckling load of the beam in figure 5.16 based on displacements with a δ correction factor of 0.006Figure 5.18: Errors for different correction factors δ

In section 4.1 the theoretical critical buckling load was derived for a structure similar to the structure in figure 5.16 and equation 5.12 was found. Using this equation for the above example, a critical buckling load of 17 967 kN is found. Compared with this value, the critical buckling load found based on displacements is just 11.3 kN or 0.6‰ off.

$$EI * \frac{m^2 * pi^2}{L^2} + k * \frac{L^2}{m^2 * pi^2} = F = F_{cr} \quad (5.12)$$

In the above example, the proposed method offers a good approach for the critical global buckling load. Before more conclusions are made to this proposed method, more examples are discussed. In appendix E 4 other examples are given, of which the lay-out is given in figure 5.19 and results are given in table 5.3. For comparison, the example given above (example A) is given as well in this table.

From the results it is visible that the 5 load cases give different results, but are well centred around the theoretical critical global buckling load of 17 967 kN. The maximal error of the calculated critical buckling load is 0.48%. If the average value is taken from the 5 calculations, the critical load becomes 17 973.9 kN, which is just 7 kN or 0.04% off from the actual value.



(a) Example B: Loaded by two moments of 100 kNm
 (b) Example C: Loaded by a point load of 100 kN
 (c) Example D: Loaded by a point load of 100 kN, a distributed load of 10 kN/m and two moments of 100 kNm
 (d) Example E: Loaded by a single moment of 100 kNm

Figure 5.19: Several load cases for the determination of the critical global buckling based on displacements

| Example | Loading | Initial displacement (mm) | Critical global buckling load (kN) | δ | error F_{cr} with average (%) | error F_{cr} with reality (%) |
|---------|--|---------------------------|------------------------------------|----------|---------------------------------|---------------------------------|
| A | $q = 100 \text{ kN/m}$ | 71.18115 | 17 955.6 | 0.006 | 0.08 | -0.06 |
| B | $M = 100 \text{ kNm}$ | 6.59123 | 17 880.2 | 0.051 | 0.72 | -0.48 |
| C | $F_v = 100 \text{ kN}$ | 11.6534 | 17 998.4 | -0.024 | 0.26 | 0.18 |
| D | $M = 100 \text{ kNm}$ $F_v = 100 \text{ kN}$ $q = 10 \text{ kN/m}$ | 25.3627 | 17 954.7 | 0.004 | 0.01 | -0.07 |
| E | $M = 100 \text{ kNm}$ | 3.7427 | 17 992.2 | -0.07 | 0.98 | 0.14 |

Table 5.3: Results of the various examples in figure 5.19

5.3. Comparison of method 1 and method 2

In the previous two sections, two methods are proposed in order to derive the critical global buckling load F_{cr} . The first method, based on Euler's derivation, gives good results and is compatible with the spring model as soil-interaction model. However, this model is not always used as soil-structure interaction model and thus it is not always possible to define F_{cr} with this model. For other soil interaction models, the second proposed method might be an outcome. However, the correctness of this method has only been confirmed for quite simple structures, not for sheet piles. This section compares both methods and will answer the question if the second method may be used for steel sheet piles.

Figure 5.20 shows an adaption of figure 5.1 to schematise a sheet pile more realistic, but the reduction of the soil stiffness k is still neglected in this example. This is done such that the method based on Euler's derivation does not approach the value of F_{cr} ⁸, but calculates the value exactly. The soil stiffness is modelled as a spring support with a variable full elastic spring stiffness, the anchor is modelled as a spring with a stiffness of 42 000 kN/m/m. Results are given in table 5.4 for three sets of parameters. The data used for the second method,

⁸The first method based on Euler's derivation uses at some places lower values for the soil stiffness as actual present. This gives that the value of F_{cr} is not determined exactly but approached if the variability of the soil stiffness is taken into account.

where F_{cr} is based on calculated displacements, is given in appendix E.3.

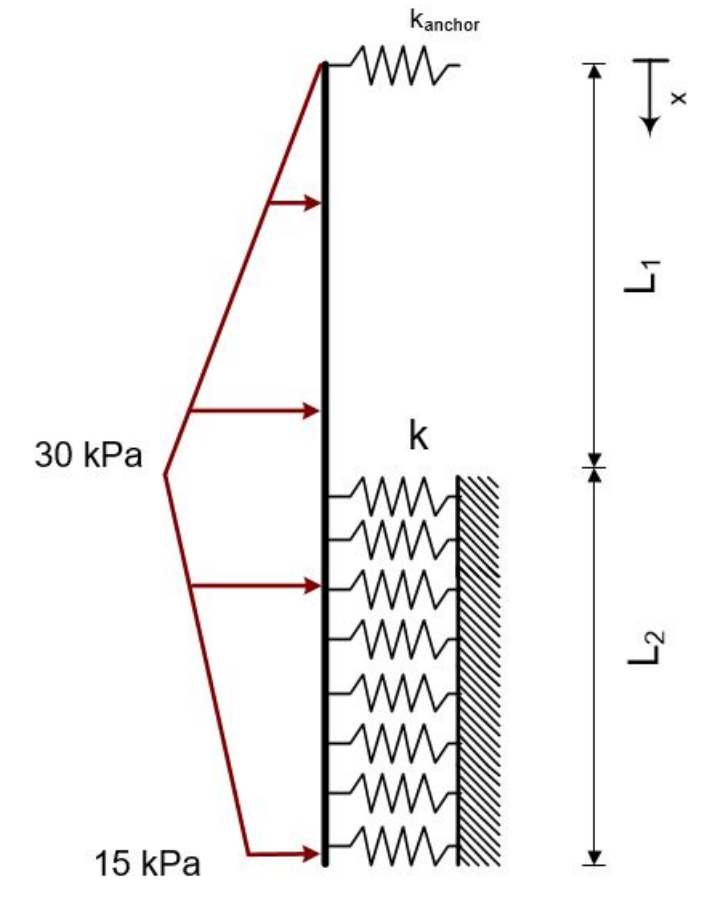


Figure 5.20: Sheet pile lay-out to compare the theoretical method with the method based on displacements

While for parameter set 2 both methods give a similar result (differential of 1.6%), parameter set 1 gives a large error of 17.3% where set 3 gives an even larger error of no less than 35.8%⁹. The critical global buckling load derived by Euler’s method is known to be correct [16]. Therefore, the value of F_{cr} can be trusted when it’s derived by the first method. Apparently, the second proposed method which uses displacements to find F_{cr} results in wrong numbers for sheet piles.

| Parameter set | L_1 (m) | L_2 (m) | EI (kNm^2) | k ($kN/m/m^2$) | F_{cr} based on displacements (kN) | δ correction factor for displacement method | F_{cr} based on Euler’s theory (kN) |
|---------------|-----------|-----------|------------------|--------------------|--------------------------------------|--|---------------------------------------|
| 1 | 5 | 5 | 79 380 | 1 000 | 9 720 | -0.745 | 8 285 |
| 2 | 5 | 5 | 79 380 | 12 000 | 24 372 | -0.350 | 23 985 |
| 3 | 5 | 10 | 79 380 | 1 000 | 11 267 | -0.474 | 8 295 |

Table 5.4: Results of both methods for different parameter sets

For the example in section 5.2 the value for F_{cr} based on displacements (method 2) approached the exact value of F_{cr} pretty well. This is in contrast with the discussed example in this section, which gave poor results. Important difference is that both ends of the beam in the example of section 5.2 are fixed and can not move,

⁹Though the sheet pile with parameter set 3 is much more embedded in the soil, the critical global buckling force is hardly affected compared to parameter set 1. Because the sheet pile gets longer, the steel resists less against global buckling in set 3 than in set 1. Because more soil must be displaced, the soil resists more against global buckling in set 3 than in set 1. Apparently, the reduction in steel resistance is more or less equals the raise in soil resistance against buckling when the parameter L_2 is raised from 5 m to 10 m.

while both pile tips in the example of this section can move. The top of the pile, at the anchor, is fixed by a stiff spring. Displacement of this anchor requires a large force, therefore the pile top is more or less fixed. The bottom half of the pile is supported by the elastic support of the soil. If this support is stiff, the pile is less able to move than when this support is weak. In the three parameter sets worked out in table 5.4, two parameter sets have a weak support of the soil ($k=1\ 000\ kN/m/m^2$) and one set has an stiff support ($k=12\ 000\ kN/m/m^2$). For the stiff support, where the pile is less able to move, the error of the found value of F_{cr} was limited (1.6%). For the other two parameter sets, with a weak support, the pile is able to move easily. Both sets gave large errors of the calculated value for F_{cr} . Apparently, the method to determine F_{cr} with the displacement becomes invalid when the structure can move quite easily. Because a sheet pile is non-fixed at the pile tip, the pile is able to move and thus the second method described in section 5.2 is not valid for sheet piles.

5.4. Proposed method compared with the Eurocode method

The proposed method, method 1, will approach the actual critical global buckling load better compared to the current method of the Eurocode, which is neglecting the soil resistance. Unfortunately, it is not possible to make a comparison of both method's for sheet piles in general. The critical global buckling load is dependent to too much parameters (soil parameters, type of sheet pile, anchor, lay-out etc.) to make a comparison valid for all sheet piles. Though, to compare both method's, an example is analysed by both method's. The lay-out of the example is given in figure 5.21, the properties of the soil and structural elements are given in table 5.5.

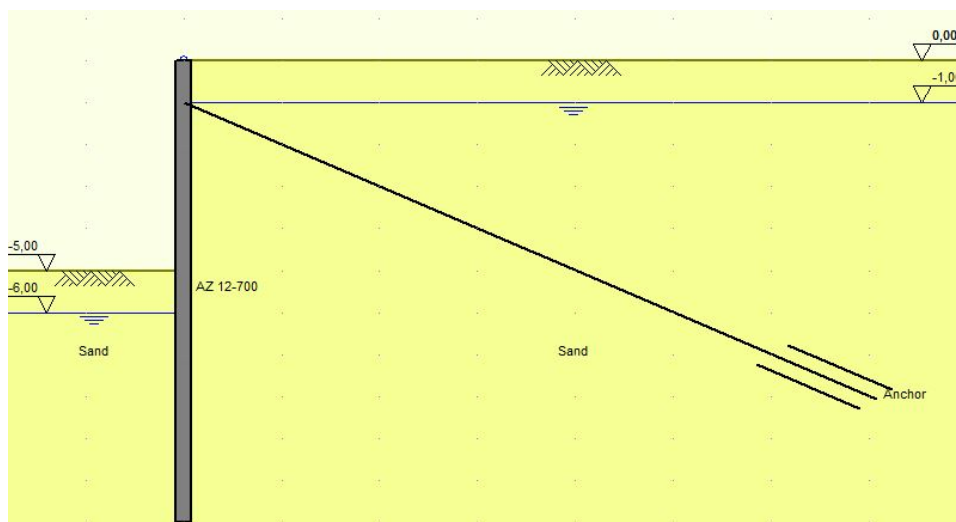


Figure 5.21: Lay-out of the example for comparison method of the proposed with the current method

| | Property | Value | Unit |
|-------------------|--|----------|-----------|
| Sand | Unsaturated unit weight sand | 18 | kN/m^3 |
| | Saturated unit weight sand | 18 | kN/m^3 |
| | Cohesion | 0 | kN/m^2 |
| | Friction angle ϕ | 30 | $^\circ$ |
| | Delta friction angle δ | 20 | $^\circ$ |
| | Spring stiffness k_1 | 12 000 | kN/m^3 |
| | Spring stiffness k_2 | 3 270 | kN/m^3 |
| | Spring stiffness k_3 | 1 000 | kN/m^3 |
| Structure lay-out | Level sheet pile tip | -11 | m |
| | Level excavation | -5 | m |
| | Original surface level | 0 | m |
| | Water level left side | -6 | m |
| | Water level right side | -1 | m |
| Sheet pile | Profile | AZ12-700 | |
| | Bending stiffness EI | 18 880 | kNm^2/m |
| | Section modulus w | 1 205 | cm^3/m |
| | Yield strength | 240 | N/mm^2 |
| | Bending moment capacity M_{Rd} | 289 | kNm |
| | Normal force capacity N_{Rd} | 2 952 | kN |
| Anchor | Level at sheet pile | -1 | m |
| | Axial stiffness EA | 840 000 | kN/m |
| | Length | 10 | m |
| | Angle | 45 | $^\circ$ |
| | Horizontal anchor stiffness k_{anchor} | 42 000 | $kN/m/m$ |

Table 5.5: Soil and material properties of the structure given in figure 5.21

The sheet pile should satisfy condition 5.13, where the u.c. (unity check) should be less than 1 for a safe design. The example has been modelled with D-sheet piling (software), which gave an first order bending moment M_{Ed} of 146.4 kNm .

Because it's assumed that the normal force will be introduced at the top of the pile, the critical buckling length is set to 11 m. The value for F_{cr} according to the current design practice would be 3 234 kN . This critical global buckling load results in a value of 0.49 for the reduction factor $\bar{\chi}_b$.

Based on the initial horizontal soil pressure determined by D-sheet piling, the available soil stiffness against the global buckling mechanism have been derived. Based on the available soil stiffness, the structural model given in figure 5.22 is used for the sheet pile. For the first meter below the soil surface, it appeared that no soil stiffness was left to resist against buckling. This model was analysed with Diana FEA, which returns a value for F_{cr} of 6 507 kN , twice the value found with the current method. This value results in a reduction factor $\bar{\chi}_b$ of 0.66.

$$\begin{aligned}
 N_{Ed} \leq 0.04 * F_{cr} : u.c. &= \frac{N_{Ed}}{N_{Rd}} + \frac{M_{Ed}}{M_{Rd}} \\
 N_{Ed} > 0.04 * F_{cr} : u.c. &= \frac{N_{Ed}}{\bar{\chi}_b N_{Rd}} + 1.15 \frac{M_{Ed}}{M_{Rd}}
 \end{aligned} \tag{5.13}$$

Based on the known data, equation 5.13 can be filled in. Based on the critical buckling load with the method from the Eurocode ($F_{cr} = 3\,234\,kN$), equation 5.14 returns. With the critical load found with the proposed method ($F_{cr} = 6\,507\,kN$), equation 5.15 is found. Both equations are plotted in figure 5.23, where it is visible that the proposed method results in lower unity checks than the current method from the Eurocode. Most significant profit of the new method is that the unfavourable check on global buckling is required from a higher normal force (from 260 kN instead of 129 kN). The higher reduction factor $\bar{\chi}_b$ of the proposed method results in a slightly lower development of the unity check compared to the current method.

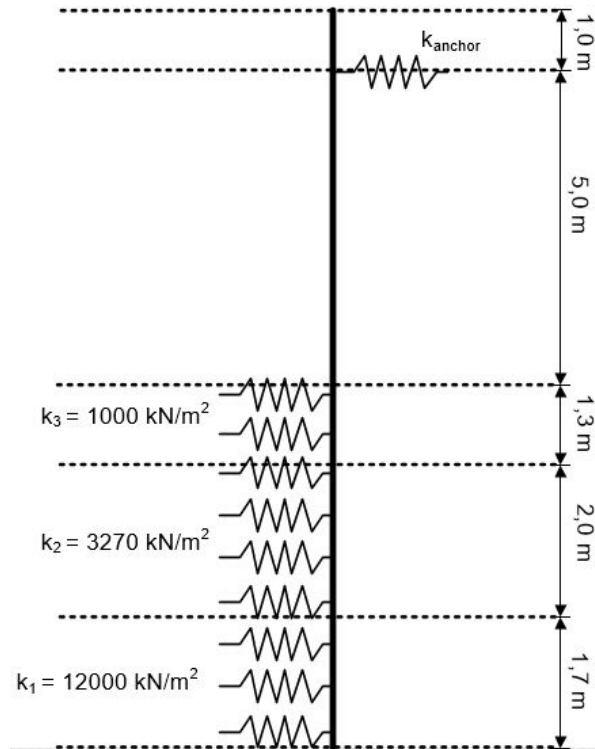


Figure 5.22: Structural model to determine F_{cr} for the sheet pile of figure 5.21

$$\begin{aligned}
 N_{Ed} \leq 129 \text{ kN} : u.c. &= \frac{N_{Ed}}{2952} + \frac{146.4}{289} \\
 N_{Ed} > 129 \text{ kN} : u.c. &= \frac{N_{Ed}}{0.49 * 2952} + 1.15 \frac{146.4}{289}
 \end{aligned} \tag{5.14}$$

$$\begin{aligned}
 N_{Ed} \leq 260 \text{ kN} : u.c. &= \frac{N_{Ed}}{2952} + \frac{146.4}{289} \\
 N_{Ed} > 260 \text{ kN} : u.c. &= \frac{N_{Ed}}{0.66 * 2952} + 1.15 \frac{146.4}{289}
 \end{aligned} \tag{5.15}$$

Section 3.2 treated the background of the factor 1.15 in equation 5.13. It stated that the factor (k_{yy})1.15 may be neglected if the second order effect to the bending moment M_{Ed} is taken into account. With this given equation 5.15 can be rewritten to equation 5.16, where M_{Ed}^{II} is the bending moment including second order effects.

$$\begin{aligned}
 N_{Ed} \leq 260 \text{ kN} : u.c. &= \frac{N_{Ed}}{2952} + \frac{146.4}{289} \\
 N_{Ed} > 260 \text{ kN} : u.c. &= \frac{N_{Ed}}{0.66 * 2952} + \frac{M_{Ed}^{II}}{289}
 \end{aligned} \tag{5.16}$$

The example above used D-sheet piling to analyse the soil-structure model, but this program is only limited able to take second order effects into account. Appendix G describes how D-sheet piling can take the second order effects into account. This has been done for the above example for 15 values of the normal force (100 to 1 500 kN), which were all modelled from the sheet pile top to the tip. Figure 5.24 represents the outcome of the current method by the Eurocode (equations 5.14 and 5.15) and method using the second order bending moment (equation 5.16). From figure 5.23 it was already concluded that the proposed method to determine F_{cr} resulted in a much more favourable unity check compared with the method described by the Eurocode.

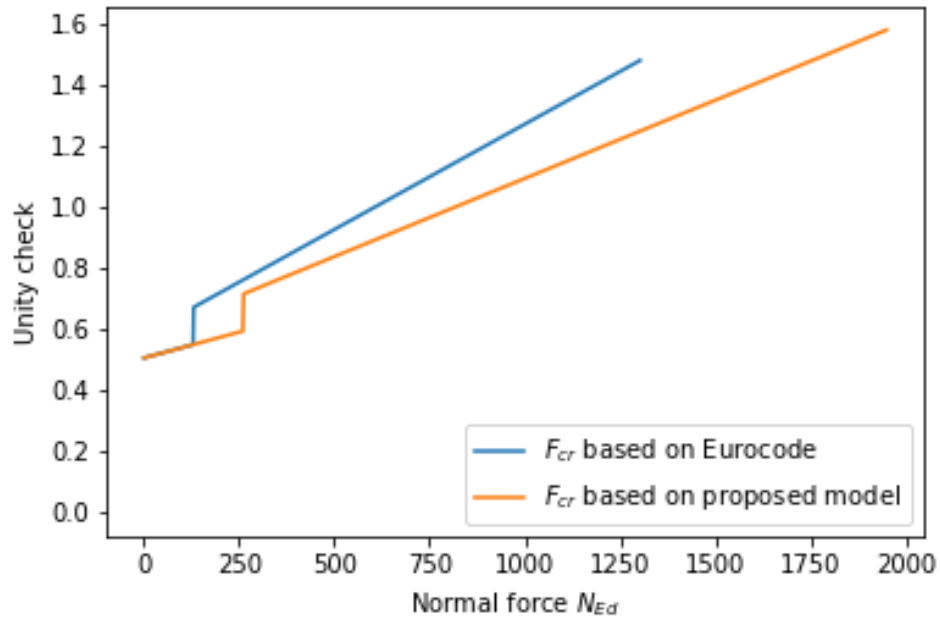


Figure 5.23: Plots of equations 5.14 and 5.15

From figure 5.24 it comes clear that when the factor 1.15 is replaced by taking the second order effects into account, the unity check becomes even more favourable for low values for the normal force N_{Ed} . For normal forces higher than 1 200 kN, taking the second order effects into account resulted in less favourable unity checks. This can be explained by the fact that from about 1 120 kN the second order effects to M_{Ed} are more than 15%, while in the current check this is set constant to 15% independent from N_{Ed} .

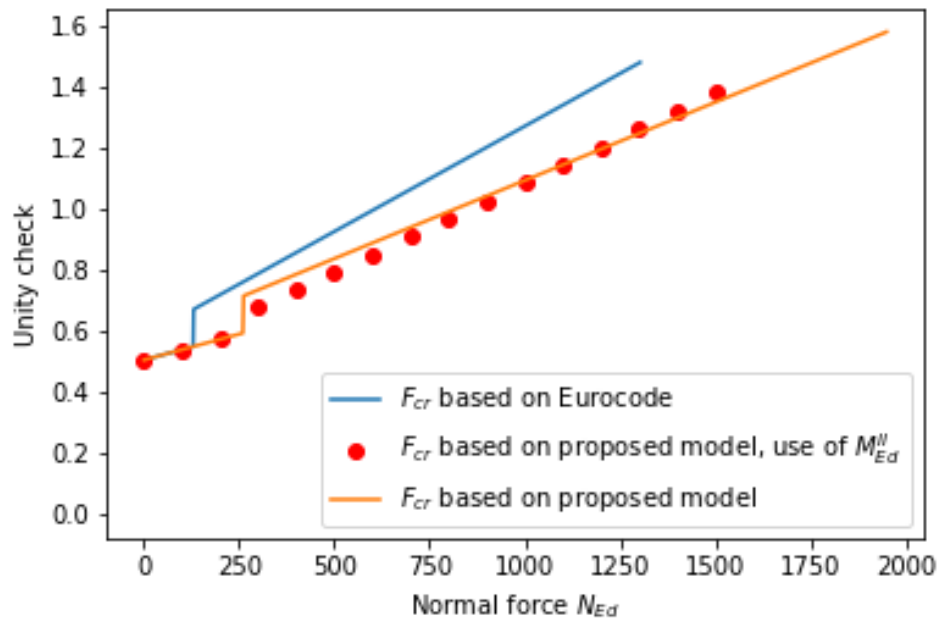


Figure 5.24: Plots of equations 5.13, 5.15 and 5.16

5.5. Conclusions to the determination of F_{cr} for sheet piles

This chapter proposed two methods to take the influence of the soil into account in the determination of the critical global buckling load. The first method, based on the Eulerian global buckling theory, is an analytical method which can be used to approach the value of F_{cr} for sheet piles if and only if the spring model is used to model the soil-structure interaction. Because the soil stiffness may decrease when the displacement of the soil grows, the soil stiffness must be underestimated at some places along the sheet pile such that the value of F_{cr} can only be approached.

Because the requirement to use the spring model is restrictive for the first described method to use, a second method is proposed. This method approaches the value of F_{cr} by the usage of the relation between the normal force and the first and second order displacements. Though quite good results were found for non-sheet piling structures with fixed boundaries, the method proved to be invalid for sheet piling structures and must therefor be rejected. The invalidity of this method seems to have an origin because the bottom tip of the sheet pile is able to move and is not fixed.

Lastly, an example is presented where the first method is used to determine the value of F_{cr} . On the top of that, the value of 1.15 in the current check on global buckling is removed as well in this example. Both improvements results in a significant reduction of the unity check. However, for higher values of the normal force, the second order effect to the bending moment starts to be significant. Though the value of 1.15 is removed, bending moment must be increased with a factor in the same or even higher order because the second order effect becomes large. Therefor, for the higher normal forces, only the better approached value of F_{cr} leads to an reduction of the unity check.

To conclude, the influence of the soil to the value of F_{cr} can be only be approached if and only if the spring model is used to model the interaction between the soil and the structure. Because this is not always the case, chapter 6 discusses alternatives to determine the effects of the global buckling mechanisms in sheet piles.

6

Effect of geometrical imperfections to the soil-structure interaction calculation model

The previous chapters have focused on the determination of the critical global buckling load F_{cr} of sheet piles. In itself, the value of F_{cr} is no point of interest, but it is used to determine the effect of the global buckling mechanism or the second order effects to the displacements or possible geometrical imperfections in sheet piles. The relation between the critical global buckling load and the second order effects is discussed in sections 3.1.1 to 3.1.3. The second order effects due to displacements caused by loading can be determined relatively simple by the use of software. This is done in section 6.1 in an attempt to describe the effects of the subsoil to the global buckling mechanism in sheet piles. Section 6.2 discusses the effect of possible geometrical imperfections in the pile. In the current method stated by the Eurocode the critical global buckling load is of importance in order to determine those effects. Section 6.2 will discuss alternative approaches to determine those effects. An important approach is to model the sheet pile with geometrical imperfections in the soil-structure interaction model. This approach has been introduced in section 3.2.2. The finite element software package Plaxis 2D is able to model a sheet pile with an imperfection. Figure 6.1 gives an example of an large imperfection ¹. Besides, the program is able to calculate second order effects ². So in principle, when Plaxis 2D is used for the design of the sheet pile, the method described in section 3.2.2 can be applied. Therefore, this software is used to evaluate the given examples. Additionally, a fourth method is described, which is a pragmatic approach of the effects of the global buckling mechanism. This chapter introduces two method's to determine the global buckling mechanism of geometrical imperfections. Section 6.3 compares this two method's with the method by the Eurocode currently used.



Figure 6.1: Extreme imperfection modelled in Plaxis 2D

¹Imperfection in the middle of the 8 m long sheet pile is set to 0.5 m (12,5%) in order to make the imperfection visible in the figure.

²To calculate second order effects with Plaxis 2D, the option *Updated Mesh* should be opt on in the settings of the calculation.

6.1. Discussion of the global buckling mechanism in sheet piles

The effect of the soil resistance against the second order effects is defined using two examples. The first example in figure 6.2a consist of a sheet pile structure which is fully surrounded by a sand soil layer with a water table one meter below the surface. More data to the sheet pile, the subsoil and model data is given in appendix H. Based by the application of an additional vertical or normal force F_{top} at top of the sheet pile, the second order effects could be determined. The structure has been analysed by Plaxis 2D, which requires that a vertical support is added at the tip of the sheet pile. This must be done because the tip resistance of the sheet pile is not calculated correctly by Plaxis [14] [20].

At first, the sheet pile and anchor are loaded by and only by the soil and water pressure resulting in the deflection of figure 6.2b. Based to this load scheme, the maximal initial displacement and bending moment in the sheet pile are respectively 63 mm and 164.9 kNm . The top of the pile, where the additional normal force is introduced, displaces with 45.58 mm .

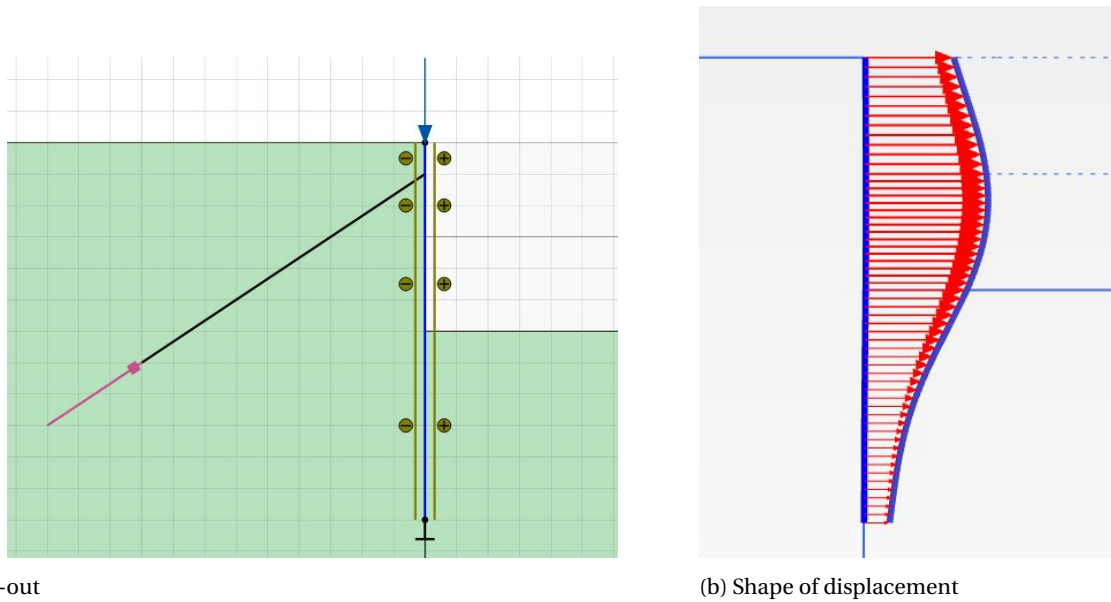


Figure 6.2: Lay-out and displacement shape of sheet pile example in sand soil layer

The additional normal force F_{top} will increase the bending moment in the deformed sheet pile causing the second order effects. To determine which part of the maximal bending moment is caused by this normal force, the horizontal distance between this normal force and the cross section with the maximal bending moment should be known. After all, the bending moment caused by the normal force equals $F_{top} \times w$. This distance is given in figure 6.3 as $w_{\text{differential}}$, which might be in the first order (neglecting the influence of the normal force) or in the second order (taking the influence of the normal force into account). For the structure of figure 6.2a the first order differential displacement $w_{\text{differential}}^I$ between the normal force and the maximal bending moment equals 16.60 mm .

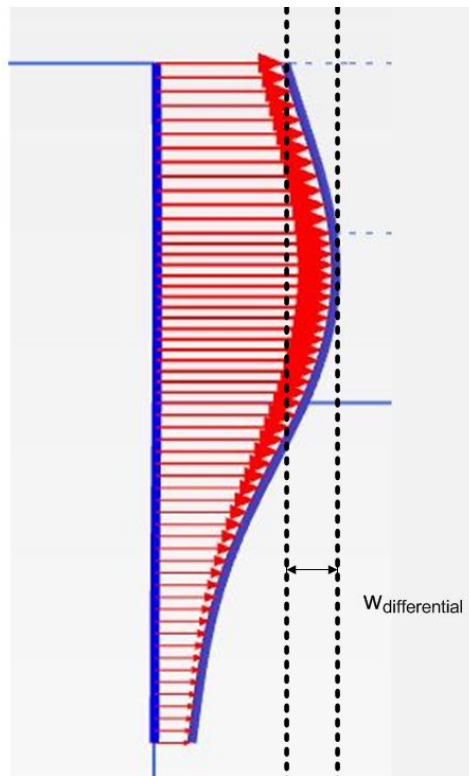


Figure 6.3: Differential displacement between the normal force and maximal displacement

The sheet pile structure of figure 6.2a has been loaded by an additional normal force F_{top} in the model. The model has been analysed for several values of F_{top} , the results are given in table 6.1. For reference, the results are discussed for a normal force F_{top} of 100 kN.

Though the displacements are increasing due to F_{top} , the second order differential displacement $w_{differential}^{II}$ between the normal force and the maximal bending reduces with (a negligible) 0.04 mm to 16.56 mm. This means that 1.6 kNm of the maximal bending moment is caused by the normal force F_{top} . However, the maximal bending moment only increases with 0.7 kNm, which means that the bending moment caused by other loads than the normal force (the soil pressure, water pressure and the anchor force) decreases with 0.9 kNm. Clearly, those forces are affected by the normal force. This effect must be explained by the soil structure interaction. The normal force causes an extra displacement of the pile and the soil, which results in an increase or decrease in the soil pressure and a disturbance of the force balance. Because the forces must be in equilibrium, the anchor force is affected as well by this redistribution of forces and thus by the normal force. This redistribution of the forces results in another value of the maximal bending moment caused by the soil pressure and the anchor force. In this example, the redistribution resulted in a decrease of 0.9 kNm for M_{Ed} .

For 18 more values of F_{top} results are given in table 6.1. This table gives the values for the first and second order differential displacement between the force F_{top} and the maximal bending moment. Based on this displacements, the bending moment caused by the normal force can be determined, based to the first order (dM^I) or the second order (dM^{II}) differential displacement. The total value of the maximal bending moment including second order effects is given by M_{Ed} . The increment of M_{Ed} with respect to the load scheme without F_{top} is expressed as dM_{Ed} .

The data shows a few trends, of which the most remarkable is that the second order differential displacement $w_{differential}^{II}$ hardly changes or even decreases (negligible) for low normal forces. $w_{differential}$ is defined as the difference between the displacement of F_{top} and the maximal bending moment. Clearly, the displacement of F_{top} grows more than the displacement at the maximal bending moment for normal forces until 300 kN. As a result, the second order differential displacement is negligible less than the first order differential displacement.

Due to the displacements, it should be expected that the maximal bending moment grows by the introduction of the normal force. The part of the maximal bending moment caused by the normal force is given by

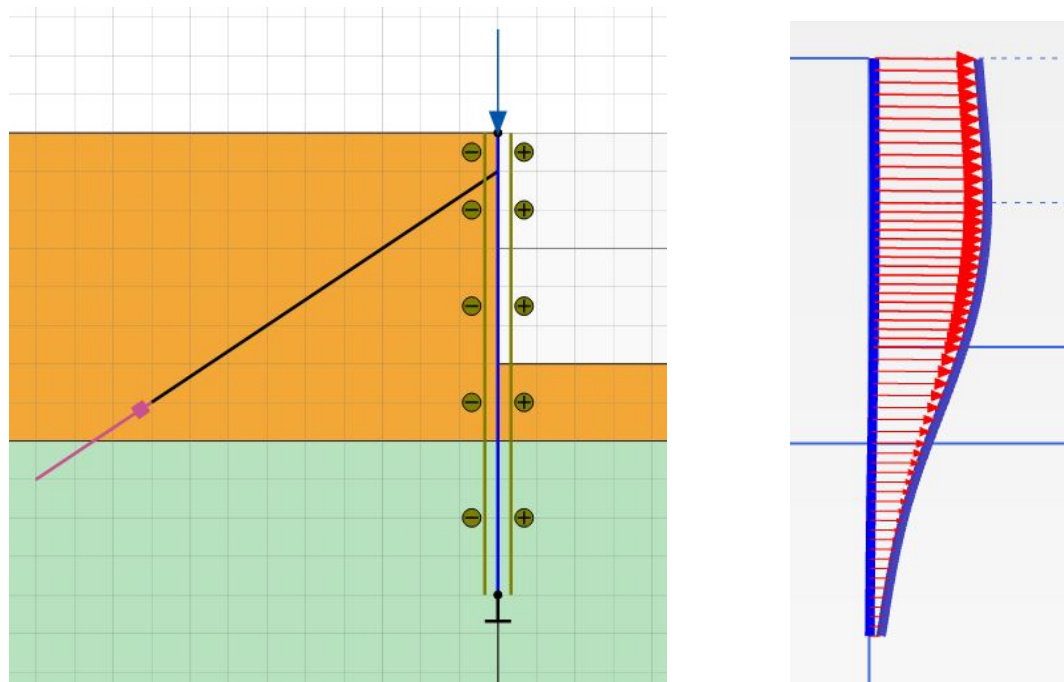
dM^{II} ($F_{top} \times w_{\text{differential}}^{II}$), this should be added to the bending moment M_{Ed} without second order effects (= 164.9 kNm) in table 6.1. However, it's observed in table 6.1 that the growth of the maximal bending moment is always less than the bending moment dM^{II} caused by the normal force. In fact, for normal forces until 1 000 kN the bending moment growth is even less than what might be expected based on the first order differential displacement (dM^I). This can be explained by the soil-structure interaction discussed before.

| F_{top} (kN) | $w_{\text{differential}}^I$ (mm) | dM^I (kNm) | $w_{\text{differential}}^{II}$ (mm) | dM^{II} (kNm) | M_{Ed} (kNm) | dM_{Ed} (kNm) |
|----------------|----------------------------------|--------------|-------------------------------------|-----------------|----------------|-----------------|
| 0 | 16.60 | 0 | 16.60 | 0 | 164.9 | 0 |
| 100 | 16.60 | 1.66 | 16.56 | 1.66 | 165.6 | 0.7 |
| 200 | 16.60 | 3.32 | 16.55 | 3.31 | 166.5 | 1.6 |
| 300 | 16.60 | 4.98 | 16.57 | 4.97 | 167.5 | 2.6 |
| 400 | 16.60 | 6.64 | 16.61 | 6.64 | 168.6 | 3.7 |
| 500 | 16.60 | 8.30 | 16.67 | 8.37 | 169.8 | 4.9 |
| 600 | 16.60 | 9.96 | 16.98 | 10.19 | 172.1 | 7.2 |
| 700 | 16.60 | 11.62 | 17.20 | 12.04 | 173.9 | 9.0 |
| 800 | 16.60 | 13.28 | 17.32 | 13.86 | 175.3 | 10.4 |
| 900 | 16.60 | 14.94 | 17.60 | 15.84 | 177.3 | 12.4 |
| 1 000 | 16.60 | 16.60 | 17.85 | 17.85 | 179.3 | 14.4 |
| 1 100 | 16.60 | 18.26 | 19.51 | 21.46 | 186.8 | 21.9 |
| 1 200 | 16.60 | 19.92 | 19.47 | 23.36 | 187.4 | 22.5 |
| 1 300 | 16.60 | 21.58 | 19.48 | 25.33 | 188.3 | 23.5 |
| 1 400 | 16.60 | 23.24 | 19.56 | 27.38 | 189.6 | 24.5 |
| 1 500 | 16.60 | 24.90 | 19.88 | 29.82 | 191.9 | 26.5 |
| 1 600 | 16.60 | 26.56 | 21.82 | 34.91 | 200.5 | 35.6 |
| 1 700 | 16.60 | 28.22 | 21.76 | 37.00 | 201.0 | 36.1 |
| 1 800 | 16.60 | 29.88 | 21.80 | 39.24 | 202.0 | 37.1 |
| 1 900 | 16.60 | 31.54 | 22.03 | 41.86 | 203.9 | 38.9 |
| 2 000 | 16.60 | 33.20 | 22.37 | 46.51 | 206.1 | 41.2 |

Table 6.1: Data on the sheet pile structure of figure 6.2a in a sand soil layer

The same analysis has been done again with the same structure, but this time a thick clay layer is present at the top of the soil profile (figure 6.4a). Results are given in table 6.2. In this case, other trends can be described compared with the previous example.

Though the second order differential displacement is strictly increasing for all normal loads, the absolute value is very small (in the order of millimetres). In figure 6.4b it becomes clear why this value is so small. A small differential displacement between the normal force on top of the sheet pile and the maximal bending moment would mean that the bending moment caused by the normal force is small to negligible. This is verified by table 6.2 (see the values for dM^{II}), but it is also found that the total maximal bending moment M_{Ed} grows significantly (see the values for dM_{Ed}). This means that the maximal bending moment caused by the soil pressure, water pressure and the anchor force is growing due to the normal force. This in contrast with the previous example, where the maximal bending moment caused by this forces is decreasing.



(a) Lay-out

(b) Shape of displacement

Figure 6.4: Lay-out and displacement shape of sheet pile example in sand-clay mixed soil profile

| F_{top} (kN) | $w_{differential}^I$ (mm) | dM^I (kNm) | $w_{differential}^{II}$ (mm) | dM^{II} (kNm) | M_{Ed} (kNm) | dM_{Ed} (kNm) |
|----------------|---------------------------|--------------|------------------------------|-----------------|----------------|-----------------|
| 0 | 2.99 | 0 | 2.99 | 0 | 211.3 | 0 |
| 100 | 2.99 | 0.30 | 3.05 | 0.30 | 212.6 | 1.3 |
| 200 | 2.99 | 0.60 | 3.16 | 0.63 | 214.2 | 2.9 |
| 300 | 2.99 | 0.90 | 3.32 | 0.99 | 215.9 | 4.6 |
| 400 | 2.99 | 1.20 | 3.86 | 1.54 | 219.3 | 8.0 |
| 500 | 2.99 | 1.49 | 4.01 | 2.00 | 220.9 | 9.6 |
| 600 | 2.99 | 1.79 | 5.08 | 3.05 | 226.1 | 14.8 |
| 700 | 2.99 | 2.09 | 5.22 | 3.66 | 227.7 | 16.4 |
| 800 | 2.99 | 2.39 | 5.43 | 4.34 | 229.6 | 18.3 |
| 900 | 2.99 | 2.69 | 6.89 | 6.20 | 236.1 | 24.8 |
| 1 000 | 2.99 | 2.99 | 7.07 | 7.07 | 237.8 | 26.5 |

Table 6.2: Data on the sheet pile structure of figure 6.4 in a clay soil layer

The two examples discussed have different behaviour when it comes to the second order effects. The second order displacement is easy to determine using Plaxis 2D. The theory of the global buckling mechanism learns that the increment of the bending moment at a certain cross section should equal the product of the normal force and the second order displacement at that specific cross section. However, based on the above two examples, it is learned that this is not valid for sheet piles. For the first example, the maximal bending moment increased less strongly than what should be expected according to the global buckling theory. However, for the second example it was found that the increase of the maximal bending moment was more than what might be expected. The interaction between the structure and the soil could be held responsible for these results. This makes it hard to describe the qualitative effects of the global buckling mechanism in sheet piles. Only thing what could be said on the qualitative effect of global buckling in sheet piles is that the maximal displacement and bending moment of the sheet pile will grow due to an extra normal force. But both are very dependent to the lay-out of the soil, the structural properties of the structure, the soil and the hydraulic conditions (water pressure etc.).

6.2. Second order effects due to geometrical imperfections

For displacements caused by loads or soil/water pressures to the structure, the second order effects could simply be determined by the use of the FE-software like Plaxis 2D. For displacements caused by geometrical imperfections, this is not so simple because the software does not take the imperfections into account, let alone the second order effects to those imperfections. The current method stated by the Eurocode to take imperfections into account uses the critical global buckling load F_{cr} . The critical load F_{cr} and the critical buckling shape are both based on elastic stiffnesses of the materials. Because the stiffness of the soil is all but elastic, it is practically impossible to determine the effect of the soil to the elastic buckling shape. When the spring model is used to model the soil-structure interaction, the soil is semi-linear and thus a linear elastic value for F_{cr} can be determined, see chapter 5. In the soil models used for FE-software, this is not possible, and thus the soil resistance to F_{cr} cannot be determined. This section presents two different approaches to determine the second order effects of the possible geometrical imperfections. To give a clear line through this document, those two approaches are named method 3 and 4, after methods 1 and 2 are already discussed in the previous chapter.

The first approach, discussed in section 6.2.1, is based on the theory in section 3.2.2, which states that the second order effects of geometrical imperfections are approached by modelling those imperfections into the soil-structure model. However, this is easier said than done. Though the maximal first order displacement caused by the imperfections is known by a generalised number it is not clear where this displacement will occur. It is given by the Eurocode that the displacements will occur in the shape of the elastic buckling mode [19], which is discussed in chapter 3. Because this buckling shape is unknown, one of the shapes of figure 6.5 should be used.

The second approach is from a new, yet to be published, version of the POVM³. This method is discussed in section 6.2.2 and gives a simplified approach to determine the bending moment caused by the normal force and the geometrical imperfection. It should be clear that this method is developed by the author's of the POVM [25], This thesis compares both proposed method's.

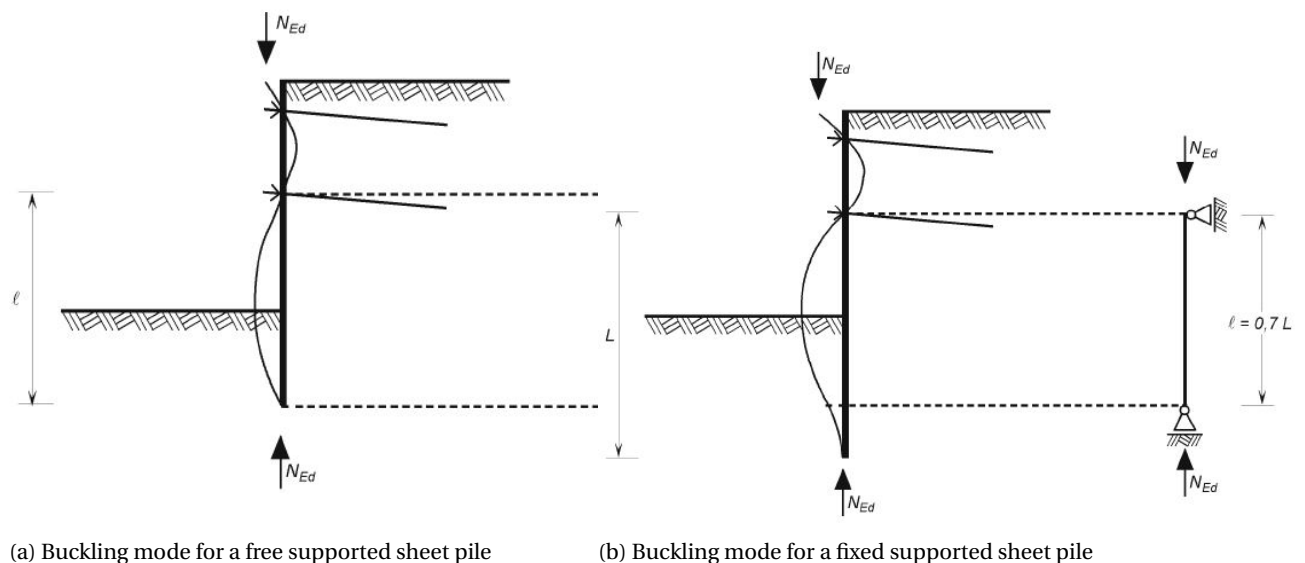


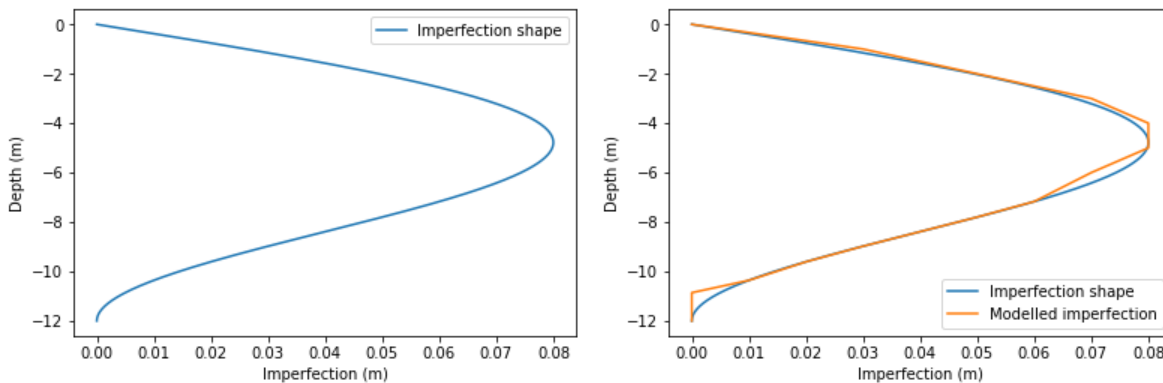
Figure 6.5: Buckling shapes as defined by Eurocode 3 part 5 (NEN-en 1993-5)

6.2.1. Method 3: Second order effects to imperfections determined by geometrical imperfections in the model

This method is based on the fact that geometrical imperfections can be introduced to the sheet pile in a soil-structure interaction model. With one of the buckling shapes of figure 6.5 the shape of the geometrical imperfections can be assumed. This method is discussed by the use of the two examples treated in section 6.1.

³Project Overstijgende Verkenning Macrostabiteit, discussed earlier in chapter 2

In both examples of section 6.1 the main part of the normal force is introduced at the top of the sheet pile by F_{top} . Therefore, geometrical imperfections are modelled over the full length of the sheet pile. The length of the piles are in both examples 12 m. For sheet piles, the Eurocode demands a maximal initial geometrical imperfection e_0 of $L/150$ [19]. This gives that the maximal geometrical imperfection equals 0.08 m , where the shape of the imperfection is given 6.6a according to figure 6.5b. Though Plaxis is able to model geometrical imperfections in a sheet pile, there are two drawbacks. The first drawback is that the imperfections must be modelled point by point, each with its own coordinate in the model. This makes modelling the sheet pile a manual and labour intensive task. Second drawback is that the coordinates can be as precise as centimetres. So if, for instance, an imperfection equals 45 mm , it should be rounded to either 40 or 50 mm , an error of 11.1% . These two drawbacks make it impossible to model the shape of the geometrical imperfections exactly. Therefore, this shape must be approached. For the two examples, this approach is presented in figure 6.6b.



(a) Shape of the initial imperfection of the sheet pile (b) Shape of the initial imperfection and the Plaxis 2D model of the sheet pile

Figure 6.6: Imperfection in a sheet pile (not to scale)

The sheet pile structure from figure 6.2a has been analysed again, but this time including the initial geometrical imperfection as given in figure 6.6b. Table 6.3 gives the maximal bending moment and as a reference, the maximal bending moment for the sheet pile without geometrical imperfections is given as well. The difference between these two values (fourth column) can be seen as the influence of the imperfection to the total bending moment. By the current method stated by the Eurocode, this extra bending moment is taken into account by applying the reduction factor χ_b to the normal force capacity. When geometrical imperfections are modelled into the soil-structure interaction model, this reduction factor is no longer necessary.

The buckling shape used to model the geometrical imperfections in the model is known to be incorrect. However, the geometrical imperfections are modelled in order to determine the effect of those imperfections to the bending moment due to the second order effect. The larger the geometrical imperfection at a cross section, the larger the extra bending moment at that section. If the largest imperfection is at the cross section with the maximal bending moment, the maximal possible bending moment will be found. In this example, the maximal bending moment is at 4.3 m below the top of the sheet pile, while the maximal imperfection (80 mm) is between 4 and 5 m below the top. It should be expected that the modelled geometrical imperfection shape has a maximal effect to the maximal bending moment. Also the other buckling shape, of figure 6.5a, has been modelled as an imperfection shape as well in Plaxis. In this case, the maximal geometrical imperfection is not at the maximal bending moment. It was found that all maximal bending moments, for each value of F_{top} , were less than those found with the geometrical imperfection shape of figure 6.5b. So out of the two buckling shapes in figure 6.5, the shape of figure 6.5b leads to the highest values of the bending moment M_{Ed} .

The imperfection shapes of figure 6.5 are also modelled to the second example of the previous section. Results of this model with the imperfection shape of figure 6.5b are given in table 6.4. Also for this example the assumed imperfection shape is likely to be wrong, but again the largest imperfection is at the same cross section where the maximal bending moment is present, creating the largest possible negative effect for the maximal bending moment. For the other imperfection shape in figure 6.5 the model has been analysed as well. With this shape, the maximal bending moment is not at the largest geometrical imperfection and less

| F_{top} | M_{Ed} without imperfections (kNm) | M_{Ed} with imperfections (kNm) | Difference (kNm) |
|-----------|--|---------------------------------------|----------------------|
| 0 | 164.9 | 166.1 | -1.2 |
| 100 | 165.6 | 174.2 | -8.6 |
| 200 | 166.5 | 177.2 | -10.7 |
| 300 | 167.5 | 189.5 | -22.0 |
| 400 | 168.6 | 195.0 | -26.4 |
| 500 | 169.8 | 205.4 | -35.6 |
| 600 | 172.1 | 213.8 | -41.7 |
| 700 | 173.9 | 219.5 | -45.6 |
| 800 | 175.3 | 231.7 | -56.4 |
| 900 | 177.3 | 240.3 | -63.0 |
| 1 000 | 179.3 | 251.6 | -72.3 |
| 1 100 | 186.8 | 263.1 | -76.3 |
| 1 200 | 187.4 | 267.0 | -79.6 |
| 1 300 | 188.3 | 285.8 | -97.5 |
| 1 400 | 189.6 | 300.2 | -110.6 |
| 1 500 | 191.6 | 313.9 | -122.3 |
| 1 600 | 200.5 | 328.6 | -128.1 |
| 1 700 | 201.0 | 342.5 | -141.5 |
| 1 800 | 202.0 | 358.5 | -156.5 |
| 1 900 | 203.9 | 375.9 | -172.0 |
| 2 000 | 206.1 | 394.0 | -187.9 |

Table 6.3: Bending moments caused by the geometrical imperfections for the example in figure 6.2a

than found with the other imperfection shape. Though it might not be the correct shape, the imperfection shape used for the results of table 6.4 seems to deliver the maximal possible bending moment in the sheet pile.

| F_{top} | M_{Ed} without imperfections (kNm) | M_{Ed} with imperfections (kNm) | Difference (kNm) |
|-----------|--|---------------------------------------|----------------------|
| 0 | 211.3 | 213.8 | -2.5 |
| 100 | 212.6 | 220.1 | -7.5 |
| 200 | 214.2 | 230.8 | -16.6 |
| 300 | 215.9 | 240.8 | -24.9 |
| 400 | 219.3 | 247.5 | -28.3 |
| 500 | 220.9 | 261.1 | -40.2 |
| 600 | 226.1 | 272.4 | -46.3 |
| 700 | 227.7 | 279.9 | -52.2 |
| 800 | 229.6 | 296.6 | -67.0 |
| 900 | 236.1 | 309.0 | -72.1 |
| 1 000 | 237.8 | 324.1 | -86.3 |
| 1 100 | 240.0 | 339.5 | -99.5 |
| 1 200 | 247.3 | 355.0 | -107.7 |
| 1 300 | 249.1 | 370.9 | -121.8 |
| 1 400 | 251.7 | 390.3 | -138.6 |
| 1 500 | 260.3 | 408.6 | -148.3 |

Table 6.4: Bending moments caused by the imperfections for the example in figure 6.4a

6.2.2. Method 4: simplified approach of the POVVM

It is clear that it is hard, maybe impossible, to predict the exact effect of imperfections to the sheet pile. The current global buckling check is based on the fact that the normal force introduces, due to the imperfections, an additional bending moment in the sheet pile. Because the shape of the imperfections is unknown, it is impossible to determine where this additional bending moment is maximal. For simplicity, the maximal bending moment caused by the normal force and imperfections should be added to the maximal bending moment caused by the soil and water pressure and the anchor force. This is done with the current global buckling check of the Eurocode by the reduction factor χ_b , as can be seen in the derivations given in chapter 3, and is the starting point of this method.

The above has led to a pragmatic method for normal forces N_{Ed} below 20% of F_{cr} , derived for the development of the POVVM [25]. In this method it is proposed to increase the bending moment by the product of the maximal normal force in the sheet pile and the maximal first order geometrical imperfection, which equals $e_0 * N_{Ed}$. This method 'forgets' that this initial imperfection e_0 and thus the additional bending moment will increase due to the normal force. To review this error, this method is applied for the first example in section 6.1. This example have been modelled with imperfections, which means that the actual effect of the imperfections are embedded in the result. Using the analysis of the examples where imperfections were not included, the new method of the POVVM could be used as well. By comparing both method's, it is possible to check the validity of the method described by the POVVM [25]. This comparison is made in table 6.5, where an e_0 of 0.08 m is used for equation 6.1.

$$M_{Ed} = M_{Ed,model} + M_{Ed,additional} = M_{Ed,model} + e_0 * N_{Ed} \quad (6.1)$$

| F_{top} | M_{Ed} with POVVM method (kNm) | M_{Ed} with imperfections in the model (kNm) | Difference (kNm) |
|-----------|----------------------------------|--|------------------|
| 0 | 164.9 | 166.1 | 1.2 |
| 100 | $165.6 + F_{top} * 0.08 = 173.6$ | 174.2 | 0.6 |
| 200 | $166.5 + F_{top} * 0.08 = 182.5$ | 177.2 | -5.3 |
| 300 | $167.5 + F_{top} * 0.08 = 191.5$ | 189.5 | -2.0 |
| 400 | $168.6 + F_{top} * 0.08 = 200.6$ | 195.0 | -5.6 |
| 500 | $169.8 + F_{top} * 0.08 = 209.8$ | 205.4 | -4.4 |
| 600 | $172.1 + F_{top} * 0.08 = 220.1$ | 213.8 | -6.3 |
| 700 | $173.9 + F_{top} * 0.08 = 229.9$ | 219.5 | -10.4 |
| 800 | $175.3 + F_{top} * 0.08 = 239.3$ | 231.7 | -7.6 |
| 900 | $177.3 + F_{top} * 0.08 = 249.3$ | 240.3 | -9.0 |
| 1 000 | $179.3 + F_{top} * 0.08 = 259.3$ | 251.6 | -7.7 |
| 1 100 | $186.8 + F_{top} * 0.08 = 274.8$ | 263.1 | -11.7 |
| 1 200 | $187.4 + F_{top} * 0.08 = 283.4$ | 267.0 | -16.4 |
| 1 300 | $188.3 + F_{top} * 0.08 = 292.3$ | 285.8 | -6.5 |
| 1 400 | $189.6 + F_{top} * 0.08 = 301.6$ | 300.2 | -1.4 |
| 1 500 | $191.6 + F_{top} * 0.08 = 311.6$ | 313.9 | 2.3 |
| 1 600 | $200.5 + F_{top} * 0.08 = 328.5$ | 328.6 | 0.1 |
| 1 700 | $201.0 + F_{top} * 0.08 = 337.0$ | 342.5 | 5.5 |
| 1 800 | $202.0 + F_{top} * 0.08 = 346.0$ | 358.5 | 12.5 |
| 1 900 | $203.9 + F_{top} * 0.08 = 355.9$ | 375.9 | 20.0 |
| 2 000 | $206.1 + F_{top} * 0.08 = 366.1$ | 394.0 | 27.9 |

Table 6.5: Bending moments caused by the imperfections for the example in figure 6.2a, based on the POVVM method (with F_{top}) and the model including geometrical imperfections in the sheet pile

Though an underestimation is expected because second order effects are neglected, the POVVM method overestimates the effect of imperfection to the maximal bending moment M_{Ed} for values of F_{top} between 200 and 1 400 kN. Because the bending moment is larger than found with the model which takes imperfections into account, this value can be used safely (though a bit conservative). For normal forces lower than 200 kN, the POVVM method seems to be invalid, but an error has been made in the determination of the results given

in table 6.5. Only the vertical force on top of the pile is taken into account, but both the skin friction as the anchor force creates additional normal forces in the sheet pile as well. Figure 6.7 shows that the normal force on top of the sheet pile has an arm of 0.08 m to the maximal imperfection, the arm of the vertical anchor force F_{anchor} has an arm of 0.05 m , causing an additional bending moment. The vertical anchor force is between 75 and 80 kN , depending on the value of F_{top} . If this force is taken into account for the POVM method, an additional bending moment of 3.75 to 4.0 kNm should be taken into account. If this value is added to the results of table 6.5, the POVM method is valid for vertical forces F_{top} smaller than $1\,600\text{ kN}$.

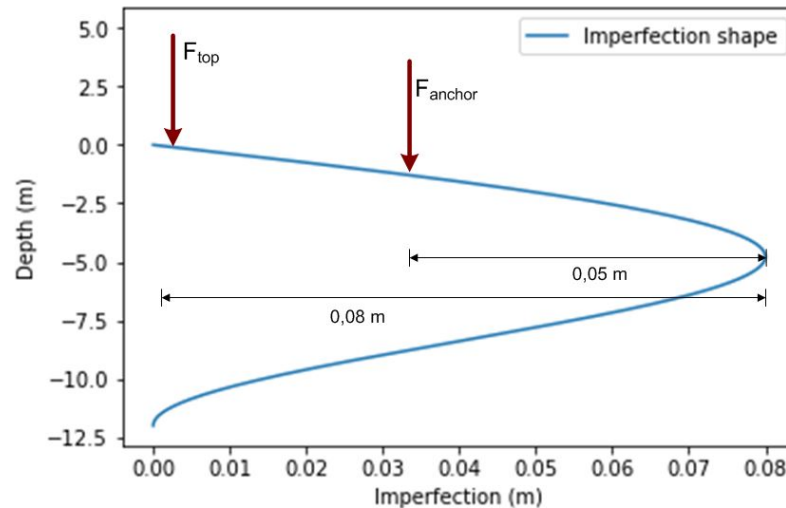


Figure 6.7: Place of the normal forces F_{top} and F_{anchor} with respect to the maximal imperfection

The normal force N_{Ed} is besides the external forces (F_{top}) and the vertical anchor force also affected by the skin friction. This skin friction is fully neglected in the above, and still the POVM method proved to be valid. In fact, it will be quite difficult to take the skin friction into account. Because the buckling and imperfection shapes are not exactly known, the distance between the friction forces and the maximal imperfection are unknown. Actually, this does also yield for the other forces (F_{top} or F_{anchor}) affecting the normal force. Though the exact displacement is unknown, the maximum first order displacement of the imperfection is known by the Eurocode ($L/150$). This value of the displacement could be used for all normal forces, no matter what the actual distance to the maximal imperfection is. In the example of figure 6.7 this would mean that the anchor force F_{anchor} should be multiplied by 0.08 m instead of 0.05 m . This does give an overestimation of the occurring bending moment due to the vertical anchor force, but it does lead to a conservative and safe design. This approach is stated by the POVM [25], which therefore replaces the global buckling check in the Eurocode by the equation given in expression 6.2. For the value of N_{Ed} , the maximal value of the normal force in the sheet pile should be taken.

$$\frac{N_{Ed}}{\chi_b N_{Rd}} + 1.15 \frac{M_{Ed}^I}{M_{Rd}} \rightarrow \frac{N_{Ed}}{N_{Rd}} + \frac{M_{Ed}^{II} + e_0 N_{Ed}}{M_{Rd}} \quad (6.2)$$

Equation 6.2 is applied to the example given above, but this time the maximal normal force N_{Ed} is used instead of F_{top} . Results of this application are given in table 6.7. For every value of F_{top} , 21 values in total, the maximal bending moment according to the POVM method is given, followed by the bending moment determined with method 3 in the previous section, where the geometrical imperfections are included in the model. From this comparison, it can be seen that the POVM method starts to underestimate the maximal bending moment from a normal force N_{Ed} of $1\,802\text{ kN}$. Therefore, for higher normal forces, the POVM method is invalid.

| F_{top} | Maximal value N_{Ed} | M_{Ed} with POVM method (kNm) | M_{Ed} with imperfections in the model (kNm) | Difference (kNm) |
|-----------|------------------------|-------------------------------------|--|----------------------|
| 0 | 107.8 | $164.9 + N_{Ed} * 0.08 = 173.5$ | 166.1 | 7.4 |
| 100 | 206.0 | $165.6 + N_{Ed} * 0.08 = 182.1$ | 174.2 | 7.9 |
| 200 | 304.5 | $166.5 + N_{Ed} * 0.08 = 190.9$ | 177.2 | 13.7 |
| 300 | 403.1 | $167.5 + N_{Ed} * 0.08 = 199.8$ | 189.5 | 10.3 |
| 400 | 501.9 | $168.6 + N_{Ed} * 0.08 = 208.8$ | 195.0 | 13.8 |
| 500 | 600.8 | $169.8 + N_{Ed} * 0.08 = 217.9$ | 205.4 | 12.5 |
| 600 | 701.2 | $172.1 + N_{Ed} * 0.08 = 228.2$ | 213.8 | 14.4 |
| 700 | 800.9 | $173.9 + N_{Ed} * 0.08 = 238.0$ | 219.5 | 18.5 |
| 800 | 900.1 | $175.3 + N_{Ed} * 0.08 = 247.3$ | 231.7 | 15.6 |
| 900 | 1 000.0 | $177.3 + N_{Ed} * 0.08 = 257.3$ | 240.3 | 17.0 |
| 1 000 | 1 100.0 | $179.3 + N_{Ed} * 0.08 = 267.3$ | 251.6 | 15.7 |
| 1 100 | 1 204.0 | $186.8 + N_{Ed} * 0.08 = 283.1$ | 263.1 | 20.0 |
| 1 200 | 1 302.0 | $187.4 + N_{Ed} * 0.08 = 291.6$ | 267.0 | 24.6 |
| 1 300 | 1 401.0 | $188.3 + N_{Ed} * 0.08 = 300.4$ | 285.8 | 14.6 |
| 1 400 | 1 499.0 | $189.6 + N_{Ed} * 0.08 = 309.5$ | 300.2 | 9.3 |
| 1 500 | 1 599.0 | $191.6 + N_{Ed} * 0.08 = 319.5$ | 313.9 | 5.6 |
| 1 600 | 1 704.0 | $200.5 + N_{Ed} * 0.08 = 336.8$ | 328.6 | 8.2 |
| 1 700 | 1 802.0 | $201.0 + N_{Ed} * 0.08 = 345.2$ | 342.5 | 2.7 |
| 1 800 | 1 900.0 | $202.0 + N_{Ed} * 0.08 = 354.0$ | 358.5 | -4.5 |
| 1 900 | 2 000.0 | $203.9 + N_{Ed} * 0.08 = 363.9$ | 375.9 | -12.0 |
| 2 000 | 2 099.0 | $206.1 + N_{Ed} * 0.08 = 374.0$ | 394.0 | -20.0 |

Table 6.6: Bending moments caused by the imperfections for the example in figure 6.2a, based on the POVM method (with N_{Ed}) and the model including geometrical imperfections in the sheet pile

In section 6.1 two example are discussed, of which the first example is used to discuss the POVM method above. For the second example, the POVM method is executed as well of which the results are given in table 6.7. Until a value of F_{top} of 1 000 kN , the POVM method is valid. From this value, the maximal bending moment is underestimated and the POVM method is no longer valid.

| F_{top} | Maximal value N_{Ed} | M_{Ed} with POVM method (kNm) | M_{Ed} with imperfections in the model (kNm) | Difference (kNm) |
|-----------|------------------------|-------------------------------------|--|----------------------|
| 0 | 104.9 | $211.3 + N_{Ed} * 0.08 = 219.7$ | 213.8 | 5.9 |
| 100 | 204.8 | $212.6 + N_{Ed} * 0.08 = 228.6$ | 220.1 | 8.5 |
| 200 | 304.8 | $214.2 + N_{Ed} * 0.08 = 238.6$ | 230.8 | 7.8 |
| 300 | 404.9 | $215.9 + N_{Ed} * 0.08 = 248.3$ | 240.8 | 7.5 |
| 400 | 505.4 | $219.3 + N_{Ed} * 0.08 = 259.7$ | 247.5 | 12.2 |
| 500 | 605.2 | $220.9 + N_{Ed} * 0.08 = 269.3$ | 261.1 | 8.2 |
| 600 | 706.2 | $226.1 + N_{Ed} * 0.08 = 282.6$ | 272.4 | 10.2 |
| 700 | 806.1 | $227.7 + N_{Ed} * 0.08 = 292.2$ | 279.9 | 12.3 |
| 800 | 906.1 | $229.6 + N_{Ed} * 0.08 = 302.1$ | 296.6 | 5.5 |
| 900 | 1 007 | $236.1 + N_{Ed} * 0.08 = 316.7$ | 309.0 | 7.7 |
| 1 000 | 1 107 | $237.8 + N_{Ed} * 0.08 = 326.4$ | 324.1 | 2.3 |
| 1 100 | 1 207 | $240.0 + N_{Ed} * 0.08 = 336.6$ | 339.5 | -2.9 |
| 1 200 | 1 308 | $247.3 + N_{Ed} * 0.08 = 351.9$ | 355.0 | -3.1 |
| 1 300 | 1 408 | $249.1 + N_{Ed} * 0.08 = 361.7$ | 370.9 | -9.2 |
| 1 400 | 1 508 | $251.7 + N_{Ed} * 0.08 = 372.3$ | 390.3 | -18.0 |
| 1 500 | 1 609 | $260.3 + N_{Ed} * 0.08 = 389.0$ | 408.6 | -19.4 |

Table 6.7: Bending moments caused by the imperfections for the example in figure 6.4a, based on the POVM method (with N_{Ed}) and the model including geometrical imperfections in the sheet pile

6.3. Comparison of proposed method's with current Eurocode method

In this chapter 3 method's are proposed in order to increase the correctness of the global buckling check for sheet piles, which is given in the left hand side of equation 6.2. The quantitative effect of this three method's is given below in figures for the two examples worked out in this chapter. Before this can be done, it must be known what the value of the critical global buckling load F_{cr} is, based on the current method neglecting the resistance of the soil. To determine this value, the critical buckling length should be estimated from the displacement diagrams, given in figure 6.8. The example with the sand profile in figure 6.8a seems to have a fixed toe, which would mean that the critical buckling length equals 70% of the sheet pile length. However, the top of the sheet pile is not really fixed and displaces quite easily. Based on this boundary, the buckling length is set to the full length of the sheet pile. The same has been done for the other example with a thick clay layer in the soil profile, of which the displacement diagram is given in figure 6.8b. With both the structures having an bending stiffness EI of $39\,648\text{ kNm}^2$ and a length of 12 m , the critical global buckling load equals $2\,717\text{ kN}$.

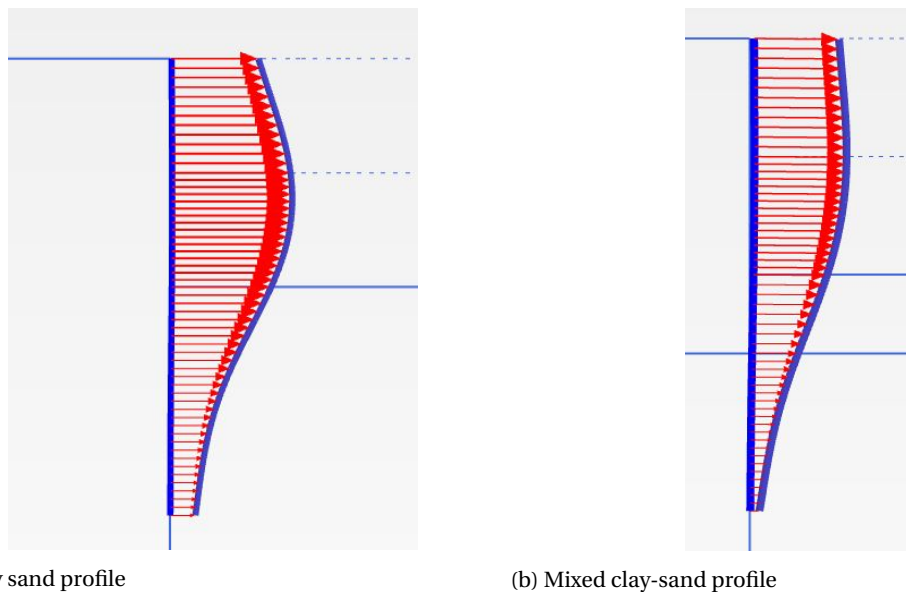


Figure 6.8: Displacements of both examples without a vertical force on top of the sheet pile

The first order bending moment for both examples are 164.9 kNm (sand soil profile) and 211.3 kNm (clay-sand soil profile). With a value for F_{cr} of $2\,717\text{ kN}$, this leads to a diagram of the current unity check in equation 6.3 for both examples as given in figure 6.9. The value 1.15 can be replaced in the global buckling check when the second order effects to the bending moment M_{Ed}^I are determined, as in equation 6.4. Since the bending moments M_{Ed}^{II} are already determined in previous sections, the improved unity check can simply be plotted against the current unity check. This plot is given in figure 6.9. For low normal forces, an significant improvement can be observed. For the high normal forces, the second order effects are around the 15%, so the removal of the factor 1.15 has a limited and unfavourable effect.

$$u.c. = \frac{N_{Ed}}{\chi_b N_{Rd}} + 1.15 \frac{M_{Ed}^I}{M_{Rd}} \quad (6.3)$$

$$u.c. = \frac{N_{Ed}}{\chi_b N_{Rd}} + \frac{M_{Ed}^{II}}{M_{Rd}} \quad (6.4)$$

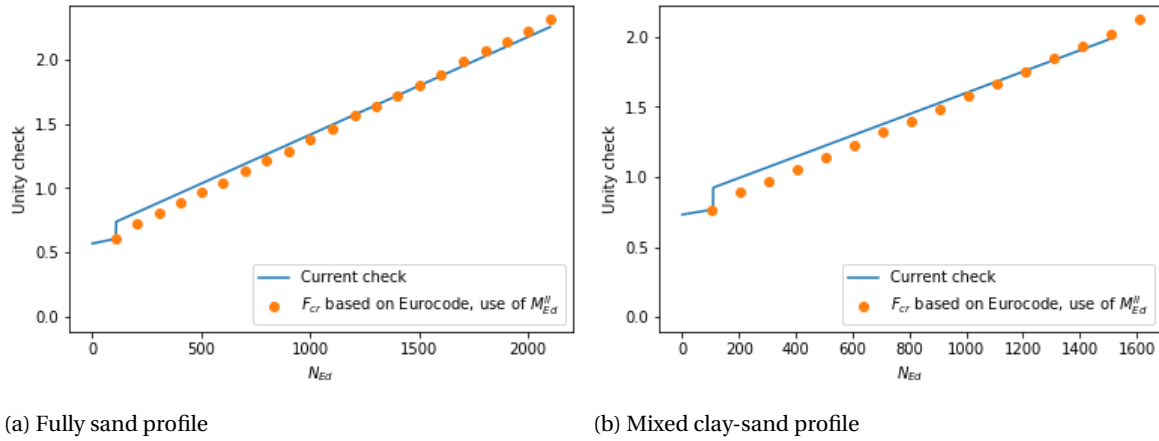


Figure 6.9: Unity check of the current check on global buckling and the improved check with the factor 1.15 replaced by M^II_{Ed}

The proposed method where the imperfections are modelled in the soil-structure interaction model and the method proposed by the POVm are compared as well with the current method. For those methods, the global buckling effect is included in the bending moment. Therefore, equation 6.5 yields as an unity check for those methods. With the data from the previous section, the unity checks could be plotted as in figure 6.10 for both examples. From this figure it can be concluded that the method proposed by the POVm and the method where imperfections were included give similar results for lower values of the normal force. Besides, both method's shows significant improvements compared to the current method. The POVm starts to underestimate the unity check for high normal forces, which is because this method uses the first order geometrical imperfection instead of the second order. This error is low to negligible for low normal forces, but becomes significant for large normal forces.

$$u.c. = \frac{N_{Ed}}{N_{Rd}} + \frac{M^II_{Ed}}{M_{Rd}} \tag{6.5}$$

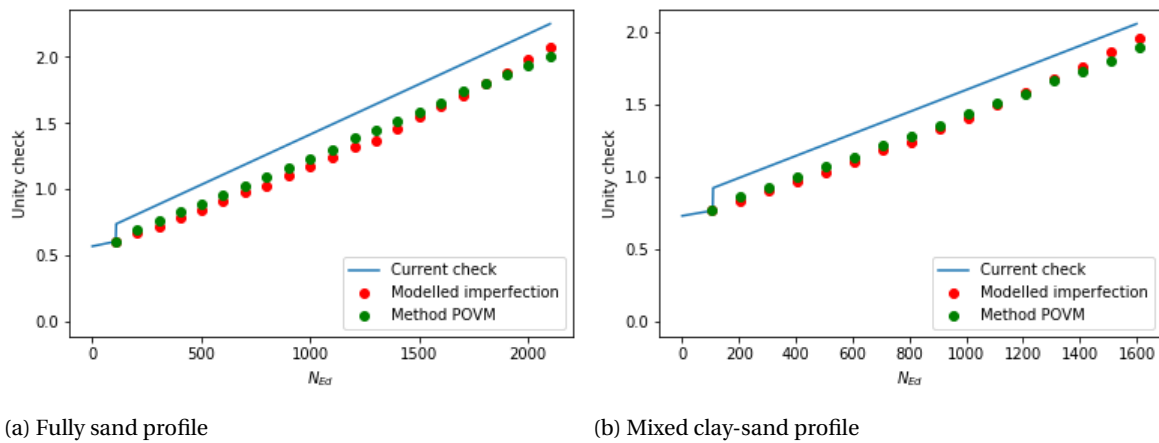


Figure 6.10: Unity check of the current check on global buckling compared with the method by modelling imperfections and the method proposed by the POVm

7

Discussion

The research done and models proposed for this thesis made some assumptions and gave some results to improve the current global buckling check. The validity, relevance and limitations of the results are dependent to the assumptions. Improvements to the current buckling check were found for the reduction factor χ_b and the value of 1.15, see equation 7.1. For each proposed improvement, the validity, relevance and limitations are discussed.

$$\gamma_{M1} \frac{N_{Ed}}{\chi_b N_{Rd}} + \gamma_{M1} * 1.15 \frac{M_{Ed}}{M_{Rd}} < 1 \quad (7.1)$$

The global buckling reduction factor χ_b is introduced to the global buckling check in order to take the effects of geometrical imperfections into account. An important parameter to determine the reduction factor χ_b is the critical global buckling load F_{cr} , which is the focus of chapter 5, proposing two models. Those models were developed in an attempt to determine the influence of the soil resistance to F_{cr} to take the influence of the soil to the global buckling mechanism into account. Though it appeared to be impossible to determine the exact value for F_{cr} if the soil resistance is taken into account, the first proposed method gave a relatively well approach after all. Several limitations come along with this method:

- The critical global buckling load F_{cr} can be approached if the spring model is used for the soil-structure interaction. Unfortunately, this model is not always used. For other soil-structure interaction models, no methods are known to determine F_{cr} .
- F_{cr} is based on an assumed constant elastic soil stiffness. Once the value of F_{cr} is known, it should be verified if the assumed soil stiffness does not decrease due to the global buckling mechanism. If the soil stiffness does decrease, F_{cr} should be re-calculated, this time with a lower soil stiffness. The verification of the soil stiffness must be done with great care because an error is made easily.
- Because the spring stiffness must be assumed and may be underestimated, it is only possible to approach the value of F_{cr} , not to determine the value exactly. Because the approach will lead to an underestimation of the critical global buckling load, it will be a safe side approach.
- Finally, F_{cr} is used to determine the value of reduction factor χ_b in order to take the effects of geometrical imperfections into account. Unfortunately, this determination requires a constant normal force in the structural element and thus in the sheet pile. However, the normal force in a sheet pile is not constant by principle because of the soil-structure friction and the anchor force, which are not introduced at the top of the sheet pile. In order to use the reduction factor χ_b safely, the maximum normal force in the sheet pile could be used. This will lead to an overestimation of the global buckling mechanism due to geometrical imperfections, but it will give a safe design of the sheet pile.

Because the first method is only applicable if the spring model is used, a second method was derived which was based on first and second order displacements. This method would be usable for all soil-structure interaction models. However, though relatively good results were found for non-sheet piling structures, the second method proved to be invalid for sheet piling structures. Based on a comparison with the first analytical method based on example calculations for a sheet piling structure, the second numerical method gave quite poor results and gave errors up to 35.8%. This error seems to be caused by the fact that the bottom tip of the pile is able to move. It was noticed that the more the tip was able to move due to lower soil stiffnesses,

the larger the error made by the numerical method becomes.

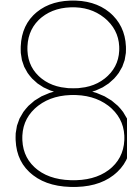
Because F_{cr} can only be approached if the spring model is used, other methods are derived to determine the global buckling effects caused by geometrical imperfections, discussed in chapter 6. In the third method the geometrical imperfections are modelled into design software for sheet piles. In contrast to the first proposed method, this method is able to take into account that the normal force is not constant in the sheet pile. However, also for this model, some limitations are present:

- Not all software is able to model a sheet pile including the geometrical imperfections. Therefore, it depends on the software used if this method is applicable or not. Typically, FE-software packages are able to model imperfections, less advanced software is not. Software available for the spring model as soil-structure interaction model is not able to model those imperfections. Therefore, the third method can not be used to describe the global buckling mechanism if the spring model is used.
- Unknown in the third method is the shape which should be used to model the geometrical imperfections. As discussed, this shape should be the same shape of the elastic buckling shape, but this is unknown. Therefore, a shape of the imperfections should be assumed which will lead to errors. However, as discussed, those errors will result in an overestimation, and therefore this method could be used safely.

The above approach has been simplified by a new approach included in the POVM, the fourth method. This approach can be used independent to which model has been used to model the soil-structure interaction. This method is a good approach which has been proven by the third method discussed. But again, also to this method are some limitations:

- For larger normal forces, the method becomes to be invalid. It is not really known what the maximal normal force is for which this method can be used. The POVM, where this method is come from, states that the method is valid until normal forces of about 20% of F_{cr} , where F_{cr} could be determined using the current method by the Eurocode neglecting the sub-soil. This is a somewhat vague boundary, not in the last place because the soil resistance to the critical global buckling load F_{cr} is neglected. More research to this boundary value might give a clear boundary.
- The prove of this method is based on two examples in this thesis, which is only a thin prove which should be strengthened with a multiple of examples. However, this method has been derived for and comes from the POVM. For this derivation, other examples has been worked out, but those are not yet published and are therefore not used.

The growth of the displacements is not only affecting the sheet pile, it is affecting the soil pressure as well. This gives that the loading to the sheet pile and a possible anchor force are changing as well due to the global buckling mechanism, resulting in another value of the bending moment caused by the soil pressure and anchor force. However, the existing global buckling equation with reduction factor χ_b does not take this influence of the global buckling mechanism into account. Therefore, even though the influence of the soil is taken into account to determine F_{cr} , the method stated by the Eurocode ignores this soil-structure interaction. The POVM method also ignores this soil-structure interaction, but for this method it has been proven that this neglect leads to only a small error and may even overestimate the bending moment caused by the global buckling mechanism.



Conclusions

The aim of this thesis is to investigate what the influence of the soil is to the global buckling mechanism in steel sheet piles. If possible, improvements to the current global buckling check given below as stated in the Eurocode, NEN-EN 1993-5, are proposed. Answers and possible improvements are found and discussed below. Once all questions are answered, a small wrap up of the two main conclusions will be given. From the answers, there are still a few questions left, which are treated by the recommendations.

$$\frac{N_{Ed}}{\chi_b N_{Rd}(\gamma_{M0}/\gamma_{M1})} + 1.15 \frac{M_{Ed}}{M_{Rd}(\gamma_{M0}/\gamma_{M1})} < 1 \quad (8.1)$$

8.1. Conclusions

In order to define the influence of the soil to the global buckling mechanism, three questions are stated. First of all, it is discussed what the background is of the global buckling mechanism. Secondly, how the current check to global buckling can be improved by taking the soil resistance into account and lastly, the quantity of those improvements are discussed.

What is the background of the current global buckling check for steel sheet piles?

The global buckling mechanism occurs if a normal force is applied to a sheet pile which is deformed. Due to the normal displacement of the deformed pile, the normal force introduces a bending moment. This moment should be taken into account by the verification of the steel stress in the sheet pile. This is done by the current check on global buckling as stated in equation 8.1. Two types of displacements occurs, to be the displacement caused by loading to the pile and the displacement caused by geometrical imperfections. The interaction between the normal force and the displacement caused by the loading is taking into account by a factor k_{yy} , which equals 1.15 in the current check for all steel sheet piling structures. For the bending moment caused by the normal force due to the imperfections, the factor χ_b has been introduced, which is dependent to the critical global buckling load F_{cr} . This load can be determined using Euler's global buckling theory, with the requirement that the materials in the structure have a linear elastic stiffness. Besides depending on F_{cr} , the value of χ_b depends to another factor as well. This factor is based on experiments and set to a constant value. From those experiments, it was concluded that the global buckling mechanism does not occur if the normal force falls below 4% of the value of F_{cr} . The unity check on global buckling should therefor not be executed in this case.

What are possible improvements to the current global buckling check to take the influence of the soil into account?

This thesis has reviewed the possibilities to take the influence of the soil to F_{cr} for steel sheet piles into account, but this appeared to be only limited possible. The problem is that F_{cr} can only be determined for structures composed by materials with a linear elastic stiffness with linear stiffnesses. Steel can be modelled with a linear elastic stiffness, the soil however has a behaviour which hardly can be described by a linear stiffness. Nevertheless, a method has been found to approach the value of F_{cr} . The interaction between the soil and the sheet pile must be modelled with a certain model, for which many models are available. Of the existing models, only the spring model is able to model the soil with a (semi-)linear elastic stiffness. Therefore, if the spring model is used, the value of F_{cr} can be approached using Euler's buckling theory. This thesis

describes a method which leads to the value of the critical global buckling force F_{cr} for steel sheet piles, including the influence of the soil. Unfortunately, there is one problem occurring which gives that the exact value of F_{cr} can not be determined. According to the spring model, the soil stiffness is dependent to the displacement of the soil. Consequently, the soil stiffness might decrease due to the extra displacement caused by the global buckling mechanism. If this is likely to happen, the soil stiffness should be modelled with the decreased value of the soil stiffness. This underestimation gives that the determined value of F_{cr} is only an approach and underestimation of the actual critical global buckling load.

A significant note to this method is that the well known and much used critical buckling length is not a point of interest. It will be quite difficult to determine the critical buckling length for steel sheet piles in the first place, general equations for the length are not available. Besides, if the critical length is known, only the influence of the soil to the critical length is known, not the influence to the critical global buckling load F_{cr} . A method using the critical buckling length would take much more time than the proposed method.

Several improvements can be made to the global buckling check stated by the Eurocode. One improvement is that the reduction factor χ_b can be replaced by taking the effects of the geometrical imperfections into account differently. This can be done by modelling a geometrical imperfect sheet pile into the calculation model. Some software is able to analyse such models and can also determine the growth of displacements due to the normal force. With this method, the effect of the global buckling mechanism initiated by geometrical imperfections can simply be calculated by the soil-structure interaction models. If this is done, applying the reduction factor χ_b to the normal force capacity would mean that the effects of the geometrical imperfections are double taken into account. Therefore, χ_b does not have to be applied and more importantly, the value of the critical global buckling load F_{cr} is no longer a point of interest.

The POVM, a Dutch design regulation for the design of dikes, gives an alternative, simplified approach. The factor of χ_b tries to represent the bending moment which is introduced by the normal force due to geometrical imperfections. In the POVM method, this bending moment is simply determined by the product of the normal force acting in the sheet pile with the value of the maximal geometrical imperfection. This should be added to the bending moment caused by the loading to the sheet pile. If this is done, the global buckling mechanism caused by geometrical imperfections is taken into account. Because this method is still relatively new, more prove is required before it can be used safely. However, for two worked out examples given in chapter 6 this method proved to be valid for relatively small values of the normal force. Therefore, this method is promising.

Above it has been discussed that the factor 1.15 is added to account for the effect of the normal force to the bending moment. Besides, the factor χ_b makes a small error, which gives that the effect of the global buckling mechanism is overestimated. This error is represented as well by the factor 1.15. This factor, which is originally expressed as k_{yy} is set constant to 1.15 and is a safe value for all sheet piling structures, independent of the loading. However, for much structures, the value of 1,15 is way to high. As alternative, the effect of the normal force to the bending moment can easily be determined with the calculation software as well. If this is done, the factor $k_{yy}(=1.15)$ should no longer represent the effect of the normal force to the bending moment, but only the error made by χ_b . However, because this error results in a small overestimation of the verification check on global buckling, it may be ignored without the design becoming unsafe.

What is the quantitative effect of the found improvements of the current global buckling check?

For the proposed method's, three examples have been treated with quantitative results, which all gave an significant improvement to the unity check on global buckling. Two quantitative effects of the improvements can be described. Firstly, a reduction to the unity check is seen because of the better approached effects of the geometrical imperfections. Secondly, the removal of the factor 1.15 by taking the global buckling effect to M_{Ed} into account gives an significant reduction of the unity check. The reduction to the unity checks of both improvements are similar for low values of the normal force.

The removal of the factor 1.15 can be done if the increment of the bending moment M_{Ed} due to the normal force is taken into account. Due to the normal force, the bending moment will certainly grow, but it is likely to be less as the 15% with the factor 1.15. The lower the normal force in the sheet pile is, the lower the growth of the bending moment will be. In other words, for large values of the normal force, the removal of the factor 1.15 will only result in a small reduction of the check on global buckling. If the bending moment grows more than 15% with the proposed method, it would be better to use the current factor 1.15. This is allowed because the

error made by χ_b is not accounted for by the proposed method, but it is accounted for by the factor 1.15. In other words, it may be beneficial to remove the factor 1.15 if the influence of the normal force to the bending moment is less than 15%.

For reference, most sheet pile structures have only a small normal force. Mostly, the influence of the normal force to the bending moment is about 0 to 10%. Though this percentage must be determined for each structure separately, it indicates the significance of this proposed improvement for much structures.

Though the removal of 1.15 is relevant for low normal forces only, the methods proposed to encounter the effects of global buckling due geometrical imperfections are relevant for both low and high values of the normal force.

To wrap up, two important conclusions can be taken from the answers to the research questions. Firstly, the effect of the global buckling mechanism due to possible imperfections can be taken into account by the reduction factor χ_b , at which the influence of the soil can be included by taking the soil resistance into account for the critical global buckling load F_{cr} . Unfortunately, the latter can only be done if the spring model is used to model the interaction between the soil and sheet pile. Because some drawbacks are in place with this method, it might be better to model the geometrical imperfections directly into available calculation software. If this is done, the effect of the imperfections to the internal forces in the sheet pile will be included in the results from the software.

Secondly, an important conclusion is that the factor 1.15 in the current Eurocode verification check on the buckling mechanism may be removed. This can simply be reached by taking the effect of the normal force to the bending moment M_{Ed} into account, a possibility most calculation software does provide. This will only have an effect if the normal force is relatively small, which is generally the case. For the unusual case that the normal force becomes large, it will be better to remain at the use of the factor of 1.15.

8.2. Recommendations

The research questions stated at the introduction are answered above, but from the answers, some new questions can be stated. Besides, other relevant questions to the global buckling check for steel sheet piles are still present. Those questions can be used for future research for which recommendations are given below.

- For future usage of the current check on global buckling, the factor 1.15 can be removed from the check if the influence of the normal force to the bending moment is taken into account in the calculation of the internal forces in the sheet pile.
- The most adequate approach to determine the effects of geometrical imperfections in the sheet pile is to model imperfections into the sheet pile. This method might provide a good alternative of the current check on global buckling stated by the Eurocode. For designs of sheet piling structures which uses the spring model to model the soil structure interaction, this is not possible. There are simply no software packages available which support the spring model and are capable to model imperfections into the sheet pile. It might be interesting to develop a program which is able to apply this method for the spring model.
- The shape in which geometrical imperfections should be modelled into the sheet pile is unknown. It is stated by the Eurocode that it should be done according to the elastic buckling shape, but this shape is unknown. More research could be done to which shape should be used.
- The method stated by the POVM is argued to be valid for relatively small values of the normal force. This thesis gives two worked out examples worked out with this method, where the method proved to be correct for those examples. Other sheet piling structures, with different conditions, might react different to the normal force. To prove that this method is valid for sheet piling structures in general, more example cases should be worked out with different. If this is done, this method gives a quite simple approach to determine the effects of global buckling in steel sheet piles.
- An additional question to the POVM method is which upper limit should be used where the method can be assumed to be valid. It is known that for large forces, the method starts to underestimate the global buckling mechanism. It is unknown from which value the method starts to become invalid. The POVM itself states that it is valid till a normal force of 20% of F_{cr} , but then the question is what the value of F_{cr} is. Additional research should be done to define the upper limit of this method.
- For the check on global buckling, safety factor should be used γ_{M1} . This factor should be used for sta-

bility checks for steel structures and equals 1.1 for steel sheet piles. The global buckling mechanism might lead to instability if the normal force goes to F_{cr} because the deformation of the structure becomes infinite. However, the normal force in sheet piles will not go to F_{cr} and instability due to global buckling will not occur. In reality, the global buckling check is more a check on the steel stress than on stability. For the steel stress, a safety factor $\gamma_{M0}(=1.0)$ should be used. It's unclear which factor should be used. As a reference, for steel structures in general, γ_{M1} is set to 1.0 according to NEN-EN 1993-1-1 instead of 1.1 for sheet piling structures according to NEN-EN 1993-5. It will be interesting to find out which value for γ_{M1} should be used, especially because the value for sheet piles differs from the value for steel structures in general.

Bibliography

- [1] Dawson-WAM. Twitter, January 2020. URL https://twitter.com/DAWSON_WAM/status/1222858825226649601.
- [2] Ir. W.F. Molenaar, Ing. M.Z. Voorendt. *Manual hydraulic structures 1*. TU-Delft, February 2017.
- [3] Nederlands normalisatie instituut. Eurocode 3: Design of steel structures - part 5: Piling, February 2008.
- [4] unknown. *Sheet piling handbook, 3rd edition*. Thyssen Krupp GfT Bautechnik, unknown.
- [5] CUR Bouw en Infra. Curpublicatie 166, part 1 and 2, 6e herziene druk, July 2012.
- [6] W. Boere A. Veruijt. *Grondmechanica*. VSSD, 1983.
- [7] M. de Koning. Master thesis tu delft, verticaal evenwicht van damwandconstructies, July 2, 2006. URL <https://repository.tudelft.nl/islandora/object/uuid%3Ac2517913-7294-4e53-b915-d67ffe20814c?collection=education>.
- [8] Deltares. D-sheet piling design of diaphragm and sheet pile walls, June 16, 2019.
- [9] Nederlands normalisatie instituut. NEN-en 1997-1+c1+a1; eurocode 7: Geotechnical design - part 1: General rules, June 2016.
- [10] Nederlands normalisatie instituut. NEN 9997-1+c2; geotechnical design of structures - part 1: General rules, November 2017.
- [11] J. G. Potyondy, M.Eng. Skinfriction between various soil and construction materials. *Géotechnique*, 11: 339-353, 1961.
- [12] D.A. Kort. Doctoral thesis tu delft, steel sheet pile walls in soft soil, February 25, 2002. URL <https://repository.tudelft.nl/islandora/object/uuid%3A6329dc40-f6bb-4791-916b-ff675422cf4b?collection=research>.
- [13] Plaxis. Plaxis material models manual 2019, 2019.
- [14] POV Macrostablieit. Povm rekentechnieken – eem toepassing binnen het ontwerp, December 20, 2018.
- [15] ir. D Grotegoed, ir. R. Spruit. Het verticale evenwicht van een verankerde damwand. *Geotechniek*, July 2012.
- [16] C. Hartsuijker, J.W. Welleman. *Module: Stablieit van het evenwicht*. TU-Delft, December 2016.
- [17] G. Sedlacek, R. Hartmann-Linden, F van Tol, A. Kort, A. Schmitt, M. Meyrer. *Development of unified design rules for steel sheet piles for introduction into Eurocode 3, Part 5*. European Union, January 1, 2002.
- [18] Nederlands normalisatie instituut. NEN 10248; warmgewalste damwandprofielen van ongelegeerde staalsoorten. deel 2: Toleranties op vorm en afmetingen, August 1995.
- [19] Nederlands normalisatie instituut. Eurocode 3: Design of steel structures - part 1-1: General rules and rules for buildings, December 2016.
- [20] Plaxis. Plaxis reference manual 2019, 2019.
- [21] G. Meinhardt, A.C. Vriend. Knikstablieit ankerpalen. *Cement*, 2009.
- [22] N. Vogt, S. Vogt. Knicken von pählen mit kleinem durchmesser in breiigen böden. *Fraunhofer IRB verlag*, 2005.
- [23] T.M.A. Lankreijer. Master thesis tu delft, buigingsknik van ankerpalen, July 3, 2014. URL <https://repository.tudelft.nl/islandora/object/uuid%3A7ad4ab46-1471-4ab8-82ea-c52567f2785a?collection=education>.

-
- [24] CUR Bouw en Infra. Curpublicatie 136, November 2011.
- [25] Ing. H. Larsen, Ir. H. Verbraken, Ir. R. van der Sman, Ir. V. Veenbergen. Pov-m publicatie stabiliteitsverhogende langconstructies, version 2020. (to be published medio 2020), 2020.
- [26] J.W. Welleman. *Work, energy methods and influence lines: Capita selecta in engineering mechanics*. Bouwen met staal, August 2016.
- [27] J. Rondal, R. Maquoi. Formulations d'ayrton-erry pour le flambement des barres métalliques, 1979.
- [28] J.W. Welleman. Knik en de voorschriften, 2016. URL http://icozct.tudelft.nl/TUD_CT/CT2031/collegestof/stabiliteit/files/KnikEUROCODE3.pdf.
- [29] Plaxis. Plaxis tutorial manual 2018, 2018.

List of Figures

| | | |
|------|---|----|
| 1 | Principle of global buckling in a sheet pile. Sheet pile anchored by a grout body anchor | |
| 1.1 | Cross sections of sheet pile profiles (figure 39-1 and 39-2 from [2]) | 1 |
| 1.2 | Visual representation of the report structure | 4 |
| 2.1 | Sheet pile profiles (figures from D-sheet piling) | 5 |
| 2.2 | Structural scheme of waling and horizontal support (top view) | 6 |
| 2.3 | Cross sectional lay-out of a wale supported sheet pile (figure 40-1 from [2])(side view) | 6 |
| 2.4 | Types of anchor systems | 7 |
| 2.5 | Sheet pile profiles [2] | 7 |
| 2.6 | Several cross sections for cimbi-walls: a) Tube piles with two Z-profiles in between; b) double U-profiles with two U-profiles in between; c) quadruple Z-profiles with two Z-profiles in between; d) and e) IPE profiles as stiffeners behind U- or Z-profiles (figure 39-21 from [2]) | 8 |
| 2.7 | Arch effect in horizontal soil pressure on combi-walls (figure 3.15 from [5]) | 9 |
| 2.8 | Soil deformation behaviour (figure 24-3 from [2] (adapted)) | 10 |
| 2.9 | Sketch of both straight (left) as curved (right) slip planes | 10 |
| 2.10 | Forces acting to the soil body sliding away (figure 34.1 from [6]) | 10 |
| 2.11 | Skinfriction angle δ based on the friction angle [10] | 12 |
| 2.12 | Reaction of sheet pile against log-scale time (figure 4.45 from [12]) | 13 |
| 2.13 | Schematisation of displacement, loading and effective loading by Blum (figure 39.7 from [2]) | 14 |
| 2.14 | Factor for embedded depth by Blum's method (table 39.4 from [2]) | 14 |
| 2.15 | Stress-deformation relationships | 15 |
| 2.16 | Spring stiffness values for different soils (table 33.1 from [2]) | 15 |
| 2.17 | Horizontal soil stress around an excavation with a sheet pile wall | 16 |
| 2.18 | interaction between horizontal soil pressure and sheet pile (figure 5.1 from [5]) | 17 |
| 2.19 | Mobilisation curve skin friction (figure 21 from [7]) | 18 |
| 2.20 | Case study Geotechniek | 19 |
| 2.21 | Structural element loaded by bending moment M and shear force V | 20 |
| 2.22 | M -, V - and N - forces on small structural element | 20 |
| 2.23 | M -, V - and N - forces on small structural element with an elastic support | 21 |
| 2.24 | Oblique bending of U-shaped sheet piles (figure 3.7 from [5]) | 22 |
| 3.1 | First order (left) and second order (right) displacement field (figure 11.4 from [16]) | 24 |
| 3.2 | Deformation w against the axial force F | 25 |
| 3.3 | Global buckling of a straight structure without initial displacement ($F_k = F_{cr}$) | 27 |
| 3.4 | Several values for the critical buckling length L_k (figure 36-2 from [2](adapted)) | 28 |
| 3.5 | Buckling length according to Eurocode | 29 |
| 3.6 | Example of fixed sheet pile with variable stiffness | 30 |
| 3.7 | Example of possible imperfections in steel sheet piling (table 9 from [18]) | 31 |
| 3.8 | Imperfections represented by eccentricity e | 32 |
| 3.9 | Experimental results of buckled sheet piles (figure 2.6-9 from [17]) | 33 |
| 3.10 | Comparison between equation 3.28 (exact equation) and equation 3.29 (simplified equation) | 34 |
| 3.11 | Test results of failure points by M-N interaction (figure 2.6-12 from [17]) | 34 |
| 3.12 | Imperfection model according to Eurocode 1993-1-1 | 35 |
| 3.13 | Example of normal force development in sheet piles (Figure from Plaxis 2D) | 37 |
| 4.1 | Displacement of an elastic supported beam (Left: elastically supported; Right: not elastically supported) (figure 7.20 from [16]) | 39 |
| 4.2 | Fourth buckling mode of a elastically supported beam (figure 7.21) from [16]) | 41 |
| 4.3 | Stress-Displacement diagram (figure 33.5 from [2]) | 41 |
| 4.4 | Comparison of several methods and tests for pile buckling (figure 7-1 from [23]) | 42 |
| 4.5 | Equilibrium of momentum at buckling (figure 2 from [22]) | 43 |

| | | |
|------|---|-----|
| 4.6 | Normal force - displacement curves based on different models (figure 3 from [22]) | 43 |
| 5.1 | Schematisation of the sheet pile neglecting the mobilisation of the soil | 47 |
| 5.2 | Determinant of coefficient matrix plotted against the normal force F | 49 |
| 5.3 | Effect of imperfections and normal force combined | 50 |
| 5.4 | Stress-Displacement diagram (figure 33.5 from [2]) | 51 |
| 5.5 | Structural model of sheet pile example | 51 |
| 5.6 | Example calculation of the global critical buckling load based on partly elastic support | 52 |
| 5.7 | Initial soil pressure mobilisation of the model | 53 |
| 5.8 | Structural model of sheet pile example | 53 |
| 5.9 | Plot of determinant against the normal force. Critical global buckling load F_{cr} equals 2 2 390 kN | 54 |
| 5.10 | Structural model for the critical buckling load calculation/approach of a sheet pile | 56 |
| 5.11 | Buckling shape computed by Diana FEA | 57 |
| 5.12 | Structural model of sheet pile in figure 5.6 | 58 |
| 5.13 | Normal distribution of soil stiffness and critical buckling load with varying soil stiffness as input | 59 |
| 5.14 | Normal distribution of bending stiffness and critical buckling load with varying bending stiffness as input | 59 |
| 5.15 | Normal distribution of bending stiffness and critical buckling load with varying bending stiffness as input | 60 |
| 5.16 | Example A: Elastic founded beam loaded by a distributed load of 100 kN/m | 62 |
| 5.17 | First and second order displacement of the example, loaded by a normal force of 2 000 kN | 62 |
| 5.18 | Errors for different correction factors δ | 63 |
| 5.19 | Several load cases for the determination of the critical global buckling based on displacements | 64 |
| 5.20 | Sheet pile lay-out to compare the theoretical method with the method based on displacements | 65 |
| 5.21 | Lay-out of the example for comparison method of the proposed with the current method | 66 |
| 5.22 | Structural model to determine F_{cr} for the sheet pile of figure 5.21 | 68 |
| 5.23 | Plots of equations 5.14 and 5.15 | 69 |
| 5.24 | Plots of equations 5.13, 5.15 and 5.16 | 69 |
| 6.1 | Extreme imperfection modelled in Plaxis 2D | 71 |
| 6.2 | Lay-out and displacement shape of sheet pile example in sand soil layer | 72 |
| 6.3 | Differential displacement between the normal force and maximal displacement | 73 |
| 6.4 | Lay-out and displacement shape of sheet pile example in sand-clay mixed soil profile | 75 |
| 6.5 | Buckling shapes as defined by Eurocode 3 part 5 (NEN-en 1993-5) | 76 |
| 6.6 | Imperfection in a sheet pile (not to scale) | 77 |
| 6.7 | Place of the normal forces F_{top} and F_{anchor} with respect to the maximal imperfection | 80 |
| 6.8 | Displacements of both examples without a vertical force on top of the sheet pile | 82 |
| 6.9 | Unity check of the current check on global buckling and the improved check with the factor 1.15 replaced by M_{Ed}^{II} | 83 |
| 6.10 | Unity check of the current check on global buckling compared with the method by modelling imperfections and the method proposed by the POVM | 83 |
| A.1 | Displacement of the force and deformation of the beam in critical global buckling (figure from [26]) | 101 |
| B.1 | Buckling curves according to European standards (The critical buckling load is referred to as Euler buckling load)(figure 2 from [28]) | 104 |
| C.1 | Linear design line when neglecting the M-N interaction factor | 108 |
| C.2 | Unity check of buckling mechanism: exactly and linear | 109 |
| C.3 | Plot of both the simplified equation (C.6) as the exact equation C.1 to model the M-N interaction with the buckling mechanism | 109 |
| C.4 | Plot of both the exact solution as the simplified solution in combination with the correction factor | 110 |
| C.5 | Amplification of a beam loaded by distributed load | 111 |

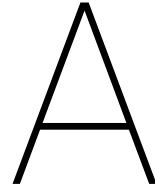
| | | |
|------|--|-----|
| D.1 | Coefficient matrix of buckling derivation for sheet pile schematisation in chapter 5.1 | 114 |
| D.2 | Determinant of the coefficient matrix of buckling derivation for sheet pile schematisation in chapter 5.1 | 115 |
| E.1 | Example A: Distributed load of 100 kN/m | 118 |
| E.2 | Example B: Double moment loading, $M = 100 \text{ kNm}$ | 120 |
| E.3 | Error against delta plot example B | 121 |
| E.4 | Example C: Point load loading, $F = 100 \text{ kN}$ | 122 |
| E.5 | Error against delta plot example C | 123 |
| E.6 | Example D: Double moment loading, $M = 100 \text{ kNm}$, distributed load loading, $q = 10 \text{ kN/m}$ and point load loading, $F_v = 100 \text{ kN}$ | 125 |
| E.7 | Error against delta plot example D | 126 |
| E.8 | Example E: single moment loading, $M = 100 \text{ kNm}$ | 127 |
| E.9 | Error against delta plot example E | 128 |
| F.1 | Structural model of example section 5.1.2 | 131 |
| F.2 | Final model of the sheet pile in Diana FEA | 133 |
| F.3 | Steps 1 and 2 of DIANA FEA stability analysis | 134 |
| F.4 | Steps 3 and 4 of DIANA FEA stability analysis | 134 |
| F.5 | Steps 5 and 6 of DIANA FEA stability analysis | 135 |
| F.6 | Steps 7 and 8 of DIANA FEA stability analysis | 135 |
| F.7 | Steps 9 of DIANA FEA stability analysis | 136 |
| F.8 | Steps 10 and 11 of DIANA FEA stability analysis | 136 |
| F.9 | Steps 12 and 13 of DIANA FEA stability analysis | 137 |
| F.10 | Steps 14 and 15 of DIANA FEA stability analysis | 137 |
| F.11 | Steps 16 and 17 of DIANA FEA stability analysis | 138 |
| F.12 | Steps 18 and 19 of DIANA FEA stability analysis | 138 |
| F.13 | Steps 20 and 21 of DIANA FEA stability analysis | 139 |
| F.14 | Steps 22 and 23 of DIANA FEA stability analysis | 139 |
| F.15 | Steps 24 and 25 of DIANA FEA stability analysis | 140 |
| F.16 | Step 26 and Mesh of DIANA FEA stability analysis | 141 |
| G.1 | Development of normal force in the sheet pile | 144 |
| G.2 | Example for second order calculation by D-sheet piling | 144 |
| H.1 | Lay-out of sheet pile structures in chapter 6 | 145 |
| H.2 | Material properties of the anchor rod | 146 |
| H.3 | Material properties of the embedded beam row | 146 |
| H.4 | Sand properties in the Plaxis models (table 3.1 from [29]) | 147 |
| H.5 | Clay properties in the Plaxis models (table 3.1 from [29]) | 148 |
| H.6 | Construction phases of the model | 149 |
| H.7 | Imperfection model in Plaxis 2D | 150 |

List of Tables

| | | |
|------|--|-----|
| 2.1 | Skin friction angle based on experience of the Rijkswaterstaat Bouwdienst [5] | 11 |
| 2.2 | f_ϕ and f_c values based on experiments (values from [11]) | 17 |
| 3.1 | Amplification factor's for both sinusoidal and parabolic displacement fields | 26 |
| 3.2 | Unity check of normal load | 36 |
| 5.1 | Soil and material properties of the structure given in figure 5.6 | 52 |
| 5.2 | Determination of critical buckling load of the beam in figure 5.16 based on displacements with a δ correction factor of 0.006 | 63 |
| 5.3 | Results of the various examples in figure 5.19 | 64 |
| 5.4 | Results of both methods for different parameter sets | 65 |
| 5.5 | Soil and material properties of the structure given in figure 5.21 | 67 |
| 6.1 | Data on the sheet pile structure of figure 6.2a in a sand soil layer | 74 |
| 6.2 | Data on the sheet pile structure of figure 6.4 in a clay soil layer | 75 |
| 6.3 | Bending moments caused by the geometrical imperfections for the example in figure 6.2a | 78 |
| 6.4 | Bending moments caused by the imperfections for the example in figure 6.4a | 78 |
| 6.5 | Bending moments caused by the imperfections for the example in figure 6.2a, based on the POVM method (with F_{top}) and the model including geometrical imperfections in the sheet pile | 79 |
| 6.6 | Bending moments caused by the imperfections for the example in figure 6.2a, based on the POVM method (with N_{Ed}) and the model including geometrical imperfections in the sheet pile | 81 |
| 6.7 | Bending moments caused by the imperfections for the example in figure 6.4a, based on the POVM method (with N_{Ed}) and the model including geometrical imperfections in the sheet pile | 81 |
| E.1 | Determination of critical buckling load of the beam in figure E.1 based on displacements rounded to the first decimal with a δ correction factor of -0.018 | 119 |
| E.2 | Determination of critical buckling load of the beam in figure E.1 based on displacements rounded to the first decimal with a δ correction factor of -0.008 | 119 |
| E.3 | Determination of critical buckling load of the beam in figure E.2 based on displacements with a δ correction factor of 0.051 | 121 |
| E.4 | Determination of critical buckling load of the beam in figure E.2 based on displacements rounded to the first decimal with a δ correction factor of 0.022 | 121 |
| E.5 | Determination of critical buckling load of the beam in figure E.2 based on displacements rounded to the first decimal with a δ correction factor of -0.051 | 122 |
| E.6 | Determination of critical buckling load of the beam in figure E.4 based on displacements with a δ correction factor of -0.024 | 123 |
| E.7 | Determination of critical buckling load of the beam in figure E.4 based on displacements rounded to the first decimal with a δ correction factor of -0.258 | 124 |
| E.8 | Determination of critical buckling load of the beam in figure E.4 based on displacements rounded to the first decimal with a δ correction factor of 0.013 | 124 |
| E.9 | Determination of critical buckling load of the beam in figure E.4 based on displacements with a δ correction factor of 0.004 | 126 |
| E.10 | Determination of critical buckling load of the beam in figure E.4 based on displacements rounded to the first decimal with a δ correction factor of -0.033 | 126 |
| E.11 | Determination of critical buckling load of the beam in figure E.4 based on displacements rounded to the first decimal with a δ correction factor of 0.001 | 127 |
| E.12 | Determination of critical buckling load of the beam in figure E.4 based on displacements with a δ correction factor of -0.07 | 128 |
| E.13 | Determination of critical buckling load of the beam in figure E.4 based on displacements rounded to the first decimal with a δ correction factor of -0.033 | 129 |

| | | |
|------|---|-----|
| E.14 | Determination of critical buckling load of the beam in figure E.4 based on displacements rounded to the first decimal with a δ correction factor of -0.019 | 129 |
| E.15 | Determination of critical buckling load for the structure in figure 5.1 with parameter set 1 based on displacements | 130 |
| E.16 | Determination of critical buckling load for the structure in figure 5.1 with parameter set 2 based on displacements | 130 |
| E.17 | Determination of critical buckling load for the structure in figure 5.1 with parameter set 3 based on displacements | 130 |
| F.1 | Data input for FEA model | 132 |
| H.1 | Properties of Plaxis models | 146 |

Appendices



Derivation of the critical global buckling load according to Rayleigh

In addition to Euler's derivation of the critical global buckling load, another method described by Rayleigh [26] is available to determine this load. This method is based on the energy required to bend the element as in figure 3.1.2. The energy required to deform the beam (both axial as bending deformation) must originate in the work delivered by the displacement of the normal force (the product of force and displacement). Figure A.1 is added to visualise the deformation of the beam and displacement of the force [26].

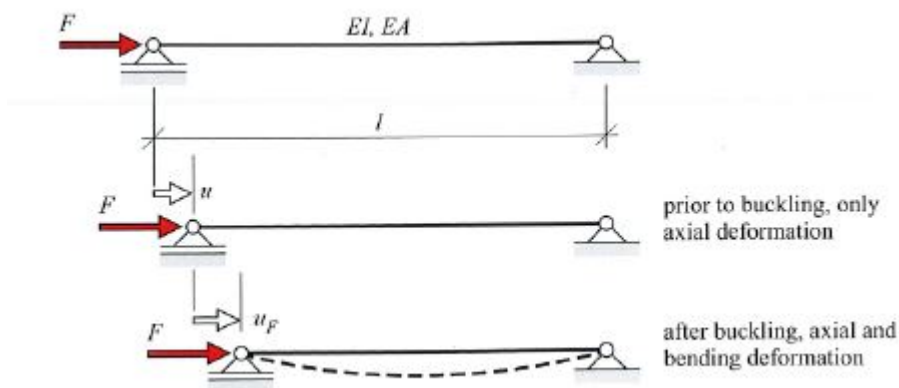


Figure A.1: Displacement of the force and deformation of the beam in critical global buckling (figure from [26])

For lower values of the normal force, the deformation of an element is purely in the axial strain of the element (middle element in figure A.1). The strain energy required to deform the element axially is introduced by the normal force and is given in equation A.1. The bending deformation of the buckled element (lower element in figure A.1) requires energy, which depends on the curvature which in turns depends on the displacement field.

The critical global buckling mechanism will occur suddenly when reaching the critical buckling load. Just before the normal force reaches this critical value, the element does not buckle and remains straight. But with minimal increment of the normal force, buckling occurs and the force will displace due to the bending. The energy delivered by this force displacement, will be the energy required for the bending deformation. The strain energy at buckling can be described by equation A.2. Since the normal force increases minimal, the first of this equation term could be eliminated. Therefore, equation A.4 could be written.

The energy stored in the beam before buckling:

$$E_v = \int_0^L \frac{1}{2} * EA * \epsilon^2 dx \quad (A.1)$$

The energy stored in the beam after buckling:

$$E_v = \int_0^L \frac{1}{2} * EA * \epsilon^2 dx + \int_0^L \frac{1}{2} * EI * \kappa^2 dx \quad (\text{A.2})$$

The displacement of the force due to the bending can be written by [26]:

$$u_f = \int_0^L \frac{1}{2} * \left(\frac{dw}{dx}\right)^2 dx \quad (\text{A.3})$$

$$\int_0^L \frac{1}{2} * EI * \left(\frac{d^2w}{dx^2}\right)^2 dx = F * u_f \quad (\text{A.4})$$

$$w(x) = \hat{w} * \sin\left(\frac{m * \pi * x}{L}\right) \quad (\text{A.5})$$

Solution to equation A.4:

$$N_{cr} = F_{cr} = \frac{\int_0^L EI * \left(\frac{d^2w}{dx^2}\right)^2 dx}{\int_0^L \left(\frac{dw}{dx}\right)^2 dx} = \frac{EI * \hat{w}^2 * \left(\frac{\pi^2}{L^2}\right)^2 * \int_0^L \sin^2\left(\frac{\pi * x}{L}\right) dx}{\hat{w}^2 * \left(\frac{\pi^2}{L^2}\right)^2 * \int_0^L \cos^2\left(\frac{\pi * x}{L}\right) dx} = \frac{\pi^2 * EI}{L^2} \quad (\text{A.6})$$

B

Derivation of global buckling reduction factor χ_b

To take imperfections into account, Eurocode 3 (steel) uses the imperfection curves given in figure B.1. The derivation of these curves starts with equation B.1. Factor C is added to the equation in order to reduce the plastic bending moment capacity if a normal force is applied. If the elastic bending moment capacity is used, this factor may be removed.

$$\frac{N_{Ed}}{N_{pl,Rd}} + C \frac{1 + \delta \frac{N_{Ed}}{N_{cr}}}{1 - \frac{N_{Ed}}{N_{cr}}} \frac{N_{Ed} * e_0}{M_{Rd}} + C \frac{M_{Ed}}{M_{Rd}} \leq 1 \quad (B.1)$$

Equation B.1 is rewritten and parameters are replaced by parameters with the same physical meaning. Since the third term of equation B.1 is independent from the normal force, this term is cancelled and reintroduced after the derivation. It takes some mathematical effort, but a generalised equation for the buckling resistance based on imperfections is found.

With the reduction factor:

$$\chi_b = \frac{N_{Ed}}{N_{pl,Rd}} \quad (B.2)$$

and relative slenderness:

$$\bar{\lambda}_b = \sqrt{\frac{N_{pl,Rd}}{N_{cr}}} \quad (B.3)$$

and the fact that $\delta=0$ gives that equation B.1 can be rewritten to:

$$\frac{N_{Ed}}{N_{pl,Rd}} + C \frac{1 + \delta \frac{N_{Ed}}{N_{cr}}}{1 - \frac{N_{Ed}}{N_{cr}}} \frac{N_{Ed} * e_0}{M_{Rd}} \Rightarrow \chi_b + C \frac{e_0 * A * f_y}{W * f_y} \frac{\chi_b}{1 - \chi_b \bar{\lambda}_b^2} \leq 1 \quad (B.4)$$

with:

A = cross sectional area

W = section modulus

Introducing:

$$\eta_b = C \frac{e_0 * A}{W} \quad (B.5)$$

gives that equation B.4 can be rewritten to:

$$\chi_b + \eta_b \frac{\chi_b}{1 - \chi_b \bar{\lambda}_b^2} \leq 1 \quad (B.6)$$

In literature ([17], p. 97) η_b is rewritten to the form given in equation B.7. The term α can be seen as a box where all the cross sectional parameters are put into with one exception. The document for the development of Eurocode 3 part 5 states the following on page 98:

'The European buckling curves a to d in EN1993-1.1 use values for α which were calibrated on tests and which are dependent on the cross sectional geometry and fabrication, see Rondal and Maquoi. The factor ε is not considered in the European buckling curves, so that the approach is safe sided for steel grades higher than S235'[17]

$$\eta_b = \alpha * \varepsilon * (\bar{\lambda}_b - 0.2) \quad (B.7)$$

$$\alpha = \frac{e * C * \frac{h}{2}}{l_0 * i * \alpha_{pl}} \sqrt{\frac{E}{235}} * \pi * \bar{\phi}_b \quad (B.8)$$

$$\varepsilon = \sqrt{\frac{235}{f_y}} \quad (B.9)$$

From tests (see [17] and [27]) it has been found that a value of 0.76 is representing the imperfection factor α sufficiently well for sheet piles (buckling curve d). To fit the curves with the test results, the relative slenderness $\bar{\lambda}_b$ was adapted with the subtraction of 0.2. This gives that the elements with a slenderness lower than 0.2 have a reduction factor χ higher than 1 (so technically it is not a reduction factor anymore). However, since the elements will fail theoretical on yielding due to normal compression instead of bending, the buckling curve is capped of for slenderness lower than 0.2. For this reason, the buckling check for structural elements do not have to be carried out for slenderness ratios below 0.2, which is also stated in Eurocode 3 [19]. This means that no buckling check is required when $N_{Rd,pl}$ is less than 4% of N_{cr} . In Eurocode 3 it is stated that the acting normal force N_{Ed} should be less than 4% of N_{cr} .

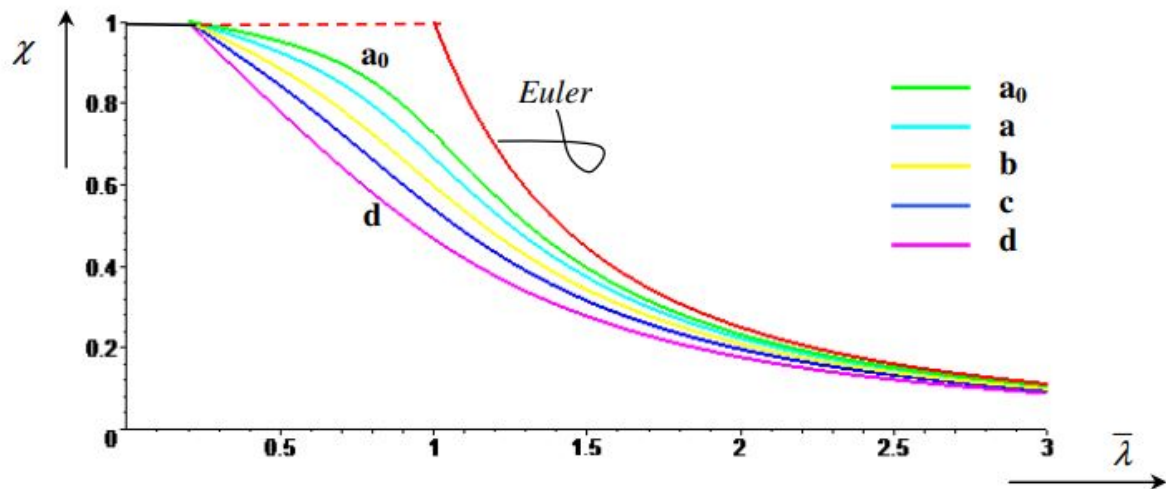


Figure B.1: Buckling curves according to European standards (The critical buckling load is referred to as Euler buckling load)(figure 2 from [28])

The value of α only yields for certain deflection values. For Z-profiles, the maximal deflection ratio e/l_0 is 5.5%, 5 %of for U piles with full interlock shear transfer and 7 %of for single U-profiles [17]. For larger imperfections, the buckling capacity reduces. The ignorance of the yield stress factor ε leads to an underestimation of approximately 10% in the case of sheet piles with S430.

With some mathematical effort the reduction factor can be expressed as:

$$\chi_b = \frac{1}{\Phi + \sqrt{\Phi^2 - \bar{\lambda}_b^2}} \quad (B.10)$$

With:

$$\Phi = 0.5(1 + \alpha * \varepsilon * (\bar{\lambda}_b - 0.2) + \bar{\lambda}_b^2) \quad (\text{B.11})$$

With the above, the buckling capacity can be determined by equation B.12, by using χ_b according to formula B.10.

$$N_{b,Rd} = \chi_b N_{pl,Rd} \quad (\text{B.12})$$

C

M-N Interaction for structural cross sections by the k_{yy} factor

Note to the reader

This appendix gives several plots which are based on the set of parameters given below. Though these parameters are irregular to steel sheet pile structures, it results in clear plots which are contributing to the explanation to the background of the factor k_{yy} for the M-N interaction. The qualitative effects are independent on the parameters.

$$\begin{aligned} N_{Rd} &= 3\,000 \text{ kN} & F_{cr} &= 1\,000 \text{ kN} \\ M_{Rd} &= 150 \text{ kNm} & e_0 &= 0.05 \text{ mm} \end{aligned}$$

Appendix B used equation C.1 to derive a generalised approach given by equation C.2. Due to two effects treated later in this appendix, a factor is required for the interaction between the bending moment and the normal force (the M-N interaction). This is called the k_{yy} factor which is taken into account in the bending moment term. For steel sheet piles, it was decided to determine a constant but conservative value. This value was set to 1.15 based on FE-experiment results [17]. If this value could be made less conservative, the buckling check on steel sheet piles could be less conservative as well. Therefore, this appendix will treat the background of this factor k_{yy} firstly, after which it is discussed how this factor could be made less conservative in use. The given equation for k_{yy} is taken from annex A from Eurocode 1993-1-1 based on elastic design (steel class 3) and the ignorance of torsional buckling related factors.

$$\frac{N_{Ed}}{N_{pl.Rd}} + \frac{1}{1 - \frac{N_{Ed}}{F_{cr}}} \frac{N_{Ed} * e_0}{M_{Rd}} + \frac{M_{Ed.2ndorder}}{M_{Rd}} < 1 \quad (C.1)$$

$$\frac{N_{Ed}}{\chi * N_{Rd}} + k_{yy} * \frac{M_{Ed}}{M_{Rd}} < 1 \quad (C.2)$$

$$\begin{aligned} k_{yy} &= C_{my} \frac{\mu_y}{1 - \frac{N_{Ed}}{F_{cr}}} \\ \mu_y &= \frac{1 - \frac{N_{Ed}}{F_{cr}}}{1 - \chi_b \frac{N_{Ed}}{F_{cr}}} \end{aligned} \quad (C.3)$$

As a reference, the design lines based on equation C.2 for several constant k_{yy} values are given in figure C.1. When a load case results in a point above such a design line, the structure does not have enough strength and will fail according to the model.

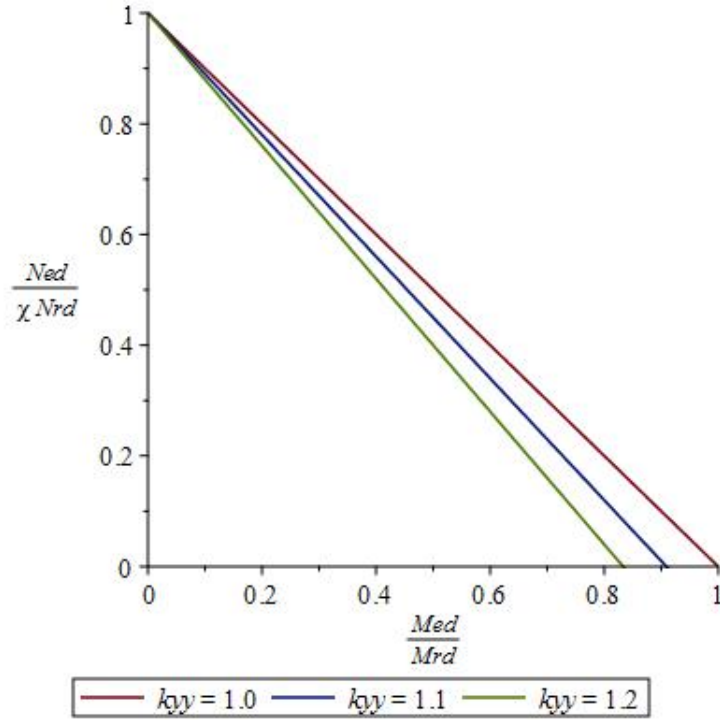


Figure C.1: Linear design line when neglecting the M-N interaction factor

C.1. Error made by the buckling equation

For a load case where the normal force is the only load, equation C.4 is valid. As mentioned earlier, equation C.4 is replaced by equation C.5. The equation is rewritten in such a way that both equations are exactly similar at a unity check of 1.0. For cases with a lower load N_{Ed} the simplified equation C.5 is an overestimation of the exact equation C.4. For larger load cases, the simplified equation is an underestimation. The latter is not a problem since the capacity (unity check = 1.0) is exceeded in both equations. Figure C.2 shows clearly that the effect of the buckling mechanism is overestimated by equation C.5 for normal loads lower than the normal buckling capacity.

$$\frac{N_{Ed}}{N_{pl,Rd}} + \frac{1}{1 - \frac{N_{Ed}}{F_{cr}}} \frac{N_{Ed} * e}{M_{Rd}} < 1 \quad (C.4)$$

$$\frac{N_{Ed}}{\chi * N_{Rd}} < 1 \quad (C.5)$$

In itself, the overestimation by equation C.5 of the buckling effect is not a problem since it should check if the capacity is exceeded or not. For both the simplified as the exact equation, the capacity is exceeded at the same normal load. It does become a problem when a bending moment is added to the check as already described by equation C.1. If this bending moment is simply added to equation C.5, equation C.6 remains. Since the first term is an overestimation of the reality, this equation is a conservative replacement of equation C.1. Figure C.3 shows the design lines of both equations. When the load exceeds the simplified design line in figure C.3, some resistance is left before the design line of the exact equation is exceeded. Partly for this reason, the M-N interaction factor k_{yy} is introduced to equation C.7.

$$\frac{N_{Ed}}{\chi_b * N_{Rd}} + \frac{M_{Ed,2ndorder}}{M_{Rd}} < 1 \quad (C.6)$$

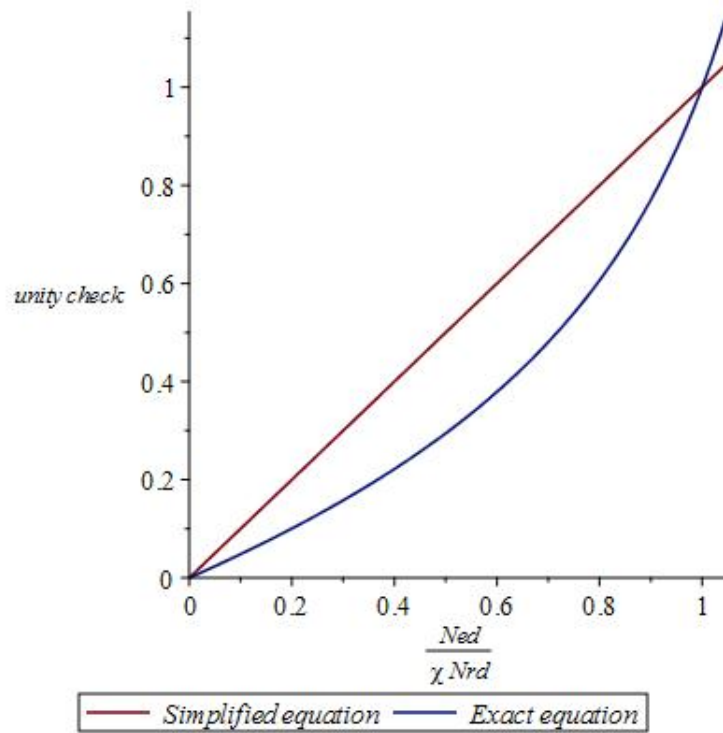


Figure C.2: Unity check of buckling mechanism: exactly and linear

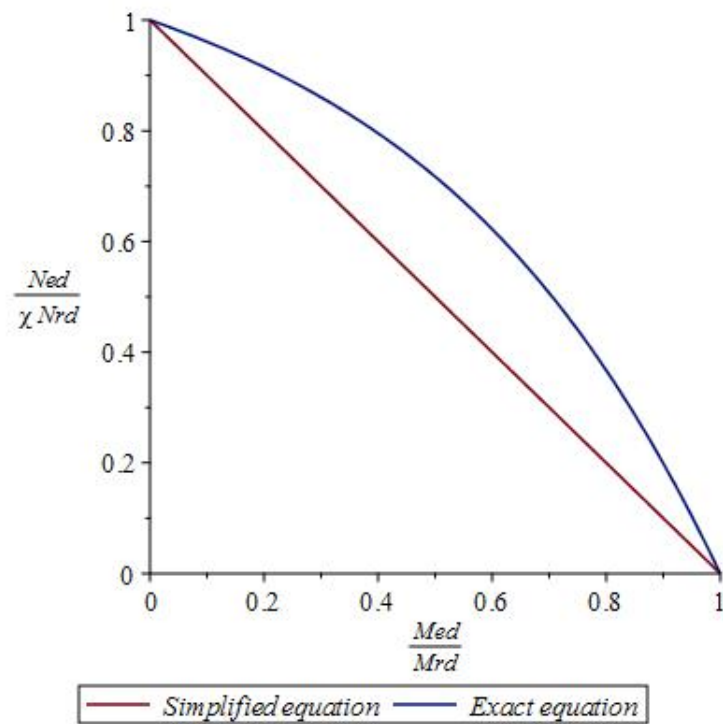


Figure C.3: Plot of both the simplified equation (C.6) as the exact equation C.1 to model the M-N interaction with the buckling mechanism

$$\frac{N_{Ed}}{\chi_b * N_{Rd}} + k_{yy} \frac{M_{Ed,2ndorder}}{M_{Rd}} < 1 \tag{C.7}$$

One part of the interaction factor k_{yy} as defined in appendix A of Eurocode 1993-1-1 is the factor μ_y . For now the factor k_{yy} is replaced by μ_y and the both design lines of the equations C.1 and C.7 are plotted, resulting in figure C.4. With the help of this figure, it is concluded that with the introduction of μ_y the simplified equation C.7 equals exactly the exact equation C.1 and therefore μ_y cancels the error made by the simplified buckling equation.

$$\mu_y = \frac{1 - \frac{N_{Ed}}{F_{cr}}}{1 - \chi_b \frac{N_{Ed}}{F_{cr}}} \quad (\text{C.8})$$

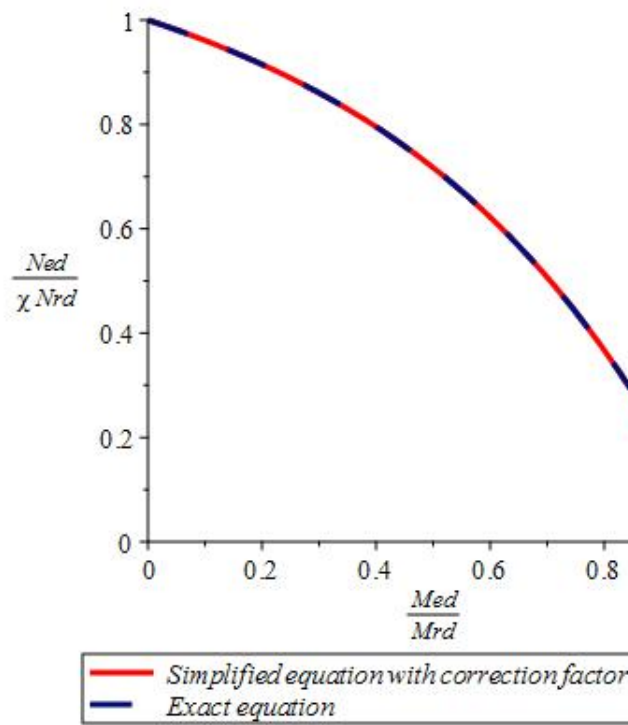


Figure C.4: Plot of both the exact solution as the simplified solution in combination with the correction factor

The error made by the buckling reduction factor χ_b is removed by the introduction of μ_y , but k_{yy} depends on more than just μ_y . In the next section, the physical meaning of the remaining part of k_{yy} will become clear.

C.2. Amplification of bending moment

The previous section describes the background of the correction parameter μ_y included in k_{yy} . If the equation for k_{yy} is written like expression C.9, the amplification factor introduced in section 3.1.1 is recognised. This indicates that instead of the second order bending moment, the first order bending moment should be used in the equations given above. This is verified by the example treated below.

$$k_{yy} = C_{my} \frac{\mu_y}{1 - \frac{N_{Ed}}{F_{cr}}} \quad (C.9)$$

$$k_{yy} = C_{my} \frac{1}{1 - \frac{N_{Ed}}{F_{cr}}} \mu_y$$

The structural element given in figure C.5 is loaded by a distributed load causing an initial displacement w_0 . Due to the application of a normal force, this displacement will grow to a displacement w_1 . Due to the displacement, the normal force will introduce a bending moment. Adding this bending moment to the initial bending moment caused by the distributed load results in the initial expression for the second order bending moment. This initial expression, given in the first line of the derivation in expression C.11, is rewritten step by step until a shape is found which is recognised as the interaction factor k_{yy} without the correction factor μ_y . The factor C_{my} is given by appendix A in Eurocode 1993-1-1 in the exact same form with the same value of 0.03. Doing the same derivation for other loading schemes also resulted in similar results for C_{my} as defined in the Eurocode. When this derivation it is concluded that the M-N interaction factor k_{yy} is introduced to take the second order effects to the bending moment into account.

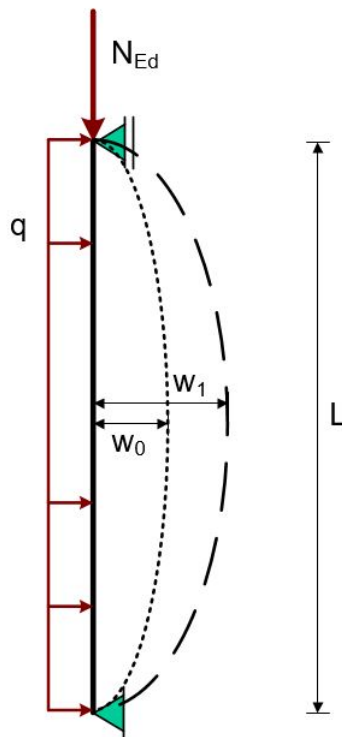


Figure C.5: Amplification of a beam loaded by distributed load

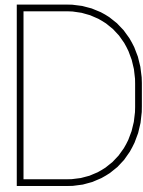
$$w_0 = \frac{5}{384} \frac{qL^4}{EI}$$

$$w_1 = \frac{5}{384} \frac{qL^4}{EI} \frac{1}{1 - \frac{N_{Ed}}{F_{cr}}} \quad (C.10)$$

$$\begin{aligned}
M_{Ed.2ndorder} &= \frac{qL^2}{8} + N * w_1 \\
&= \frac{qL^2}{8} + N_{Ed} \frac{1}{1 - \frac{N_{Ed}}{F_{cr}}} \frac{5qL^4}{384EI} \\
&= \frac{qL^2}{8} \left(1 + \frac{N_{Ed}}{1 - \frac{N_{Ed}}{F_{cr}}} \frac{5L^2}{48EI} \right) \\
&= \frac{qL^2}{8} \left(1 + \frac{N_{Ed}}{1 - \frac{N_{Ed}}{F_{cr}}} \frac{5L^2}{48EI} \frac{F_{cr}}{F_{cr}} \right) \\
&= \frac{qL^2}{8} \left(1 + \frac{N_{Ed}}{1 - \frac{N_{Ed}}{F_{cr}}} \frac{5L^2}{48EI} \frac{\pi^2 EI}{L^2 F_{cr}} \right) \\
&= \frac{qL^2}{8} \left(1 + \frac{N_{Ed}}{1 - \frac{N_{Ed}}{F_{cr}}} \frac{5\pi^2}{48F_{cr}} \right) \\
&= \frac{qL^2}{8} \left(1 + \frac{N_{Ed}}{1 - \frac{N_{Ed}}{F_{cr}}} \frac{1.03}{F_{cr}} \right) \\
&= \frac{qL^2}{8} \left(1 + \frac{1.03 \frac{N_{Ed}}{F_{cr}}}{1 - \frac{N_{Ed}}{F_{cr}}} \right) \\
&= \frac{qL^2}{8} \left(\frac{1 + 0.03 \frac{N_{Ed}}{F_{cr}}}{1 - \frac{N_{Ed}}{F_{cr}}} \right) \\
&= \frac{C_{my}}{1 - \frac{N_{Ed}}{F_{cr}}} M_{Ed.1storder} \\
&= \frac{k_{yy}}{\mu_y} M_{Ed.1storder} \\
C_{my} &= 1 + 0.03 \frac{N_{Ed}}{F_{cr}}
\end{aligned} \tag{C.11}$$

C.3. Conclusions to the k_{yy} interaction factor

In this appendix it has been found that the M-N interaction factor k_{yy} is used for two effects: to account for the error made with the use of the buckling reduction factor χ_b and to account for the second order bending moment. As mentioned earlier, the factor k_{yy} is set to 1.15 for steel sheet piles. This factor can be removed when one calculates the second order bending moment with the use of software. When this is done, the error made by the reduction factor χ_b by the simplified buckling equation C.5 is neglected instead of being removed by k_{yy} . However, this does not lead to unsafe design of the pile because neglecting this overestimation will be conservative. For steel sheet piles, the second order bending moment is usually in the order of 5% higher than the first order bending moment. This is less than the 15% currently taken into account, and thus sheet piles can be designed more economically.

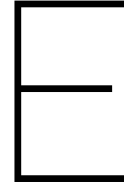


Determinant of schematised sheet pile chapter 5.1

In chapter 5.1 the critical global buckling load for a simplified sheet piled has been derived by the Euler theory. Because of the size of the both the coefficient matrix as the it's determinant, both the matrix as the determinant are given below.

$$\begin{vmatrix}
 0, 0, 0, F, 0, 0, 0, 0, \\
 1, 0, 0, 1, 0, 0, 0, 0, \\
 \frac{-10F - 10\sqrt{F^2 - 317520000}}{126} e^{\frac{\sqrt{F^2 - 317520000}}{126}} + e^{\frac{-10F + 10\sqrt{F^2 - 317520000}}{126}} + \frac{-10F + 10\sqrt{F^2 - 317520000}}{126} e^{\frac{-10F - 10\sqrt{F^2 - 317520000}}{126}} \\
 0, 0, 0, e^{\frac{-10F - 10\sqrt{F^2 - 317520000}}{126}} + e^{\frac{-10F + 10\sqrt{F^2 - 317520000}}{126}} + \frac{-10F + 10\sqrt{F^2 - 317520000}}{126} e^{\frac{-10F - 10\sqrt{F^2 - 317520000}}{126}} \\
 0, 0, 0, \frac{-10F - 10\sqrt{F^2 - 317520000}}{20} e^{\frac{-10F - 10\sqrt{F^2 - 317520000}}{126}} + \frac{-10F - 10\sqrt{F^2 - 317520000}}{20} e^{\frac{-10F + 10\sqrt{F^2 - 317520000}}{126}} + \frac{-10F + 10\sqrt{F^2 - 317520000}}{20} e^{\frac{-10F - 10\sqrt{F^2 - 317520000}}{126}} \\
 \frac{-10F + 10\sqrt{F^2 - 317520000}}{20} e^{\frac{-10F + 10\sqrt{F^2 - 317520000}}{126}} \\
 0, 0, F \sin\left(\frac{\sqrt{5}\sqrt{F}}{126}\right), F \cos\left(\frac{\sqrt{5}\sqrt{F}}{126}\right), \frac{-10F - 10\sqrt{F^2 - 317520000}}{20} e^{\frac{-10F - 10\sqrt{F^2 - 317520000}}{126}} + \frac{-10F - 10\sqrt{F^2 - 317520000}}{20} e^{\frac{-10F + 10\sqrt{F^2 - 317520000}}{126}} + \frac{-10F + 10\sqrt{F^2 - 317520000}}{20} e^{\frac{-10F - 10\sqrt{F^2 - 317520000}}{126}} \\
 \frac{-10F + 10\sqrt{F^2 - 317520000}}{20} e^{\frac{-10F + 10\sqrt{F^2 - 317520000}}{126}} + \frac{-10F + 10\sqrt{F^2 - 317520000}}{20} e^{\frac{-10F - 10\sqrt{F^2 - 317520000}}{126}} \\
 0, -1, \frac{\sqrt{5}\sqrt{F} \cos\left(\frac{\sqrt{5}\sqrt{F}}{126}\right)}{630}, \frac{\sqrt{5}\sqrt{F} \sin\left(\frac{\sqrt{5}\sqrt{F}}{126}\right)}{630}, \frac{-10F - 10\sqrt{F^2 - 317520000}}{1260} e^{\frac{-10F - 10\sqrt{F^2 - 317520000}}{126}} + \frac{-10F - 10\sqrt{F^2 - 317520000}}{1260} e^{\frac{-10F + 10\sqrt{F^2 - 317520000}}{126}} + \frac{-10F + 10\sqrt{F^2 - 317520000}}{1260} e^{\frac{-10F - 10\sqrt{F^2 - 317520000}}{126}} \\
 \frac{-10F + 10\sqrt{F^2 - 317520000}}{1260} e^{\frac{-10F + 10\sqrt{F^2 - 317520000}}{126}} + \frac{-10F + 10\sqrt{F^2 - 317520000}}{1260} e^{\frac{-10F - 10\sqrt{F^2 - 317520000}}{126}} \\
 0, F, \frac{F^2 | 2 \sqrt{5} \cos\left(\frac{\sqrt{5}\sqrt{F}}{126}\right)}{315}, \frac{F^2 | 2 \sqrt{5} \sin\left(\frac{\sqrt{5}\sqrt{F}}{126}\right)}{315}, \frac{-10F - 10\sqrt{F^2 - 317520000}}{25200} e^{\frac{-10F - 10\sqrt{F^2 - 317520000}}{126}} + \frac{-10F - 10\sqrt{F^2 - 317520000}}{25200} e^{\frac{-10F + 10\sqrt{F^2 - 317520000}}{126}} + \frac{-10F + 10\sqrt{F^2 - 317520000}}{25200} e^{\frac{-10F - 10\sqrt{F^2 - 317520000}}{126}} \\
 \frac{-10F + 10\sqrt{F^2 - 317520000}}{25200} e^{\frac{-10F + 10\sqrt{F^2 - 317520000}}{126}} + \frac{-10F + 10\sqrt{F^2 - 317520000}}{25200} e^{\frac{-10F - 10\sqrt{F^2 - 317520000}}{126}} \\
 + \frac{F \sqrt{-10F + 10\sqrt{F^2 - 317520000}}}{1260} e^{\frac{-10F + 10\sqrt{F^2 - 317520000}}{126}} + \frac{F \sqrt{-10F - 10\sqrt{F^2 - 317520000}}}{1260} e^{\frac{-10F - 10\sqrt{F^2 - 317520000}}{126}} + \frac{F \sqrt{-10F + 10\sqrt{F^2 - 317520000}}}{1260} e^{\frac{-10F - 10\sqrt{F^2 - 317520000}}{126}} \\
 \frac{F \sqrt{-10F - 10\sqrt{F^2 - 317520000}}}{1260} e^{\frac{-10F + 10\sqrt{F^2 - 317520000}}{126}} \\
 1, 5, \sin\left(\frac{\sqrt{5}\sqrt{F}}{126}\right), \cos\left(\frac{\sqrt{5}\sqrt{F}}{126}\right), -e^{\frac{-10F - 10\sqrt{F^2 - 317520000}}{252}} + e^{\frac{-10F - 10\sqrt{F^2 - 317520000}}{252}} + \frac{-10F - 10\sqrt{F^2 - 317520000}}{252} e^{\frac{-10F + 10\sqrt{F^2 - 317520000}}{252}} \\
 -e^{\frac{-10F + 10\sqrt{F^2 - 317520000}}{252}} + \frac{-10F + 10\sqrt{F^2 - 317520000}}{252} e^{\frac{-10F - 10\sqrt{F^2 - 317520000}}{252}} - e^{\frac{-10F - 10\sqrt{F^2 - 317520000}}{252}} + \frac{-10F - 10\sqrt{F^2 - 317520000}}{252} e^{\frac{-10F + 10\sqrt{F^2 - 317520000}}{252}}
 \end{vmatrix}$$

Figure D.1: Coefficient matrix of buckling derivation for sheet pile schematisation in chapter 5.1



Examples of displacement based critical buckling loads

This appendix gives the data of examples treated in the main report of which the critical global buckling load was calculated based on displacements. Of each example, the displacements have been determined using the theory given in section E.1.

E.1. Calculation of deformation

Section 2.3.2 introduced the relation between the displacements and forcing of a elastic founded structural element. The relation is repeated in equation E.1. Because the normal force N is assumed positive as a tensile force, it can be replaced by compressive force $-F$. With the use of Maple TA equation E.2 is found. The 4 unknowns can be solved by stating 4 boundary conditions. Once this is done, the exact displacements can be found for elastic supported structural elements.

$$EI \frac{d^4 w}{dx^4} - N \frac{d^2 w}{dx^2} = q - k * w \quad (E.1)$$
$$EI \frac{d^4 w}{dx^4} + F \frac{d^2 w}{dx^2} + k * w = q$$

$$w(x) = \frac{q}{k} + C1 e^{-\frac{\sqrt{2} \sqrt{-EI(F - \sqrt{-4EI k + F^2})} x}{2EI}} + C2 e^{\frac{\sqrt{2} \sqrt{-EI(F - \sqrt{-4EI k + F^2})} x}{2EI}} + C3 e^{-\frac{\sqrt{2} \sqrt{-EI(F + \sqrt{-4EI k + F^2})} x}{2EI}} + C4 e^{\frac{\sqrt{2} \sqrt{-EI(F + \sqrt{-4EI k + F^2})} x}{2EI}} \quad (E.2)$$

$$M(x) = -EI \frac{d^2}{dx^2} w(x) \quad (E.3)$$

E.2. Calculations of displacements for the examples in section 5.2.1

In section 5.2.1 the critical global buckling load of the beam in figure E.1 has been determined based on displacements. For 5 load cases, the displacements has been evaluated to find the critical load. This section gives the data of the displacements of each load case. The general properties of the beam are given below.

- Bending stiffness $EI = 79380 kNm^2$ (sheet pile profile AZ18-700)
- Length $L = 10m$
- Elastic foundation stiffness $k = 1000 kN/m^2$

E.2.1. Example A

This section gives the results of example A given in section 5.2.1 and given again in figure E.2.

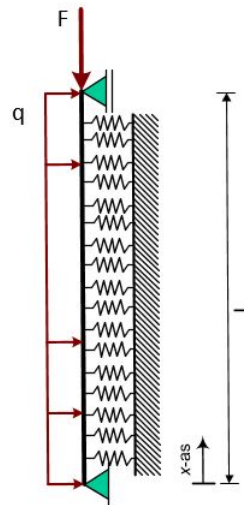


Figure E.1: Example A: Distributed load of 100 kN/m

Determination of displacements

The displacements are based on the general formula E.2 combined with the boundary conditions. At the both sides ($x=0$ and $x=L$), it is known that both the displacement as the bending moment are zero. This results in equation E.4 for the displacement field of this example. The imaginary part of the solutions is negligible to the real part (order of $1e-16$ compared to an order of $1e-2$ m).

$$\begin{aligned}
 w(x, F, q, k, EI) = & \frac{q}{k} - (0.05332968020 + 0.003733681400I) e^{-0.7071067810 \frac{\sqrt{-1.0EI(F-1.0\sqrt{-4.0EI k+F^2}}}{EI} x} \\
 & + (0.003329680196 + 0.003733681401I) e^{0.7071067810 \frac{\sqrt{-1.0EI(F-1.0\sqrt{-4.0EI k+F^2}}}{EI} x} \\
 & - (0.05332968020 - 0.003733681400I) e^{-0.7071067810 \frac{\sqrt{-1.0EI(F+\sqrt{-4.0EI k+F^2}}}{EI} x} \\
 & + (0.003329680196 - 0.003733681401I) e^{0.7071067810 \frac{\sqrt{-1.0EI(F+\sqrt{-4.0EI k+F^2}}}{EI} x}
 \end{aligned} \tag{E.4}$$

Determination of the critical global buckling load based on displacements This section gives the values which are used to find the critical global buckling load based on displacements. Because the main report treats the determination based on displacements defined to the 5th decimal, this section only treats the determination based on displacements defined to the first and second decimal.

Displacements rounded to the first decimal

| N_{Ed} (kN) | w^I (mm) | w^{II} (mm) | w^{II}/w^I | n | F_{cr} | Error (‰) |
|---------------|------------|---------------|--------------|--------|----------|-----------|
| 500 | 71.2 | 73.2 | 1.0281 | 35.959 | 17 980 | 17.78 |
| 1 000 | 71.2 | 75.4 | 1.0590 | 17.647 | 17 647 | 1.03 |
| 1 500 | 71.2 | 77.7 | 1.0913 | 11.757 | 17 635 | 1.73 |
| 2 000 | 71.2 | 80.2 | 1.1264 | 8.769 | 17 537 | 7.25 |
| 2 500 | 71.2 | 82.8 | 1.1629 | 7.027 | 17 569 | 5.48 |
| 3 000 | 71.2 | 85.5 | 1.2008 | 5.889 | 17 668 | 0.15 |
| 3 500 | 71.2 | 88.5 | 1.2430 | 5.042 | 17 645 | 1.14 |
| 4 000 | 71.2 | 91.7 | 1.2879 | 4.411 | 17 643 | 1.29 |
| 4 500 | 71.2 | 95.1 | 1.3357 | 3.925 | 17 665 | 0.54 |
| 5 000 | 71.2 | 98.8 | 1.3876 | 3.533 | 17 666 | 0.50 |
| Average | | | | | 17 665 | 0.360 |

Table E.1: Determination of critical buckling load of the beam in figure E.1 based on displacements rounded to the first decimal with a δ correction factor of -0.018**Displacements rounded to the second decimal**

| N_{Ed} (kN) | w^I (mm) | w^{II} (mm) | w^{II}/w^I | n | F_{cr} | Error (‰) |
|---------------|------------|---------------|--------------|--------|----------|-----------|
| 500 | 71.19 | 73.22 | 1.0287 | 35.618 | 17 809 | 2.35 |
| 1 000 | 71.19 | 75.40 | 1.0591 | 17.775 | 17 775 | 0.41 |
| 1 500 | 71.19 | 77.71 | 1.0916 | 11.831 | 17 747 | 1.14 |
| 2 000 | 71.19 | 80.16 | 1.1260 | 8.873 | 17 746 | 1.20 |
| 2 500 | 71.19 | 82.76 | 1.1625 | 7.104 | 17 759 | 0.44 |
| 3 000 | 71.19 | 85.55 | 1.2017 | 5.918 | 17 754 | 0.77 |
| 3 500 | 71.19 | 88.52 | 1.2434 | 5.075 | 17 763 | 0.26 |
| 4 000 | 71.19 | 91.71 | 1.2882 | 4.442 | 17 766 | 0.06 |
| 4 500 | 71.19 | 95.13 | 1.3363 | 3.950 | 17 775 | 0.41 |
| 5 000 | 71.19 | 98.82 | 1.3881 | 3.556 | 17 780 | 0.70 |
| Average | | | | | 17 767 | 0.77 |

Table E.2: Determination of critical buckling load of the beam in figure E.1 based on displacements rounded to the first decimal with a δ correction factor of -0.008

E.2.2. Example B

This section gives the results of example B given in section 5.2.1 and given again in figure E.2. With an error of 0.083 ‰ and a δ correction factor of 0.042, a critical buckling load of 17 757 kN is found. Figure E.3 gives the error plot as a function of δ .

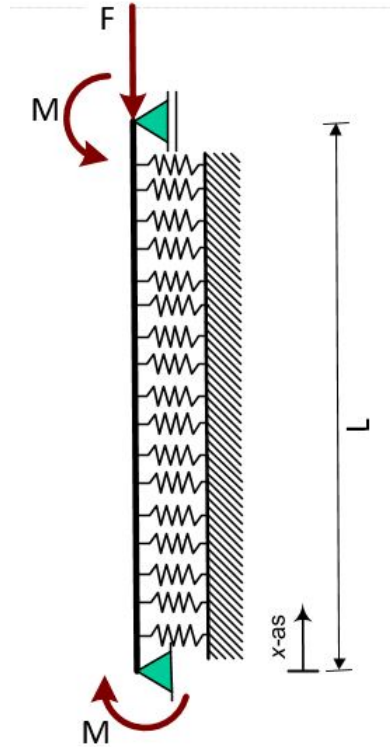


Figure E.2: Example B: Double moment loading, $M = 100 \text{ kNm}$

Determination of displacements

The displacements are based on the general formula E.2 combined with the boundary conditions. At the both sides ($x=0$ and $x=L$), it is known that the displacements are zero and the bending moment equals the external moment. This results in equation E.5 for the displacement field of this example.

$$\begin{aligned}
 w(x, F, k, EI) = & (-0.0004190653059 + 0.005985679127I) e^{-0.7071067810 \sqrt{\frac{-1.0EI(F-1.0\sqrt{-4.0EI k+F^2}}{EI}} x} \\
 & + (0.0004190653075 - 0.0003737205469I) e^{0.7071067810 \sqrt{\frac{-1.0EI(F-1.0\sqrt{-4.0EI k+F^2}}{EI}} x} \\
 & - (0.0004190653059 + 0.005985679127I) e^{-0.7071067810 \sqrt{\frac{-1.0EI(F+\sqrt{-4.0EI k+F^2}}{EI}} x} \\
 & + (0.0004190653075 + 0.0003737205469I) e^{0.7071067810 \sqrt{\frac{-1.0EI(F+\sqrt{-4.0EI k+F^2}}{EI}} x}
 \end{aligned} \tag{E.5}$$

Determination of the critical global buckling load based on displacements

This section gives the values which are used to find the critical global buckling load based on displacements.

| N_{Ed} (kN) | w^I (mm) | w^{II} (mm) | w^{II}/w^I | n | F_{cr} | Error (‰) |
|---------------|------------|---------------|--------------|--------|----------|-----------|
| 1 000 | 6.59123 | 7.00101 | 1.062 | 17.905 | 17 905.1 | 1.40 |
| 2 000 | 6.59123 | 7.46304 | 1.132 | 8.946 | 17 892.0 | 0.66 |
| 3 000 | 6.59123 | 7.98756 | 1.212 | 5.961 | 17 883.4 | 0.18 |
| 4 000 | 6.59123 | 8.58811 | 1.303 | 4.469 | 17 876.4 | 0.21 |
| 5 000 | 6.59123 | 9.28235 | 1.408 | 3.574 | 17 870.8 | 0.52 |
| 6 000 | 6.59123 | 10.09380 | 1.531 | 2.978 | 17 866.8 | 0.75 |
| 7 000 | 6.59123 | 11.05460 | 1.677 | 2.552 | 17 864.3 | 0.89 |
| 8 000 | 6.59123 | 12.20980 | 1.852 | 2.233 | 17 863.5 | 0.93 |
| 9 000 | 6.59123 | 13.62450 | 2.067 | 1.985 | 17 864.5 | 0.88 |
| 10 000 | 6.59123 | 15.39660 | 2.336 | 1.787 | 17 867.2 | 0.72 |
| 11 000 | 6.59123 | 17.67997 | 2.682 | 1.625 | 17 871.9 | 0.46 |
| 12 000 | 6.59123 | 20.73197 | 3.145 | 1.490 | 17 878.7 | 0.08 |
| 13 000 | 6.59123 | 25.01706 | 3.796 | 1.376 | 17 887.5 | 0.41 |
| 14 000 | 6.59123 | 31.46810 | 4.774 | 1.278 | 17 898.5 | 1.03 |
| 15 000 | 6.59123 | 42.27584 | 6.414 | 1.194 | 17 911.9 | 1.78 |
| Average | | | | | 17 880.2 | 0.73 |

Table E.3: Determination of critical buckling load of the beam in figure E.2 based on displacements with a δ correction factor of 0.051

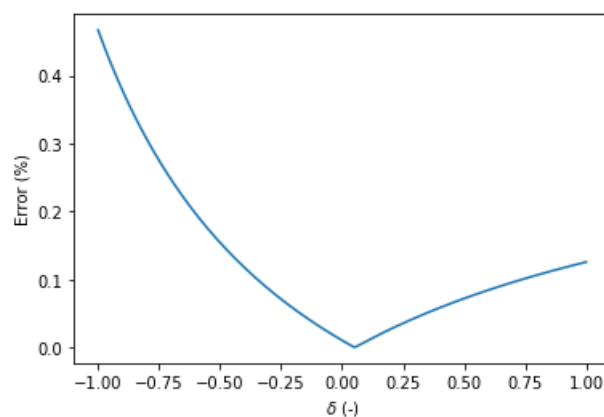


Figure E.3: Error against delta plot example B

Displacements rounded to the first decimal

| N_{Ed} (kN) | w^I (mm) | w^{II} (mm) | w^{II}/w^I | n | F_{cr} | Error (‰) |
|---------------|------------|---------------|--------------|--------|----------|-----------|
| 500 | 6.6 | 6.8 | 1.0303 | 33.274 | 16 637 | 18.69 |
| 1 000 | 6.6 | 7.0 | 1.0606 | 17.137 | 17 137 | 10.81 |
| 1 500 | 6.6 | 7.2 | 1.0909 | 11.758 | 17 637 | 40.30 |
| 2 000 | 6.6 | 7.5 | 1.1364 | 8.172 | 16 344 | 35.97 |
| 2 500 | 6.6 | 7.7 | 1.1667 | 6.868 | 17 170 | 12.75 |
| 3 000 | 6.6 | 8.0 | 1.2121 | 5.611 | 16 832 | 7.20 |
| 3 500 | 6.6 | 8.3 | 1.2576 | 4.797 | 16 789 | 9.70 |
| 4 000 | 6.6 | 8.6 | 1.3030 | 4.227 | 16 910 | 2.61 |
| 4 500 | 6.6 | 8.9 | 1.3485 | 3.806 | 17 129 | 10.33 |
| 5 000 | 6.6 | 9.3 | 1.4091 | 3.391 | 16 953 | 0.03 |
| Average | | | | | 16 954 | 14.84 |

Table E.4: Determination of critical buckling load of the beam in figure E.2 based on displacements rounded to the first decimal with a δ correction factor of 0.022

Displacements rounded to the second decimal

| N_{Ed} (kN) | w^I (mm) | w^{II} (mm) | w^{II}/w^I | n | F_{cr} | Error (‰) |
|---------------|------------|---------------|--------------|---------|----------|-----------|
| 500 | 6.59 | 6.79 | 1.0304 | 35.631 | 17 815 | 3.24 |
| 1 000 | 6.59 | 7.00 | 1.0622 | 17.893 | 17 893 | 1.10 |
| 1 500 | 6.59 | 7.22 | 1.0956 | 11.994 | 17 991 | 6.57 |
| 2 000 | 6.59 | 7.46 | 1.1320 | 8.961 | 17 922 | 2.73 |
| 2 500 | 6.59 | 7.72 | 1.1715 | 7.129 | 17 823 | 2.80 |
| 3 000 | 6.59 | 7.99 | 1.2124 | 5.947 | 17 842 | 1.77 |
| 3 500 | 6.59 | 8.28 | 1.2565 | 5.098 | 17 844 | 1.64 |
| 4 000 | 6.59 | 8.59 | 1.3035 | 4.463 | 17 852 | 1.18 |
| 4 500 | 6.59 | 8.92 | 1.3536 | 3.973 | 17 877 | 0.19 |
| 5 000 | 6.59 | 9.28 | 1.4082 | 3.575 | 17 874 | 0.03 |
| | | | | Average | 17 873 | 2.12 |

Table E.5: Determination of critical buckling load of the beam in figure E.2 based on displacements rounded to the first decimal with a δ correction factor of -0.051

E.2.3. Example C

This section treats example C given in section 5.2.1 and given again in figure E.4. With an error of 0.02 ‰ and a δ correction factor of -0.021, a critical buckling load of 18 042 kN is found. Figure E.5 gives the error plot as a function of δ .

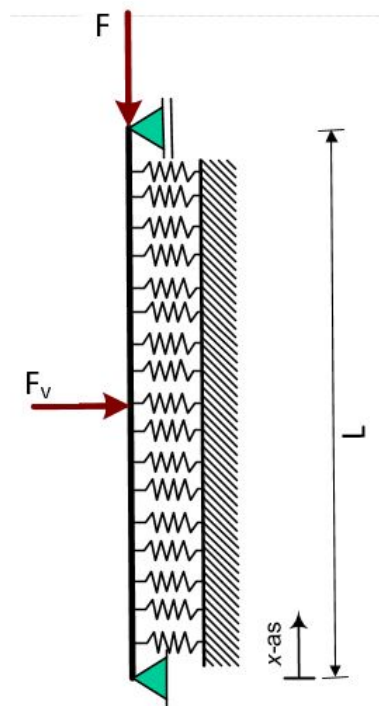


Figure E.4: Example C: Point load loading, $F = 100$ kN

Determination of displacements

The displacements are based on the general formula E.2 combined with the boundary conditions. Because a point load is attached in the middle, two displacements fields are used: one left and one right of the load. This results in 8 unknown parameters. At both boundaries (right and left end of the beam), the conditions of zero displacements and bending moment yields. At the transition of both fields, 4 conditions can be defined: equal displacements, rotation and bending moments in both fields. The 4th condition is that the value of

the shear force (first derivative of the bending moment) equals 0.5*F. This results in equation E.6 for the left displacement field of this example. The right displacement field similar to the left field but mirrored.

$$\begin{aligned}
 w(x.F.k.EI) = & (-0.002592342356 + 0.0008855765544I) e^{-0.7071067810 \frac{\sqrt{-1.0EI(F-1.0\sqrt{-4.0EI k+F^2})}x}{EI}} \\
 & + (0.002592342356 - 0.0008855765544I) e^{0.7071067810 \frac{\sqrt{-1.0EI(F-1.0\sqrt{-4.0EI k+F^2})}x}{EI}} \\
 & - (0.002592342357 + 0.0008855765541I) e^{-0.7071067810 \frac{\sqrt{-1.0EI(F+\sqrt{-4.0EI k+F^2})}x}{EI}} \\
 & + (0.002592342357 + 0.0008855765541I) e^{0.7071067810 \frac{\sqrt{-1.0EI(F+\sqrt{-4.0EI k+F^2})}x}{EI}}
 \end{aligned}
 \tag{E.6}$$

Determination of the critical global buckling load based on displacements

This section gives the values which are used to find the critical global buckling load based on displacements.

| N_{Ed} (kN) | w^I (mm) | w^{II} (mm) | w^{II}/w^I | n | F_{cr} | Error (%) |
|---------------|------------|---------------|--------------|---------|----------|-----------|
| 1 000 | 11.65340 | 12.32284 | 1.057 | 17.990 | 17 989.9 | 0.47 |
| 2 000 | 11.65340 | 13.07570 | 1.122 | 8.997 | 17 993.4 | 0.28 |
| 3 000 | 11.65340 | 13.92870 | 1.195 | 5.999 | 17 996.3 | 0.11 |
| 4 000 | 11.65340 | 14.90320 | 1.279 | 4.500 | 17 999.3 | 0.05 |
| 5 000 | 11.65340 | 16.02740 | 1.375 | 3.600 | 18 001.5 | 0.17 |
| 6 000 | 11.65340 | 17.33879 | 1.488 | 3.001 | 18 003.1 | 0.26 |
| 7 000 | 11.65340 | 18.88850 | 1.621 | 2.572 | 18 004.1 | 0.32 |
| 8 000 | 11.65340 | 20.74824 | 1.780 | 2.251 | 18 004.5 | 0.34 |
| 9 000 | 11.65340 | 23.02170 | 1.976 | 2.000 | 18 004.3 | 0.33 |
| 10 000 | 11.65340 | 25.86460 | 2.219 | 1.800 | 18 003.3 | 0.28 |
| 11 000 | 11.65340 | 29.52210 | 2.533 | 1.637 | 18 001.7 | 0.18 |
| 12 000 | 11.65340 | 34.40367 | 2.952 | 1.500 | 17 999.3 | 0.04 |
| 13 000 | 11.65340 | 41.24860 | 3.540 | 1.384 | 17 996.0 | 0.13 |
| 14 000 | 11.65340 | 51.54164 | 4.423 | 1.285 | 17 992.0 | 0.36 |
| 15 000 | 11.65340 | 68.76950 | 5.901 | 1.199 | 17 987.0 | 0.63 |
| | | | | Average | 17 998.4 | 0.26 |

Table E.6: Determination of critical buckling load of the beam in figure E.4 based on displacements with a δ correction factor of -0.024

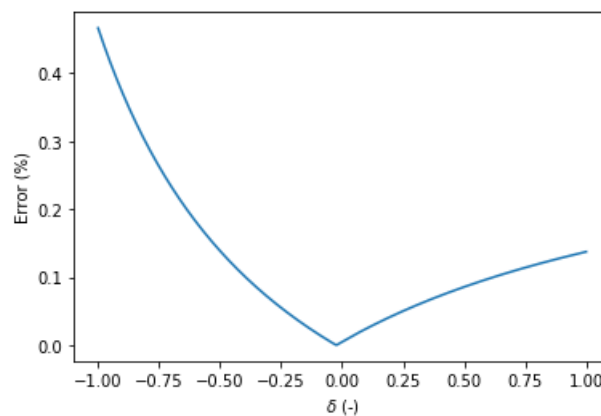


Figure E.5: Error against delta plot example C

Displacements rounded to the first decimal

| N_{Ed} (kN) | w^I (mm) | w^{II} (mm) | w^{II}/w^I | n | F_{cr} | Error (‰) |
|---------------|------------|---------------|--------------|---------|----------|-----------|
| 500 | 11.7 | 12.0 | 1.0256 | 28.938 | 14 969 | 7.90 |
| 1 000 | 11.7 | 12.3 | 1.0513 | 15.469 | 15 469 | 41.57 |
| 1 500 | 11.7 | 12.7 | 1.0855 | 9.681 | 14 522 | 22.19 |
| 2 000 | 11.7 | 13.1 | 1.1197 | 7.201 | 14 402 | 30.28 |
| 2 500 | 11.7 | 13.5 | 1.1539 | 5.823 | 14 558 | 19.81 |
| 3 000 | 11.7 | 13.9 | 1.1880 | 4.946 | 14 838 | 0.90 |
| 3 500 | 11.7 | 14.4 | 1.2308 | 4.215 | 14 754 | 6.60 |
| 4 000 | 11.7 | 14.9 | 1.2735 | 3.713 | 14 852 | 0.01 |
| 4 500 | 11.7 | 15.4 | 1.3162 | 3.346 | 15 059 | 13.93 |
| 5 000 | 11.7 | 16.0 | 1.3675 | 3.019 | 15 095 | 16.36 |
| | | | | Average | 14 852 | 15.95 |

Table E.7: Determination of critical buckling load of the beam in figure E.4 based on displacements rounded to the first decimal with a δ correction factor of -0.258

Displacements rounded to the second decimal

| N_{Ed} (kN) | w^I (mm) | w^{II} (mm) | w^{II}/w^I | n | F_{cr} | Error (‰) |
|---------------|------------|---------------|--------------|---------|----------|-----------|
| 500 | 11.65 | 11.98 | 1.0283 | 36.762 | 18.381 | 7.04 |
| 1 000 | 11.65 | 12.32 | 1.0575 | 18.614 | 18 614 | 5.55 |
| 1 500 | 11.65 | 12.69 | 1.0893 | 12.348 | 18 521 | 0.54 |
| 2 000 | 11.65 | 13.08 | 1.1228 | 9.253 | 18 506 | 0.32 |
| 2 500 | 11.65 | 13.49 | 1.1579 | 7.414 | 18 535 | 1.25 |
| 3 000 | 11.65 | 13.93 | 1.1957 | 6.176 | 18 528 | 0.91 |
| 3 500 | 11.65 | 14.40 | 1.2361 | 5.291 | 18 520 | 0.47 |
| 4 000 | 11.65 | 14.90 | 1.2790 | 4.631 | 18 525 | 0.73 |
| 4 500 | 11.65 | 15.44 | 1.3253 | 4.114 | 18 512 | 0.05 |
| 5 000 | 11.65 | 16.03 | 1.3760 | 3.694 | 18 472 | 2.13 |
| | | | | Average | 18 511 | 1.90 |

Table E.8: Determination of critical buckling load of the beam in figure E.4 based on displacements rounded to the first decimal with a δ correction factor of 0.013

E.2.4. Example D

This section treats example D given in section 5.2.1 and given again in figure E.6. With an error of 0.011 ‰ and a δ correction factor of 0.003, a critical buckling load of 17 941 kN is found. Figure E.7 gives the error plot as a function of δ .

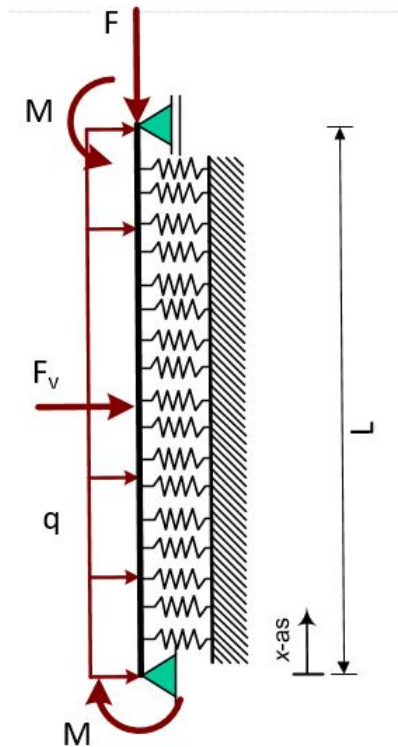


Figure E.6: Example D: Double moment loading, $M = 100 \text{ kNm}$, distributed load loading, $q = 10 \text{ kN/m}$ and point load loading, $F_v = 100 \text{ kN}$

Determination of displacements

As a combi of the previous 3 examples, this example is made. The displacement field for the left side of the point load is given in equation E.7.

$$\begin{aligned}
 w(x.F.q.k.EI) = & \frac{q}{k} - (0.008344375680 - 0.006497887541I) e^{-0.7071067810 \sqrt{\frac{-1.0EI(F-1.0\sqrt{-4.0EI k+F^2}}{EI}}x} \\
 & + (0.003344375682 - 0.0008859289615I) e^{0.7071067810 \sqrt{\frac{-1.0EI(F-1.0\sqrt{-4.0EI k+F^2}}{EI}}x} \\
 & - (0.008344375668 + 0.006497887533I) e^{-0.7071067810 \sqrt{\frac{-1.0EI(F+\sqrt{-4.0EI k+F^2}}{EI}}x} \\
 & + (0.003344375680 + 0.0008859289609I) e^{0.7071067810 \sqrt{\frac{-1.0EI(F+\sqrt{-4.0EI k+F^2}}{EI}}x}
 \end{aligned} \tag{E.7}$$

Determination of the critical global buckling load based on displacements

This section gives the values which are used to find the critical global buckling load based on displacements.

| N_{Ed} (kN) | w^I (mm) | w^{II} (mm) | w^{II}/w^I | n | F_{cr} | Error (‰) |
|---------------|------------|---------------|--------------|--------|----------|-----------|
| 1 000 | 25.36272 | 26.86434 | 1.059 | 17.958 | 17 957.8 | 0.174907 |
| 2 000 | 25.36272 | 28.55442 | 1.126 | 8.978 | 17 956.5 | 0.102194 |
| 3 000 | 25.36272 | 30.47077 | 1.201 | 5.985 | 17 955.3 | 0.036703 |
| 4 000 | 25.36272 | 32.66201 | 1.288 | 4.489 | 17 954.3 | 0.018466 |
| 5 000 | 25.36272 | 35.19177 | 1.388 | 3.591 | 17 953.5 | 0.063111 |
| 6 000 | 25.36272 | 38.14495 | 1.504 | 2.992 | 17 952.9 | 0.096631 |
| 7 000 | 25.36272 | 41.63740 | 1.642 | 2.565 | 17 952.5 | 0.117640 |
| 8 000 | 25.36272 | 45.83150 | 1.807 | 2.244 | 17 952.4 | 0.126147 |
| 9 000 | 25.36272 | 50.96205 | 2.009 | 1.995 | 17 952.5 | 0.121263 |
| 10 000 | 25.36272 | 57.38175 | 2.262 | 1.795 | 17 952.8 | 0.102210 |
| 11 000 | 25.36272 | 65.64581 | 2.588 | 1.632 | 17 953.4 | 0.068134 |
| 12 000 | 25.36272 | 76.68167 | 3.023 | 1.496 | 17 954.3 | 0.018235 |
| 13 000 | 25.36272 | 92.16369 | 3.634 | 1.381 | 17 955.5 | 0.048514 |
| 14 000 | 25.36272 | 115.45472 | 4.552 | 1.283 | 17 957.0 | 0.133066 |
| 15 000 | 25.36272 | 154.45190 | 6.0901 | 1.197 | 17 958.9 | 0.236454 |
| Average | | | | | 17 954.6 | 0.10 |

Table E.9: Determination of critical buckling load of the beam in figure E.4 based on displacements with a δ correction factor of 0.004

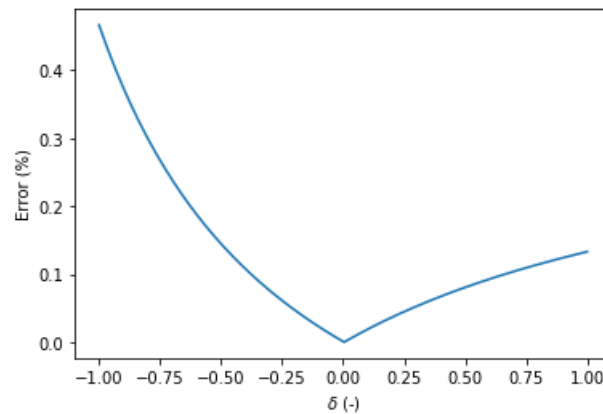


Figure E.7: Error against delta plot example D

Displacements rounded to the first decimal

| N_{Ed} (kN) | w^I (mm) | w^{II} (mm) | w^{II}/w^I | n | F_{cr} | Error (‰) |
|---------------|------------|---------------|--------------|--------|----------|-----------|
| 500 | 25.4 | 26.1 | 1.0276 | 36.088 | 18 044 | 29.33 |
| 1 000 | 25.4 | 26.9 | 1.0591 | 17.375 | 17 375 | 8.87 |
| 1 500 | 25.4 | 27.7 | 1.0906 | 11.679 | 17 519 | 0.65 |
| 2 000 | 25.4 | 28.6 | 1.1260 | 8.676 | 17 351 | 10.20 |
| 2 500 | 25.4 | 29.5 | 1.1614 | 6.991 | 17 477 | 3.04 |
| 3 000 | 25.4 | 30.5 | 1.2008 | 5.816 | 17 448 | 4.67 |
| 3 500 | 25.4 | 31.5 | 1.2402 | 5.027 | 17 593 | 3.59 |
| 4 000 | 25.4 | 32.7 | 1.2874 | 4.365 | 17 459 | 4.07 |
| 4 500 | 25.4 | 33.9 | 1.3347 | 3.890 | 17 503 | 1.52 |
| 5 000 | 25.4 | 35.2 | 1.3858 | 3.506 | 17 532 | 0.01 |
| Average | | | | | 17 530 | 6.60 |

Table E.10: Determination of critical buckling load of the beam in figure E.4 based on displacements rounded to the first decimal with a δ correction factor of -0.033

Displacements rounded to the second decimal

| N_{Ed} (kN) | w^I (mm) | w^{II} (mm) | w^{II}/w^I | n | F_{cr} | Error (‰) |
|---------------|------------|---------------|--------------|--------|----------|-----------|
| 500 | 25.36 | 26.09 | 1.0288 | 35.775 | 17 887 | 1.14 |
| 1 000 | 25.36 | 26.86 | 1.0592 | 17.924 | 17 924 | 0.89 |
| 1 500 | 25.36 | 27.68 | 1.0915 | 11.942 | 17 913 | 0.30 |
| 2 000 | 25.36 | 28.55 | 1.1258 | 8.958 | 17 916 | 0.44 |
| 2 500 | 25.36 | 29.48 | 1.1625 | 7.162 | 17 904 | 0.22 |
| 3 000 | 25.36 | 30.47 | 1.2015 | 5.968 | 17 903 | 0.24 |
| 3 500 | 25.36 | 31.53 | 1.2433 | 5.114 | 17 900 | 0.42 |
| 4 000 | 25.36 | 32.66 | 1.2879 | 4.477 | 17 910 | 0.12 |
| 4 500 | 25.36 | 33.88 | 1.3360 | 3.980 | 17 908 | 0.01 |
| 5 000 | 25.36 | 35.19 | 1.3876 | 3.582 | 17 912 | 0.25 |
| Average | | | | | 17 908 | 0.40 |

Table E.11: Determination of critical buckling load of the beam in figure E.4 based on displacements rounded to the first decimal with a δ correction factor of 0.001

E.2.5. Example E

This section treats example E given in section 5.2.1 and given again in figure E.8. With an error of 0.100 ‰ and a δ correction factor of -0.057 a critical buckling load of 18 189 kN is found. Figure E.9 gives the error plot as a function of δ .

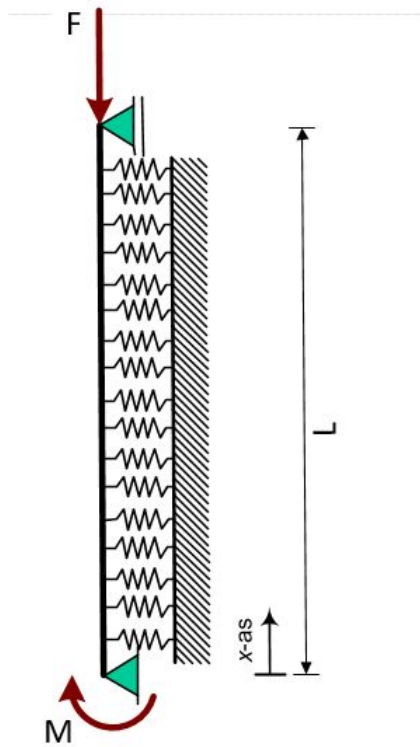


Figure E.8: Example E: single moment loading, $M = 100 \text{ kNm}$

Determination of displacements

As an adaption to example B example E is done. The displacement field for the left side of the point load is given in equation E.8.

$$\begin{aligned}
 w(x.F.q.k.EI) = & \frac{q}{k} - (0.00004914548928 - 0.005612782817I) e^{-0.7071067810 \sqrt{\frac{-1.0EI(F-1.0\sqrt{-4.0EI k+F^2}}{EI}}x} \\
 & + (0.00004914548996 - 0.0000008242373932I) e^{0.7071067810 \sqrt{\frac{-1.0EI(F-1.0\sqrt{-4.0EI k+F^2}}{EI}}x} \\
 & - (0.00004914548928 + 0.005612782817I) e^{-0.7071067810 \sqrt{\frac{-1.0EI(F+\sqrt{-4.0EI k+F^2}}{EI}}x} \\
 & + (0.00004914548996 + 0.0000008242373932I) e^{0.7071067810 \sqrt{\frac{-1.0EI(F+\sqrt{-4.0EI k+F^2}}{EI}}x}
 \end{aligned} \tag{E.8}$$

Determination of the critical global buckling load based on displacements

This section gives the values which are used to find the critical global buckling load based on displacements.

| N_{Ed} (kN) | w^I (mm) | w^{II} (mm) | w^{II}/w^I | n | F_{cr} | Error (%) |
|---------------|------------|---------------|--------------|---------|----------|-----------|
| 1 000 | 3.74270 | 3.94805 | 1.055 | 17.950 | 17 950.1 | 2.33 |
| 2 000 | 3.74270 | 4.17868 | 1.116 | 8.984 | 17 967.3 | 1.39 |
| 3 000 | 3.74270 | 4.43969 | 1.186 | 5.994 | 17 981.8 | 0.58 |
| 4 000 | 3.74270 | 4.73763 | 1.266 | 4.498 | 17 993.8 | 0.09 |
| 5 000 | 3.74270 | 5.08108 | 1.358 | 3.601 | 18 003.4 | 0.62 |
| 6 000 | 3.74270 | 5.48155 | 1.465 | 3.002 | 18 010.4 | 1.01 |
| 7 000 | 3.74270 | 5.95475 | 1.591 | 2.574 | 18 014.7 | 1.25 |
| 8 000 | 3.74270 | 6.52279 | 1.743 | 2.252 | 18 016.1 | 1.33 |
| 9 000 | 3.74270 | 7.21771 | 1.929 | 2.002 | 18 014.8 | 1.25 |
| 10 000 | 3.74270 | 8.08781 | 2.161 | 1.801 | 18 010.6 | 1.02 |
| 11 000 | 3.74270 | 9.20931 | 2.461 | 1.637 | 18 003.9 | 0.65 |
| 12 000 | 3.74270 | 10.70990 | 2.862 | 1.500 | 17 995.0 | 0.16 |
| 13 000 | 3.74270 | 12.82064 | 3.426 | 1.383 | 17 984.5 | 0.43 |
| 14 000 | 3.74270 | 16.00656 | 4.277 | 1.284 | 17 973.5 | 1.04 |
| 15 000 | 3.74270 | 21.36132 | 5.707 | 1.198 | 17 963.4 | 1.60 |
| | | | | Average | 17 992.2 | 0.98 |

Table E.12: Determination of critical buckling load of the beam in figure E.4 based on displacements with a δ correction factor of -0.07

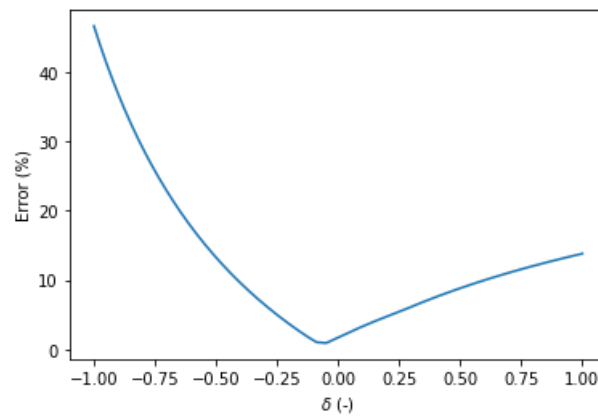


Figure E.9: Error against delta plot example E

Displacements rounded to first decimal

| N_{Ed} (kN) | w^I (mm) | w^{II} (mm) | w^{II}/w^I | n | F_{cr} | Error (‰) |
|---------------|------------|---------------|--------------|---------|----------|-----------|
| 500 | 3.7 | 3.8 | 1.0270 | 36.779 | 18 390 | 46.82 |
| 1 000 | 3.7 | 3.9 | 1.0541 | 18.890 | 18 890 | 75.28 |
| 1 500 | 3.7 | 4.1 | 1.1081 | 9.945 | 14 917 | 150.85 |
| 2 000 | 3.7 | 4.2 | 1.1351 | 8.156 | 16 312 | 71.47 |
| 2 500 | 3.7 | 4.3 | 1.1622 | 6.963 | 17 408 | 9.06 |
| 3 000 | 3.7 | 4.4 | 1.1892 | 6.113 | 18 334 | 43.65 |
| 3 500 | 3.7 | 4.6 | 1.2432 | 4.975 | 17 414 | 8.71 |
| 4 000 | 3.7 | 4.7 | 1.2703 | 4.5779 | 18 312 | 42.38 |
| 4 500 | 3.7 | 4.9 | 1.3243 | 3.982 | 17 917 | 19.93 |
| 5 000 | 3.7 | 5.1 | 1.3784 | 3.556 | 17 778 | 12.02 |
| | | | | Average | 17 567 | 48.02 |

Table E.13: Determination of critical buckling load of the beam in figure E.4 based on displacements rounded to the first decimal with a δ correction factor of -0.033**Displacements rounded to second decimal**

| N_{Ed} (kN) | w^I (mm) | w^{II} (mm) | w^{II}/w^I | n | F_{cr} | Error (‰) |
|---------------|------------|---------------|--------------|---------|----------|-----------|
| 500 | 3.74 | 3.84 | 1.0267 | 37.689 | 18 845 | 8.32 |
| 1 000 | 3.74 | 3.95 | 1.0562 | 18.471 | 18 471 | 11.67 |
| 1 500 | 3.74 | 4.06 | 1.0856 | 12.465 | 18 698 | 0.47 |
| 2 000 | 3.74 | 4.18 | 1.1177 | 9.339 | 18 677 | 0.66 |
| 2 500 | 3.74 | 4.31 | 1.1524 | 7.437 | 18 592 | 5.21 |
| 3 000 | 3.74 | 4.44 | 1.1872 | 6.241 | 18 724 | 1.86 |
| 3 500 | 3.74 | 4.58 | 1.2246 | 5.368 | 18 787 | 5.24 |
| 4 000 | 3.74 | 4.74 | 1.2674 | 4.669 | 18 676 | 0.72 |
| 4 500 | 3.74 | 4.90 | 1.3102 | 4.163 | 18 733 | 2.34 |
| 5 000 | 3.74 | 5.08 | 1.3583 | 3.738 | 18 690 | 0.04 |
| | | | | Average | 18 689 | 3.65 |

Table E.14: Determination of critical buckling load of the beam in figure E.4 based on displacements rounded to the first decimal with a δ correction factor of -0.019**E.3. Critical buckling loads based on displacement of sheet piles in section 5.3**

Section 5.3 treats the comparison between the theoretical method and method based on displacements in order to find the critical global buckling load. In order to do this, a large amount of displacements are required for the method based on displacements. The data of this method is given in this section. Each set of parameters in section 5.3 is represented by a table below.

| N_{Ed} (kN) | w^I (mm) | w^{II} (mm) | w^{II}/w^I | n | F_{cr} | Error (%) with average | δ corection factor |
|---------------|------------|---------------|--------------|---------|----------|---------------------------|------------------------------|
| 800 | 28.82533 | 29.53431 | 1.025 | 11.343 | 9 074.6 | 66.4 | -0.745 |
| 1 600 | 28.82533 | 30.32670 | 1.052 | 5.884 | 9 414.9 | 31.4 | -0.745 |
| 2 400 | 28.82533 | 31.22986 | 1.083 | 4.050 | 9 719.4 | 0.12 | -0.745 |
| 3 200 | 28.82533 | 32.28822 | 1.120 | 3.118 | 9 976.5 | 26.33 | -0.745 |
| 4 000 | 28.82533 | 33.57966 | 1.165 | 2.542 | 10 169.7 | 46.21 | -0.745 |
| 4 800 | 28.82533 | 35.25497 | 1.223 | 2.141 | 10 274.5 | 57.00 | -0.745 |
| 5 600 | 28.82533 | 37.64978 | 1.306 | 1.831 | 10 253.6 | 54.85 | -0.745 |
| 6 400 | 28.82533 | 41.68741 | 1.446 | 1.570 | 10 048.9 | 33.79 | -0.745 |
| 7 200 | 28.82533 | 51.09382 | 1.773 | 1.329 | 9 571.0 | 15.38 | -0.745 |
| 8 000 | 28.82533 | 112.43001 | 3.900 | 1.087 | 8 701.7 | 104.81 | -0.745 |
| | | | | Average | 9 720.5 | 43.6 | |

Table E.15: Determination of critical buckling load for the structure in figure 5.1 with parameter set 1 based on displacements

| N_{Ed} (kN) | w^I (mm) | w^{II} (mm) | w^{II}/w^I | n | F_{cr} | Error (%) with average | δ correction factor |
|---------------|------------|---------------|--------------|---------|----------|---------------------------|-------------------------------|
| 1 000 | 5.5574 | 5.71186 | 1.02779 | 24.386 | 24 386.7 | 1.6 | -0.35 |
| 2 000 | 5.5574 | 5.87998 | 1.05805 | 12.198 | 24 369.4 | 1.2 | -0.35 |
| 3 000 | 5.5574 | 6.06363 | 1.09109 | 8.136 | 24 407.1 | 0.8 | -0.35 |
| 4 000 | 5.5574 | 6.26511 | 1.12735 | 6.104 | 24 416.9 | 0.4 | -0.35 |
| 5 000 | 5.5574 | 6.48715 | 1.16730 | 4.885 | 24 426.2 | 0.0 | -0.35 |
| 6 000 | 5.5574 | 6.73309 | 1.21155 | 4.073 | 24 435.0 | 0.4 | -0.35 |
| 7 000 | 5.5574 | 7.07069 | 1.2723 | 3.492 | 24 442.7 | 0.7 | -0.35 |
| 8 000 | 5.5574 | 7.31420 | 1.31612 | 3.056 | 24 449.5 | 1.0 | -0.35 |
| 9 000 | 5.5574 | 7.66096 | 1.37852 | 2.717 | 24 455.1 | 1.2 | -0.35 |
| 10 000 | 5.5574 | 8.05564 | 1.44953 | 2.446 | 24 459.4 | 1.4 | -0.35 |
| 11 000 | 5.5574 | 8.50906 | 1.53112 | 2.224 | 24 462.1 | 1.5 | -0.35 |
| 12 000 | 5.5574 | 9.03557 | 1.62586 | 2.039 | 24 462.8 | 1.5 | -0.35 |
| 13 000 | 5.5574 | 9.65470 | 1.73727 | 1.882 | 24 461.2 | 1.5 | -0.35 |
| 14 000 | 5.5574 | 10.39368 | 1.87024 | 1.747 | 24 456.9 | 1.3 | -0.35 |
| 15 000 | 5.5574 | 11.29173 | 2.03184 | 1.630 | 24 449.2 | 1.0 | -0.35 |
| 16 000 | 5.5574 | 12.40751 | 2.23261 | 1.527 | 24 437.4 | 0.5 | -0.35 |
| 17 000 | 5.5574 | 13.83298 | 2.48911 | 1.437 | 24 420.5 | 0.2 | -0.35 |
| 18 000 | 5.5574 | 15.72111 | 2.82886 | 1.355 | 24 397.4 | 1.2 | -0.35 |
| 19 000 | 5.5574 | 18.34695 | 3.30135 | 1.282 | 24 366.4 | 2.4 | -0.35 |
| 20 000 | 5.5574 | 22.26053 | 4.00557 | 1.216 | 24 325.3 | 4.1 | -0.35 |
| | | | | Average | 24 372.0 | 3.1 | |

Table E.16: Determination of critical buckling load for the structure in figure 5.1 with parameter set 2 based on displacements

| N_{Ed} (kN) | w^I (mm) | w^{II} (mm) | w^{II}/w^I | n | F_{cr} | Error (%) with average | δ correction factor |
|---------------|------------|---------------|--------------|---------|----------|---------------------------|-------------------------------|
| 800 | 27.25713 | 28.62324 | 1.050 | 11.495 | 11 494.9 | 11.3 | -0.474 |
| 1 600 | 27.25713 | 30.24617 | 1.110 | 5.797 | 11 593.2 | 2.9 | -0.474 |
| 2 400 | 27.25713 | 32.21767 | 1.182 | 3.890 | 11 670.8 | 3.8 | -0.474 |
| 3 200 | 27.25713 | 34.68350 | 1.272 | 2.931 | 11 722.3 | 8.2 | -0.474 |
| 4 000 | 27.25713 | 37.89236 | 1.390 | 2.348 | 11 740.5 | 9.8 | -0.474 |
| 4 800 | 27.25713 | 42.31160 | 1.552 | 1.952 | 11 714.2 | 7.5 | -0.474 |
| 5 600 | 27.25713 | 48.94833 | 1.796 | 1.661 | 11 626.8 | 0.0 | -0.474 |
| 6 400 | 27.25713 | 60.48382 | 2.219 | 1.432 | 11 452.0 | 15.0 | -0.474 |
| | | | | Average | 11 627 | 7.3 | |

Table E.17: Determination of critical buckling load for the structure in figure 5.1 with parameter set 3 based on displacements

F

Input data of Diana FEA

In chapter 5.1 the theoretical critical buckling load based on Euler's theory has been determined. Because it took quite some effort to do this manually, this appendix treats how the example from section 5.1.2 can be determined using software program Diana FEA. The structural model of the example is given in figure F.1. Data is given in table F.1. For simplicity, the sheet pile will be modelled as one straight plate with the same bending stiffness. To reach this stiffness, a plate with a thickness of 165.54 mm and a width of 1 m will be modelled.

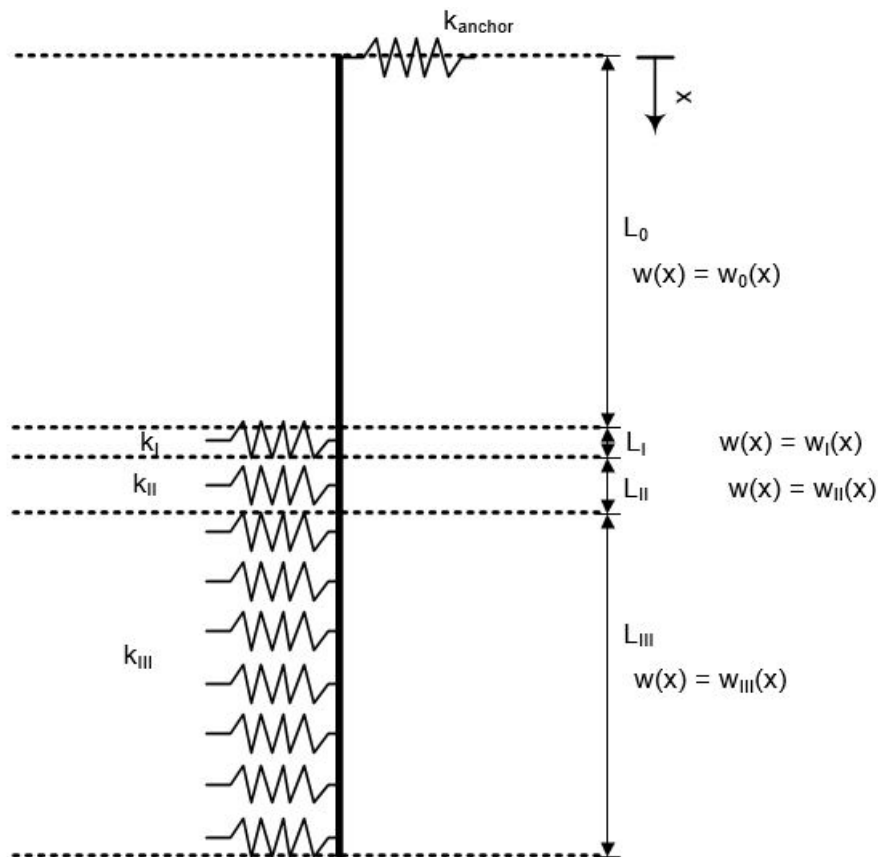


Figure F.1: Structural model of example section 5.1.2

| Parameter | Value | Unit |
|-------------------|--------|------------|
| Length sheet pile | 10 | m |
| L_0 | 4.2 | m |
| L_I | 0.3 | m |
| L_{II} | 1.1 | m |
| L_{III} | 4.4 | m |
| k_I | 1 000 | $kN/m/m^2$ |
| k_{II} | 3 270 | $kN/m/m^2$ |
| k_{III} | 12 000 | $kN/m/m^2$ |
| k_{anchor} | 42 000 | $kN/m/m$ |
| EI | 79 380 | kNm^2 |

Table F1: Data input for FEA model

F.1. Diana FEA model

The final result of the FEA model is given in figure F2. Compared to figure F.1, a few things are added. In order to provided the vertical and longitudinal ¹, extra rigid supports are added. This supports won't restrict the deformation in the buckling direction and will therefor not affect the global critical buckling load. The anchor is modelled as five separate springs on top of the sheet pile. The points visible at the lower part of the pile in figure F2 are the springs which represents the soil. Diana is not able to model an elastic support like in figure F.1 which is therefor replaced by enough springs. Those are placed each 0.1 m in height and each 0.2 m in width. Below, the input to get this model is given step by step.

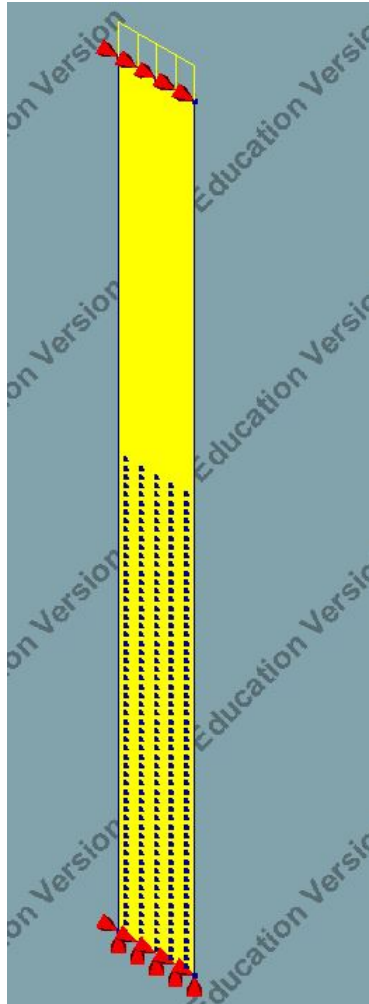
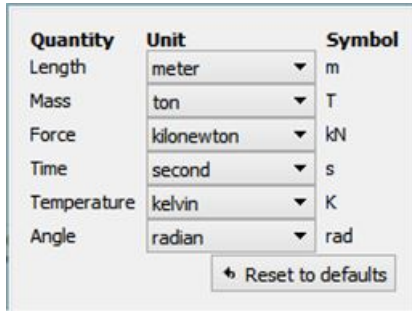
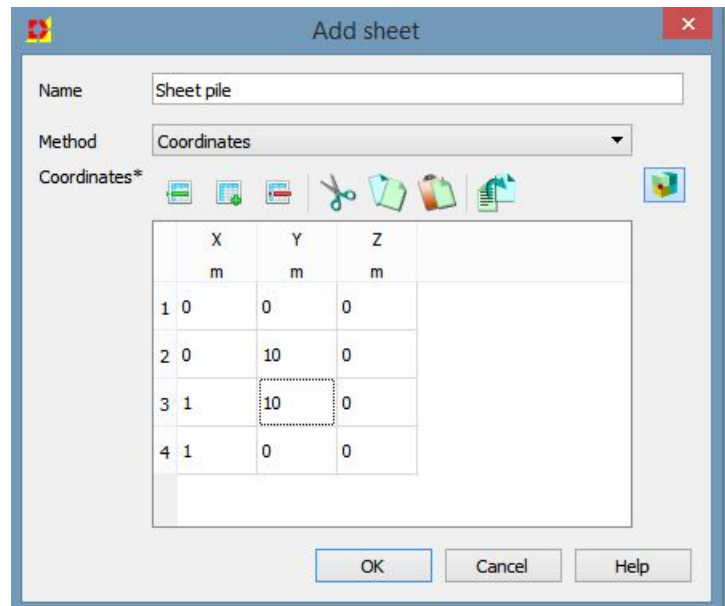


Figure E2: Final model of the sheet pile in Diana FEA

¹This direction is not given in the 2D figure F.1

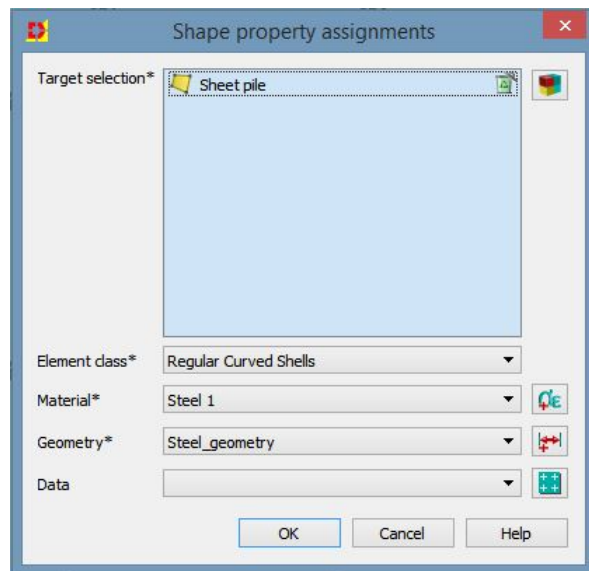


(a) Step 1: Units used in the model

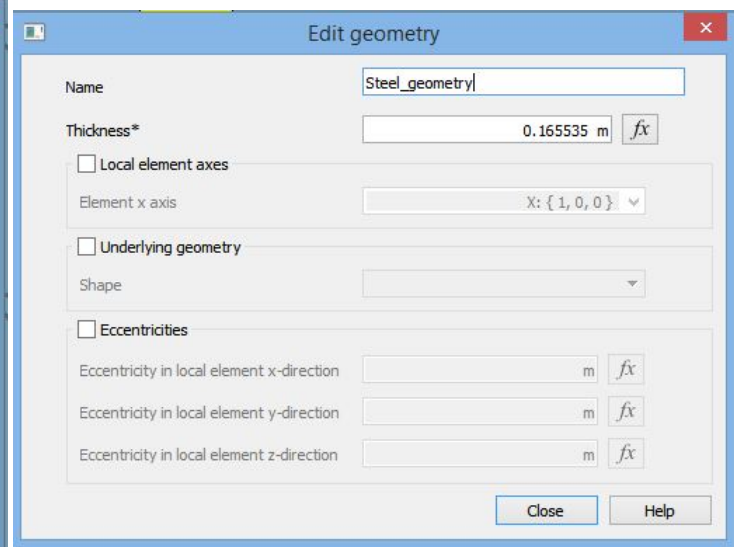


(b) Step 2: Shape of the sheet pile

Figure E3: Steps 1 and 2 of DIANA FEA stability analysis

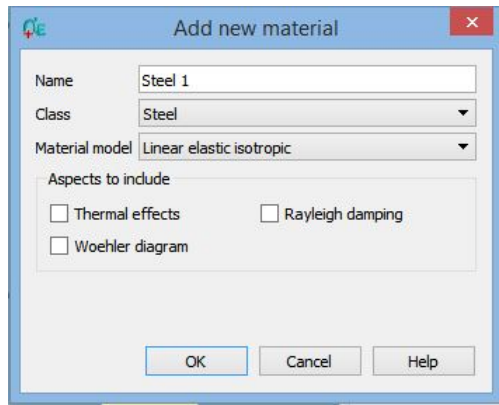


(a) Step 3: Steel property assignment

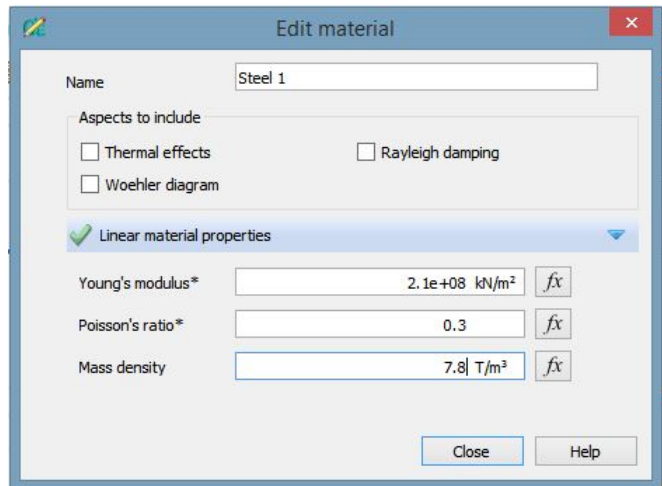


(b) Step 4: Input of steel geometry

Figure E4: Steps 3 and 4 of DIANA FEA stability analysis

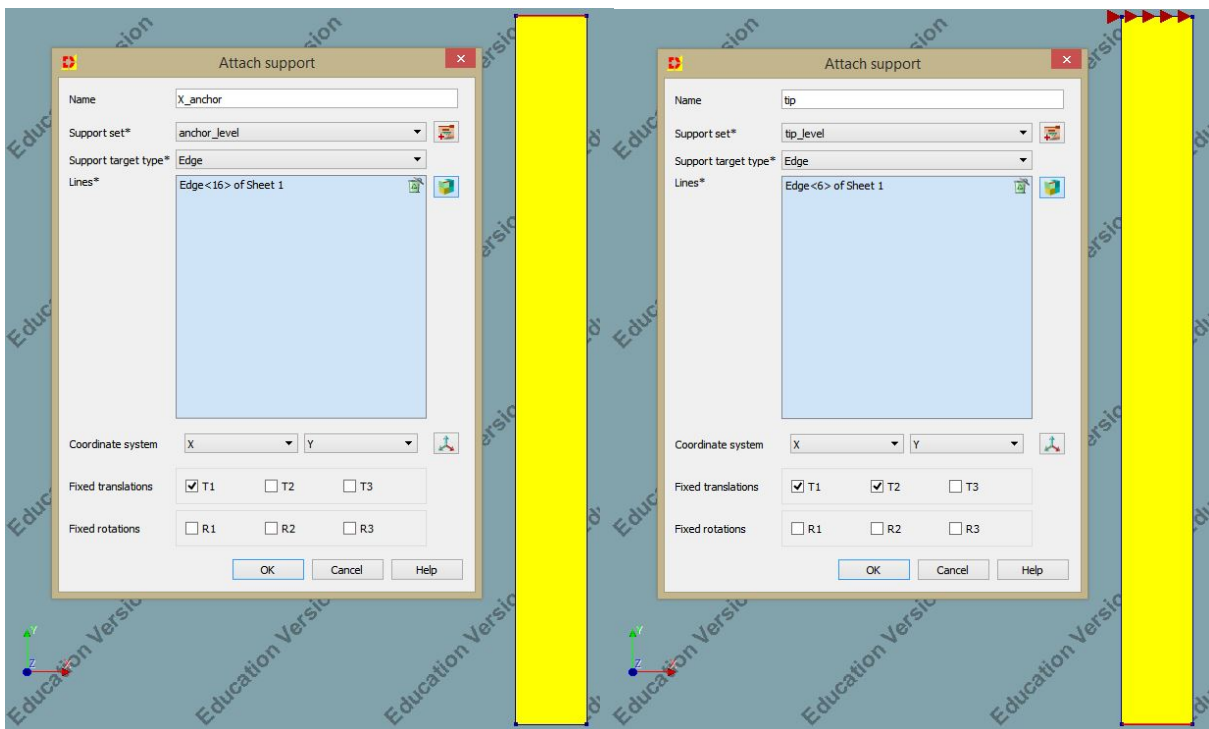


(a) Step 5: Input of steel model



(b) Step 6: Input of steel properties

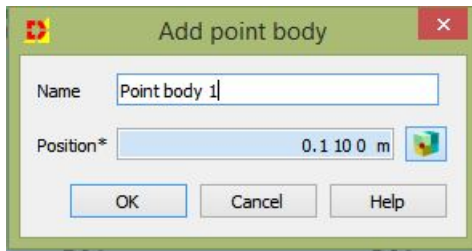
Figure E.5: Steps 5 and 6 of DIANA FEA stability analysis



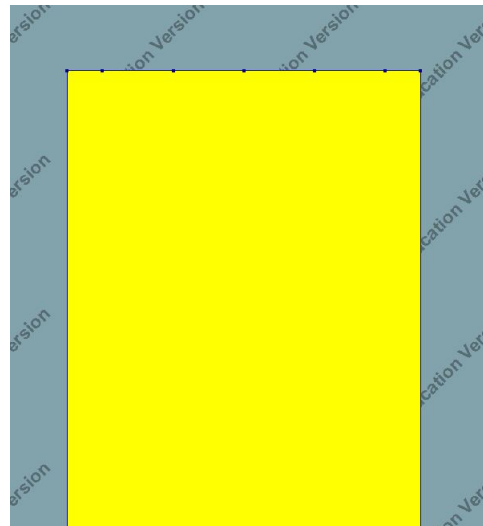
(a) Step 7: Input of rigid supports at anchor level (note the red coloured (selection) edge)

(b) Step 8: Input of rigid supports at sheet pile tip (note the red coloured (selection) edge)

Figure E.6: Steps 7 and 8 of DIANA FEA stability analysis

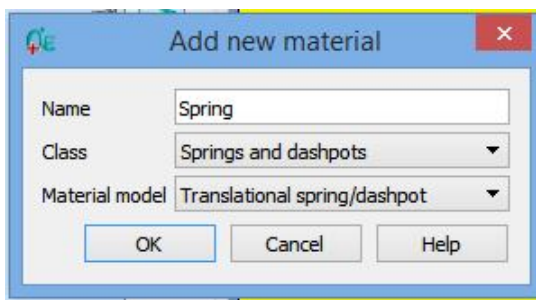


(a) Step 9: Input of point at anchor level to connect anchor spring

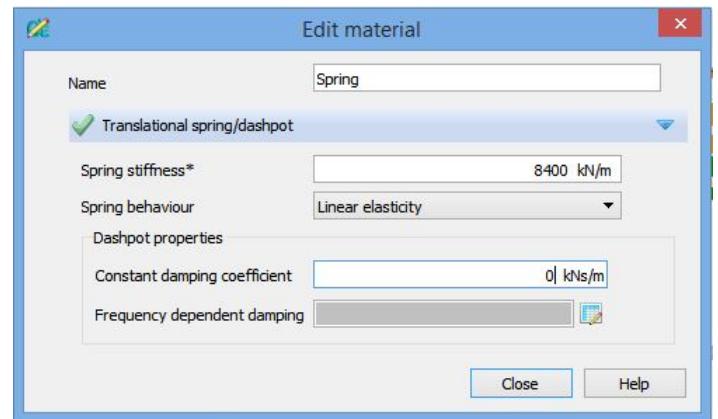


(b) 5 points where the anchor spring will be attached

Figure E7: Steps 9 of DIANA FEA stability analysis

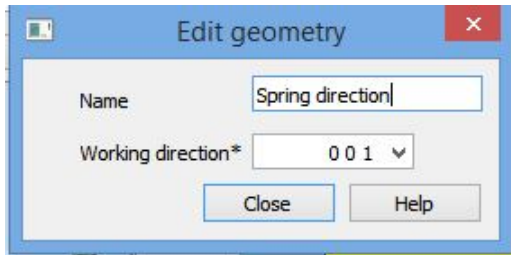


(a) Step 10: Material model of the springs

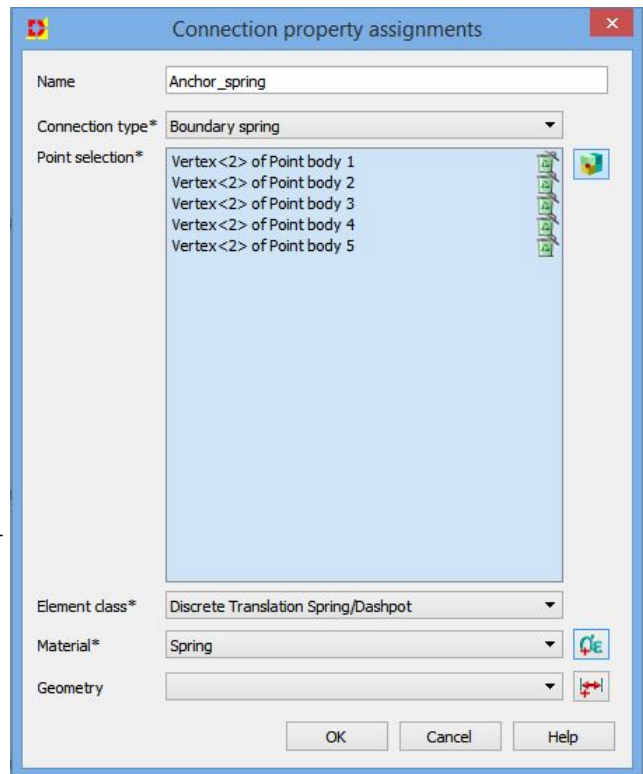


(b) Step 11: Input of material parameters of the anchor spring

Figure E8: Steps 10 and 11 of DIANA FEA stability analysis

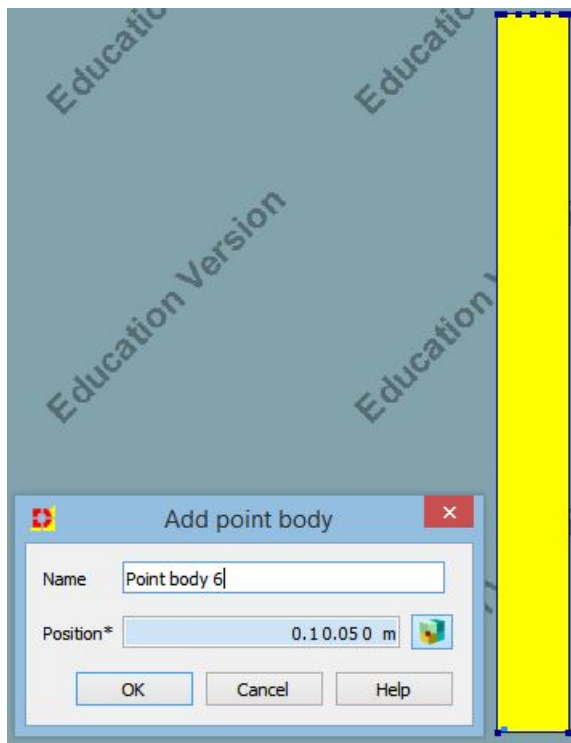


(a) Step 12: Input of spring direction using element geometry

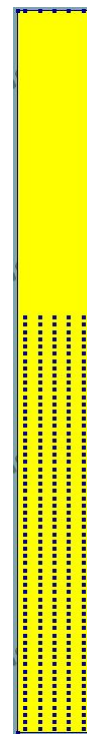


(b) Step 13: Property assignment of anchor spring

Figure E9: Steps 12 and 13 of DIANA FEA stability analysis



(a) Step 14: Input of spring point for elastic soil foundation



(b) Step 15: Copying first spring point to 270 spring points

Figure E10: Steps 14 and 15 of DIANA FEA stability analysis

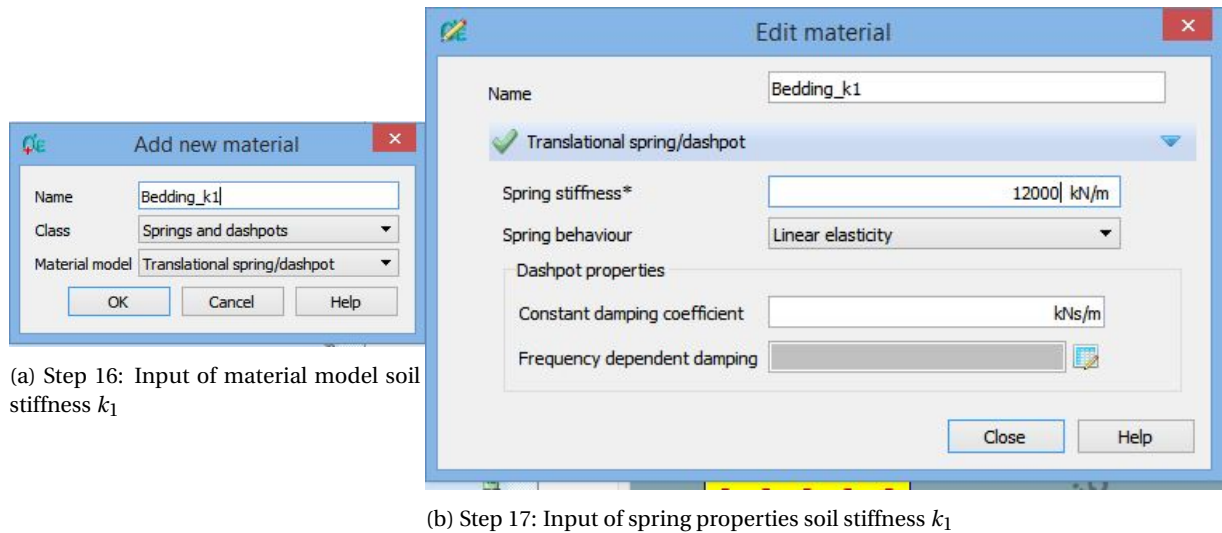


Figure F.11: Steps 16 and 17 of DIANA FEA stability analysis

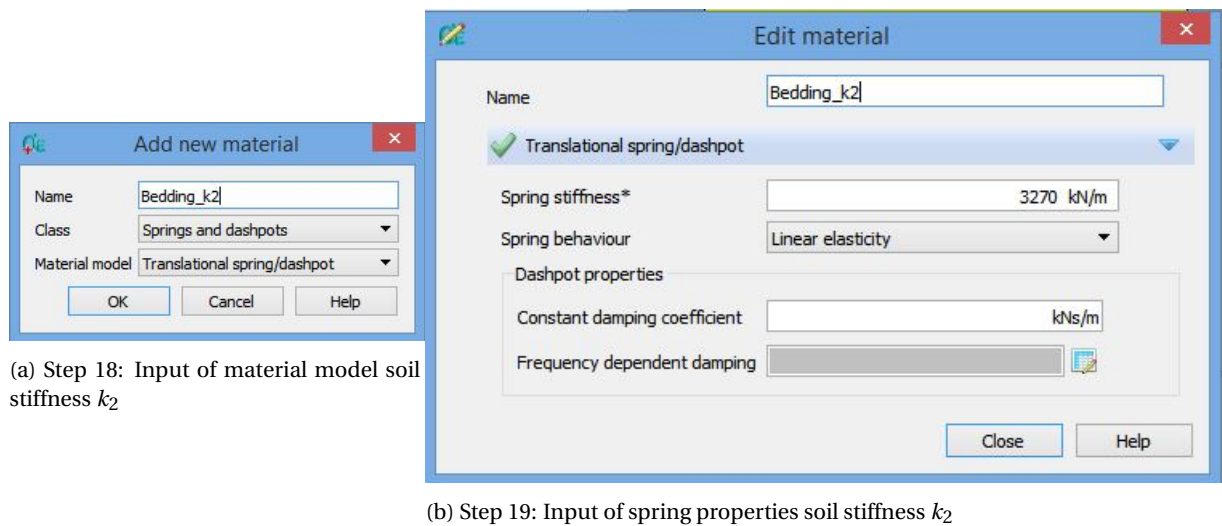
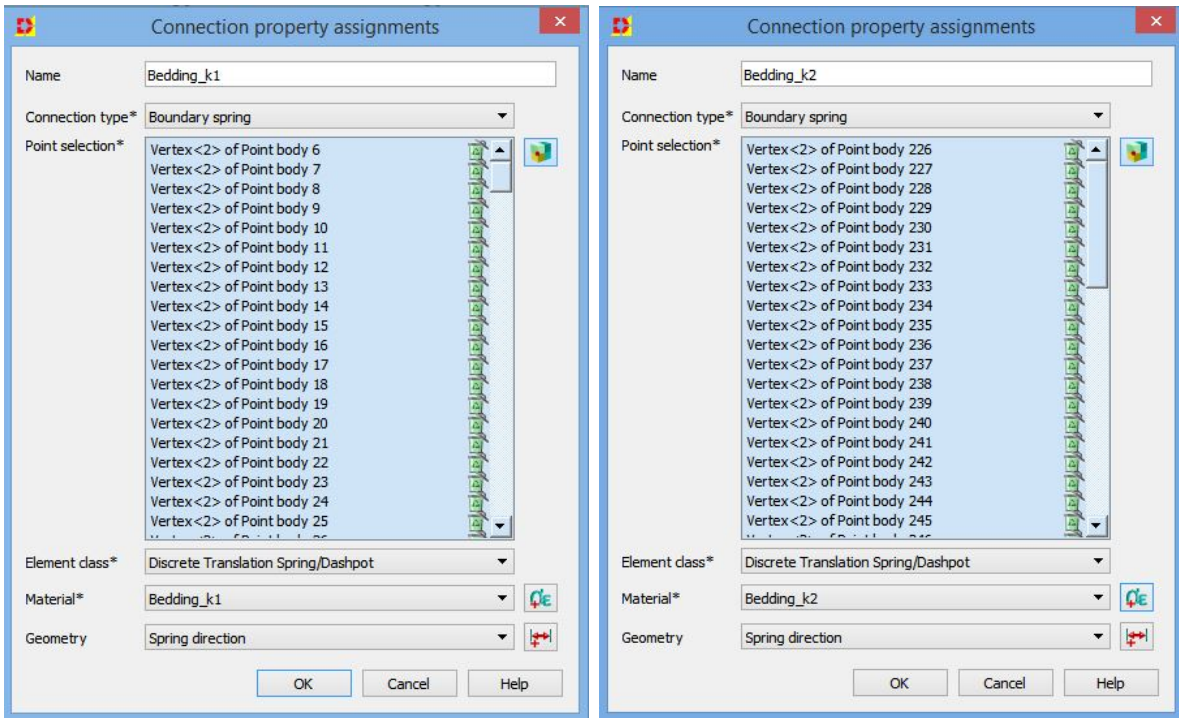


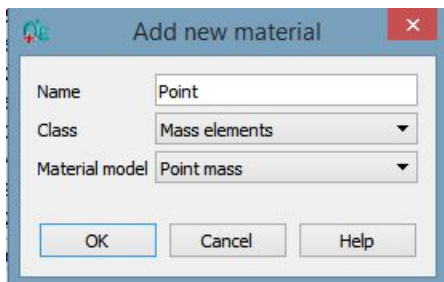
Figure F.12: Steps 18 and 19 of DIANA FEA stability analysis



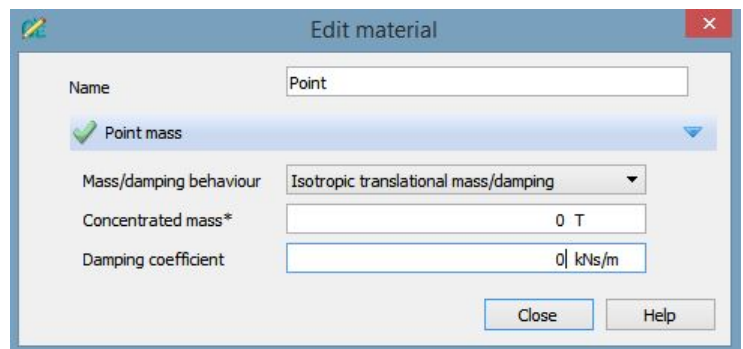
(a) Step 20: Property assignment of 215 spring representing the elastic support k_1

(b) Step 21: Property assignment of 55 spring representing the elastic support k_2

Figure F.13: Steps 20 and 21 of DIANA FEA stability analysis



(a) Step 22: Input of material model for points



(b) Step 23: Input of material properties for point material

Figure F.14: Steps 22 and 23 of DIANA FEA stability analysis

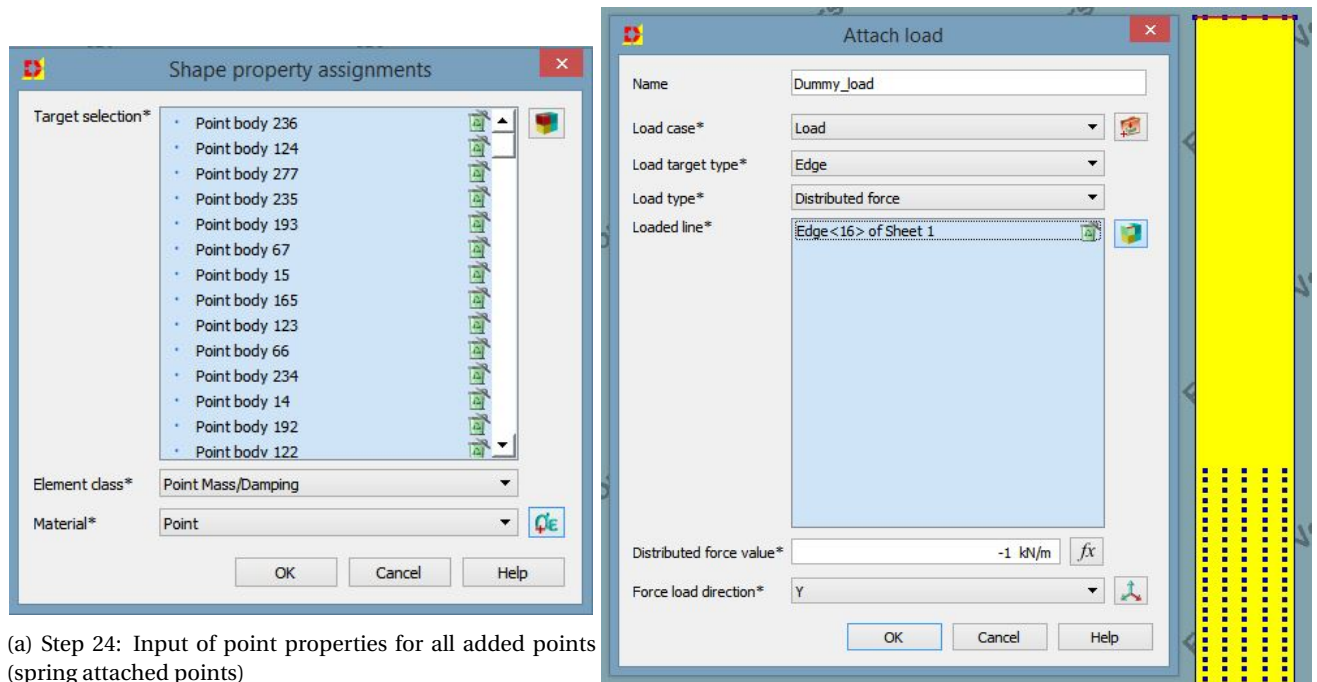
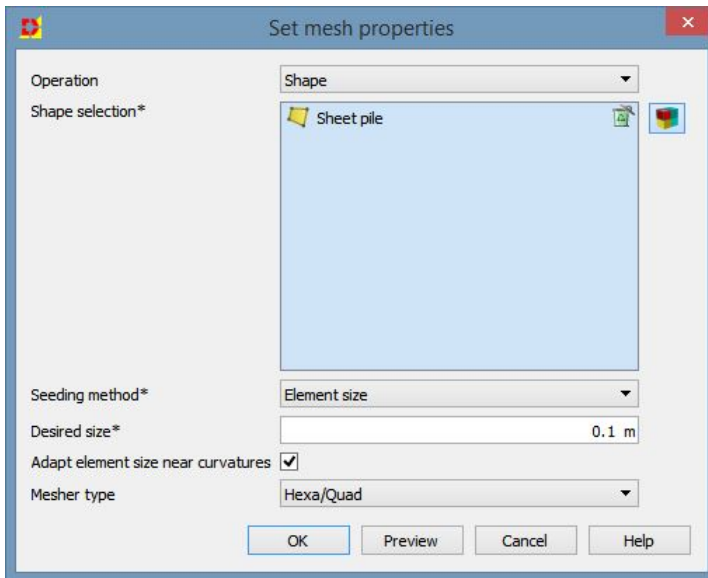
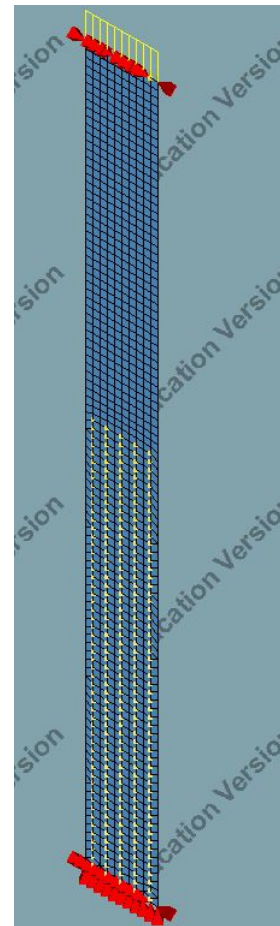


Figure F.15: Steps 24 and 25 of DIANA FEA stability analysis

The model in figure E.2 can be reached by applying step 1 to step 25. With an stability analysis Diana FEA returns a value for a certain load case. This value induces how much times this load case can be applied before buckling occurs. For this reason, a load of -1 kN was applied such that if the stability analysis returns a value of 1 000, the critical buckling load equals 1 000 kN . Before this analysis can be done, the mesh must be defined. The input of the mesh and the mesh itself is given figure F.16.



(a) Step 26: Defining the mesh size



(b) Mesh of the model

Figure E.16: Step 26 and Mesh of DIANA FEA stability analysis

G

Second order effects determined by D-sheet piling

The software package D-sheet piling is able to calculate the second order effect due to a normal force, but there are some serious limitations. Firstly, the second order effects are only determined if the normal force is manually defined. The anchor force or the wall friction to the pile are not taken into account for the second order effects. This is proven in the example calculation given below. Therefore, the anchor forces and skin friction must be calculated firstly. With the results of this calculations, the development of the normal force inside the sheet pile could manually defined. Once this is done, the second order effects can be determined with a second calculation. This second order effects might affect the anchor force and the skin friction, which would require third calculation. With this method, the second order effects are known by D-sheet piling, which replaces the factor 1.15 in equation 5.13.

Drawback to the second order calculation is that the development of the normal force can only limited be defined at four points along the sheet pile: at the pile top and tip and at both surface levels (left and right surface). Because one of the surface levels is often at the same level as the sheet pile top, the normal force can practically only be defined at three levels. Due to this reason, the effect of the normal force can only be approached. An example of such an approach is given by figure G.1, which gives both the diagrams of the actual normal force as the modelled normal force. Fortunately, Deltares, the developers of the program, have said that in future versions of the program will be able to define the normal force at more points than the four points discussed (Deltares, personal E-mail, November 25, 2019).

Example calculation second order bending moment

The sheet pile structure in figure G.2 is designed to support a soil level difference of 7 m. On the top of the pile a vertical force of 1 000 *kN* is present. Analysing this model results in a bending moment at the excavation level of -136.42 *kNm*, the vertical and horizontal anchor force are both 61.46 *kN*. At the excavation level, the soil pressure at the right side equals 42 kPa, which develops fully linear from the soil surface. The bending moment at the excavation level caused by the soil pressure equals 343 *kNm*, the horizontal anchor force causes a bending moment of -430.22 *kNm* and the vertical load of 1 000 *kN* causes -49.1 *kNm*. The sum of those three contributions is -136.32 *kNm*, while the program calculates a value of -136.42 *kNm*. The vertical anchor force should introduce a bending moment of 3 *kNm*, which is not found by the results of the program. It can be concluded that, strangely enough, the vertical external load is the only normal load which is taken into account for the second order effects.

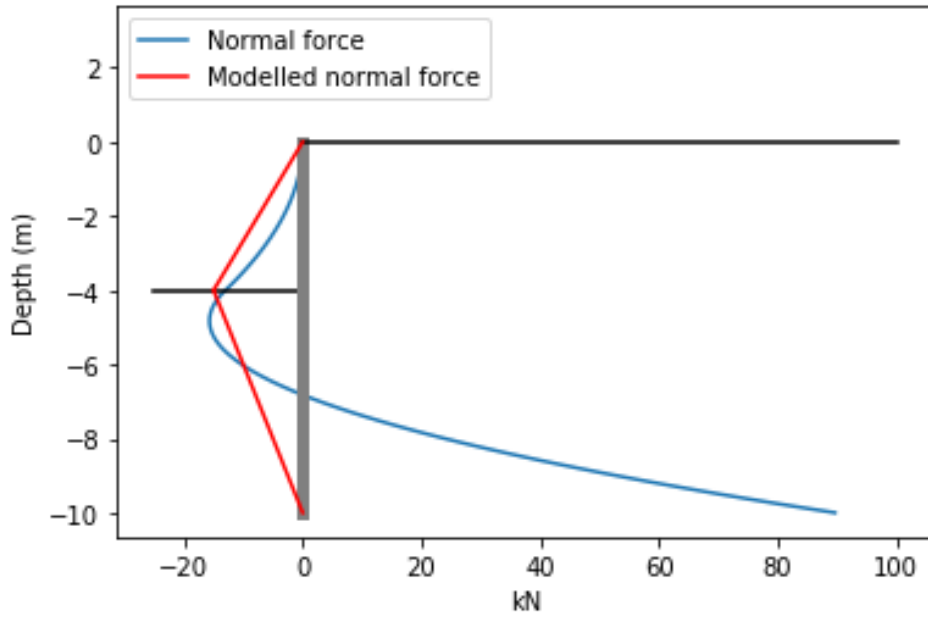


Figure G.1: Development of normal force in the sheet pile

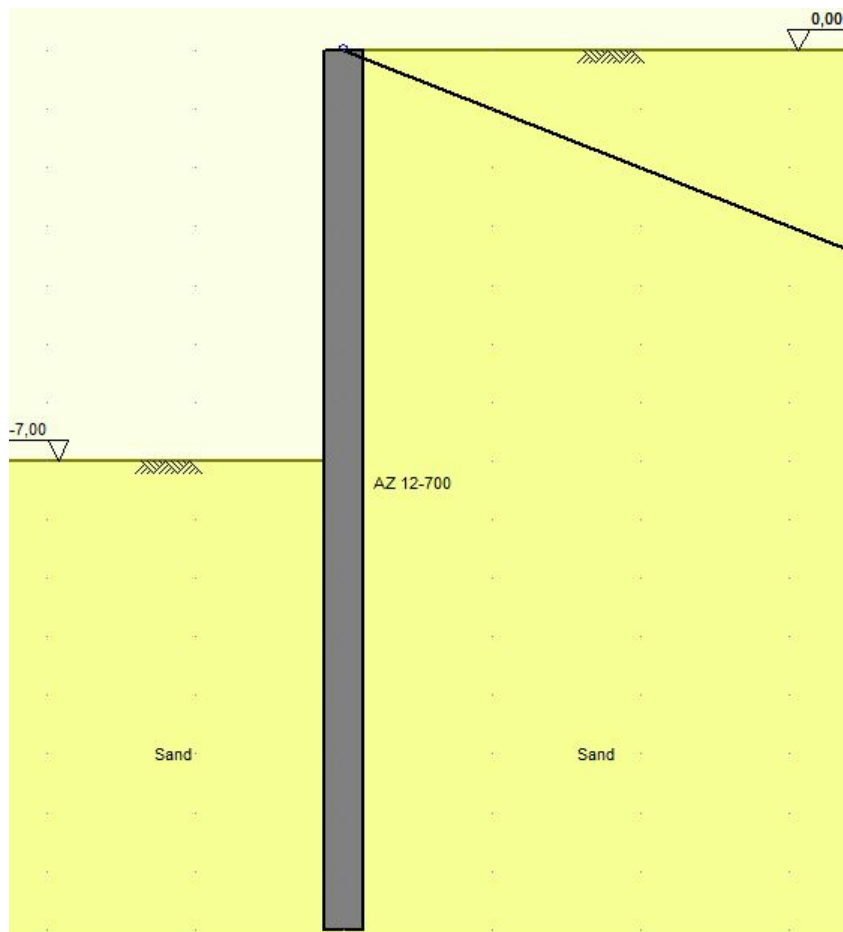
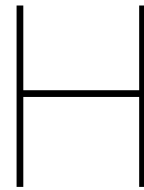


Figure G.2: Example for second order calculation by D-sheet piling



Plaxis model data

Below the data is given for the Plaxis models used for the examples in chapter 6. As a reminder, the lay-out of the structure is given in figure H.1.

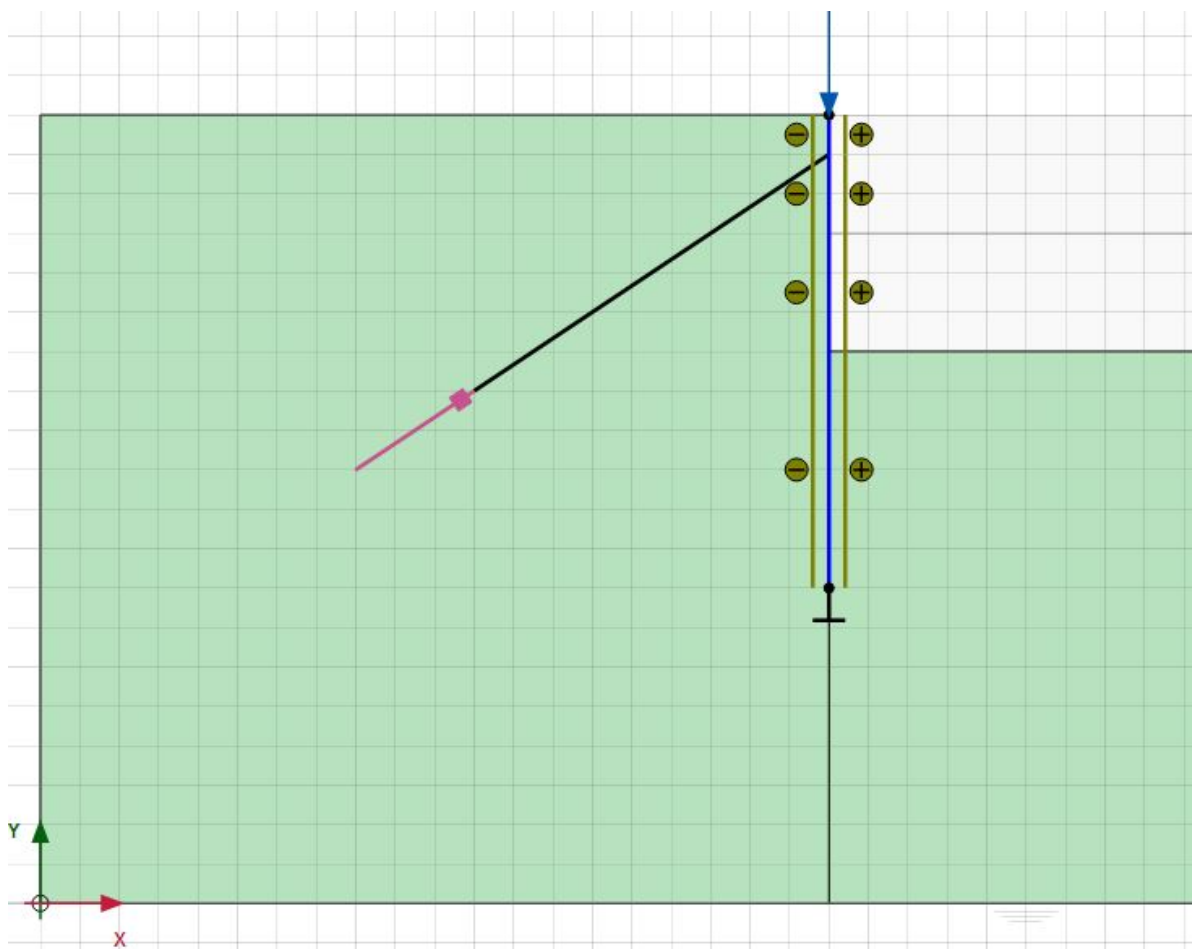


Figure H.1: Lay-out of sheet pile structures in chapter 6

| Property | Value | Unit |
|------------------------------------|-----------------------|------------------|
| Model width | 50 | M |
| Model height | 20 | M |
| Sheet pile type | AZ 12-700 | - |
| Material type | Elastic | - |
| Axial stiffness EA | 2.587e6 | kN/m |
| Bending stiffness | 39.648 | kNm ² |
| Weight | 0 | kg/m |
| Isotropic | Yes | - |
| Interfaces | Positive and Negative | - |
| Right coordinate anchor rod | (20.19) | - |
| Left coordinate anchor rod | (11.13) | - |
| Right coordinate embedded beam row | (11.13) | - |
| Left coordinate embedded beam row | (8.11) | - |
| Mesh type | Medium | - |

Table H.1: Properties of Plaxis models

| Parameter | Name | Value | Unit |
|----------------------|----------------|-----------------------|------|
| Material type | Type | Elastic | - |
| Normal stiffness | EA | 5.0 · 10 ⁵ | kN |
| Spacing out-of-plane | L _s | 2.5 | m |

Figure H.2: Material properties of the anchor rod

| Parameter | Name | Value | Unit |
|----------------------------|-----------------------------|------------------------|-------------------|
| Material type | Type | Elastic | - |
| Stiffness | E | 7.07 · 10 ⁶ | kN/m ² |
| Unit weight | γ | 0 | kN/m ³ |
| Beam type | Type | Predefined | - |
| Predefined beam type | Type | Massive circular beam | - |
| Diameter | D | 0.3 | m |
| Pile spacing | L _{spacing} | 2.5 | m |
| Skin resistance | T _{skin,start,max} | 400 | kN/m |
| | T _{skin,end,max} | 400 | kN/m |
| Base resistance | F _{max} | 0 | kN |
| Interface stiffness factor | - | Default values | - |

Figure H.3: Material properties of the embedded beam row

| Parameter | Name | Silt | Sand | Loam | Unit |
|--|------------------|-----------------------|-----------------------|-----------------------|-------------------|
| General | | | | | |
| Material model | <i>Model</i> | Hardening soil | Hardening soil | Hardening soil | - |
| Type of material behaviour | <i>Type</i> | Drained | Drained | Drained | - |
| Soil unit weight above phreatic level | γ_{unsat} | 16 | 17 | 17 | kN/m ³ |
| Soil unit weight below phreatic level | γ_{sat} | 20 | 20 | 19 | kN/m ³ |
| Parameters | | | | | |
| Secant stiffness in standard drained triaxial test | E_{50}^{ref} | 2.0 · 10 ⁴ | 3.0 · 10 ⁴ | 1.2 · 10 ⁴ | kN/m ² |
| Tangent stiffness for primary oedometer loading | E_{oed}^{ref} | 2.0 · 10 ⁴ | 3.0 · 10 ⁴ | 8.0 · 10 ³ | kN/m ² |
| Unloading / reloading stiffness | E_{ur}^{ref} | 6.0 · 10 ⁴ | 9.0 · 10 ⁴ | 3.6 · 10 ⁴ | kN/m ² |
| Power for stress-level dependency of stiffness | <i>m</i> | 0.5 | 0.5 | 0.8 | - |
| Cohesion | c_{ref}^s | 1.0 | 0.0 | 5.0 | kN/m ² |
| Friction angle | φ^s | 30 | 34 | 29 | ° |
| Dilatancy angle | ψ | 0.0 | 4.0 | 0.0 | ° |
| Poisson's ratio | ν_{ur}^s | 0.2 | 0.2 | 0.2 | - |
| K_0 -value for normal consolidation | K_0^{nc} | 0.5 | 0.4408 | 0.5152 | - |
| Groundwater | | | | | |
| Data set | - | USDA | USDA | USDA | - |
| Model | - | Van Genuchten | Van Genuchten | Van Genuchten | - |
| Soil type | - | Silt | Sand | Loam | - |
| < 2 μm | - | 6.0 | 4.0 | 20.0 | % |
| 2 μm – 50 μm | - | 87.0 | 4.0 | 40.0 | % |
| 50 μm – 2 mm | - | 7.0 | 92.0 | 40.0 | % |
| Use defaults | - | From data set | From data set | From data set | - |
| Permeability in horizontal direction | k_x | 0.5996 | 7.128 | 0.2497 | m/day |
| Permeability in vertical direction | k_y | 0.5996 | 7.128 | 0.2497 | m/day |
| Interfaces | | | | | |
| Interface strength | - | Manual | Manual | Rigid | - |
| Strength reduction factor inter. | R_{inter} | 0.65 | 0.70 | 1.0 | - |
| Consider gap closure | - | Yes | Yes | Yes | - |
| Initial | | | | | |
| K_0 determination | - | Automatic | Automatic | Automatic | - |
| Over-consolidation ratio | <i>OCR</i> | 1.0 | 1.0 | 1.0 | - |
| Pre-overburden pressure | <i>POP</i> | 0.0 | 0.0 | 25.0 | kN/m ² |

Figure H.4: Sand properties in the Plaxis models (table 3.1 from [29])

| Parameter | Name | Clay | Sand | Unit |
|--|------------------|---------------------|------------------|-------------------|
| General | | | | |
| Material model | <i>Model</i> | Soft soil | Hardening soil | - |
| Type of material behaviour | <i>Type</i> | Undrained (A) | Drained | - |
| Soil unit weight above phreatic level | γ_{unsat} | 16 | 17 | kN/m ³ |
| Soil unit weight below phreatic level | γ_{sat} | 18 | 20 | kN/m ³ |
| Initial void ratio | e_{init} | 1.0 | 0.5 | - |
| Parameters | | | | |
| Modified compression index | λ^* | $3.0 \cdot 10^{-2}$ | - | - |
| Modified swelling index | κ^* | $8.5 \cdot 10^{-3}$ | - | - |
| Secant stiffness in standard drained triaxial test | E_{50}^{ref} | - | $4.0 \cdot 10^4$ | kN/m ² |
| Tangent stiffness for primary oedometer loading | E_{oed}^{ref} | - | $4.0 \cdot 10^4$ | kN/m ² |
| Unloading / reloading stiffness | E_{ur}^{ref} | - | $1.2 \cdot 10^5$ | kN/m ² |
| Power for stress-level dependency of stiffness | m | - | 0.5 | - |
| Cohesion (constant) | c_{ref}' | 1.0 | 0.0 | kN/m ² |
| Friction angle | φ' | 25 | 32 | ° |
| Dilatancy angle | ψ | 0.0 | 2.0 | ° |
| Poisson's ratio | ν_{ur}' | 0.15 | 0.2 | - |
| K_0 -value for normal consolidation | K_0^{nc} | 0.5774 | 0.4701 | - |
| Groundwater | | | | |
| Permeability in horizontal direction | k_x | 0.001 | 1.0 | m/day |
| Permeability in vertical direction | k_y | 0.001 | 1.0 | m/day |
| Interfaces | | | | |
| Interface strength | - | Manual | Manual | - |
| Strength reduction factor inter. | R_{inter} | 0.5 | 0.67 | - |
| Initial | | | | |
| K_0 determination | - | Automatic | Automatic | - |
| Over-consolidation ratio | <i>OCR</i> | 1.0 | 1.0 | - |
| Pre-overburden pressure | <i>POP</i> | 5.0 | 0.0 | kN/m ² |

Figure H.5: Clay properties in the Plaxis models (table 3.1 from [29])

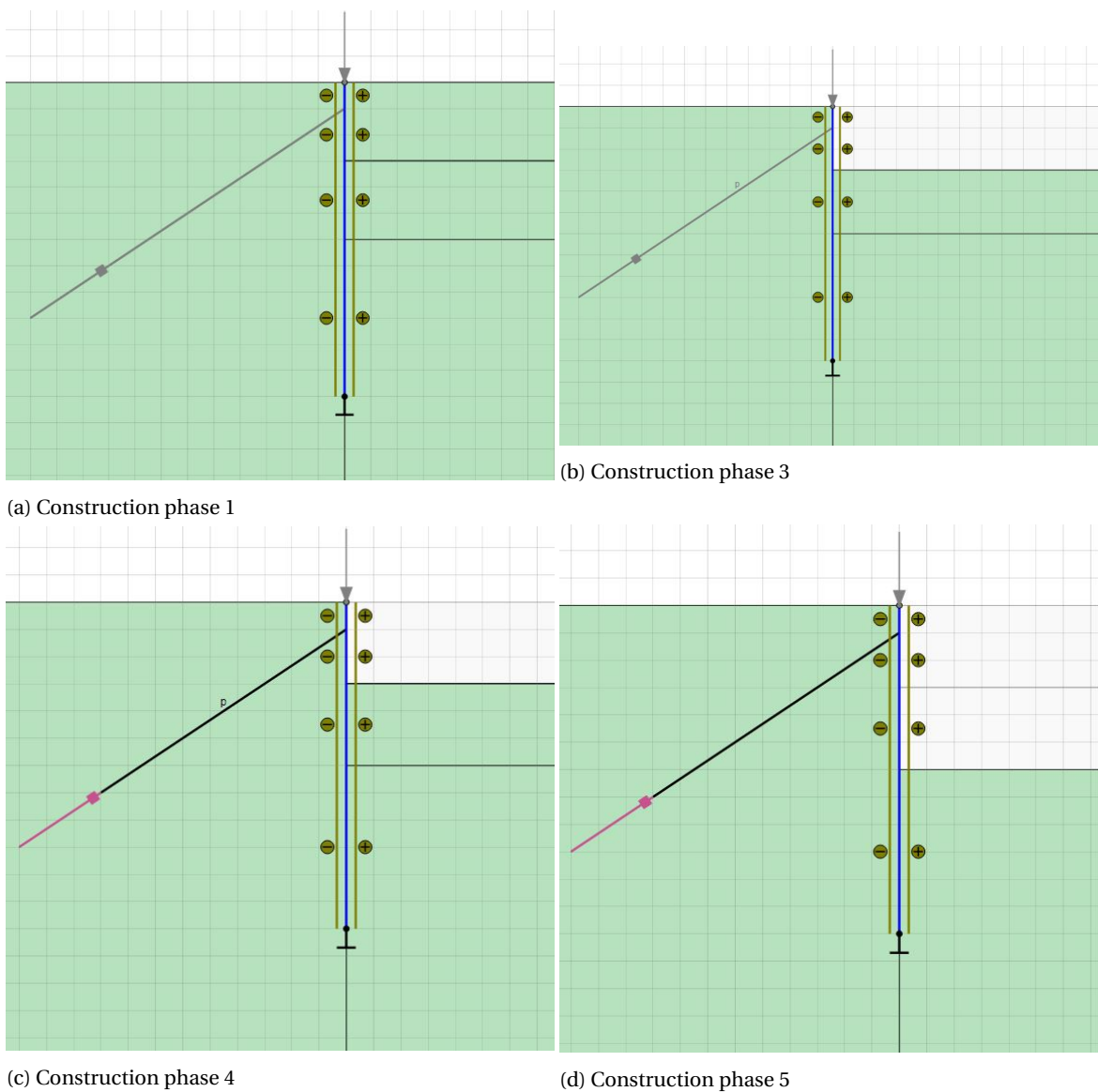


Figure H.6: Construction phases of the model

The construction of a sheet pile must be done in phases. For the models in the example of chapter 6, some of the phases are represented in figure H.6. Phase 1 represents the installation of the sheet pile, the water head in the soil is at +19 m (1 m below the surface). In phase 2, the water head at the right side is lowered with 6 m to +13 m. In phase 3 the soil at the right side is excavated for 3 m, so the anchor can be installed in phase 4. The anchor is pre-stressed with a force of 200 kN. Finally, in phase 5 the soil is excavated for 3 more meters. After this phase, the normal force on top of the sheet pile is increased step by step to get the results given in chapter 6.

In order to determine the effect of imperfections, the imperfections might be modelled. This is for example given in figure H.7, where the pile geometry is defined by 15 points so that the initial imperfections occur. Two imperfection shapes are used as an example. For the fixed imperfection shape, the following coordinates are used:

(20;20).(20.03;19).(20.05;18).(20.07;17).(20.08;16).(20.08;15).(20.08;14).(20.06;12.83).(20.05;12.20).(20.0;11.61),
(20.03;11.02).(20.02;10.39).(20.01;9.64).(20;19.14).(20;8)

For the simple imperfection shape, the coordinates are as given below:

(20;20).(20.02;19).(20.04;18).(20.06;17).(20.07;15.9).(20.08;15).(20.08;14).(20.08;13).(20.07;12.10).(20.06;11).
(20.04;10).(20.02;9).(20.0;8)

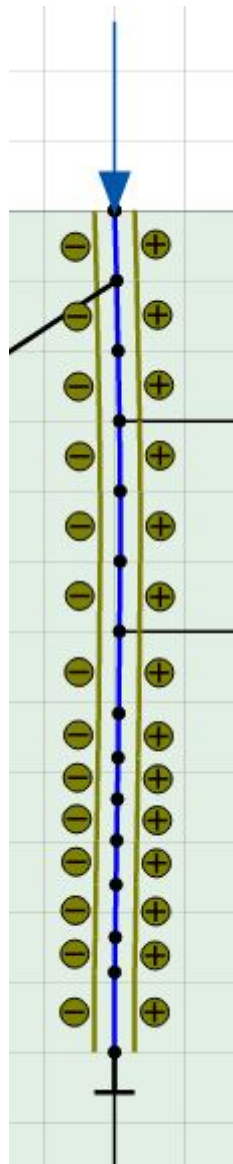


Figure H.7: Imperfection model in Plaxis 2D